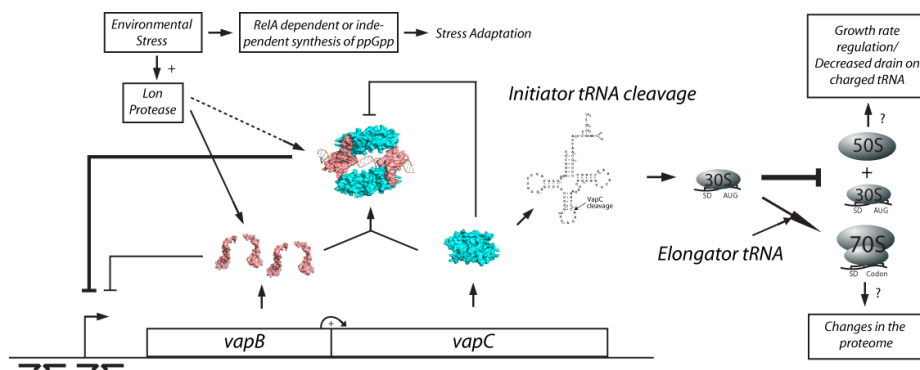


Molecular Target of Enteric VapC Toxins and Regulation of *vapBC* Transcription by Conditional Cooperativity



PhD Thesis

Kristoffer Skovbo Winther

Institute for Cell and Molecular Biosciences
Newcastle University
September 2011

Abstract

The ubiquitous Type II toxin – antitoxin (TA) loci encode two proteins, a toxin and an antitoxin. The antitoxin combines with and neutralizes a cognate toxin. Usually, the TA genes form an operon that is transcribed by a single promoter located upstream of the genes. In most cases, the antitoxin autoregulates the TA operon via binding to operator sites in the promoter region. In almost all such cases, the toxin act as a co-repressor of transcription as the toxin enhances the DNA binding of the antitoxin. Recently, it has been shown that toxins play an additional role in stimulating transcription, as the antitoxin and toxin ratio is important for cooperative binding of the complex to DNA. The antitoxin is rapidly degraded by cellular proteases under conditions of stress and treatment with antibiotics, which leads to activation of the toxin.

The toxins of TAs belong to different gene families. The most abundant TA gene family is *vapBC* that, in some organisms, have expanded into cohorts of genes. For example, the major human pathogen *Mycobacterium tuberculosis* contains at least 88 TAs, 45 of which are *vapBC* loci. VapC toxins encoded by *vapBC* loci are PIN domain proteins (PilT N-terminal). Eukaryotic PIN domain proteins are site-specific ribonucleases involved in quality control, metabolism and maturation of mRNA and rRNA. From *in vitro* experiments it has been postulated that VapC toxins are RNases or DNases but their exact cellular target has remained elusive.

Here I show that VapC encoded by *Shigella flexneri* 2a virulence plasmid pMYSH6000 and the chromosome of *Salmonella enterica* serovar Typhimurium LT2 are site-specific endoribonucleases that specifically cleave tRNA^{fMet} in the anticodon stem-loop *in vivo* and *in vitro*. Furthermore, I show that VapC dependent depletion of tRNA^{fMet} leads to bacteriostatic inhibition of global translation, which surprisingly induces low-level initiation of translation at elongator codons that are correctly positioned relative to a Shine & Dalgarno sequence.

I also show that VapC forms a complex with VapB and acts as a co-repressor of *vapBC* transcription. During steady state growth VapB is in excess of VapC. However, nutrient stress or treatment with antibiotics leads to Lon protease dependent decrease in VapB levels. Furthermore, I show that VapC in excess of VapB directly interferes with cooperative DNA binding of the VapBC complex, which is dependent on the dimerisation of the VapC toxin.

In conclusion, I show that enteric VapCs not only regulate global cellular translation by tRNA^{fMet} cleavage, but also regulate *vapBC* transcription by conditional cooperativity.

Acknowledgements

First I would like to thank my supervisor Kenn Gerdes for giving me the opportunity to do research in his lab. I am grateful that Kenn has believed in my skills and has supported my work to the completion of this thesis.

Secondly, I would like to thank present and past members of Kenn Gerdes' lab for stimulating and interesting scientific discussions as well as the not so scientific discussions. I would also like to thank people working in the CBCB for their technical expertise and great nights out. In particular I would like to thank Daniel Castro-Roa, Patricia Dominguez-Cuevas and Soren Ulrik Nielsen for their scientific know-how and helpful discussions. I would also like to thank David Guymer and Henrik Strahl for critical reading of this thesis.

Finally, I would like to thank my family and friends for all the support and encouragement in the world. Especially, I would like to thank Patricia for her oceans of patience and love.

Kristoffer Skovbo Winther

September 2011

Table of Contents

Abstract	1
Acknowledgements	3
Abbreviations	7
Introduction	9
Chapter 1: Families	12
Toxin-antitoxin loci: Families, distribution and phylogeny	12
Chapter 2: Toxins	19
Structure and activity of Toxins.....	19
Toxin targets outside the translation machinery – CcdB, ParE, Zeta and YeeV	19
<i>Inhibitors of DNA gyrase – CcdB and ParE</i>	19
<i>Targeting peptidoglycan synthesis and cell division – Zeta and YeeV</i>	21
Toxin targets inside the translation machinery	21
<i>The ribosome and translation</i>	21
<i>Trans-translation</i>	24
<i>Ribosome dependent mRNA Interferases – RelE and HigB</i>	25
<i>Ribosome independent mRNA interferases – MazF, HicA, and MqsR</i>	28
<i>Targeting the ribosome – Doc and HipA</i>	31
<i>Prokaryotic PIN domains - VapC</i>	33
<i>Diverse toxin families which target the translational machinery of E. coli</i>	38
Chapter 3: Antitoxins	41
Structure and activity of Antitoxins.....	41
<i>CcdA and the CcdAB TA complexes</i>	41
<i>MazEF and Kis-Kid TA complexes</i>	44
<i>RelBE TA complexes</i>	46
<i>Phd-Doc TA complexes</i>	49
<i>FitAB and other VapBC complexes</i>	51
New regulatory interactions with TAs.....	54
Chapter 4: Models	56
Models for the biological function(s) of chromosomal TAs.....	56
<i>Implications of TAs in bacterial stress response and pathogenesis</i>	56
<i>TAs in Persistence – tolerance to antibiotics</i>	61
<i>Programmed Cell Death and phage abortive system</i>	62
Results Section I: The Molecular and Cellular target of Enteric VapC toxins	64
Introduction to the experimental work	64

VapC toxin expression leads to bacteriostatic inhibition of translation	65
VapC expression activates endogenous YoeB mRNA interferase to cleave mRNA at stop codons	67
Ribosome dependent YoeB cleavage reveals possible ectopic initiation of translation at elongator codons, which depends on Shine & Dalgarno sequence	69
VapC expression does not decrease stability of model mRNAs <i>in vivo</i> in the absence of YoeB activation but inhibits translation	72
VapC toxins decrease polysomes, but does not specifically associate with the ribosome or ribosomal subunits	73
Purified VapC inhibits translation	76
VapC specifically cleaves tRNA ^{fMet} <i>in vitro</i> and <i>in vivo</i> without affecting stability of other tRNAs	77
tRNA ^{fMet} is most-likely the sole target of VapC	81
VapC cleavage occurs at the anticodon stem-loop of tRNA ^{fMet}	82
An abrupt decrease in the rate of translation induces VapC cleavage of tRNA ^{fMet} from plasmid resident <i>vapBC</i> locus	84
Depletion of tRNA ^{fMet} by VapC results in ectopic initiation of translation at elongator codons	85
Discussion Section I	87
Future Perspectives for Results Section I.....	95
Results Section II: Transcriptional regulation of <i>vapBC</i>_{LT2}	97
Introduction to experimental work	97
Strict translational coupling between <i>vapB</i> _{LT2} and <i>vapC</i> _{LT2} ensures excess levels of VapB _{LT2} during steady state growth	98
Lon protease is responsible for VapB _{LT2} degradation which activates <i>vapBC</i> _{LT2} transcription during nutritional stress and by chloramphenicol.....	100
VapB _{LT2} specifically binds its own promoter DNA and VapC _{LT2} increase the affinity of VapB _{LT2} for DNA	102
VapC _{LT2} in excess decreases the affinity of VapB _{LT2} for DNA which is reversible	104
VapB _{LT2} binds independently to two inverted repeats in the promoter region with different affinity <i>in vitro</i> and <i>in vivo</i>	105
VapC _{LT2} toxin in excess disrupts DNA-binding of VapB _{LT2} to <i>vapO1</i> and shows conditional repression <i>in vitro</i> and <i>in vivo</i>	107
VapC _{LT2} dimerisation is important for transcriptional repression and conditional cooperativity.....	111
Discussion for Results Section II	116
Future Perspectives for Results Section II.....	122
Conclusion	123

Materials and Methods	125
Bacterial Strains, Plasmids and Growth Conditions.....	125
Standard procedures.....	125
Strains Constructed.....	130
Plasmids Constructed	130
Rates-of protein, RNA and DNA synthesis.....	142
RNA purification	143
<i>Total RNA purification</i>	143
<i>tRNA purification</i>	143
Preparation of VapC and VapB	144
Inhibition of <i>in vitro</i> translation extract.....	144
<i>VapC activity assay</i>	145
<i>Resuming translation in a VapC inhibited extract</i>	145
<i>In vitro</i> RNA cleavage analysis	145
<i>In vitro</i> cleavage site mapping	146
Analysis of the <i>in vivo</i> cleavage site in tRNA ^{fMet}	146
Ribosome Profiles generated by ultracentrifugation	146
Luciferase activity assays.....	147
Northern blot analysis.....	148
<i>mRNA Northern blot analysis</i>	148
<i>tRNA Northern blot analysis</i>	148
Primer extension analysis.....	149
<i>Identification of the transcriptional start site of the vapBC_{LT2} promoter</i>	149
<i>Identification of cleavage sites generated by YoeB mRNA interferase</i>	149
Western blot analysis	150
<i>Degradation of VapB_{LT2} in the cell</i>	150
<i>Western blot analysis on ribosome fractions</i>	150
Electrophoretic mobility shift assays and DNase I footprinting.....	151
<i>DNase I footprinting</i>	151
MW estimation of VapBC _{LT2} complex bound to DNA.....	152
β-galactosidase assays	152
Quantitative PCR	152
<i>In vitro</i> translation of <i>vapBC_{LT2}</i> mRNA	153
<i>In vitro</i> cross-linking of purified VapC _{LT2}	153
References	155
Publications	177

Abbreviations

A	adenosine
Amp	ampicillin
ATP	adenosine triphosphate
bp	base pair(s)
BLAST	basic local alignment search tool
C	cytosine
°C	degrees Celsius
CM	chloramphenicol
C-terminus	carboxy terminus
Da	Daltons
DNase	deoxyribonuclease
dNTP	deoxynucleotide triphosphate
EDTA	Ethylenediaminetetraacetic acid
EF	elongation factor
EMSA	electrophoretic mobility shift assay
EtBr	Ethidium Bromide
FD	Formamide
G	guanine
h	hour
HEPES	4-(2-hydroxyethyl)-1-piperazineethanesulfonic acid
His-tag	poly-histidine tag
HTH	helix turn helix
IF	initiation factor
IPTG	isopropylthio- β -D-galactosidase
IR	inverted repeat
Kan	kanamycin
kb	kilobase
LB	luria bertani
LHH	looped helix helix
mi	mRNA interferase
min	minutes
mRNA	messenger RNA

Native-PAGE	non-denaturing PAGE
ND	not determined
NMD	nonsense mediated decay
NMR	nuclear magnetic resonance
N-terminus	amino terminus
MW	molecular weight
OD	optical density
ON	over night
ORF	open reading frame
PAGE	polyacrylamide gel electrophoresis
PBS	phosphate buffered saline
PCR	polymerase chain reaction
PDB	protein data bank
PIN	PilT N-terminal domain
PNK	polynucleotide kinase
ppGpp	guanosine tetraphosphate
PSK	post segregational killing
RHH	ribbon helix helix
rpm	revolutions per minute
RNase	ribonuclease
rRNA	ribosomal RNA
SDS	Sodium dodecyl sulphate
σ	sigma factor
T	thymine
TA	toxin antitoxin
Tris	tris-(hydroxymethyl)-aminomethane
tRNA	transfer RNA
tRNAse	transfer RNA ribonuclease
U	uracil
UTR	untranslated region
Vap	virulence associated protein
WT	wild type

Introduction

Prokaryotes have evolved elaborate strategies to inherit unstable plasmids by actively preventing loss during cell division. In most cases prokaryotic plasmids contain centromere-like gene cassettes that actively segregate plasmids before cell division occurs (Gerdes *et al.*, 2004). Others rely on gene cassettes, which selectively restrict the reproduction of plasmid-free daughter cells (Jensen and Gerdes, 1995). The latter type of system is also referred to as toxin-antitoxin systems (TAs).

Early genetic screening for genes involved in stabilisation of plasmid R1 revealed a small locus named *hok/sok* (*host killing/ suppression of killing*) (Gerdes *et al.*, 1986). This system is represented by three genes; *mok* (*modulator of killing*), *hok* and *sok*. The *mok* gene encodes a small peptide, which overlaps with *hok* reading frame and is necessary for *hok* translation. The *sok* gene, which is a *cis* encoded small RNA that inhibits Hok synthesis in two ways; indirectly by interfering with *mok* translation and directly by decreasing the stability of *hok* mRNA in a RNase III dependent manner (Thisted and Gerdes, 1992; Gerdes *et al.*, 1992). If continuous synthesis of unstable *sok* mRNA is lost e.g. if the plasmid is not inherited to one of the daughter cells after cell division, left over stable *hok* mRNA will result in Hok synthesis and selective killing of plasmid free cells. This phenotype is also referred to as postsegregational killing or PSK. A general trait of all TAs is that they encode an unstable antitoxin and a stable toxin, which evidently, if plasmid is resident, will lead to plasmid addiction and a PSK phenotype. It is now clear that TAs are not only restricted to mobile genetic elements such as plasmids or phages, but are also present on prokaryotic chromosomes (Gerdes and Wagner, 2007; Fozo *et al.*, 2010). Hence, chromosomal TAs may play other roles.

TAs come in several forms and have been divided into three different types with respect to the nature of their component parts; *hok/sok* TA system is a type I TA (Figure 1A). The second class, Type II TAs, are strictly proteic systems in which the antitoxin neutralises the toxin by direct interactions between antitoxin and toxin (Gerdes *et al.*, 2005; van Melderen, 2010) (Figure 1B). The third class is type III TAs, which are similar to type I having an RNA antitoxin and similar to the type II systems in that the antitoxin makes direct interactions with the toxin and hereby neutralizes its activity (Figure 1C). Type III TAs are a quite recent discovery and the only well described example is plasmid resident ToxIN (ToxN for toxin and ToxI for toxin

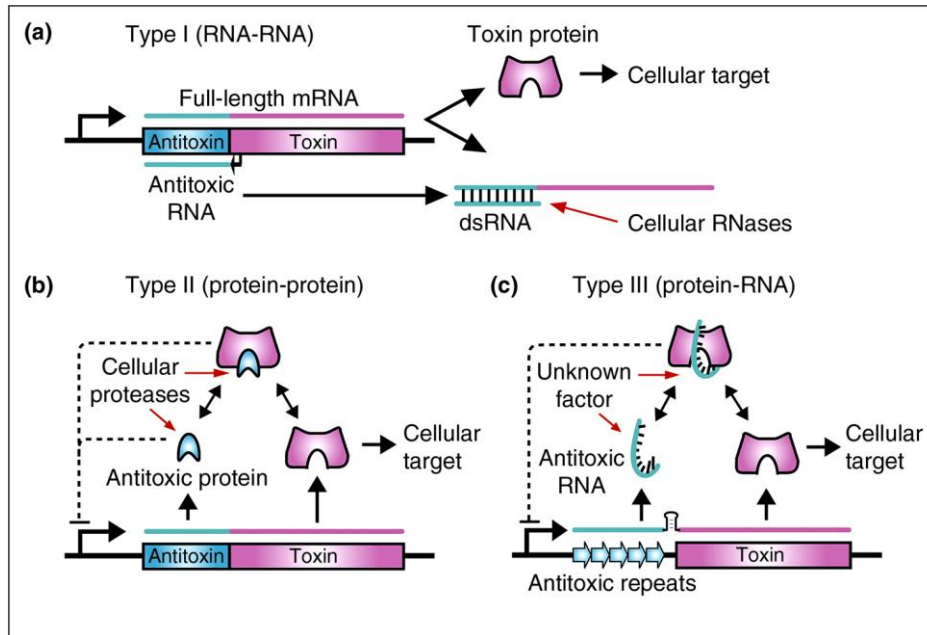


Figure 1 Overview of Toxin-Antitoxin types. **A)** Type I TAs encode a small Antisense RNA antitoxin which inhibits translation of toxin mRNA as well as promoting the degradation by cellular ribonucleases such as RNase III. If synthesis of RNA antitoxin is discontinued toxin is translated and activated. **B)** Type II TAs are strictly proteic and encode an unstable antitoxin and a stable toxin which forms a non-toxic complex. Antitoxin inhibits transcription, which is enhanced by the toxin in TA complex. When antitoxin is degraded by cellular proteases, toxin liberated to act on its target. **C)** Type III TAs encode an RNA antitoxin, which is generated from antitoxin repeats and a protein toxin. RNA antitoxin neutralises toxin activity by binding to the toxin which also negatively regulates transcription. As yet unidentified factor(s) are predicted to degrade or interfere with the antitoxin, which in turn activates the toxin. Adapted from (Blower *et al.*, 2011a).

inhibitor) from *Erwinia carotovora* Atroseptica (Fineran *et al.*, 2009). The TA locus was found to be an efficient abortive infection (Abi) system that gives resistance to multiple types of phages, by restricting growth of infected cells. The recent solving of ToxIN crystal structure revealed, ToxI as a 36-nucleotide RNA pseudo-knot, which makes extensive RNA-protein contacts with ToxN (Blower *et al.*, 2011b). Interestingly, the structure also revealed that ToxN is involved in generating ToxI by endonuclease activity on a repetitive ToxI precursor.

Most TA research to date has concerned Type II TAs and will also be the main subject of this introduction. Bioinformatic reports from several groups in recent years have made it apparent that type II TAs are highly abundant not only on plasmids but especially on chromosomes of both bacteria and archaea (Anantharaman and Aravind, 2003; Pandey and Gerdes, 2005; Makarova *et al.*, 2009). This makes type II TAs far more common than either type I or type III TAs.

Type II TAs have been extensively studied over the years, but their biological roles are still not clear and several possibilities have been suggested, which might not be

exclusive. These include: stress response elements and pathogenesis systems (Gerdes *et al.*, 2005; Ramage *et al.*, 2009), persistence (Korch *et al.*, 2003; Keren *et al.*, 2004; Vazquez-Laslop *et al.*, 2006), quorum sensing and biofilm formation (Kim *et al.*, 2009; Wang *et al.*, 2011), protection from phage infection (Hazan and Engelberg-Kulka, 2004), protection against loss of DNA (Szekeres *et al.*, 2007; Wozniak and Waldor, 2009), programmed cell death (Aizenman *et al.*, 1996) and even anti-addiction modules (Saavedra De *et al.*, 2008).

Generally, type II TAs constitute a single genetic unit where the toxin gene is positioned downstream of the antitoxin gene (Gerdes *et al.*, 2005). In the majority of TAs the antitoxin TGA stop-codon overlaps with ATG start-codon of the toxin gene in an ATGA sequence (-2bp overlap), however TGATG sequence (-1bp) is also frequent. These gene overlaps reflect translational coupling, which has been shown for the *parD/pem* TA-locus of plasmid R1/R100 (Ruiz-Echevarria *et al.*, 1995).

However, for some families of type II TAs including *higBA*, *hicAB* and *mqsRA* the antitoxin gene is positioned downstream of the toxin gene (Pandey and Gerdes, 2005; Jorgensen *et al.*, 2009; Brown *et al.*, 2009). In these cases antitoxin and toxin levels are balanced by rare start codons or an additional promoter.

The antitoxin gene encodes a proteic antitoxin (~70-150 amino acids), which generally contains an N-terminal DNA binding domain that binds in the TA promoter region and represses TA operon transcription. Antitoxins generally bind toxins (~90-440 amino acids) by high affinity interactions between the antitoxin C-terminus and the toxin. The TA complex formation usually enhances the affinity of the antitoxin for promoter DNA. Generally antitoxins, as opposed to toxins, are unstructured proteins, which render them metabolically unstable and prone to proteolysis by cellular proteases (summarised in Figure 1B).

The following chapter, Chapter 1, will be an overview of Type II TA families, phylogeny and distribution. Chapter 2 will describe the structures of Type II toxins and their molecular targets. Chapter 3 will focus on mechanisms of toxin inactivation and how Type II TAs are regulated. The final chapter, Chapter 4, will concern the different aspects of Type II TAs function and proposed biological roles.

Chapter 1: Families

Toxin-antitoxin loci: Families, distribution and phylogeny

By the development of shotgun sequencing methods, the first bacterial genome was sequenced in 1995 (Fleischmann *et al.*, 1995). This led to an explosion in the number of sequenced genomes over the last 15 years and now more than 1600 genomes are available on National Centre for Biotechnology Information genome homepage (<http://www.ncbi.nlm.nih.gov/genome>). Bioinformatic analysis on vast sequence data sets allows new connections and predictions to be made regarding the biology of bacteria and archaea. Bioinformatics in particular has been central for the understanding of type II TAs and the distribution and phylogeny of chromosomal Type II TAs. Even predictions of new TA families have been made possible.

Type II toxin-antitoxin systems were first discovered as efficient PSK systems, which can stabilise mobile genetic elements such as *ccd* locus of *Escherichia coli* F-plasmid (Ogura and Hiraga, 1983). Several distinct families of plasmid encoded Type II TAs have since been identified: *parD/pem* of R1/R100 (Bravo *et al.*, 1987), *vapBC* of *Salmonella* Dublin virulence plasmid (Pullinger and Lax, 1992), *parDE* of RK2 (Roberts and Helinski, 1992), *phd-doc* of bacteriophage P1 (Lehnherr *et al.*, 1993), *higBA* of Rts1 (Tian *et al.*, 1996) and *relBE* of P307 (Gronlund and Gerdes, 1999).

For *parD* TA locus of plasmid R1, *kis-kid* (killing suppressor and determinant), chromosomal homologues *chpA* and *chpB* (chromosomal homolog of *pem*) were soon after identified in *Escherichia coli* (Masuda *et al.*, 1993). At present, *chpA* is generally referred to as *mazEF* (Aizenman *et al.*, 1996). It is now known that *chpA* toxin, ChpAK, more commonly referred to as MazF, does not actually kill the cells and MazF-inhibited cells can easily be resuscitated by subsequent *chpAI/MazE* production (Pedersen *et al.*, 2002). Similar early observations were made for *relBE* of plasmid P307, which was found to have chromosomal homologues not only in bacteria but also in archaea (Gotfredsen and Gerdes, 1998; Gronlund and Gerdes, 1999). Observations like these have questioned whether plasmid-resident Type II TAs in fact kill plasmid-free cells or, rather, restrict growth when TA resident plasmids are lost. Identification of a striking abundance of TAs on the chromosomes of prokaryotes led to the idea that TAs might have other biological roles than stabilising DNA (Gerdes, 2000; Anantharaman and Aravind, 2003; Pandey and Gerdes, 2005).

Table 1 Summary of prokaryotic Type II TA loci in 964 prokaryotic genomes¹

TA family	Antitoxin	DNA – binding domain ^{1,2}	Protease	Toxin	Activity	Number of loci ¹	Phylogenetic distribution ²
CcdAB	CcdA	RHH	Lon	CcdB	Inhibition of DNA gyrase	8	Gram ⁻
MazEF	MazE	Xre/HTH, RHH, XF1863/RHH & AbrB	ClpAP/Lon	MazF	mRNA cleavage	126	Gram ⁻ & Gram ⁺
RelBE	RelB	Xre/HTH, RHH, COG1753/RHH, AbrB & Phd	Lon	RelE	Ribosome dependent mRNA cleavage	889	Gram ⁻ , Gram ⁺ & Archaea
ParDE	ParD	RHH & Phd	ND	ParE	Inhibition of DNA gyrase	50	Gram ⁻
HigBA	HigA	COG5606/HTH & RHH	Lon	HigB	Ribosome dependent mRNA cleavage	54	Gram ⁻ & Gram ⁺
Phd-Doc	PhD	RHH, Phd YhfG	ClpXP	Doc (fic)	Associating with 30S ribosomal subunit	92	Gram ⁻ & Gram ⁺
VapBC	VapB	Xre/HTH, COG2442/HTH, COG2886/HTH, MerR/HTH RHH, COG2880/AbrB, AbrB & Phd	ND	VapC (PIN)	Ribonuclease	1316	Gram ⁻ , Gram ⁺ & Archaea
HipBA	HipB	Xre/HTH	Lon	HipA	Phosphorylation of translation factor EF-Tu	258	Gram ⁻ , Gram ⁺ & Archaea
HicAB	HicB	HicB	Lon	HicA	mRNA cleavage	247	Gram ⁻ , Gram ⁺ & Archaea
ω - ϵ - ζ	ω	RHH	N/A	ζ	Phosphorylation of peptidoglycan precursor	16	Gram ⁺

The table excludes 117 and 615 loci which could only be assigned to specific superfamilies of MazF/CcdB and RelE/ParE, respectively. ¹(Makarova *et al.*, 2009) ²(Shao *et al.*, 2011).

To date, at least ten type II TA-families from plasmids and chromosomes have been identified, which have been divided according to sequence similarity of the toxin (summarised in Table 1). Most prokaryotic TAs encode toxins which inhibit translation, these are: MazF, RelE, HigB, Doc, VapC, HipA and HicA. Only a few toxins inhibit replication, ParE and CcdB, and one peptidoglycan synthesis, ζ (Toxin targets will be discussed in detail in Chapter 2).

An early bioinformatic study revealed by high resolution sequence alignments that in fact ParE and RelE belong to a super family of toxin proteins, the ParE/RelE super family, which share conserved residues forming the core of secondary structural elements (Anantharaman and Aravind, 2003). The HigB toxin family is also part of the ParE and RelE super family, yielding a larger RelE/ParE/HigB superfamily of toxins, as HigB shares low but significant sequence similarities with RelE and is a ribosome dependent mRNA interferase (Anantharaman and Aravind, 2003; Pandey and Gerdes, 2005). HigBA is, however, easily distinguished from RelBE or ParDE as the antitoxin is positioned downstream of the toxin. Similar observations have been made for CcdB and MazF which share a SH3 barrel structural fold and therefore also constitutes a superfamily, the CcdB/MazF super family (Loris *et al.*, 1999; Kamada *et al.*, 2003; Buts *et al.*, 2005). These observations are intriguing as it seems that RelE and ParE or MazF and CcdB have evolved from the same ancestral proteins to target both replication and translation. Furthermore, that proteins from two different structural superfamilies such CcdB and ParE have evolved independently to acquire the same cellular target. The other toxin families have evolved independently and constitute their own structural super families including: Doc, VapC, HipA, HicA and ζ .

Antitoxins can be classified by their N-terminal DNA domain, but are far less conserved compared to toxins. The common classes of DNA-binding domains employed by antitoxins are; Helix-Turn-Helix (HTH), Ribbon-Helix-Helix (RHH), AbrB and Phd. Interestingly, DNA-binding domains are not restricted to a specific TA family and often antitoxins within the same TA family utilises different classes of DNA-binding domains (Anantharaman and Aravind, 2003; Pandey and Gerdes, 2005; Makarova *et al.*, 2009; Leplae *et al.*, 2011) (see Table 1).

These observations all suggest that TAs undergo rapid evolution and prone to gene shuffling events. It has become increasingly clear that TAs belong to a prokaryotic 'mobileome' which refer to genes that rapidly spread via horizontal gene transfer (HGT) (Makarova *et al.*, 2009; Leplae *et al.*, 2011). The mobilome also includes prophages, restriction modification systems (RMs) and clustered regularly interspaced short palindromic repeats (CRISPR) with CRISPR associated systems (CRISPR-Cas), which are thought to be anti-phage immunity systems (Barrangou *et al.*, 2007). The mobilome has recently been reviewed (Koonin and Wolf, 2008).

From Table 1 it is observed that translational inhibitors (including the mRNA interferases) have far the greatest representation ~98%, whereas *vapBC* is the most represented TA loci family ~ 43%. While *mazEF*, *higBA*, *cddAB*, *parDE*, *phd-doc* and ω - ϵ - ζ TA loci are more or less restricted to bacteria, *hicAB*, *relBE*- and *vapBC*-homologues are widely distributed in both bacteria and archaea.

There is a distinct phyletic pattern of TA loci distribution: bacteria that have drastically reduced genomes such as obligate host-associated parasites or symbiotes only retain a few loci (Pandey and Gerdes, 2005;Makarova *et al.*, 2009;Leplae *et al.*, 2011). There are, however, exceptions which include intracellular pathogens of the *Rickettsia* family, but this group only recently evolved and the genomes are still undergoing reductive evolution (Ogata *et al.*, 2001). This observation led Gerdes and co-workers to suggest that TA loci might be specifically beneficial to free-living prokaryotes (Pandey and Gerdes, 2005;Gerdes *et al.*, 2005;Sevin and Barloy-Hubler, 2007).

However, there is also a relationship between the genome size and number of TAs and the lack of TAs in organisms with small genomes could also be a consequence of TA abundance scaling with genome size (Makarova *et al.*, 2009;Leplae *et al.*, 2011). Nevertheless, there is enrichment for TAs in organisms belonging to the phyla of *proteobacteria*, *cyanobacteria*, *green sulphur bacteria* and *actinobacteria* often characterized by high phenotypic plasticity. These include proteobacteria such as *Nitrosomonas europaea* (~59 TAs) which has a very versatile metabolism and *Photobacterium luminescens* (~66 TAs), with a versatile life cycle (Leplae *et al.*, 2011). Both organisms have high numbers of insertion sequences in their genomes.

Another example is the human pathogen *Mycobacterium tuberculosis* which contains up to 88 TA loci (Ramage *et al.*, 2009)(Figure 2C). In stark contrast obligate intracellular *Mycobacterium leprae* contains only one predicted TA and several pseudo TAs (non-functional TAs) (Pandey and Gerdes, 2005;Leplae *et al.*, 2011). *M. leprae* has evolved from *M. tuberculosis* by massive reductive evolution and the presence of several pseudo genes indicates it is still undergoing decay (Cole *et al.*, 2001). *M. tuberculosis* has a persistent growth state, which is highly tolerant to antibiotics and has an extracellular and intracellular growth phase (Stewart *et al.*, 2003). This observation also supports a theory that TAs might be beneficial to *M. tuberculosis* as it needs to be more versatile to confront more varied environments than *M. leprae*. Organisms with high phenotypic plasticity seem to share common

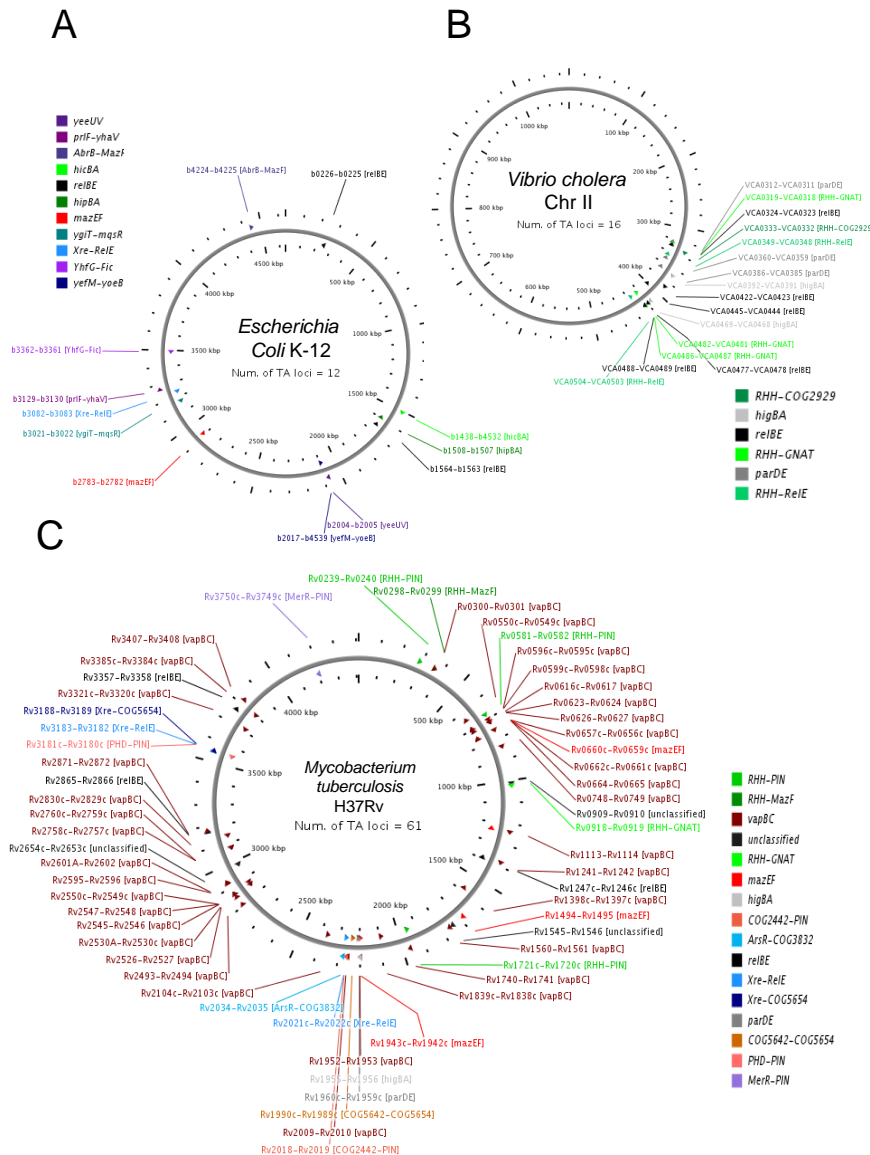


Figure 2 Predicted and verified TA loci on selected bacterial chromosomes. **A)** *Escherichia coli* K-12 (4.6 Mb) with 12 TAs. This prediction does not include recently described *yafNO* (which is homologues to RelBE TA-family (Christensen-Dalsgaard *et al.*, 2010) **B)** *Vibrio cholerae* Chr II (1.1Mb) with 16 TAs **C)** *Mycobacterium tuberculosis* H37Rv (4.4Mb) with 61 TAs. The TAs are either classified by TA-family or DNA-binding domain and toxin family. New putative TA families include; YhfG–Fic; which is a predicted Fic (Doc-like) toxin with a new YhfG antitoxin family. RHH-COG2929; RHH containing antitoxin with COG2929 toxin (distant RelE homologue). RHH-GNAT; RHH containing antitoxin with GNAT toxin (Predicted N-acetyltransferase). COG2442-PIN; COG2442 (Predicted helical RNA/DNA binding protein) antitoxin and PIN domain toxin (VapC). ArsR-COG3832; AsrR antitoxin (Predicted HTH binding domain) and COG3832 toxin (homologues to eukaryotic stress proteins). Xre-COG5654 and COG5642-COG5654; Xre and COG5652 antitoxins (HTH DNA binding domains) with predicted COG5654 toxin (conserved protein of unknown function). Adapted from (Makarova *et al.*, 2009;Shao *et al.*, 2011).

traits as many are characterised by very low growth rates and therefore TAs might contribute to or be beneficial during slow growth (Pandey and Gerdes, 2005).

Model organism *Escherichia coli* K-12 is known to have at least ten TA-systems, seemingly scattered throughout its genome, and are primarily of the type which

inhibit translation by mRNA cleavage (Figure 2A). However, TAs are not in all cases randomly scattered as there are chromosomal gene contexts which have higher TA frequency than others. These contexts can be highly diverse even between closely related species (Pandey and Gerdes, 2005;Makarova *et al.*, 2009).

An example is the *mazEF* locus of *Escherichia coli* K-12, *E. coli* O157 and *E. coli* EDL933 (Pandey and Gerdes, 2005). In these strains *mazEF* is positioned just downstream of the *relA* gene. Interestingly, in closely related species such as *E. coli* CFT073 and *Shigella flexneri* 2A a TA locus in this position is completely absent. What is more striking is that in related species as *Salmonella* Typhimurium LT2, *S. typhi* and *S. typhi* 2A, *mazEF* in this position is substituted for a *parDE* TA locus (Pandey and Gerdes, 2005). Variability in TAs between closely related organisms was recently analysed using 41 genome sets of closely related prokaryotic organisms which drew the same conclusion, as variability was strikingly high (Makarova *et al.*, 2009).

It is therefore conceivable that specific places on the chromosome such as the position downstream of the *relA* gene are “hot spots” for TA integration. Another extreme example of preferential localization patterns has been observed for *Vibrio cholerae* where all TAs, including those predicted and verified experimentally, reside inside a mega integron on chromosome II in close proximity of *attC* recombination sites (Pandey and Gerdes, 2005;Makarova *et al.*, 2009) (Figure 2B). Highly clustered TAs are also found in *Mycobacterium tuberculosis* and *Nitrosomonas europaea* as the majority of TAs seem to reside inside “TA Islands” on the chromosome (Pandey and Gerdes, 2005;Makarova *et al.*, 2009) (Figure 2C).

With increasing numbers of available sequenced genomes, comparative genomics approaches have been widely used to identify new TA families. The *hicAB* locus was discovered in a pilus gene cluster of *Haemophilus influenzae* also called *hif* cluster (*H. Influenzae* fimbriae). Bioinformatic approaches such as comparative genomics predicted *hicAB* to be a new TA family. This was recently verified experimentally (Makarova *et al.*, 2006;Jorgensen *et al.*, 2009). Numerous TAs have been identified by searching the genetic context of a putative toxin for antitoxin-like or predicted DNA-binding proteins (Makarova *et al.*, 2009;Leplae *et al.*, 2011). These putative TAs are often restricted to certain phyla or plasmids which complicates their identification.

Several three-component type II TAs have also been described, which are variations on the two component systems. Some of these have been described including: ω - ϵ - ζ of broad-range plasmid pSM19035 of *Bacillus subtilis*, *pasABC* of pTF-CF2 from *Thiobacillus ferrooxidans* and *paaR-paaA-parE* of *Escherichia coli* O157:H7 (de la Hoz *et al.*, 2000; Smith and Rawlings, 1997; Hallez *et al.*, 2010). These types of TAs are commonly found on plasmids and often the antitoxic and DNA-binding activities are encoded by two separate proteins rather than one.

Bioinformatic approaches have also revealed the presence of solitary toxins in prokaryotic genomes, which might have evolved alternative functions. A studied example is the solitary *mazF* toxin of *Myxococcus xanthus*, which has been shown to induce programmed cell death as a part of a complex multicellular developmental program (Nariya and Inouye, 2008). In about 5% of identified VapC toxins the reading frame was found to be without any antitoxin partner, but in these cases the VapC toxin was found to fused with a TRAM domain (RNA binding), KH domains (RNA binding) and AAA+ ATPase domains, which suggests that the toxin has adapted alternative functions (Anantharaman and Aravind, 2003).

The following chapter, Chapter 2, will outline the structural aspects and the molecular target of the toxin of type II TAs and related cytotoxins.

Chapter 2: Toxins

Structure and activity of Toxins

In recent years the numbers of identified TA and TA-like systems have expanded rapidly and this chapter will focus on the structure and activity of different characterised toxin families. *Escherichia coli* K-12 is the major bacterial model organism and consequently its TAs have been studied in greatest detail including; *dinj-yafQ* (*relBE* TA-family), *yafNO* (*relBE* TA-family), *hicAB* (renamed from *yncN-ydcQ*), *hipBA*, *relBE*, *yeeUV* (new putative TA-family), *yefM-yoeB* (*relBE* TA-family), *mazEF* (renamed from *chpA*), *mqsR-mqsA* (renamed from *ygiU-ygiT*), *higBA* (renamed from *ygjN-ygjM*), *prlF-yhaV* (*relBE* TA-family), *chpB* (*chpS-chpB/mazEF* TA-family) (Figure 2A).

To date the majority of identified toxin targets have been shown to target the translational machinery, which is also the case for TAs of *E. coli* K-12. The majority of all toxins inhibit translation by ribonuclease activity which in most cases is dependent on the ribosome. A few other described toxin families have evolved different targets inside the translation machinery or in distinct cellular processes outside the translation machinery. Toxin expression in general results in bacteriostatic growth inhibition from which the cells can be resuscitated by subsequent expression of antitoxin. The following section separates the toxin from the antitoxin counterparts to define the structural features and cellular activity of toxins.

Toxin targets outside the translation machinery – CcdB, ParE, Zeta and YeeV

Inhibitors of DNA gyrase – CcdB and ParE

Both CcdB and ParE target the DNA gyrase, which is an essential type II topoisomerase in *E. coli* (Bernard *et al.*, 1993; Jiang *et al.*, 2002).

The structure of CcdB revealed a N-terminal five-stranded β sheet, a 13 residue C-terminal α -helix, and central three small stranded β -sheet containing a loop (Figure 3A left) (Loris *et al.*, 1999). CcdB forms a dimer and the structure resembles that of MazF despite the fact that they only share low sequence similarity (Figure 3A right). Enigmatically, MazF is an mRNA interferase, whereas CcdB does not cleave RNA and, accordingly, residues involved in RNA hydrolysis are not present (Buts *et al.*,

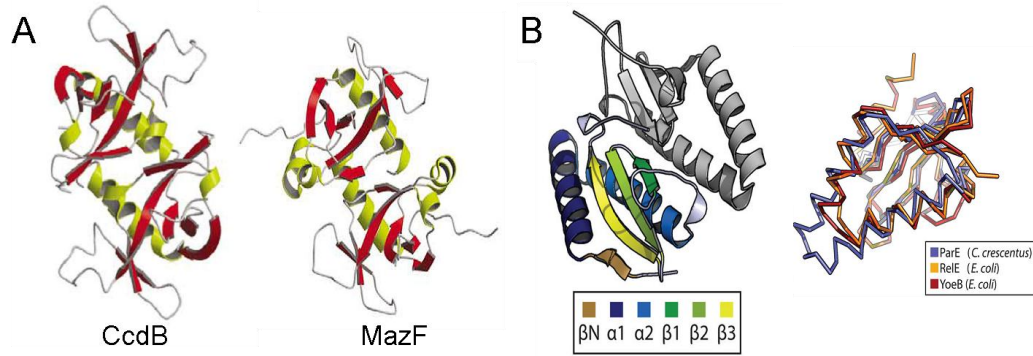


Figure 3 Structures of CcdB and ParE. **A**) Left the Structure of CcdB dimer and right *E. coli* MazF dimer structure. α -Helices (yellow) and β -sheets (Red) **B**) Left the structure of ParE dimer from *C. crescentus* with structural features coloured in one monomer and right ParE superimposed on *E. coli* RelE and YoeB. Adapted from (Dao-Thi *et al.*, 2005;Buts *et al.*, 2005;Dalton and Crosson, 2010).

2005). The crystal structure of ParE from *Caulobacter crescentus* has recently been solved (Dalton and Crosson, 2010). The structure revealed a ParE dimer of monomers with two N-terminal α -helices connected by a single tryptophan W26 forming an antiparallel hairpin structure which packs against a three stranded β -sheet (Figure 3B left). Intriguingly, ParE structure resembles that of RelE and YoeB from *Escherichia coli*, which like MazF are mRNA interferases (Figure 3B right). These observations suggest a similar evolutionary origin (Buts *et al.*, 2005).

Instead of cleaving RNA, CcdB and ParE are DNA gyrase inhibitors which have evolved from two distinct structural superfamilies. DNA gyrase is a topoisomerase that induces negative supercoiling as well as resolves interlinked plasmids, making it essential in replication, transcription, DNA repair and recombination (Bernard and Couturier, 1992;Nollmann *et al.*, 2007). The gyrase consists of two subunits, GyrA containing a catalytic domain and GyrB containing ATP-binding domain, which in concert facilitate double-stranded DNA break as well as rejoining activity. The crystal structure of CcdB bound to its target has been solved (Dao-Thi *et al.*, 2004;Dao-Thi *et al.*, 2005). CcdB binds to a fragment of GyrA by three C-terminal residues W99, G100 and I101, causing two distinct effects whether the DNA gyrase is associated with DNA or not. If GyrA is in its free state or bound to GyrB in the absence of DNA, CcdB forms GyrA-CcdB or GyrA-GyrB-CcdB complexes which are inactive. When DNA gyrase is in its catalytically active state with DNA, CcdB blocks the closing of GyrA subunits which creates DNA roadblocks that inhibit replication and transcription. The W99 residue in CcdB dimer interacts with Arg462 in GyrA dimer,

and CcdB resistant DNA gyrases are obtained by a Arg462Cys substitution (Dao-Thi *et al.*, 2005).

ParE also inhibits DNA gyrase, which prevents initiation of replication at *oriC* (Jiang *et al.*, 2002). However, ParE seems to act by a distinct mechanism as ParE from *Vibrio cholera* has been shown to bind GyrA but not GyrA fragments as observed for CcdB. Furthermore, a strain containing a GyrA Arg462Cys substitution mutation is still sensitive to ParE (Yuan *et al.*, 2010). Nevertheless, CcdB and ParE both result in DNA strand breaks as DNA is not resolved by DNA gyrase and both efficiently inhibit replication and cell division (Couturier *et al.*, 1998)

Targeting peptidoglycan synthesis and cell division – Zeta and YeeV

Zeta is the toxin of three component TA system ϵ - ω - ζ which has been described from plasmid pSM19035 and *pezAT* (pneumococcal ω ζ) from the chromosome of *Streptococcus pneumoniae* (Zielenkiewicz and Ceglowski, 2005; Khoo *et al.*, 2007). Crystal structures of Zeta and PezT revealed monomeric proteins folding into α/β structures similar to that of phosphotransferases with a ATP/GTP-binding pocket (Meinhart *et al.*, 2003; Khoo *et al.*, 2007). More recently it has been shown that PezT inhibits cell wall synthesis by phosphorylating peptidoglycan precursor diphosphate-N-acetylglucosamine (UNAG) using ATP (Mutschler *et al.*, 2011).

YeeV is the toxin component of a new putative TA system *yeeUV* present on the chromosome of *E. coli* K-12 (Brown and Shaw, 2003). It has recently been shown that YeeV might constitute a new toxin family, different from CcdB and ParE, which inhibits cell division (Tan *et al.*, 2011). YeeV was found not only to inhibit the GTPase activity and GTP-dependent polymerisation of FtsZ, an essential tubulin-like cell division protein, but also the ATP-dependent polymerisation of MreB, an actin-like protein involved in cell division and determination of cell shape.

Toxin targets inside the translation machinery

The ribosome and translation

The main actor of the translation machinery is the ribosome. In bacteria, translation involves formation of a 70S ribosomal initiation complex of 50S and 30S ribosomal subunits with the aid of mRNA, fMet-tRNA^{fMet} and initiation factors (IF1, IF2 and IF3) (Figure 4A). Selection of translation initiation site is often governed by the interaction of a unique mRNA leader sequence, referred to as the Shine & Dalgarno

sequence, with the anti-Shine & Dalgarno sequence of 16S rRNA. However, this mechanism is not exclusive as other structural features of the mRNA also increase specificity and leaderless translation initiation has also been found to occur (Laursen *et al.*, 2005; Nakamoto, 2009). Initiator fMet-tRNA^{fMet} contains universally conserved structural features as the G-C stem of the anticodon stemloop, which increases its selection in 30S ribosomal subunit P-site. This selection is increased in the presence of initiation factors (Hartz *et al.*, 1989; Antoun *et al.*, 2006). It has recently been shown that multiple copies of tRNA^{fMet} genes in *E. coli* ensure high cellular levels of tRNA^{fMet}, which might also be crucial for the fidelity in P-site selection (Kapoor *et al.*, 2011). After the formation of 70S translation initiation complexes, cycles of translation elongation can occur. Cognate aminoacyl charged tRNA bound to Elongation factor-Tu (EF-Tu) with GTP enters in the ribosomal A-site and peptidyl transfer occurs (Figure 4B). Peptidyl transfer is followed by translocation stimulated by elongation factor G (EF-G) and GTP, which moves the ribosome forward and uncharged P-site tRNA is moved to E-site and A-site tRNA with peptide chain to the P-site, this leaves the A-site vacant on the next codon for subsequent rounds of translation elongation (Shoji *et al.*, 2009). Translation is terminated when ribosomal A-site reaches a stop codon (UAG, UAA or UGA), which is recognised by peptide chain release factor 1 or 2 (RF1 or RF2) (Loh and Song, 2010). Release factors trigger the hydrolysis of the tRNA peptide ester bond and release of the peptide (Figure 4B). Subsequently, the GTPase activity of Release factor 3 (RF3) catalyses release of RF1 and RF2. Post termination complexes are recycled by combined action of Ribosome recycling factor RRF and EF-G, mRNA and deacylated tRNA is finally removed by IF3, which also has anti-association activity preventing 30S and 50S re-assembly (Seshadri and Varshney, 2006; Petry *et al.*, 2008).

The *E. coli* ribosome incorporates amino acids into a peptide chain with elongation rates ranging from 10-18 amino acids/sec depending on the doubling rate of the cell (Dennis and Bremer, 1974). To avoid mistranslation, the ribosome has adapted mechanisms which increase translation fidelity..

Key steps in translation quality control involves correct selection during aminoacyl-tRNA synthesis (recognition of correct amino acid and tRNA by aminoacyl-tRNA synthases), EF-Tu binding, aminoacyl-tRNA selection in the ribosomal A-site and post peptide bond formation selection in ribosomal P-site (Reynolds *et al.*, 2010).

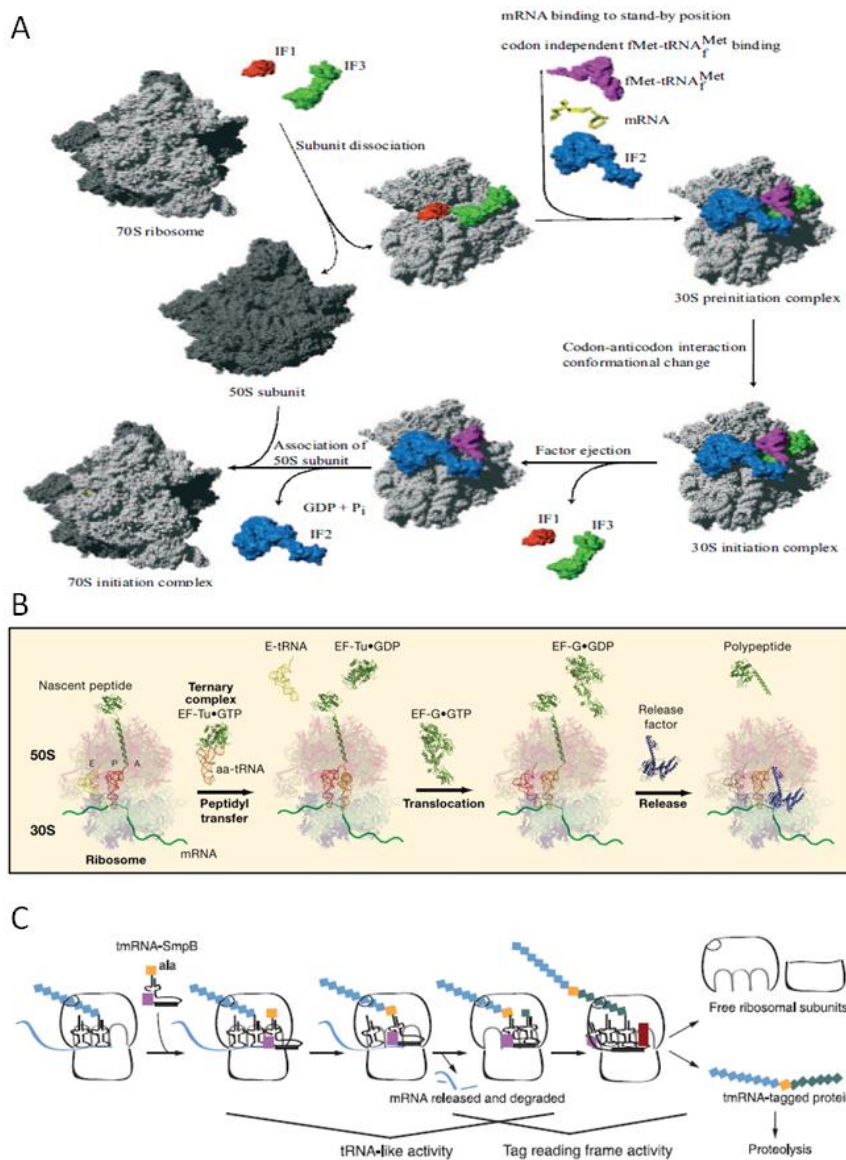


Figure 4 Overview of translation **A)** Translation initiation. IF1 (red) and IF3 (green) associates with 30S and keeps 50S and 30S dissociated. fMet-tRNA_f^{Met} (purple) with IF2 (blue) and GTP associates with mRNA (yellow) and 30S ribosomal subunit in an 30S preinitiation complex. Anticodon interaction leads to conformational changes and ejection of IF1 and IF3. 50S ribosomal subunit associates with 30S initiation complex by IF2-GTP hydrolysis and ejection of IF2-GDP + Pi. **B)** Translation elongation and termination. Ternary complex of EF-Tu-GTP bound aminoacyl-tRNA binds in vacant ribosomal A-site. Peptidyl transfer of aminoacyl group of tRNA in P-site to aminoacyl-tRNA in ribosomal A-site occurs and translation factor ejection is mediated by hydrolysis of GTP. The ribosome moves one codon by hydrolysis of EF-G-GTP which positions P-site deacylated tRNA in the E-site and A-site tRNA with peptide in the P-site. Translation is terminated when A-site reaches a stop codon and peptide released by the action of release factors. **C)** The trans-translation mechanism. Alanine acylated tmRNA (Alanyl group, orange square) bound to SmpB (purple square) and EF-Tu-GTP (not shown) enters the ribosomal A-Site of a ribosome stalled on a mRNA 3'-end. tmRNA accepts the peptide chain from P-site tRNA by peptidyl transfer and translation resumes on tmRNA reading frame which encodes proteolytic tag. The mRNA (blue) is released and degraded by cellular RNases. Translation terminates normally on the protease tag reading frame stop codon by Release factor (Red rectangle) mediated peptide release. The tmRNA tagged peptides (green squares) are now targeted for proteolysis by cellular proteases. Adapted from (Laursen *et al.*, 2005; Zaher and Green, 2009; Keiler and Ramadoss, 2011).

These quality control mechanisms result in low incorporation error rates with an average of 3.4×10^{-4} per codon, which can vary slightly depending on the tRNA abundance of a specific codon (Kramer and Farabaugh, 2007).

Trans-translation

If the mRNA is damaged or if ribosomes are deprived from terminating, ribosomes will normally stall (Sunohara *et al.*, 2004; Li *et al.*, 2007). Ribosome stalling is also induced by depletion of aminoacyl-tRNA either by amino acid starvation or by consecutive rare codons (decoded by low abundance aminoacyl-tRNA) in an mRNA (Li *et al.*, 2008b; Garza-Sanchez *et al.*, 2008). Ribosome stalling has been observed to induce mRNA cleavage in the ribosomal A-site (Hayes and Sauer, 2003; Garza-Sanchez *et al.*, 2009). This is induced either by an unknown endoribonuclease and/or by the action of 3'-5' exoribonuclease RNase II by degradation of mRNA which is not protected by ribosomes (The possible role of mRNA cleaving toxins in A-site cleavage will be discussed).

This results in a non-stop mRNA (mRNA without a stopcodon) containing a stalled ribosome on mRNA 3'-end and trailing ribosomes, which are deprived of an opportunity of terminating translation normally. The ribosome can be released and recycled by a process referred to as *trans*-translation, which simultaneously facilitates the degradation of damaged truncated mRNA and translated peptide (figure 4C and recently reviewed (Keiler and Ramadoss, 2011)). The central player in *trans*-translation is tmRNA which only functions in concert with protein SmpB and EF-Tu-GTP. The tmRNA is unique as it contains a 5'- and 3'-end tRNA-like domain resembling a tRNA with an amino acyl acceptor stem a T-arm and a D-loop, as well as a short 10 codon mRNA reading frame (Komine *et al.*, 1994; Tu *et al.*, 1995). Alanyl tRNA-synthase (alaRS) is required as tRNA-like domain of tmRNA has to be charged with an alanyl group before it is recognized by EF-Tu-GTP (Barends *et al.*, 2001). SmpB is a crucial partner as it not only mimics tRNA anti-codon in the ribosome but also facilitates the interaction of tmRNA with alaRS, thus, the resumption of translation on tmRNA reading frame (Karzai *et al.*, 1999; Hanawa-Suetsugu *et al.*, 2002). *Trans*-translation is independent of normal translation initiation and tmRNA contains a GCA codon (resume codon) on which translation resumes (Williams *et al.*, 1999). Resuming of translation on tmRNA reading frame leads to release of non-stop mRNA, which is degraded primarily by the activity of

RNase R, and tagging of truncated peptide for proteolysis by cellular proteases (Lies and Maurizi, 2008;Ge *et al.*, 2010). Resumption of translation allows ribosomes to terminate normally and to be recycled. The *trans*-translation mechanism seems to be important for translation quality control in *E. coli*, but might also be an integral part in gene regulation as it affects the timing of DNA replication in *Caulobacter crescentus* and affects virulence in *Salmonella enterica* and *Yersinia pestis* (Julio *et al.*, 2000;Keiler and Shapiro, 2003;Okan *et al.*, 2010). Recently, two additional proteins ArfA (YhgL) and YaeJ have been identified in *E. coli*, which can perform tmRNA independent peptide release and ribosome rescue (Chadani *et al.*, 2010;Chadani *et al.*, 2011). ArfA was shown to be synthetic lethal with tmRNA in *E. coli*, which indicates the importance of a functional ribosome rescue system.

The majority of Type II TA toxins have cellular targets inside the translation machinery and are all potent inhibitors of translation. These include; RelE, HigB, MazF, HicA, MqsR, Doc, HipA and VapC. The term mRNA interferases (mi) has been adopted by Inouye and co-workers to describe proteins which inhibit translation by mRNA cleavage, and is now generally used to describe: RelE, HigB, MazF, HicA and MqsR toxins.

Ribosome dependent mRNA Interferases – RelE and HigB

The *relBE* locus of the *E. coli* chromosome is one of the best described TA loci. The *relB* gene was first identified in a screen for relaxed (*rel*) mutants during amino acid starvation (Diderichsen *et al.*, 1977). On the onset of amino acid starvation, synthesis of ribosomal RNA stalls, which is a result of accumulation of RNA polymerase binding alarmone ppGpp, synthesized by RelA in response to a decrease in cellular level of charged tRNA (Potrykus and Cashel, 2008) (discussed in Chapter 4). Relaxed mutants continue rRNA transcription in response to amino acid starvation.

It was observed that a mutation in *relB* resulted in a “delayed relaxed response”, which was different from the relaxed phenotype, since rRNA synthesis was delayed for about 10 min upon onset of amino acid starvation (Diderichsen *et al.*, 1977;Bech *et al.*, 1985). It is now known that *relB* is the antitoxin component of TA locus *relBE*, and the “delayed relaxed” response is due to hyper-activation of the toxin RelE during amino acid starvation in a RelB¹⁰¹ mutant with a A39T substitution which renders RelB less stable (Gotfredsen and Gerdes, 1998;Christensen and Gerdes, 2004).

This phenomenon can be explained by rapid and efficient Lon protease dependent activation of RelE in a RelB¹⁰¹ mutant during amino acid starvation. RelE toxin inhibits global translation which reduces the turnover of charged tRNA pools in the cell and results in decreased ppGpp and continued rRNA synthesis, hence the term “delayed relaxed” (Christensen and Gerdes, 2004).

RelE-mediated inhibition of translation is caused by mRNA cleavage between the second and third base of an mRNA codon positioned in the ribosomal A-site (Christensen and Gerdes, 2003; Pedersen *et al.*, 2003). RelE acts catalytically with codon base preferences. Not only Stop codons UAG and UAA are cleaved efficiently *in vitro* with K_m/K_{cat} ($s^{-1}\mu M^{-1}$) values of 17 and 2.7, respectively but also sense codons CAG and UCG with K_m/K_{cat} 11 and 22, respectively (Pedersen *et al.*, 2003). This codon preference could also be confirmed *in vivo* (Christensen and Gerdes, 2003). Interestingly, RF1 (peptide chain release factor 1) can compete with RelE for UAG stop codon cleavage, which suggests competition in the ribosomal A-site and indeed, RelE does not cleave mRNA in the absence of the ribosome (Pedersen *et al.*, 2003).

E. coli RelE is an 11.2 kDa protein (95 amino acids) which consists of a compact, four-stranded antiparallel β sheet flanked by three α helices (Figure 10B) that is very similar to that of RelE from archaea *Pyrococcus horikoshii* OT3 (Figure 5A) and *Methanococcus jannaschii* (Takagi *et al.*, 2005; Francuski and Saenger, 2009; Neubauer *et al.*, 2009; Li *et al.*, 2009). The archaeal RelE homologues are both toxic in *E. coli* and RelE of *M. jannaschii* has also been shown to cleave inside the mRNA reading frame *in vivo*, which indicates conservation in the mechanism cleavage (Christensen and Gerdes, 2003; Shinohara *et al.*, 2010). *Mycobacterium tuberculosis* encodes three *relBE* homologues (Figure 2C) that are all functional TA systems and inhibit growth of *Mycobacterium smegmatis* (Korch *et al.*, 2009; Yang *et al.*, 2010). A RelE homologue from the gram-positive organism *Streptococcus pneumoniae* was also found to be active and to cleave mRNA in the reading frame (Christensen and Gerdes, 2003; Nieto *et al.*, 2006).

Recently, the crystal structures of *E. coli* RelE in complex with 70S ribosome of *Thermus thermophilus* containing mRNA in pre-cleavage (3.3Å) and post-cleavage state (3.6Å) were solved (Neubauer *et al.*, 2009). The structures confirmed that RelE occupies the ribosomal A- site (Figure 5B) and induces cleavage of mRNA after the second base by re-orienting and activating mRNA for 2'OH dependent hydrolysis

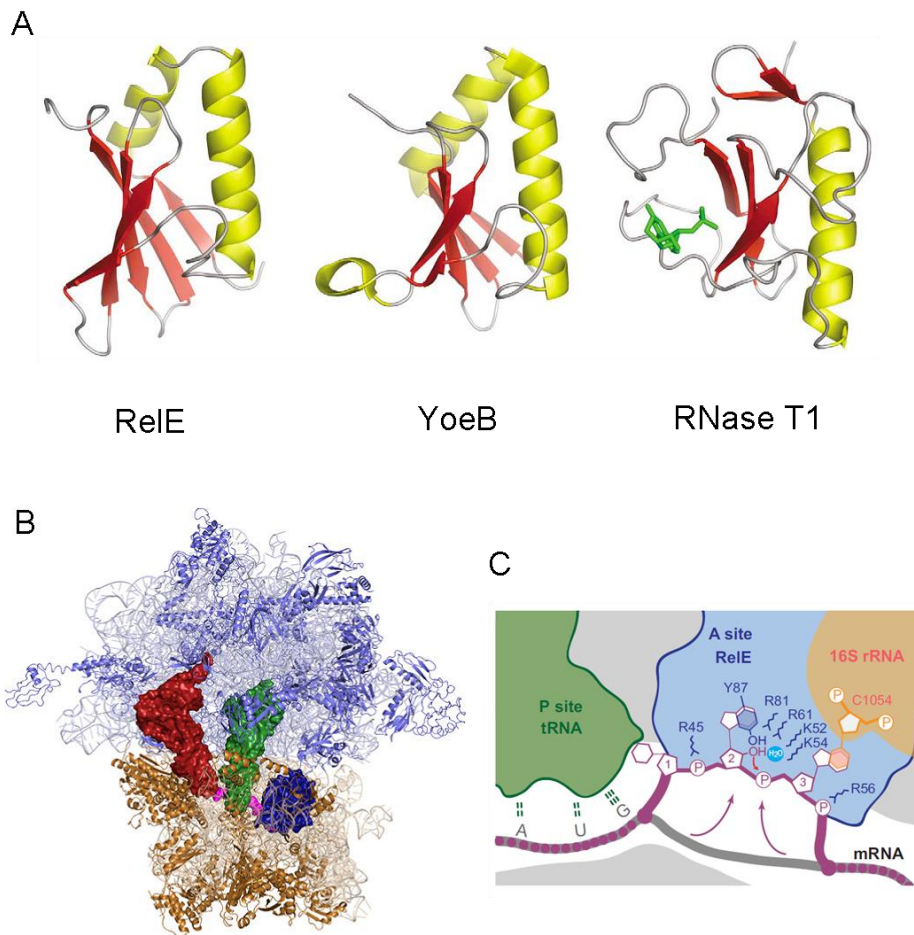


Figure 5 RelE structure and activity **A)** RelE (*P. horikoshii* OT3) and YoeB (*E. coli*) contains an α/β -fold which shares similarity to that of RNase T1 (*Aspergillus oryzae*). α -helices (yellow) and β -sheets (Red) 2'guanosine monophosphate is shown in green sticks in the activity site of RNase T1. **B)** *Thermophilus thermophilus* 70S ribosome (50S blue, 30S wheat) containing RelE (A site, blue), tRNA^{fMet} (P site, green), a noncognate tRNA^{fMet} (E site, red), and mRNA (magenta) in pre-cleavage state. **C)** Model for RelE activity. RelE (blue) occupies the A site where it pulls the mRNA (purple) into its active site (arrows). Here, the second nucleotide ("2") of the mRNA stacks with Y87 of RelE (blue), while the third nucleotide ("3") stacks with C1054 of 16S rRNA (orange). Additional relevant basic residues in the active site are shown including water molecule used in the catalysis. The red arrow indicates the nucleophilic attack of the 2'-O. Adapted from (Buts *et al.*, 2005; Neubauer *et al.*, 2009).

(Figure 5C). This mechanism also explains the strict requirement of the ribosome in mRNA cleavage and suggests preferences for a pyrimidine in the first codon base and purines in the second and third position (Neubauer *et al.*, 2009).

E. coli K-12 contains at least five other TAs of the *relBE* and *higBA* family: *yefM/yoeB*, *prlF-yhaV*, *dinJ-YafQ*, *yafNO* and *higBA*. The *E. coli* YoeB crystal structure revealed an α/β fold very similar to that of RelE (Figure 5A) (Kamada and Hanaoka, 2005). Interestingly, YoeB and RelE seem to share structural similarities to RNase T1, barnase and RNase Sa, and active site residues of RNase T1 are also

present in YoeB, which could explain non-specific RNase activity observed by YoeB *in vitro* (Figure 5A). YoeB associates with 70S ribosomes and 50S ribosomal subunits and cleave translated mRNA preferentially in the second codon of mRNA and in stop codons (Christensen-Dalsgaard and Gerdes, 2008; Zhang and Inouye, 2009).

YhaV and YafQ toxins have been shown to have RNase activity *in vitro*, whereas YafQ and YafO inhibit translation by mediating ribosome dependent mRNA cleavage *in vivo* (Schmidt *et al.*, 2007; Prysak *et al.*, 2009; Zhang *et al.*, 2009; Christensen-Dalsgaard *et al.*, 2010). HigBAs from the *Vibrio cholera* mega integron and from *E. coli* have recently been characterized and HigB was observed to inhibit translation by ribosome-dependent mRNA cleavage, but with a different cleavage pattern to RelE (Christensen-Dalsgaard and Gerdes, 2006; Budde *et al.*, 2007; Christensen-Dalsgaard *et al.*, 2010).

In conclusion, generally toxins of the *relBE* TA family cleave mRNA in the ribosomal A-site. Evidently, RelE mediated mRNA cleavage will lead to ribosome stalling on the 3'-end of a non-stop mRNA, which is the substrate for *trans*-translation. Indeed it has been observed that a tmRNA deficient mutant is hypersensitive to RelE and that over expression of tmRNA and *smpB* can counteract RelE toxicity (Christensen and Gerdes, 2003). Furthermore, tmRNA seems to be required for complete resuscitation of RelE inhibited cells and rapid recovery of translation by RelB expression. This suggests that tmRNA counteracts RelE toxicity by rescue of stalled ribosomes from damaged mRNAs. A similar observation has been made for mRNA interferases MazF and ChpBK (Christensen *et al.*, 2003). These observations suggest that that mRNA-cleaving toxins could be integral components of the same quality control management program as tmRNA (discussed in Chapter 4). Consistent with this interpretation both RelE and MazF have been reported to cleave mRNA during amino acid starvation, however their specific roles remain elusive (Christensen *et al.*, 2003)

Ribosome independent mRNA interferases – MazF, HicA, and MqsR

E. coli K-12 has two chromosomal *mazEF* TA loci, *mazEF* (*chpA*) and *chpB* (Masuda *et al.*, 1993). MazEF from *E. coli* chromosome and *Kis-Kid* of ParD from plasmid R1 are the most extensively described TAs of the *mazEF* TA family. The crystal structure of MazEF revealed that the toxin MazF, a ~12 kD protein (111 AA) forms dimers with an α/β -fold very similar to that of CcdB (Figure 3A) (Kamada *et al.*, 2003).

Conditional overexpression of MazF and ChpBK (toxin of *chpB*) inhibits cell growth, which can be reversed by cognate antitoxins MazE and ChpBI (Masuda *et al.*, 1993; Pedersen *et al.*, 2002). *In vitro* and *in vivo* studies have shown that MazF and ChpBK are ribosome-independent ribonucleases, which cleave primarily single stranded RNA at specific sequences that result in inhibition of translation. *E. coli* MazF exclusively cleaves ACA sequences, whereas ChpBK cleaves ACY sites (where Y is A, G or U). (Zhang *et al.*, 2003b; Zhang *et al.*, 2005). MazF is thought not to cleave rRNA and tRNA (Suzuki *et al.*, 2005).

Recently, it has been shown that a pentapeptide “quorum sensing” molecule produced under certain conditions, greatly increases the endoribonucleolytic activities of both MazF and ChpBK (Belitsky *et al.*, 2011) (discussed in Chapter 4).

Several MazF homologues have been characterised, including MazF_{sa} from *Staphylococcus aureus* and several MazF_{mt} from *Mycobacterium tuberculosis*. MazF_{sa} cleaves the pentad sequence U*ACAU (*indicates the cleavage site), which is highly abundant in several mRNAs including *sraP* mRNA encoding a protein known to be important for adhesion of the pathogen (Zhu *et al.*, 2009). Up to seven MazF homologues have been identified on the chromosome of *M. tuberculosis* and cause growth inhibition when expressed in *E. coli* (Zhu *et al.*, 2006). MazF_{mt-1} cleaves A*UC, MazF_{mt-3} cleaves UU*CCU/CU*CCU, MazF_{mt-6} cleaves U-rich regions (U/C)U*(A/U)C(U/C) and MazF_{mt-7} U*CGCU, all single stranded RNA substrates (Zhu *et al.*, 2006; Zhu *et al.*, 2008). The Kid toxin of ParD of plasmid R1 cleaves AU(A/C/U) in mRNA, but it has recently been shown that Kid cleaves more specifically in UUACU sequences which are rare but present in an RNA that represses plasmid R1 replication (Pimentel *et al.*, 2005). This suggests that Kid activation simultaneously may regulate growth rate and plasmid-copy number, which is a mechanism quite different from PSK. The fact that some MazF homologue toxins seem to have very specific RNA cleavage sites suggest that MazF might play a role in regulating specific mRNAs (discussed in Chapter 4).

The *hicAB* TA family has recently been discovered (Makarova *et al.*, 2006). *E. coli* HicA, a 6.8 kDa protein (58 AA), was predicted to contain a double stranded RNA binding fold and HicB, a 16.1 kDa protein (145 AA), a reduced RNase H fold fused to a HTH DNA-binding domain. A recent study showed that HicA is the toxin component as ectopic expression of HicA led to growth inhibition, which is

counteracted by HicB expression (Jorgensen *et al.*, 2009). HicA was found to inhibit global translation by mRNA cleavage, which is not dependent on the translation machinery, as non-translated mRNAs were cleaved efficiently. In a more recent study homologues of *hicAB* were identified in *Streptococcus pyogenes*, where both HicA and HigB were found to be toxic in *E. coli* cells, indicating an alternative function of this locus (Leplae *et al.*, 2011). Deletion of *hicB* antitoxin gene in *E. coli* does not affect growth; however cells are more sensitive to envelope stress (Button *et al.*, 2007). Interestingly $\Delta hicB$ cells show down-regulated extracytoplasmic stress response mediated by alternative sigma factor, σ^E , and curiously σ^E is no longer essential in this strain. This indicates that $\Delta hicB$ cells have low level constitutive activity of HicA, which acts on a subset of mRNAs involved in extracytoplasmic stress.

Similar to *hicAB*, *mqsR-mqsA* (motility quorum sensing R and A renamed from *ygiU-ygiT*) is a relatively recent discovery (Gonzalez Barrios *et al.*, 2006). The *mqsR* gene was found to be necessary for efficient biofilm formation, which will be discussed in Chapter 4. More recently it has been shown that MqsR is a ribosome-independent mRNA interferase, which inhibits translation by cleaving mRNA at GCU sequences *in vivo* and *in vitro* (Yamaguchi *et al.*, 2009; Christensen-Dalsgaard *et al.*, 2010). In both studies MqsA was found to counteract the activity of MqsR, which gives *mqsR-mqsA* a similar genetic setup as *hicAB* and *higBA*.

MqsR is a 11.2 kDa protein (98AA) that does not share any sequence homology with MazF, but has been shown to contain an α/β -fold structure similar to that of RelE (Brown *et al.*, 2009). Interestingly, the HTH DNA-binding domain of MqsA was found to reside in the C-terminal domain, whereas interactions with the toxin are found to occur through the N-terminus. This is the first example of a structural RelE homologue which cleaves mRNA ribosome-independently *in vivo*.

Even though ribosome-independent mRNA interferases are site specific, a recent study has shown that translation can drastically stimulate mRNA cleavage, probably by unfolding structured mRNA, thus making otherwise protected sites available to cleavage (Christensen-Dalsgaard and Gerdes, 2008).

Targeting the ribosome – Doc and HipA

The most common activity of toxins is to inhibit translation by ribonuclease activity which is often dependent on the translation machinery. However, a small group of toxins, including Doc and HipA toxins, have evolved distinct mechanisms.

Association with 30S ribosomal subunit – Doc

Bacteriophage P1 encodes the *phd-doc* TA locus (*preventing host death, death on curing*), which has now also been identified on many bacterial chromosomes. The *phd-doc* TA locus has been demonstrated to aid the maintenance of lysogenic P1 bacteriophage inside *E. coli* (Lehnherr *et al.*, 1993; Lehnherr and Yarmolinsky, 1995). Early studies on *phd-doc* showed that the molecular target of Doc toxin likely had to reside within the translation machinery as toxin activation inhibited global protein synthesis (Hazan *et al.*, 2001). The Doc toxin is highly toxic to *E. coli* cells and has now been shown to interact with 30S ribosomal subunits in 70S ribosomes, inhibiting elongation of translation, which results in polysome accumulation (Liu *et al.*, 2008). Interestingly, Doc toxin, though being significantly larger, seems to mimic the activity of aminoglycoside antibiotic hygromycin B, which binds to Helix 44 in 16S ribosomal RNA. This observation was further substantiated as a hygromycin B resistant mutation in ribosomes also conferred resistance to Doc toxicity (Liu *et al.*, 2008). A non-toxic Doc^{H66Y} mutant has recently been crystallized with the C-terminus of PhD, which revealed a small, strictly α -helical protein (Figure 6A) (Garcia-Pino *et al.*, 2008).

Doc shares structural similarities to bacterial Fic proteins (*filamentation induced by cAMP*) and AvrB, a secreted bacterial toxin, which suggests a similar evolutionary origin. Fic proteins have a central conserved HXFX(D/E)(A/G)N(K/G)R motif that is also present in Doc (Figure 6A) and are predicted to retain adenosine monophosphate transferase activity (Garcia-Pino *et al.*, 2008; Arbing *et al.*, 2010). However, whether there is a functional relationship remains elusive.

Phosphorylation of translation elongation factor EF-Tu – HipA

HipA was first identified in a screen for *E. coli* mutants showing increased tolerance to ampicillin; these mutants were persistent and therefore termed persisters (Moyed and Bertrand, 1983). An isolated HipA7 mutant showed high persistence (Hip)

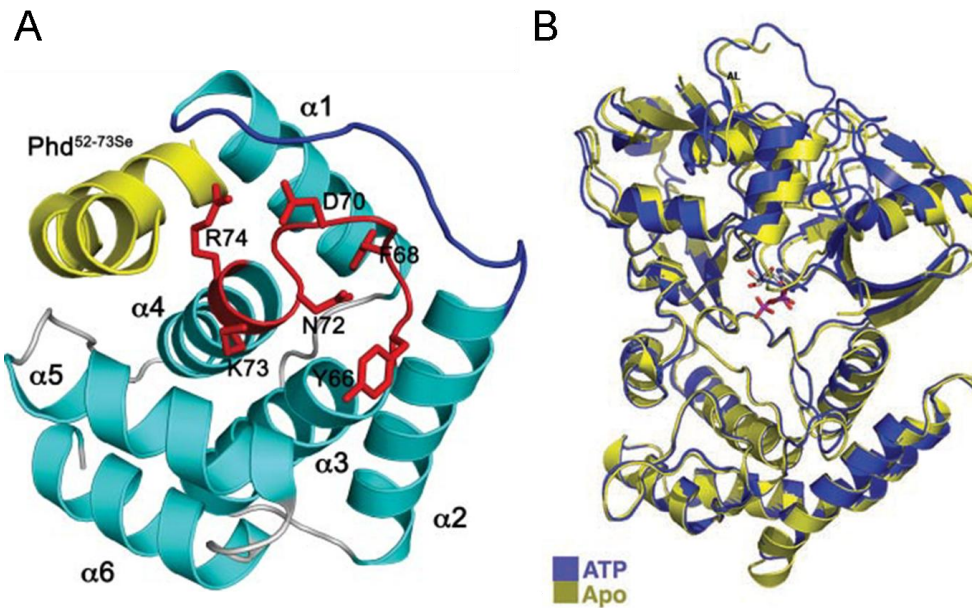


Figure 6 Structure of Doc and HipA **A)** Crystal structure of Doc^{H66Y} monomer (Teal) with Phd^{52-73Se} (Yellow). Doc is an α -helical bundle protein consisting of six α -helices, stacking in three consecutive helix-loop-helix elements. Central α 3 and α 4 have high hydrophobic residue content which facilitates stacking of α 1 and α 2 on one side and α 5 and α 6 on the other. Residues conserved in Fic proteins are shown in red. **B)** Crystal structure of HipA in ATP bound (blue) and unbound (yellow) state, position of ATP is shown in magenta. The N-terminal is a α/β -fold, whereas the C-terminal is all α -helical. ATP binding results in a small rotation (\sim 4%) in N-terminal and C-terminal domains. Adapted from (Garcia-Pino *et al.*, 2008;Schumacher *et al.*, 2009).

frequencies of 10^{-2} compared to wild type *E. coli* which only produces persisters in frequencies of 10^{-6} - 10^{-5} . Much later it was shown that *hipA* in fact forms a TA locus with its antitoxin *hipB* (Black *et al.*, 1991;Black *et al.*, 1994). The HipA7 mutant contains substitutions G22S and D291A, which are both needed to give high persistence frequencies, in a ppGpp dependent manner (Korch *et al.*, 2003) (ppGpp is described in Chapter 4). HipA inhibits bacterial growth by decreasing protein synthesis, whereas HipA7 does so only to a lesser extent (Korch and Hill, 2006). The inhibition was observed to be bacteriostatic as the inhibition could be counteracted by subsequent HipB expression. HipA encodes a 440 AA residue protein with a structural fold similar to that of eukaryotic ATP-binding serine/threonine kinases, which bind ATP (Figure 6B) (Schumacher *et al.*, 2009). EF-Tu was observed to strongly interact with HipA in the presence of ATP and magnesium. This was stimulated by GDP, which leaves EF-Tu in an open form. These data, combined with structure of HipA-EF-Tu peptide substrate, shows that HipA might phosphorylate Thr382 which blocks aminoacyl-tRNA binding by EF-Tu, as EF-Tu cannot bind GTP when phosphorylated (Schumacher *et al.*, 2009).

Prokaryotic PIN domains - VapC

The *vapBC* locus (virulence associated protein) was first identified and described from a virulence plasmid of *Salmonella* Dublin and later found in regions flanking virulence genes on the chromosome of *Dichelobacter nodosus* (Pullinger and Lax, 1992; Bloomfield *et al.*, 1997). Inactivation of *vagC* (now referred to as *vapB*) in *S. dublin* led to growth inhibition on selected media and loss of plasmid-associated virulence due to impairment of plasmid stability. Similar phenomena were also reported for virulence plasmid pMYSH6000 of *Shigella flexneri* 2a YSH6000 as *vapBC* locus *mvpAT* (maintenance of virulence plasmid) stabilise plasmids by PSK and work in concert with another conventional partitioning system to efficiently stabilise pMYSH6000 (Radnedge *et al.*, 1997; Sayeed *et al.*, 2000; Sayeed *et al.*, 2005). A more recent study on *vapBC* locus of *Leptospira interrogans* revealed stronger evidence that *vapBC* are in fact *bona fide* TA loci as this study not only showed that *vapBC* could stabilise plasmids by PSK, but also that over expression of VapC inhibited growth, which could be counteracted by VapB expression (Zhang *et al.*, 2004). An early bioinformatic study predicted the *vapBC* locus to constitute a new toxin-antitoxin family as *vapB* genes contained DNA binding motifs and were encoded upstream of *vapC*, which contained predicted PIN domains (Anantharaman and Aravind, 2003).

PIN domains make up a large structural domain family, which are found in bacteria, archaea and eukaryotes. The domain was originally identified in the N-terminus of an ATPase involved in biosynthesis of type IV pili in *Myxococcus xanthus* (*pilT* N-terminal domain). However, the functional relationship between the ATPase and the PIN domain still remains unclear (Wall and Kaiser, 1999). An early bioinformatic study using PSI-BLAST to detect remote sequence homologies, revealed that though PIN domains generally share only low sequence similarity, conserved residues could still be detected (Clissold and Ponting, 2000). PIN domains were found to contain four to five highly conserved acidic amino acid residues (glutamate or aspartate) and a single hydroxyl residue (serine and threonine). This pattern of acidic residues are often found in proteins which bind divalent metal ions (Mg^{2+} and Mn^{2+}) and Clissold and Ponting predicted PIN domains to produce a nuclease active site similar to that of 5'-nuclease domain families (nuclease domain of *taq* polymerase, T4 RNase H and 5'3' FLAP endonucleases). This relationship was confirmed with the crystal structure

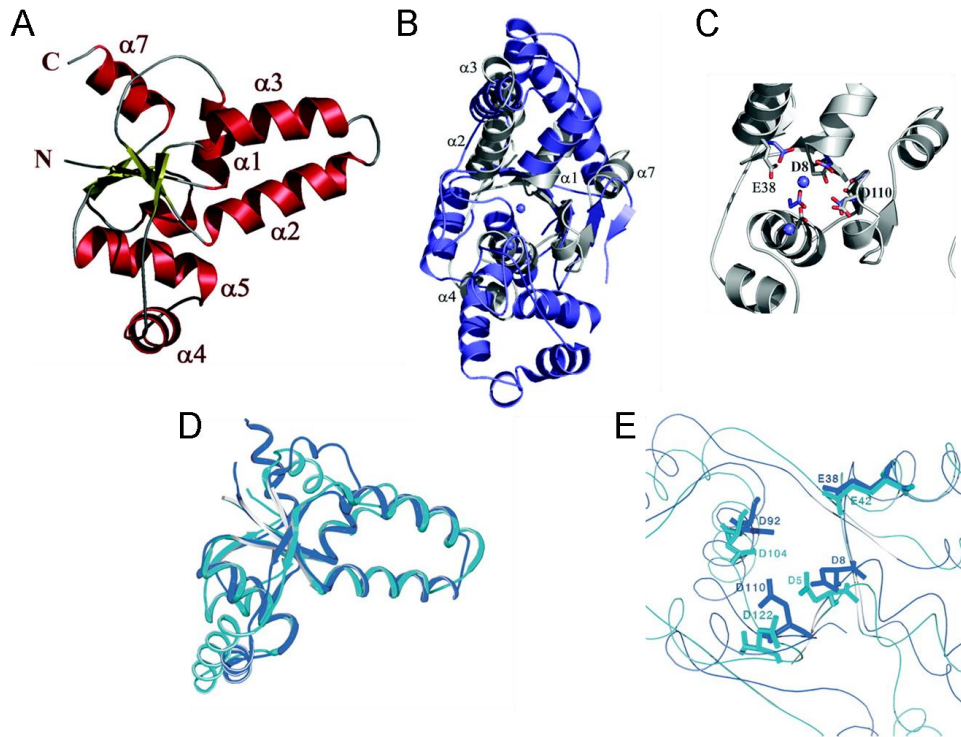


Figure 7 Structures of VapC PIN domain proteins **A**) PAE2754 monomer α -Helices shown in red (numbered except α_6) and central twisted parallel β -sheets shown in green. **B**) T4 RNase H (blue) superimposed onto PAE2754 (grey). **C**) Close-up on proposed active site of PAE2754 (grey) with active site residues of T4 RNase H (blue). **D**) FitB (cyan) superimposed onto PAE2754 (blue). **E**) putative active site residues of FitB (cyan) and PAE2754 (blue). Adapted from (Arcus *et al.*, 2004;Mattison *et al.*, 2006).

of the PIN domain of PAE2754 from *Pyrobaculum aerophilum* (Arcus *et al.*, 2004). PAE2754 was found to form a tetramer in solution by association of two PAE2754 dimers. The PAE2754 monomer contains $\alpha/\beta/\alpha$ - fold with seven α -helices and central twisted parallel β -sheets (Figure 7A). As predicted by Clissold and Ponting PAE2754 PIN domain did not share any similarity with T4 RNase H (Figure 7B), however it was observed that active site residues involved in coordinating metal ions could be aligned (Figure 7C). In addition, PAE2754 showed weak Mg^{2+} - and Mn^{2+} -dependent nuclease activity on single stranded DNA substrates, suggesting nuclease activity (Arcus *et al.*, 2004). To date 11 PIN domain structures are available in the Protein Data Bank (PDB), which all share low sequence similarity, but nevertheless show the same conserved three-dimensional fold (Arcus *et al.*, 2011). More recently it has been shown that VapC most likely is a ribonuclease as VapC-1 (of *vapBC-1*) from non-typable *Haemophilus influenzae* was shown to degrade total RNA *in vitro*, which was inhibited in the presence of VapB-1 (Daines *et al.*, 2007). VapC-1 did not show any activity towards double stranded and single stranded DNA. RNase activity of VapC *in*

Table 2 summary of reported VapC RNase activity

Name/organism	Condition	Substrate	Metal ion dependency	Counteract toxicity	Reference
<i>Haemophilus influenzae</i> VapC-1 (HI0322)	<i>In vitro</i>	Total RNA	ND	VapB-1 (HI0321)	(Daines et al., 2007)
<i>Mycobacterium tuberculosis</i> VapBC-5 (Rv0626-Rv0627)	<i>In vitro</i>	RNA hairpin-loop	Mg ²⁺	RNase-OUT	(Miallau et al., 2009)
VapC (Rv0301)	<i>In vitro</i>	MS2 RNA	ND	VapB (Rv0300)	(Ramage et al., 2009)
VapC (Rv1561)	<i>In vitro</i>	MS2 RNA	ND	N/A	(Ramage et al., 2009)
VapC (Rv0065)	<i>In vitro</i>	150nt RNA	Mg ²⁺	VapB (Rv0065A)	(Ahidjo et al., 2011)
VapC (Rv0617)	<i>In vitro</i>	150nt RNA	Mg ²⁺	VapB (Rv0616A)	(Ahidjo et al., 2011)
<i>Sulfolobus solfataricus</i> VapC-6 (SSO1493)	<i>In vitro</i>	Total RNA, <i>dppB-1</i> mRNA, <i>tetR</i> mRNA and <i>vapB-6</i> mRNA	Mg ²⁺	VapB-6 (SSO1494)	(Maezato et al., 2011)
<i>Piscirickettsia salmonis</i> VapC (Ps-tox)	<i>In vitro</i>	Total RNA	ND	VapB (Ps-antitox)	(Gomez et al., 2011)

ND (Not Described)

vitro has now been reported from several independent studies, which are summarised in Table 2. These observations all support that VapC toxins are ribosome independent ribonucleases.

PIN domains are present in many Eukaryotic proteins, and are involved in conserved processes of rRNA maturation and RNA quality control (recent review on eukaryotic endoribonucleases (Tomecki and Dziembowski, 2010)). Yeast Dis3 (also called Rrp44) is the catalytic domain of the eukaryotic exosome, which is involved in the degradation of rRNA processing by-products and cryptic unstable transcripts (CUTs) in the nucleus. Dis3/Rrp44 contains a C-terminal RNase II-like 3'-5' exoribonuclease domain and an N-terminal PIN domain (Schneider *et al.*, 2009; Schaeffer *et al.*, 2009). The PIN domain was found not only to exhibit Mn²⁺-dependent endoribonuclease activity on single stranded hairpin-loop RNA, but also to assist the binding of Dis3 to

the exosome. Interestingly, Dis3/Rrp44 was found to specifically degrade hypermodified damaged tRNA_i^{Met} (initiator tRNA) *in vitro*, although recognition did not seem to be linked to the N-terminal PIN domain as mutations in RNase II domain abolished tRNA_i^{Met} binding (Schneider *et al.*, 2007)

Yeast also harbours a second PIN domain protein Swt1 which is involved in RNA surveillance on exported nuclear mRNPs (messenger ribonucleoprotein particles)(Skruzny *et al.*, 2009). Swt1 was found to cleave unstructured regions of RNA *in vitro* independently of metal ion addition. Other yeast PIN domains are Nob1 and Utp24, which are necessary for processing of 18S ribosomal RNA (Bleichert *et al.*, 2006; Lamanna and Karbstein, 2009). Utp24 acts in the early steps of rRNA maturation, whereas Nob1 only acts on 20S pre-rRNA. Nob1 showed specific manganese-dependent endoribonuclease activity on a RNA substrate containing 20S pre-rRNA cleavage site (also referred to as D-site) *in vitro* (Pertschy *et al.*, 2009). A fifth PIN domain found in eukaryotes is SMG6 which is involved in nonsense mediated messenger decay (NMD). It is governed by an mRNA quality control system which degrades mRNAs containing premature termination codons (Huntzinger *et al.*, 2008). Human SMG6 showed manganese-dependent ribonuclease activity *in vitro* on single stranded RNA (Glavan *et al.*, 2006). An interesting pattern seems to appear as most of the PIN domain proteins are involved in quality control where the PIN domain endoribonucleolytic activity initiates RNA degradation by 3'-5' exoribonucleases. This has some analogy to prokaryotic RNase E and G, that initiate RNA maturation or degradation events by RNA cleavage, which is followed by exoribonuclease mediated RNA degradation (Recently reviewed (Picard *et al.*, 2009)).

Despite that our knowledge of Eukaryotic PIN domains has advanced greatly in recent years, the targets and specific activities of prokaryotic PIN domains are still not clear.

Previously it has been reported that mutation in *ntrR* of *ntrPR* of plant symbiont *Sinorhizobium meliloti* increased the expression of nodulation (*nod*) and nitrogen fixation (*nif*) genes (Olah *et al.*, 2001). The *ntrR* gene is a *vapC* homologue and *ntrP* contains an AbrB-like DNA binding domain. The expression of *ntrR* was found to decrease the growth of *E. coli* cells by an unknown mechanism (Bodogai *et al.*, 2006). A transcriptome analysis of *ntrR* deletion strain showed that several genes were

affected including metabolic genes and not only *not* and *nif* symbiotic genes (Puskas *et al.*, 2004). This suggests that *ntrR* might, by an unknown mechanism, interfere with general regulatory mechanisms, especially under anaerobic growth.

Another well described *vapBC* locus is *fitAB* from the human pathogen *Neisseria gonorrhoea*. The *fitAB* (fast intracellular trafficking) locus was identified in a genetic screen for mutations which gives a fast trafficking phenotype in a monolayer of epithelial cells (Hopper *et al.*, 2000). Mutations in *fitAB* allowed mutants to transverse the epithelial barrier 5-6 times faster than wild type cells and it was suggested that *fitAB* regulates the intracellular growth rate during pathogenesis. The FitAB TA-complex has been crystallised bound to DNA and revealed a [FitA₂-FitB₂]₂ hetero octamer (Mattison *et al.*, 2006). FitA is a RHH DNA-binding protein and FitB a PIN domain protein, which perfectly aligns with the structure of PAE2754 including the proposed acidic catalytic residues of PAE2754 (Figure 7D & E). It is however still unknown how FitB regulates the intracellular growth rate of *N. gonorrhoea*.

Transcriptome analysis in the crenarchaeon *Sulfolobus solfataricus* have shown that many of the 26 chromosomal *vapBC* loci are upregulated in response to heat shock (Tachdjian and Kelly, 2006; Cooper *et al.*, 2009). It is therefore suggested that VapC might be involved in adjusting metabolism in response to heat shock. More recently it has been shown that inactivation of *vapBC-6* locus results in heat shock sensitivity and heat shock dependent reduction in the growth rate of *S. solfataricus* (Maezato *et al.*, 2011). By quantitative PCR a preferential increase in *dppB-1* dipeptide transporter (~20-fold) and *tetR* (~5-fold) transcriptional regulator in *vapBC-6* deficient strain, suggesting that these genes are regulated by *vapBC-6*. *In vitro* these transcripts were degraded by purified VapC-6 and it was suggested that VapC targets these transcripts during heat shock (Maezato *et al.*, 2011). Interestingly, a *vapBC-6* deficient strain also showed decreased transcripts house keeping sigma factor (*rpoD*) and eIF2 gamma domain, of Initiation factor 2 during heat shock, which could account for the observed sensitivity to heat shock. However, it is still unclear how *vapBC-6* assists the heat shock response in *S. solfataricus*.

It is now known that ectopic expression of several VapCs (including VapC from *Mycobacterium smegmatis*, as well as several *Mycobacterium tuberculosis* VapCs (Rv0301, Rv1561 and Rv1829c) inhibit cell growth by decreasing the global rate of translation, without substantial effects to transcription and replication (Robson *et al.*,

2009;Ramage *et al.*, 2009). Despite these observations, the specific molecular target of the VapC toxin has evaded exposure.

Diverse toxin families which target the translational machinery of E. coli

Similar to ribosome-dependent mRNA interferases, colicin D treatment has been shown to induce ribosomal A-site cleavage in response to ribosomal pausing (Garza-Sanchez *et al.*, 2008). Colicin D belongs to a group of colicins that target the translation machinery (recently reviewed (Cascales *et al.*, 2007)). Colicins share many similarities with TAs as they are often plasmid resident and encode toxic proteins, which are neutralised by host-encoded immunity proteins. Colicins are secreted from producer cells and transported to the cytosol of target cells by outer membrane receptors and imported to the cytosol by translocation (Kleanthous, 2010). Colicin E3 cleaves 16S ribosomal RNA between A1493 and G1494 near the 3'-end, which interferes with the decoding center of the ribosomal A-site and abolishes protein synthesis (Bowman *et al.*, 1971).

Colicin E5 and colicin D inhibit protein synthesis by cleaving in the tRNA anticodon loop (Ogawa *et al.*, 1999;Tomita *et al.*, 2000). Colicin E5 cleave tRNA^{Tyr}, tRNA^{His}, tRNA^{Asn} and tRNA^{Asp} between position 34 and 35 containing a queuine (a modified guanine) at the wobble base and colicin D cleave all tRNA^{Arg} between position 38 and 39. Treatment of *E. coli* with colicin D has been shown to induce ribosome stalling on arginine codons as the cells are depleted of amino acylated tRNA^{Arg} (Garza-Sanchez *et al.*, 2008). This in turn induces mRNA cleavage in the ribosomal A-site, which is dependent on an unknown ribonuclease or could be mediated by mRNA interferases. Arginine, tryptophan, histidine and serine starvation has also been shown to induce similar A-site cleavage (Li *et al.*, 2008b;Garza-Sanchez *et al.*, 2008).

Another anticodon nuclease is encoded by the *prr* locus of clinical *E. coli* strains and has been shown to be induced upon phage T4 infection and potentially cleave its own tRNA^{lys} (Depew and Cozzarelli, 1974;David *et al.*, 1982). The anticodon nuclease gene *prrC* is integrated into the *prrABD* gene cluster, which encodes EcoPrnI: a type I restriction modification system (Amitsur *et al.*, 1992). Upon phage T4 infection, phage encoded peptide Stp suppresses EcoPrnI, which leads to activation of PrrC. PrrC cleaves 5' to the anticodon of tRNA^{lys} between position 33 and 34 with required modified wobble base (David *et al.*, 1982;Amitsur *et al.*, 1987;Jiang *et al.*, 2001). PrrC expression does not immediately lead to cell death as T4 phage encode an RNA

repair system with a 3'-phosphatase-polynucleotide kinase which hydrolyses 2',3'-cyclic phosphate and phosphorylate 5'-OH, which can be joined by phage-encoded RNA ligase restoring intact tRNA^{lys}. Therefore, PrrC is only a potential phage abortive system as the phage, ingeniously, can repair the RNA damage.

Similar to PrrC, both colicin E5 and colicin D produces 5'-cleavage products with 3' 2',3'-cyclic phosphate and 3'-cleavage products with 5'-hydroxyl groups, although no homology exists between these three nucleases (Ogawa *et al.*, 1999;Tomita *et al.*, 2000). Archaea (and eukaryotes) hold a number of intron-containing tRNA genes, which are cut out by an tRNA splicing endonuclease (Peebles *et al.*, 1983). Cleavage generates a 5' exon with a 2',3'-cyclic phosphate terminus and a 3'exon with a 5'-hydroxyl group, which is the substrates of 3'phosphate RNA ligase RtcB, that creates the functional tRNA (Englert *et al.*, 2011). *E. coli* encodes a homologue of 3'phosphate ligase, RtcB, which is situated in a putative RNA repair operon (Tanaka and Shuman, 2011). *E. coli* RtcB has been shown to actively ligate cleavage products of *Kluyveromyces lactis* γ -toxin anticodon nuclease, which produces similar cleavage products to PrrC, colicin E5 and colicin D. This could indicate an evolutionary and functional link between tRNases and RNA ligase repair systems.

More recently, a new group of toxin systems have been identified in proteobacteria. These systems are thought to be intercellular communication systems, which mediate contact-dependent growth inhibition (CDI) (Aoki *et al.*, 2005;Hayes *et al.*, 2010). The CDI systems consist of a CdiB/CdiA two-partner secretion system (TPS) and an additional immunity protein CdiI. CdiB facilitates the translocation of CdiA "exo protein" onto the cell surface and CdiI protects against autoinhibition. If CDI⁺ bacteria get in direct contact with other bacteria, CdiA "exo protein" is taken up by concerted action of BamA receptor protein and AcrB membrane transport protein and if the cell fails to produce cognate immunity proteins (CDI⁻) it leads to growth inhibition.

It has recently been shown that the C-terminal domain of CdiA protein is responsible for growth inhibition, CdiA-CT (Aoki *et al.*, 2010). CdiA-CT₃₉₃₇₋₂ of plant pathogen *Dickaya dadantii* showed efficient Mg²⁺-dependent DNase activity *in vitro*, whereas CdiA-CT₅₃₆ from uropathogenic *E. coli* showed specific tRNase activity (confirmed degradation of tRNA^{His} and tRNA^{ala}, without degradation of ribosomal RNA (Aoki *et al.*, 2010). In CdiA-CT the nuclease activity was inhibited in the presence of immunity proteins. Interestingly growth inhibited CDI⁻ cells could be recovered by

subsequent expression of CdiI *in trans* from a plasmid, suggesting that the metabolic downshift mediated by CdiA is reversible (Aoki *et al.*, 2009).

It is clear that a multitude of toxin targets exist within the cell. The toxin targets are primarily placed within the translation machinery, but all affect growth and cell division. The following chapter, Chapter 3, will focus on the activity of the antitoxin and the structures of toxin-antitoxin complexes. Furthermore it includes a discussion on how antitoxins contribute to DNA binding and neutralisation of the toxin. Chapter 3 will also outline the transcriptional repression mechanisms by TA complexes and how transcription can be activated by protease-dependent degradation of antitoxins and more directly by toxin molecules, affecting cooperative binding and repression of the TA promoter.

Chapter 3: Antitoxins

Structure and activity of Antitoxins

The most important role of the antitoxin is to prevent the cognate toxins from inhibiting their cellular targets. This is achieved by direct non-covalent protein-protein interactions, leading to the formation of inactive TA complexes. The metabolic stability of antitoxins should be sufficiently low as to allow liberation from the toxin. In addition, the antitoxin autoregulates transcription of the TA operon, which maintains tight control of toxin and antitoxin levels in the cell. These functions are all programmed within these small molecules (~70-150 amino acids) in different domains of the protein. Despite the functional relationship between all antitoxins and their small size, the sequence and structures are quite diverse. Even cognate antitoxins of structurally homologous toxins can be quite different and contain different DNA-binding domains. This diversity is suggested to have evolved by gene-shuffling events (see Chapter 1) (Anantharaman and Aravind, 2003;Makarova *et al.*, 2009). Interestingly, degradation of antitoxins by cellular proteases activates TA transcription, but it is not an exclusive mechanism. Recently, it has become clear that changes in antitoxin/toxin ratio also affect the ability of a TA complex to repress transcription: a condition now generally referred to as conditional cooperativity.

In the following Chapter, structural and functional relationship between antitoxins and TA complexes of the best characterised TA systems (i.e. CcdAB, MazEF/Kis-Kid, RelBE, Phd-Doc and VapBC) will be described in detail.

CcdA and the CcdAB TA complexes

CcdA antitoxin encoded by *E. coli* F plasmid forms a dimer of two 8.4 kDa monomers containing a N-terminal RHH-like DNA binding domain and a highly flexible C-terminus. These RHH-like domains are found transcriptional repressor proteins like CopG, MetJ and Arc. The CcdA dimer was also found to specifically bind three direct repeats in the *ccdAB* promoter of which the first one overlaps with the promoter (Figure 8A) (Madl *et al.*, 2006). Binding of one CcdA dimer to a direct repeat ($K_d \sim 149 \mu\text{M}$) cooperatively increases the affinity of binding of the second dimer ($K_d \sim 71 \mu\text{M}$) and subsequently the third dimer ($K_d \sim 59 \mu\text{M}$), which could be due to unspecific interactions between antitoxin dimers or bending of DNA. These

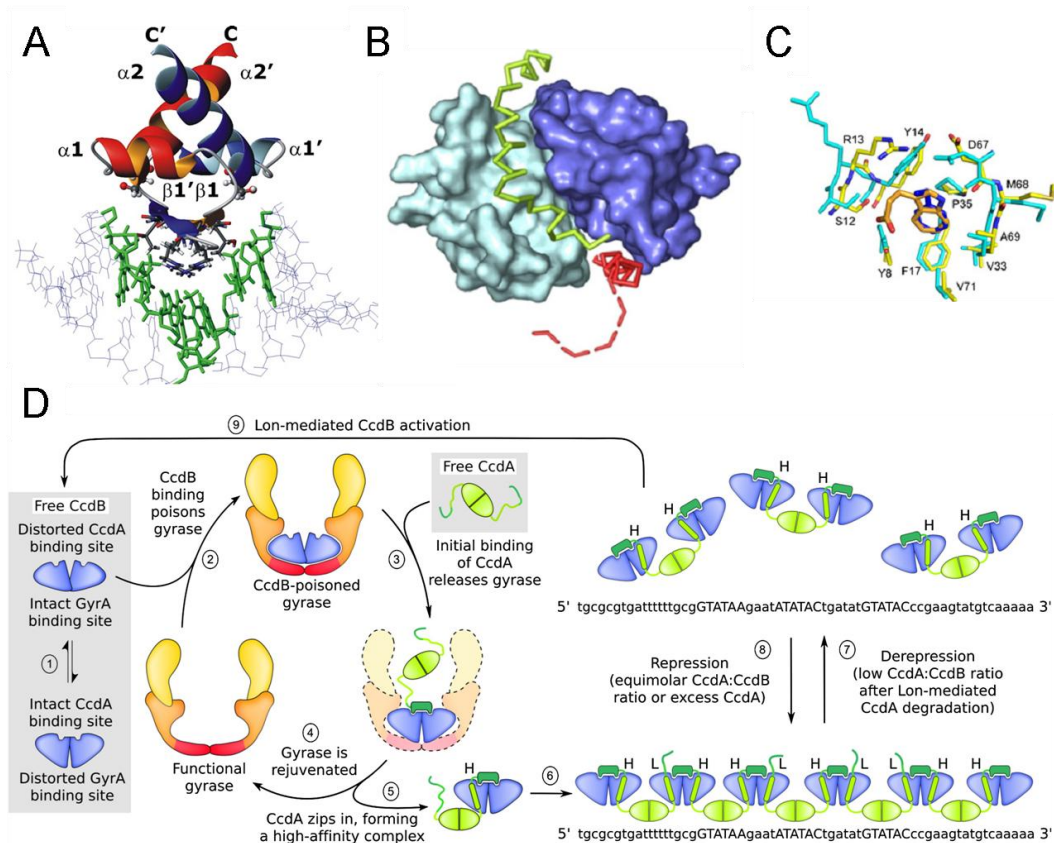


Figure 8 Regulation of *ccdAB* and gyrase rejuvenation **A**) Structure of CcdA dimer N-terminal RHH domain (in red and blue) binding to major groove of B-form DNA (6bp palindrome 5'-GTATAC-3' shown in green). Arg4, Thr6 and Thr8 from each dimer beta sheet form base-specific contracts. **B**) CcdB dimer (cyan and blue) with two CcdA³⁷⁻⁷² bound with high affinity (green) and low affinity (red). Both CcdA³⁷⁻⁷² bind CcdB dimer with Arg40-Met61 segments, but only one (green) binds with Ser64-Trp72 which results the other CcdA³⁷⁻⁷² C-terminal (Red dashed line) to be unstructured and disordered. **C**) Hydrophobic binding pockets on CcdB dimer can accommodate both Phe65 and Trp72 of CcdA³⁷⁻⁷² monomer. The interactions of the hydrophobic binding pocket of one CcdB monomer (cyan) with Phe65 (blue) and the other CcdB monomer (yellow) interactions with Trp72. **D**) The complete model of CcdA and CcdB activities. 1) CcdB dimer (blue) converts between two conformations. 2) In a conformation with distorted CcdA binding site and intact GyrA binding site CcdB binds to gyrase which result in poisoning. 3) Initial binding of CcdA⁶⁵⁻⁷² to CcdB dimer changes the conformation of CcdB to a form with distorted GyrA binding site. 4) CcdA₂-CcdB₂ complexes are released from gyrase and it is rejuvenated. 5) In free CcdA₂-CcdB₂ complexes, CcdA³⁷⁻⁶⁵ zips in and forms High affinity complexes (H) and with one free CcdA C-terminal. 6) The free CcdA C-terminal can bind with low affinity to another High affinity complex and chains of CcdA₂-CcdB₂ complexes, which bind to direct repeats in the promoter region will polymerise along the DNA. 7) When CcdA levels decrease in response to Lon protease dependent degradation it leads to increases in CcdB which resolve repression complexes by CcdA titration on high affinity binding sites. 8) This leads to transcriptional derepression and increased *de novo* synthesis of CcdA which in turn allows CcdA₂-CcdB₂ complexes to be formed which repress transcription. 9) When Lon mediated degradation of CcdA out competes the *de novo* synthesis of CcdA, CcdB is freed to act on its target. Adapted from (Madl *et al.*, 2006;De *et al.*, 2009)

affinities are however low, and affinity and specificity of CcdA for DNA is drastically increased in the presence of CcdB (Dao-Thi *et al.*, 2002). This is also consistent with the observation that CcdA only represses transcription *in vivo* in the presence of gyrase toxin, CcdB (Tam and Kline, 1989).

Upon binding of CcdA C-terminus to CcdB dimer, which can be free or in complex with its target GyrA, CcdA becomes structured. CcdA C-terminal residues 46-73 are shielded by CcdB by binding to hydrophobic pockets on either CcdB monomer (Madl *et al.*, 2006;De *et al.*, 2009) (Figure 8B). This leads to an allosteric change in CcdB which favours CcdA binding and decreases affinity of CcdB for GyrA.

Recent crystal structures revealed that when CcdA/CcdB ratios are 1:1, CcdA binds to two sites in the CcdB dimer, one with high affinity which requires the interaction of the complete C-terminus of one CcdA dimer and another with low affinity which only requires residues 40-61 of an additional CcdA dimer (Figure 8B and C)(De *et al.*, 2009). Previously, it has been shown that CcdA and CcdB bind DNA in a 1:1 complex of $[\text{CcdA}_2\text{-CcdB}_2]_n$ protecting a region of ~113 bp from DNase I nuclease degradation *in vitro* and using cell extracts *in vivo* (Tam and Kline, 1989;Dao-Thi *et al.*, 2002). This observation suggests that $[\text{CcdA}_2\text{-CcdB}_2]_n$ bind to direct repeats in the promoter region and that complexes extend from there in both directions as helical polymers. In these complexes a free CcdA C-terminus from one $\text{CcdA}_2\text{-CcdB}_2$ tetramer interacts with the low affinity site on CcdB in the neighbouring $\text{CcdA}_2\text{-CcdB}_2$ hereby increasing the affinity of the next complex for DNA (Figure 8D)

The unstructured features of CcdA in solution render it vulnerable to proteolytic degradation and it is degraded by the ATP-dependent Lon protease *in vitro* and *in vivo* (van Melderen *et al.*, 1996). *In vivo*, CcdA has a $T_{1/2} \sim 30$ min and in the presence of CcdB it is increased to $T_{1/2} \sim 60$ min. If *de novo* synthesis of CcdA does not keep up with Lon-dependent degradation of CcdA it results in a decreased CcdA:CcdB ratio. An early study has shown that a CcdA:CcdB ratio of 1:2 results in formation of $[\text{CcdA}_2\text{-CcdB}_4]_n$ complexes, which have drastically decreased affinity for DNA (Afif *et al.*, 2001). This is caused by preferential binding of CcdA to the high affinity site of CcdB dimer, and when CcdA levels are low, CcdA bound in the low affinity site will be titrated to high affinity sites. The non-toxic $\text{CcdA}_2\text{-CcdB}_4$ complexes are sterically hindered in the DNA binding of CcdA and therefore have decreased affinity for DNA (Madl *et al.*, 2006;De *et al.*, 2009).The decreased repression of *ccdAB* promoter, allows *de novo* syntheses of CcdA and the return of a 1:1 ratio of CcdA:CcdB, favouring formation of repression competent complexes $[\text{CcdA}_2\text{-CcdB}_2]_n$. The complete interaction diagram of *ccd* with rejuvenation of CcdB poised DNA gyrases is summarised in Figure 8D.

MazEF and Kis-Kid TA complexes

The *mazEF* locus of *E. coli* K-12 is a chromosomal homologue of *kis-kid* of plasmid R1 (Masuda *et al.*, 1993). The Kid toxin is smaller than MazF 12.1/14.8kD, but shares 25% sequence identity, and Kis antitoxin shares 33 % sequence identity with MazE antitoxin. MazE is an intrinsically unstructured protein, which upon interaction with DNA or MazF becomes structured and dimerises whereby the N-terminal domain forms a barrel-like structure in which both monomers contribute a pair of β -sheets connected by a short α -helix (Loris *et al.*, 2003). An identical structure has been reported for Kis antitoxin (Kamphuis *et al.*, 2007). The crystal structure of MazEF revealed a MazF₂-MazE₂-MazF₂ structure, where two extended C-termini of a MazE dimer reach out into each of two MazF dimers (Figure 9A) (Kamada *et al.*, 2003). The MazF dimer contains two identical mRNA binding sites which change conformation upon binding of one MazE C-terminus, accounting for the inactivation of MazF (Li *et al.*, 2006). Residues 48-76 of MazE interact with the MazF dimer with four surface regions including one by the N-terminal globular domain and three by the C-terminus. NMR structural data on Kis-Kid showed that they most likely resemble those of the MazE-MazF complex (Kamphuis *et al.*, 2007).

Both MazE and MazF, and Kis and Kid, are required for transcriptional autoregulation of *mazEF* and *parD*, respectively (Ruiz-Echevarria *et al.*, 1991; Marianovsky *et al.*, 2001). The N-terminal globular domain formed by two MazE dimers resembles the N-terminal domain of homodimeric AbrB repressor protein of *Bacillus subtilis*, which contains a looped hinge helix (LHH) fold (Figure 9B) (Bobay *et al.*, 2005). The N-terminal DNA binding domain binds DNA by interactions from central β -sheets into the major groove of DNA (Figure 9C). In the MazF₂-MazE₂-MazF₂ crystal structure, a MazE dimer only occupies two of four possible sites in two MazF dimers which could allow binding of an additional MazE dimer and formation of [MazE₂-MazF₂]_n in which MazF dimers bridges between MazE dimers bound to DNA (Kamada *et al.*, 2003).

The *mazEF* locus is primarily transcribed from a single promoter (P2) which contains alternating palindromes with an inverted repeat overlapping with -10 pribnow box (5'-ATTGATATATACTGTATCTACATA-3') of P2 and a single repeat overlapping with -35 sequence (5'-TCGTATCTACAAT-3') (Marianovsky *et al.*, 2001). The promoter is only partially repressed in the presence of only MazE and

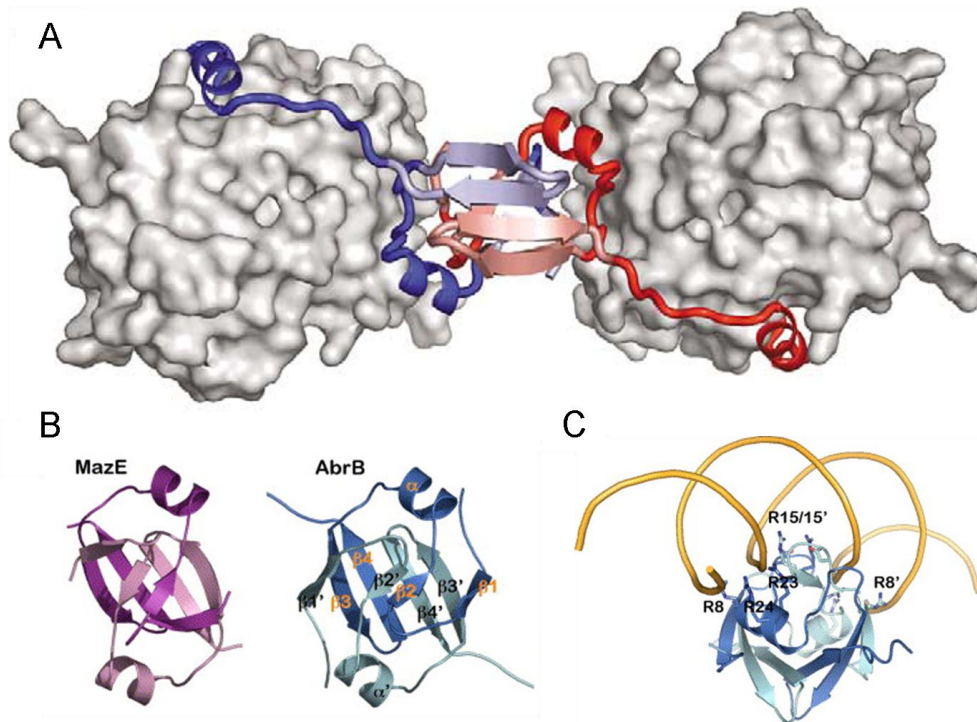


Figure 9 Structure of MazEF TA complex. **A)** Crystal structure of MazF₂-MazE₂-MazF₂ complex. MazE₂ dimer (Red and blue) forms a globular domain with the N-termini. The C-terminal of each dimer reaches out into the mRNA binding pocket of MazF₂ dimer (grey). This conformation leaves two unoccupied mRNA binding pockets. **B)** Structures of N-terminal domain of MazE (purple) and N-terminal domain of AbrB (blue with secondary structure labelled). **C)** Model of N-terminal domain of AbrB binding to bent DNA. The interaction is predicted to be mediated by several Arg (or Lys) residues in AbrB N-terminal. Adapted from (Buts et al., 2005; Bobay et al., 2005).

MazF acts as a co-repressor (Marianovsky *et al.*, 2001; Zhang *et al.*, 2003a). Crude cell extracts of MazEF expressing cells were found to protect a 47 bp region containing the alternating palindromes from DNase I nuclease activity, consistent with MazEF binding. The *parD* locus contains two inverted repeats, one imperfect (-52 to -70, 5'-AAGTTATATTTTATTAAACATT-3'), and one perfect which overlaps with the -10 sequence and transcriptional start site (-15 to +3, 5'-ATGTTATATTTAAATATAACTT-3'). Heterooctameric species of Kis₂-Kid₂-Kis₂-Kid₂ complexes were identified to protect these two inverted repeats from hydroxyl radical treatment indicating that these sites are bound by Kis-Kid (Monti *et al.*, 2007). In addition, Kis-Kid complexes were found to bind the perfect inverted repeat with higher affinity than the imperfect repeat, suggesting it to be important for transcriptional repression. Interestingly, Kis antitoxin alone binds operator DNA with low affinity, but showed low unspecific cooperative binding similar to that reported for CcdA.

During steady state growth, the ATP-dependent protease ClpAP degrades MazE ($T_{1/2}$ ~30 min) and during amino acid starvation, MazE is degraded by the ATP-dependent Lon protease ($T_{1/2}$ ~30 min) (Aizenman *et al.*, 1996; Christensen *et al.*, 2003).

The antitoxin/toxin ratio decreases when *de novo* synthesis of antitoxin does not keep up with the degradation by proteases. Hence, Lon-dependent degradation of MazE during amino acid starvation leads to transcriptional activation of *mazEF* (Christensen *et al.*, 2003). It is known that when the Kis/Kid ratios are low ~ 1:2, a hexameric form of Kid₂-Kis₂-Kid₂ complexes are formed which have decreased affinity for DNA as 80% of the complexes present were not associated with DNA (Monti *et al.*, 2007). Whether the hexameric Kis-Kid complexes observed are similar to the first published hexameric structure of MazEF is not known (Figure 9A). It could indicate that MazEF also forms hexameric complexes, when toxin is in excess, which would result in low DNA affinity due steric clashes between toxin-complexed dimers as suggested for Kis-Kid (Monti *et al.*, 2007).

The *mazEF* locus has additional interesting features as it is positioned downstream of the *relA* gene encoding ppGpp synthase and has been proposed to have a concerted function in response to ppGpp (Aizenman *et al.*, 1996) (discussed in Chapter 4). Furthermore, a FIS binding site was identified immediately upstream of the third repeat in the promoter region and was shown to bind FIS protein *in vivo* and *in vitro* (Marianovsky *et al.*, 2001). FIS is a nucleoid associated protein, which regulates various processes including transcription, recombination and replication (reviewed (Browning *et al.*, 2010) and was shown to increase the transcription of *mazEF* 1.6-fold. FIS levels are high in exponentially growing cells in which *mazEF* is tightly repressed. The specific role of FIS in *mazEF* transcriptional regulation is however unknown (Marianovsky *et al.*, 2001).

RelBE TA complexes

The *relBE* locus of *E. coli* K-12 is resident inside Qin prophage and is transcribed from a single promoter, which in addition to *relB* and *relE* also contains *hokD* (or *relF*), a type I TA locus (Pedersen and Gerdes, 1999). However, *hokD* is suggested to be inactive as upstream regulatory elements are lacking.

E. coli RelB is a 9.35 kDa protein (79 AA), which contains an N-terminal RHH-like DNA binding domain that in solution dimerises and forms multimers in the absence

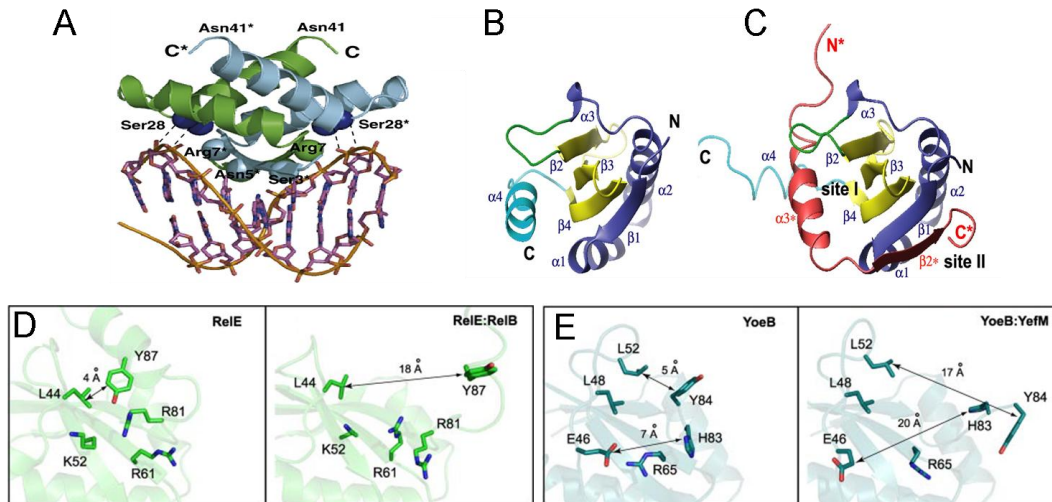


Figure 10 Interactions in the RelBE TA complex **A)** Structure of RelB N-terminal RHH domain residues 1-41 modelled onto 12bp 5'-TTGTAATTACAA-3' halfsite inverted repeat. RelB monomers are Green and blue, respectively and important residues interacting with DNA are shown. **B)** NMR structure of unbound RelE monomer. **C)** NMR structure of RelE with bound RelB C-terminal. Secondary structure is indicated including interaction sites I and II. **D)** Structure of RelE active site residues in presence and absence of RelB. **E)** Structure of YoeB active site in the presence and absence of YefM. Adapted from (Li *et al.*, 2008;Li *et al.*, 2009).

of RelE (Cherny *et al.*, 2007;Li *et al.*, 2008a). By DNase I protection and hydroxyl radical footprinting it was shown that two RelB dimers bind an inverted DNA repeat of 26 bp (5'-CTTGTAAATGACATTTGTAATTACAAG-3') in the promoter region between the -10 sequence (pribnow box) and the ribosome binding site (also referred to as *relO*) (Overgaard *et al.*, 2008;Li *et al.*, 2008a). Each 12 bp half-site of the inverted repeat can be subdivided into two small 6 bp imperfect inverted repeat which is bound by a single RelB dimer (Figure 10A). RelB has relatively low affinity for *relO* DNA ($K_d \sim 12.5 \mu\text{M}$), which is drastically increased in the presence of RelE ($K_d \sim 3.4 \text{ nM}$). Interestingly, RelB¹⁻⁵⁰ (lacking C-terminus) had even lower affinity ($K_d \sim 197\mu\text{M}$) than full length RelB in the absence of RelE suggesting that RelB, through its C-terminus, can itself mediate unspecific weak cooperative binding to *relO* (Overgaard *et al.*, 2008;Li *et al.*, 2008a). RelE does not bind DNA, but mediates strong cooperative binding of RelB to DNA, which acts to repress transcription of the *relBE* promoter (Gotfredsen and Gerdes, 1998;Overgaard *et al.*, 2008). Mutations in residues of the RelB RHH-like DNA binding domain (e.g Arg7) lead to decreased DNA binding and de-repression of *relBE* promoter (Li *et al.*, 2008a;Overgaard *et al.*, 2009). The C-terminus of RelB interacts with RelE to neutralise its activity *in vivo* and *in vitro* (Cherny *et al.*, 2007;Li *et al.*, 2009). The recent NMR structure of the RelB C-terminus bound to low toxic RelE^{R81A/R83A} revealed that RelB induces a

catalytic-incompetent structure of RelE^{R81A/R83A} which involves displacement of α -helix 4 of RelE^{R81A/R83A} (Figure 10B & C). RelB interacts with RelE^{R81A/R83A} in two sites. Site 1 interaction involves an α -helix of the RelB C-terminus (α H3*) with the surface of β -sheet core of RelE^{R81A/R83A} which perturbs the active site (see Chapter 2) by displacing Tyr87 and neutralisation of charged Arg61, Lys52, Lys54 and Arg81 (The position of Arg81 is predicted as it was substituted for an alanine) (Figure 10D). Site 2 anchors the RelB C-terminus to the surface of RelE^{R81A/R83A} in a hydrophobic patch formed by β -sheet 1 and α -helix hairpin of H1 and H2. Similar active site perturbation is induced by YefM upon binding to the RelE homologue YoeB (Figure 10 E) (Kamada and Hanaoka, 2005). This change renders RelE or YoeB catalytically inactive, either by directly interfering with toxin activity and/or by restricting the access of the toxin to the ribosomal A-site.

RelB is degraded by the ATP-dependent Lon protease *in vitro* and *in vivo* ($T_{1/2} < 15$ min) (Christensen *et al.*, 2001; Overgaard *et al.*, 2009). A decrease in rate-of translation induced by amino acid starvation or treatment with chloramphenicol leads to a decrease in *de novo* synthesis of RelB and increased turnover leads to a decrease in RelB/RelE ratio and transcriptional de-repression which is independent of stringent alarmone ppGpp (Christensen *et al.*, 2001). However, transcription was observed to increase more rapidly than Lon-mediated RelB decrease, which suggests an additional mechanism activating transcription (Overgaard *et al.*, 2008). Consistent with this observation, overexpression of non-toxic RelE^{C6} (Deleted for six C-terminal AA) induced *relBE* transcription while the protein levels of RelB did not decrease (Overgaard *et al.*, 2008). By gel shift assays and SPR (Surface Plasmon Resonance) it was observed that at a RelB/RelE ratio of 2:1, the TA complex had highest affinity for DNA, suggesting a DNA-binding complex of RelB₂-RelE. Interestingly, when the RelB/RelE ratio is shifted towards 1:1, the affinity for DNA drastically decreases suggesting the presence of RelB₂-RelE₂ complexes, which have low affinity for DNA. The decrease in affinity for DNA is dependent on the presence of both inverted repeats of *relO*, which suggests that the cooperative binding of two RelB-RelE complexes is crucial for this mechanism. This phenomenon was therefore termed conditional cooperativity (Overgaard *et al.*, 2008). It was suggested that the strong cooperativity of RelB₂-RelE complexes could be mediated by RelE bridging between a RelB₂ dimer such that RelB could interact with RelE in two distinct sites with different affinity (similar to CcdAB): The C-terminus of one RelB protomer binding

to a high affinity site in RelE and another RelB C-terminus binding to a low affinity site. Excess of free RelE with unoccupied high affinity binding sites would titrate low affinity bound RelB C-termini and lead to decreased cooperativity and consequently affinity for DNA (Overgaard *et al.*, 2008). The presence of high and low affinity RelB binding sites has not yet been confirmed and the exact mechanism still remains elusive. The phenomenon of conditional cooperativity has more recently been reported for three different *relBE* homologues of *Mycobacterium tuberculosis* (Yang *et al.*, 2010). For two of the three RelBE complexes it was observed that RelB:RelE ratios of 1:1 or lower greatly decreased the affinity of complex for promoter DNA, which could suggest a mechanism very similar to *E. coli* RelBE. The crystal structure of the YefM-YoeB complex revealed a YefM₂-YoeB complex, which makes it plausible that RelB-RelE forms a complex with similar stoichiometry (Kamada and Hanaoka, 2005). This is, however, in contrast to Archaeal RelB-RelE complexes from *Pyrococcus horikoshii* OT3 and *Methanococcus Jannaschii*, which both make RelB₂-RelE₂ complexes that are significantly different from each other and may therefore regulate transcription by different mechanisms (Takagi *et al.*, 2005; Francuski and Saenger, 2009).

Phd-Doc TA complexes

The *phd-doc* locus of bacteriophage P1 is autoregulated by Phd antitoxin *in vivo* leading to ~ 9-10 fold repression in the absence of Doc and ~ 40-100 fold repression in the presence of Doc, hence Doc acts as a co-repressor (Magnuson *et al.*, 1996; Magnuson and Yarmolinsky, 1998). The Phd antitoxin is an 8 kDa protein (73 aa), which, in the absence of Doc or DNA, shows intrinsic disorder as it exists in different forms (Garcia-Pino *et al.*, 2010). In the folded conformation Phd forms a dimer with a globular N-terminal domain that has a central six-stranded β -sheet sandwiched between four α -helices. This overall resembles the fold of antitoxin YefM (Kamada and Hanaoka, 2005). By DNase I footprinting Phd has previously been shown to protect an inverted repeat (5'-ATTGTGTACACATAACGAGTACACGAG-3') in the promoter region between the -10 sequence and the Shine & Dalgarno sequence, consistent with an operator site for Phd (O_{R1/2}) (Magnuson *et al.*, 1996). Each half site of the inverted repeat has been shown to be occupied by a Phd₂ dimer which binds with K_d ~ 3 μ M and Doc increases the affinity 10-fold by forming a Phd₂-Doc^{H66Y} complex as interaction of the

Phd C-terminus with Doc^{H66Y} promotes allosteric folding of the Phd N-terminal domain and dimerisation (Garcia-Pino *et al.*, 2010). The Doc-induced folding of Phd is aided through an α -helix, which connects the C-terminus with the N-terminal DNA-binding domain.

Doc^{H66Y} has previously been crystallised with Phd^{52-73Se} C-terminal donor, which revealed that the Phd C-terminus forms a kinked α -helix, which in one part makes hydrophobic interactions (residues 54-62) with Doc^{H66Y} and in another makes charge complementation (residues 64-72) with positive charges on the Doc^{H66Y} surface (Figure 6A) (Garcia-Pino *et al.*, 2008). The Doc toxin contains a reduced Fic-fold (discussed in Chapter 2) in which a missing α -helix that is present in Fic, is provided by the C-terminal α -helix of Phd. This suggests fold complementation and that Doc and Fic share an evolutionary origin. Phd does not directly interfere with putative conserved active site residues of Doc and Phd most likely either inhibits access to the ribosome or induces a conformational change in Doc (Figure 6A) (Garcia-Pino *et al.*, 2008).

In its free state, Phd is an intrinsically unstructured protein, which makes it susceptible to proteases and it has been shown that Phd is degraded by the ATP-dependent protease ClpXP *in vivo* ($T_{1/2} \sim 120$ min) (Lehnerr and Yarmolinsky, 1995). A recent crystal structure of Phd-Doc revealed a Phd₂-Doc-Phd₂ complex in which Doc toxin bridges two Phd₂ dimers (Figure 11A) (Garcia-Pino *et al.*, 2010). The C-terminus of one Phd₂ dimer interacts with Doc by high affinity interactions as described above, the C-terminus of the other Phd₂ dimer however only makes low affinity hydrophobic interactions (residues 52-62) with Doc, which occurs at a distinct binding site (Figure 11B). This particular configuration explains the observed increased cooperative binding of Phd to *phd-doc* operator in the presence of Doc (Garcia-Pino *et al.*, 2010). Gel shift assays with *phd-doc* operator at different Doc:Phd ratios revealed that Phd-Doc can form complexes with different stoichiometry, which also bind DNA with high affinity. At Doc:Phd ratios from 0.25 to 0.75 Phd-Doc form complexes which are consistent with; Phd₂-Doc-Phd₂, Doc-Phd₂-Doc-Phd₂ and Doc-Phd₂-Doc-Phd₂-Doc complexes. However at a Doc:Phd ratio of 1 and above only smaller complexes with a low affinity for DNA are observed, which are consistent with Doc-Phd₂-Doc complexes. This can be explained as the low affinity bound Phd₂ C-termini are titrated on to high affinity binding sites on free Doc at a Doc:Phd ratio of 1. The Doc-Phd₂-Doc complexes formed are deficient in

FitA binds to *fitAB* operator relatively strong in the absence of FitB ($K_d \sim 176$ nM), but the affinity is increased about 38-fold in presence of FitB ($K_d \sim 4.5$ nM) (Wilbur *et al.*, 2005). The crystal structure of FitA-FitB bound to IR36 has been solved (Figure 12A) (Mattison *et al.*, 2006). The structure revealed that FitA, similarly to CcdA and RelB, interacts with DNA through a two-stranded antiparallel β -sheet formed by dimerisation of two FitA monomers. The C-terminus of a FitA monomer makes intimate contacts with α -Helix (α) 1, 2 and 4 of a FitB monomer (Figure 12B). In the DNA bound complex FitB forms a homodimer, which bridges between FitA dimers bound to binding sites in the DNA (Figure 12A). The dimerisation of FitB is mediated by extensive contacts between α 3 of one FitB monomer with α 5 of the other. Phe78 in the α 4- α 5 loop is a key residue in this dimerisation, as are several hydrophobic residues in α 3 (Ala41, Leu45 and Ala48) and α 5 (Tyr86, Ala87 and Ser91) and a single salt bridge (formed between Arg44 (α 3) and Glu80 (α 5)). This configuration of FitA and FitB dimers forms a closed circular unit of two heterotetramers [FitA₂-FitB₂]₂. This allows the FitB dimer to act as a bridge between the FitA dimer bound to each half-site of the DNA inverted repeat, which mediates strong cooperative binding of FitA to operator DNA. The interactions of the two FitA₂ dimers with operator DNA in the crystal structure was mapped to each of the half sites in the inverted repeat, which is consistent with the DNase I footprint of FitA (Figure 12E). Interestingly, the α 3 of the FitA C-terminus wraps around the FitB monomer and positions a positive Arg68 residue in the otherwise negative FitB active site composed of Asp5, Glu42, Asp104 and Asp122 (Figure 12C). The position of Arg68 is thought to expel any divalent metal ions bound to the active site and inactivate the enzyme (Mattison *et al.*, 2006). A similar mechanism has more recently been proposed for neutralisation of VapBC-6 of *M. tuberculosis*. VapB-6 positions Arg75 in the vicinity of the active site of VapC-6, which is suggested to affect metal ion acquisition (Figure 12D) (Miallau *et al.*, 2009).

Autoregulation has also been described for *vapBC* from *M. smegmatis* and the *vapBC* homologue *ntrPR* of *S. meliloti* (Bodogai *et al.*, 2006; Robson *et al.*, 2009). NtrP antitoxin contains an N-terminal AbrB-like DNA binding domain similar to MazE. The *ntrPR* locus is transcribed from a single promoter and a 34 bp stretch in the promoter region is protected by *E. coli* extracts containing NtrP and NtrR in DNase I footprinting assays. The protected region contains a direct repeat, which acts as *ntrPR* operator site (5'-TTCGGCATATACATTTAGGCATATACAAGG-3'). In the

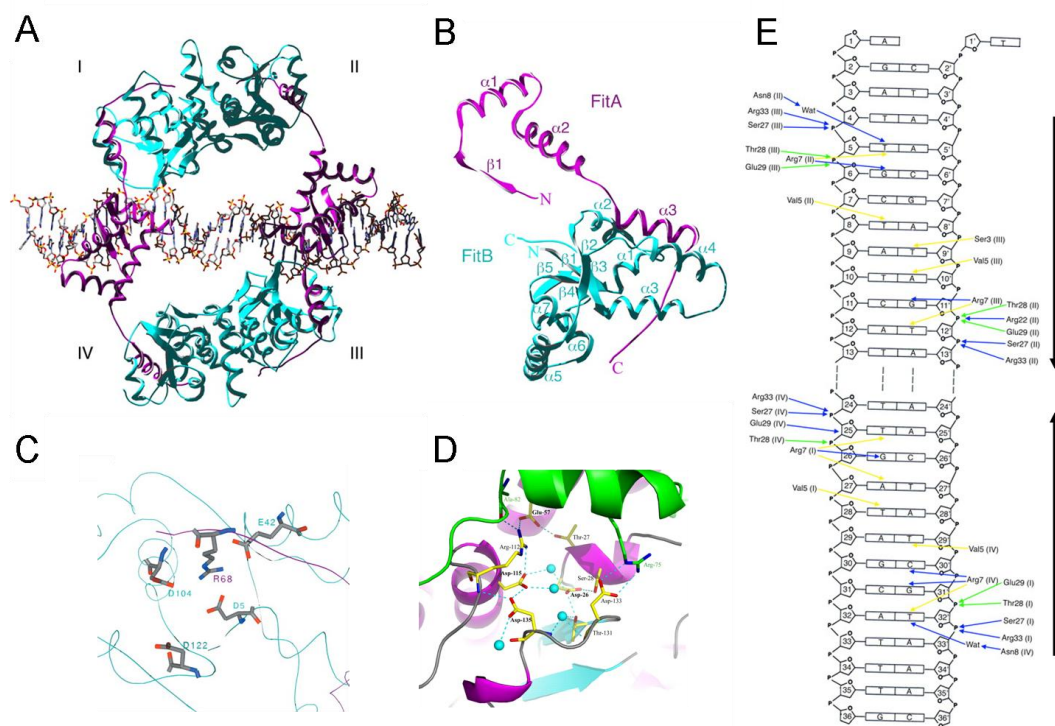


Figure 12 Interactions in the VapBC TA complex. **A**) [*FitA*₂-*FitB*₂]₂ octamer of four heterodimers bound to DNA containing *fitAB* operator site (IR36). The *fitA* and *FitB* proteins are coloured in magenta and cyan, respectively. **B**) *FitA* and *FitB* heterodimer secondary structure is labelled and position of N and C-termini. **C**) Interactions of Arg68 of *FitA* C-terminal with the active site of *FitB*. **D**) Interactions of Arg75 of *VapB*-5 C-terminal (Green) with the active site of *VapC*-5 (Magenta, Residues in yellow sticks). **E**) Interactions made by *FitA* dimer N-terminal residues with DNA operator sites (indicated by black inverted arrows). Blue arrows are side chain DNA hydrogen bonds, Green arrows are amide-DNA hydrogen bonds and Yellow arrows are Van der Waals contacts. Adapted from (Mattison et al., 2006; Miallau et al., 2009).

absence of NtrR, NtrP failed to significantly bind the *ntrPR* operator *in vivo*, which suggests that NtrR acts as a corepressor and is needed for efficient repression of transcription (Bodogai *et al.*, 2006). Gel shifts using a probe lacking one of the direct repeats abolished NtrP-NtrR binding, suggesting that NtrR mediates cooperative binding of NtrP to the operator sites. This mechanism is consistent with *FitA*-*FitB* mediated operator binding and though operator sites have different architecture, could represent a general mechanism for transcriptional autoregulation for *vapBC* TA loci. No data is available on the stability of *VapB*/*FitA*. However, *FitA* has a secondary structure similar to RelB, which suggest a short half-life, especially in its unbound state. Although transcriptional regulation of different TA families has been extensively studied over the years, the regulation of *vapBC* TA family still remains unclear.

New regulatory interactions with TAs

It is clear that TAs have evolved conserved strategies to maintain the toxin and antitoxin levels in equilibrium in the cell, which is dependent on the antitoxin/toxin ratio.

Several of the chromosome encoded Type I TAs (e.g. *symRE*, *tisAB*) of *E. coli* are induced by the SOS response (Gerdes and Wagner, 2007). The SOS response refers to genes that are up-regulated upon DNA damage, and LexA repressor protein plays a central role in transcriptional repression under non-damage conditions (Reviewed in (Butala *et al.*, 2009)). SOS induced genes include; *dinB*, *recA*, *ruvA* and *ruvB*, which are required for stress-induced mutagenesis. Recently, LexA binding boxes have been identified in promoter regions of two *E. coli* type II TAs *dinJ-yafQ* and *yafNO*, whereas both genes were up-regulated in response to DNA damage (Prysak *et al.*, 2009; Singletary *et al.*, 2009; Christensen-Dalsgaard *et al.*, 2010). LexA was shown to specifically bind the LexA box in *dinJ-yafQ* promoter region *in vitro*, consistent with repression. The majority of *yafNO* up regulation in response to SOS was, however, found to result from co-transcription from the upstream *dinB* SOS gene (Singletary *et al.*, 2009). The function of these TAs in the SOS response are still unclear and TA deletion mutants did not show any effect on viability in response to DNA damage (Prysak *et al.*, 2009; Singletary *et al.*, 2009).

TA transcription can also be regulated by transcriptional activators. γ -proteobacteria *Haemophilus influenza* and *Vibrio cholera* are naturally competent and encode genes involved in DNA uptake and processing (Redfield *et al.*, 2005). Competence related genes are transcriptionally activated by Sxy protein in concert with cyclic AMP receptor proteins (CRP). *E. coli* is not naturally competent but contains *sxy* gene and CRP-S binding sites, which are also found to be present in promoter regions of *prlF-yhaV*, *hicAB*, *higBA* and *chpB* TAs (Sinha *et al.*, 2009). Interestingly, microarray analysis of *sxy* overexpression led to increased transcription of these TAs, suggesting that Sxy and cAMP-CRP could stimulate activity of TAs. Whether this regulation is genuine and whether TAs are involved in competence is still unknown.

Utilisation of host transcription factors is, however, not the only way TAs can be incorporated into general stress response pathways. Very recently, a SecB-like chaperone (Rv1957) has been identified in *M. tuberculosis*, which specifically prevents aggregation and degradation of HigA of the *higBA* TA locus (Bordes *et al.*,

2011). In bacteria, the SecB chaperone binds and presents preproteins targeted for secretion to the SecA motor component of the sec translocon (Reviewed (Driessen and Nouwen, 2008)). SecB has general chaperone properties and can, to some extent, complement the activities of DnaK and Trigger factor (Ullers *et al.*, 2004). Rv1957 ORF overlaps with the stop codon of *higA* ORF, which suggest that Rv1957 is part of a TAC system (*toxin antitoxin chaperone*). The TAC system has the potential to respond to export stress as the chaperone can be titrated by other proteins. This in turn inhibits the activity of HigA and activates HigB toxin (Bordes *et al.*, 2011). Observations like this suggest that there might be a cohort of undiscovered mechanisms by which TAs can be adapted into regulatory pathways. The following Chapter will concern the different models of proposed biological functions of TAs.

Chapter 4: Models

Models for the biological function(s) of chromosomal TAs

At present the toxin-antitoxin research field is rapidly expanding and several research groups have presented models for the biological function of chromosome encoded TAs.

The simplest biological model is that chromosomal TAs perform similar tasks to their plasmid encoded counterparts. It has recently been shown that TAs might stabilise mobile genetic elements such as superintegrons or integrative and conjugative elements (ICE). SXT is an ICE found in clinical isolates of *Vibrio cholerae* often carrying antibiotic resistance genes (Wozniak and Waldor, 2009). For SXT to undergo conjugation, it is excised from the chromosome and circulated and under this condition SXT stability is maintained by a TA locus, *mosAT*. Similar observations have been made for the superintegron of *Vibrio vulnificus* in which TAs have been suggested to stabilise flanking DNA regions, preventing loss during recombination events (Szekeres *et al.*, 2007).

In addition to the function of TAs in stabilising DNA, the opposite has also been proposed (Saavedra De *et al.*, 2008). Chromosomal TAs are suggested to be able to stimulate loss of DNA containing homologous TAs by counteracting toxin activation, which results in anti-addiction. Whether the biological function is to promote stability or anti-addiction or just a unspecific consequence of the antitoxin and toxin properties is still unclear and few examples have been reported.

In recent years it has become apparent that the activities of toxins induce bacteriostatic growth inhibition, which suggests that TAs are involved in growth rate regulation rather than cell killing (Gerdes *et al.*, 2005). The fact that type II TAs are prevalent in free-living organisms and can be activated by proteolysis of an unstable antitoxin makes TAs capable of responding to changes in the rate of translation and increased protease activity. In the following section the more commonly applied models for TA function will be outlined.

Implications of TAs in bacterial stress response and pathogenesis

Free-living bacteria have evolved elaborate strategies to survive and adapt to changes in their environment such as changes in osmotic potential, temperature and nutrient

availability. Bacteria sense environmental changes and respond through changes in the global gene expression profile, which shuts down or turns on expression of genes that assist the cell in restoring homeostasis and environmental tolerance. This is mainly governed by two-component systems and alternative dissociable sigma factors of RNA polymerase (Krell *et al.*, 2010; Osterberg *et al.*, 2011). In the utilization of alternative sigma factors, ppGpp has a central function, whereas it affects the efficiency of alternative σ factors in competition with σ^{70} housekeeping sigma factor for core RNA polymerase. σ^{70} has the highest affinity for core RNA polymerase and therefore the majority of RNA polymerases are occupied with σ^{70} during steady state growth: approximately 70% are employed in transcribing rRNA operons (Raffaello *et al.*, 2005). However, when the level and activity of alternative sigma factors increase e.g. during stress or when entering stationary phase, alternative sigma factors compete with σ^{70} for core RNA polymerase directing transcription to other genes. Stationary phase/stress induced molecules as ppGpp and Rsd (anti-sigma factor) increase the ability of alternative sigma factors to compete for core polymerase (Bernardo *et al.*, 2006; Jishage *et al.*, 2002; Jishage and Ishihama, 1998). Gram-negative bacteria uses two different pathways to produce (p)ppGpp (guanosine 3'-diphosphate 5' triphosphate, which is subsequently hydrolyzed to ppGpp): a RelA- and a SpoT-dependent pathway. RelA associates with the ribosome and synthesizes (p)ppGpp in response to deacylated tRNA in the ribosomal A-site and therefore responds to amino acid limitations (Wendrich *et al.*, 2002). This is also referred to as the stringent response. SpoT is a bifunctional (p)ppGpp synthetase that also has hydrolase activity and regulates the (p)ppGpp levels in response to most conditions other than amino acid starvation. However, mechanisms for SpoT activation are still unclear (Gentry and Cashel, 1996; Potrykus and Cashel, 2008). The alarmone, ppGpp, binds RNA polymerase and exerts both direct negative and positive effects on transcription depending on the promoter (Kvint *et al.*, 2000). Generally, σ^{70} -dependent promoters involved in growth and proliferation are negatively regulated, while σ^{70} -dependent promoters involved in maintenance and stress defence are positively regulated during stringent response (Chang *et al.*, 2002). The mechanism for how ppGpp directly exerts this dualistic function depending on the type of promoter is still unclear and different models have been suggested (Magnusson *et al.*, 2005). These include effects on RNA polymerase open complex formation and stability, thereby affecting mostly

promoters with intrinsically unstable open complexes (e.g. rRNA promoters), but also promoter clearance has been proposed.

The direct effects of ppGpp is enhanced by DksA, a protein that has structural resemblance to transcriptional elongation factor GreA, and binds the RNA polymerase (Perederina *et al.*, 2004;Paul *et al.*, 2005). Both ppGpp and alternative general stress response sigma factor σ^S (encoded by *rpoS*) have been found to be important not only for stress but also virulence (Dalebroux *et al.*, 2010;Dong and Schellhorn, 2010).

Early studies have shown that protein degradation increases during conditions of amino acid starvation and is important for adaptation. This is primarily due to the activity of ATP-dependent proteases (e.g Lon , Clp and FtsH) (Sussman and Gilvarg, 1969;Maurizi, 1992). More recently it has been shown that activity of Lon protease changes in response to accumulating levels of polyphosphate, which is a consequence of ppGpp mediated inhibition of PPX (exopolyphosphatase) activity (Kuroda *et al.*, 1997;Kuroda *et al.*, 2001). Polyphosphate binds to Lon and stimulates degradation of idling ribosomal proteins and could thus establish a link between protein turnover and stringent response creating an endogenous source of amino acids (Kuroda, 2006). Increased protease activity is not only observed under nutrient deprivation, but also under conditions of heat shock where proteases help to regulate alternative sigma factors and chaperones as well as degrading misfolded proteins (Meyer and Baker, 2011).

In general, TAs are up-regulated in response to translation inhibition induced either by amino acid starvation or treatment with antibiotics, which depends on activities of cellular proteases (Christensen *et al.*, 2001;Christensen *et al.*, 2003;Jorgensen *et al.*, 2009;Christensen-Dalsgaard *et al.*, 2010). This is in agreement with the turnover of labile antitoxins when *de novo* synthesis is decreased, which in turn liberates the toxin to act on its target and reduce the growth rate.

Induction of TAs in response to antibiotics has also been reported in organisms as diverse as *Streptococcus pneumoniae* and *Mycobacterium tuberculosis* (Singh *et al.*, 2010;Nieto *et al.*, 2010). In *M. tuberculosis* several TAs were also found to be up-regulated during anoxic growth and in infected human macrophages (Korch *et al.*, 2009;Ramage *et al.*, 2009). Interestingly, some TAs were up-regulated specifically under anoxic growth, whilst others were only up-regulated during macrophage infection. This indicates that these TAs might respond to virulence and different

environmental cues. In addition to these observations, mutants of *vapBC* homologue *fitAB* of *Neisseria gonorrhoea* were shown to increase replication during intracellular growth in epithelial cells (Hopper *et al.*, 2000). This did not affect host-independent growth, which suggests that *fitAB* can affect the growth rate during infection. Similarly, mutants of another *vapBC* homologue, *ntrPR* of *Sinorhizobium meliloti*, allow the bacterium to form root nodules with leguminous plants more efficiently, and fix more nitrogen than wild-type, consistent with mutants having higher transcription and translation capacity (Olah *et al.*, 2001;Puskas *et al.*, 2004). It appears that these TAs limit bacterial growth upon encountering eukaryotic host cells.

Recently it has been observed that TAs in archaea also respond to stress as several *vapBC* loci of *Solfolubus solfataricus* are up-regulated in response to heat shock (Tachdjian and Kelly, 2006;Cooper *et al.*, 2009). Interestingly, disruption of a single *vapBC* locus (out of ~26 TA loci) resulted in significant loss of viability after heat shock, which suggest that this specific *vapBC* locus is involved in heat shock survival. Ectopic expression of Lon protease in *E. coli*, which inhibits translation, has been shown to induce strong cleavage in the ribosomal A-site dependent on the *yefM/yoeB* TA-system (Christensen *et al.*, 2004). A-site cleavage is observed in response to amino acid starvation and ectopic expression of mRNA interferases such as RelE and MazF (see Chapter 2). Interestingly, A-site cleavage has also recently been observed by ectopic expression of Doc toxin in *E. coli*, which is a result of *trans*-activation of mRNA interferases from the *E. coli* chromosome. Doc inhibits translation and was found to activate RelE-dependent A-site cleavage (Garcia-Pino *et al.*, 2008). This observation also suggests that the mechanism by which translation is inhibited can activate specific TAs to cleave mRNA (see Chapter 2). Ribosomal A-site cleavage and *trans*-translation activity in response to amino acid starvation is also observed in a strain deleted for five chromosomal TAs ($\Delta 5$: *relBE,yefM/yoeB,dinj/yafQ,mazF, chpB*) (Li *et al.*, 2008b). This suggests that these five systems are not required for A-site cleavage, but does not exclude that other mRNA interferases, which are present in *E. coli*, may contribute to *trans*-translation and mRNA quality control. Activation of toxins that cleavage mRNA during amino acid starvation are therefore suggested to rapidly contribute to adjustment of rates of nutrient and energy consumption to a lower level (Gerdes *et al.*, 2005). The toxin-mediated reduction in the global rate of translation results in a lower drain on charged tRNA pools which would produce a lower level of translational errors (Sorensen *et al.*, 1994;Sorensen, 2001;Dittmar *et*

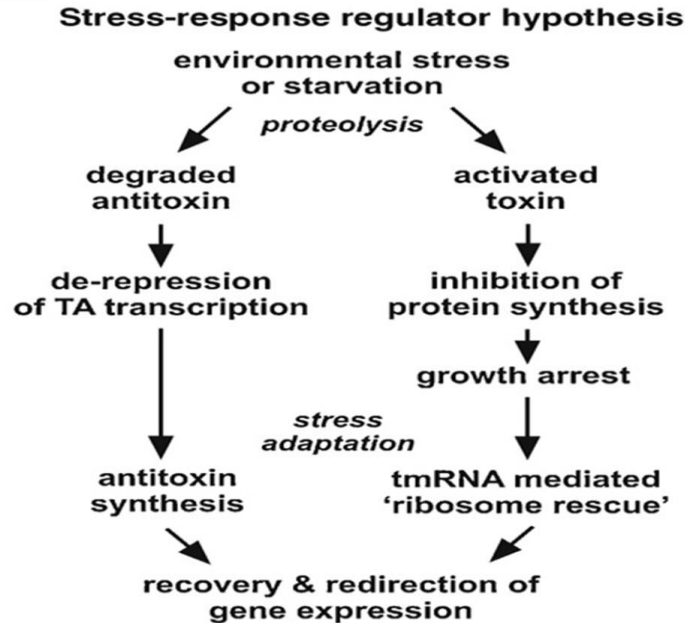


Figure 13 The stress response model for TAs. Environmental stress or starvation leads to proteolysis of the antitoxin and activation of the toxin. The toxin inhibits translation by mRNA cleavage, which results in growth inhibition and adjustments in the translation machinery. This may help stress adaptation as stalled ribosomes are recycled by *trans*-translation and redirected to translate certain mRNAs or reduces translation with increased fidelity. Stress adaptation results in antitoxin production and toxin neutralisation, which in turn recovers translation and growth. Adapted from (Hayes and Low, 2009).

al., 2005) Stalled ribosome complexes can be recycled by toxin-dependent or -independent A-site cleavage and subsequent *trans*-translation.

An alternative model predicts specific environmental cues as activators of TAs to degrade specific mRNAs, which redirects translation to those which are not cleaved (Ramage *et al.*, 2009; Wang and Wood, 2011). Proteome remodelling has been proposed to be important for heat shock in *S. solfataricus* in which VapC mediates degradation of specific mRNAs, resulting in increased survival during heat shock (Maezato *et al.*, 2011). Similar models have been proposed for MazF_{sa} of *Staphylococcus aureus* and MazF_{mt-3} and MazF_{mt-7} of *M. tuberculosis* as the toxins have very rare cleavage sites (Zhu *et al.*, 2008; Zhu *et al.*, 2009) (summarised in Figure 13).

An interesting new interaction with the general stress response has recently been discovered, mediated by the *mqsR-mqsA* TA locus of *E. coli* (recently reviewed in (Wang and Wood, 2011)). The *mqsR-mqsA* TA locus is up-regulated in *E. coli* biofilms and its deletion significantly reduces biofilm formation (Ren *et al.*, 2004; Gonzalez Barrios *et al.*, 2006; Kasari *et al.*, 2010). MqsA antitoxin has recently been shown not only to autoregulate *mqsR-mqsA* transcription, but also directly

represses transcription of DNA replication inhibitor *cspD* and alternative stress sigma factor σ^S by binding to *mqsR-mqsA*-like inverted repeats in the promoter region (Kim *et al.*, 2010; Wang *et al.*, 2011). Lon protease degrades MqsA and is necessary for the activity of *mqsR-mqsA*, which makes it a protease-sensitive switch. Degradation of MqsA is suggested to increase transcription of *rpoS* as well as to liberate MqsR toxin to cleave mRNA and redirect translation. MqsR is a GCU-specific RNase and fourteen GCU-deficient mRNAs exist in *E. coli*, of which six are up-regulated in biofilms, which suggest a possible link (Yamaguchi *et al.*, 2009).

Other TAs have also been suggested to be involved in biofilm formation as a strain deleted for five TAs (*mazEF*, *relBE*, *chpB*, *yefM-yoeB*, *dinj-yafQ*) as well as single deletions showed decreased production of biofilm (Kim *et al.*, 2009; Kolodkin-Gal *et al.*, 2009).

Multicellular communities of biofilms are highly tolerant to antibiotics in which the organisms often adopt a dormant growth state resembling that of persisters (Shah *et al.*, 2006). It has been suggested that MqsR and toxins in general can contribute to such a quasi-dormant growth state (Wang and Wood, 2011).

TAs in Persistence – tolerance to antibiotics

Persisters are dormant non-dividing variants of normal cells that form stochastically in a microbial population, particularly in biofilms, which serve as a protective habitat for persisters. Recently reviewed (Lewis, 2010). When cells are treated with antibiotics, most bacterial cells die but persisters survive; if survivors are re-inoculated with antibiotics the same biphasic pattern is observed. Hence, these cells are tolerant rather than resistant. Persisters have been implicated in the recalcitrance of chronic infectious disease to antibiotic treatment.

Several independent studies have implicated TAs in persistence. Persistence was initially linked to TAs by isolation of *E. coli* mutants of *hipA* which induced high level of persisters (see Chapter 2) (Moyed and Bertrand, 1983). Recently, key insights to *hipBA*-mediated increase in persisters have been made, which describes a threshold based model that determines persistence depending on the level of HipA in the cell (Rotem *et al.*, 2010). Overexpression of toxins leads to a quasi-dormant growth state very similar to persisters, which are both highly tolerant to antibiotics (Vazquez-Laslop *et al.*, 2006).

Consistent with TAs being involved with persister cell formation, several TAs (*mazEF*, *dinj-yafQ*, *relBE*, *yefM-yoeB*, *mqsR-mqsA*) were up regulated in isolated persisters (Shah *et al.*, 2006). The deletion of *mqsR-mqsA* or only *mqsR* in both cases decreases the number of persisters, which could be reverted by MqsR-MqsA production suggesting that the toxin is involved in facilitating dormancy (Kim and Wood, 2010). In addition to type II TAs, Type I TA *tisAB* has been shown to increase persistence in response to DNA damage induced by ciprofloxacin treatment (Dorr *et al.*, 2010).

Very recently it was shown that successive deletions of ten mRNA interferase toxins in *E. coli* were shown to decrease the persister frequency 100- to 200-fold after treatment with ciprofloxacin or ampicillin (Maisonneuve *et al.*, 2011). This indicates strong redundancy between mRNA interferases as the strongest effect on persister frequency was observed after successive deletion of five TAs. The decrease in persister frequency was dependent on Lon protease, which is consistent with Lon-dependent stochastic degradation of the antitoxin in a subpopulation of growing cells.

Programmed Cell Death and phage abortive system

Biofilm formation often involves cell-to-cell signals such as quorum sensing molecules (Davies *et al.*, 1998). The *mqsR-mqsA* TA locus has previously been linked to the autoinducer-2- quorum sensing system which stimulates biofilm formation in response to autoinducer-2 (AI-2) (Gonzalez Barrios *et al.*, 2006).

An early study by Engelberg-Kulka and co-workers showed that *mazEF* expression is inhibited by increased levels of ppGpp (Aizenman *et al.*, 1996). This is proposed to decrease transcription of *mazEF* and to stimulate MazE degradation and MazF activation. This in turn kills a subpopulation of cells by an altruistic suicide mechanism beneficial to the surrounding population and is also referred to as programmed cell death (PCD). Similarly, mutants lacking *mazEF* were also shown to be significantly more resistant to a variety of stress conditions including different antibiotics, thymine-/amino acid starvation, high temperatures and oxidative stress (Sat *et al.*, 2001; Sat *et al.*, 2003; Kolodkin-Gal and Engelberg-Kulka, 2006; Hazan *et al.*, 2004). Analogous to biofilm autoinducers, *mazEF* has recently been shown to be activated in response to a small pentapeptide quorum sensing molecule, referred to as extracellular death factor (EDF) (Kolodkin-Gal *et al.*, 2007). The EDF molecule (Asn-Asn-Trp-Asn-Asn) is secreted in response to high culture density and increases

MazF mediated cell killing. Very recently it has been shown that EDF most likely acts by amplifying the endoribonucleolytic activity of MazF and the MazF homologue ChpBK (Belitsky *et al.*, 2011).

A role for MazF-mediated PCD in preventing spreading of phage P1 infections has also been proposed (Hazan and Engelberg-Kulka, 2004). Interestingly, this observation requires cross-talk between two different TA-loci namely, *phd-doc* from P1 phage and the *mazEF* locus of the *E. coli* chromosome. A similar role has also been proposed for a new putative TA locus *rnIAB* (*RNase LS*) as it was shown to efficiently inhibit reproduction of T4 Phage (Koga *et al.*, 2011).

Whether *mazEF* mediated PCD is a universal or a strain specific observation is not clear, as this phenomenon has not yet been observed by other groups (Gerdes *et al.*, 2005;van Melderen, 2010). It is obvious that many models exists, which describe the possible benefits by having TAs on the chromosome. Nevertheless it is still far from clear and will undoubtedly be the subject of many future studies.

Results Section I: The Molecular and Cellular target of Enteric VapC toxins

Introduction to the experimental work

The subject of this thesis concerns the characterization of prokaryotic *vapBC* loci. Since the discovery of the first *vapBC* locus in 1992, *vapBC* TA loci have been the topic of many studies and, though VapC homologues are now identified as PIN domain proteins with proposed nucleolytic activity, the cellular target and physiological function of *vapBC* and PIN domains in general are still unknown. The vast number of *vapBC* loci identified in both Bacteria and especially Archaea makes *vapBC* a very interesting TA locus. In addition, interesting observations have been made regarding its possible involvement in pathogenesis and growth under stress conditions.

The experimental work presented in Results Section I focuses on the identification of the cellular target of VapC. *E. coli* K-12 is used as a model organism in all *in vivo* studies presented here.

The bioinformatics study by Pandey and Gerdes showed that *Escherichia coli* K-12 does not contain chromosomally encoded *vapBC* loci (Pandey and Gerdes, 2005). However recent protein-protein BLAST (<http://blast.ncbi.nlm.nih.gov/Blast.cgi>) searches for VapC-like proteins revealed the presence of homologues in several recently sequenced isolates of pathogenic *E. coli* including strain: EIEC 53638, EHEC MS146-1, EHEC H120 and EHEC M863. Enteroinvasive (EIEC) *E. coli* share similarities with *S. flexneri* and *Salmonella* Typhimurium as they invade and proliferate inside epithelial cells (Tsolis *et al.*, 2008). VapC has previously been phenotypically linked to intracellular growth of human pathogen of *Neisseria gonorrhoea* which makes these VapCs an interesting subject of study (Hopper *et al.*, 2000).

The *vapBC* locus of the human pathogen *Salmonella enterica* serovar Typhimurium LT2 was selected as the model system for this study. The *vapBC* locus of *S. enterica* LT2 chromosome (STM3034, STM3033) has been predicted to have the same genetic organization as *E. coli* K-12 *relBE* (Pandey and Gerdes, 2005). Furthermore, *vapBC* homologue, *mvpAT* from *Shigella flexneri* 2a YSH6000 virulence plasmid pMYSH6000, which have been shown to be active in *E. coli* K-12 derivatives (Sayeed

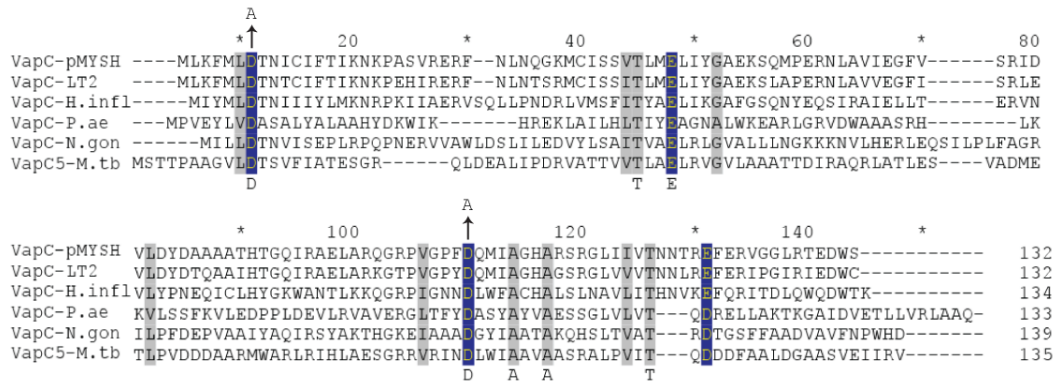


Figure 14 Alignment of experimentally analysed Prokaryotic VapC PIN-domain proteins. The quartet of highly conserved negatively charged amino acid residues that form the catalytic site and bind Mg^{2+} are shown as blue columns. The D to A change in VapC_{LT2} is indicated with an arrow. PIN domains were initially suggested to have RNase activity due to structural features shared with RNase H and Flap endonucleases that have a quartet of conserved acidic residues stabilising an Mg^{2+} in its catalytic centre. This was later confirmed by crystal structures (Clissold and Ponting, 2000; Arcus *et al.*, 2004). VapC_{H.infl} from *Haemophilus influenzae* has non-specific ribonuclease activity in HEPES buffer containing 15 mM NaCl (Daines *et al.*, 2007); VapC from the archaon *Pyrobaculum aerophilum* has a Mg^{2+} dependent exonuclease activity in 20 mM NaCl + 10 mM $MgCl_2$ (Arcus *et al.*, 2004). The *vapBC* (*fitAB*) locus of *Neisseria gonorrhoeae* delays intercellular trafficking of the bacterium in an *in vitro* infection model (Mattison *et al.*, 2006); VapC5 of *M. tuberculosis* has Mg^{2+} dependent, non-specific RNase activity (Miallau *et al.*, 2009).

et al., 2000), is also investigated in this study. An alignment of *S. enterica* LT2, STM3033 (referred to as VapC_{LT2}), *S. flexneri* 2a pMYSH6000 MvpT (referred to as VapC) with previously characterised VapCs show that, despite the overall low sequence similarity between the different PIN domain proteins, the putative active site residues of the PIN domain are conserved (Figure 14). The primary objective of this section is to identify the molecular and cellular target of enteric VapC toxins.

VapC toxin expression leads to bacteriostatic inhibition of translation

To test the activity of VapC_{LT2} of *S. enterica* LT2 and VapC from *S. flexneri* YSH600 virulence plasmid pMYSH6000 in *E. coli* K-12, VapC_{LT2} and VapC were cloned onto low copy plasmids in front of an arabinose inducible promoter. In addition, corresponding antitoxins, VapB_{LT2} and VapB were cloned onto low copy R1 plasmids in front of an IPTG inducible promoter. The activity of toxin and antitoxin was assayed by counting the colony forming units (CFU) of cells expressing toxin with and without subsequent antitoxin expression (Figure 15). It is observed that VapC_{LT2} and VapC are potent toxins in *E. coli* K-12 cells, which reduce CFU $\sim 10^4$ -fold 30 min after addition of arabinose. Furthermore, it is observed that if cells are plated onto agar plates containing IPTG, which allows transcription of antitoxin, cells regain almost full viability (compared with vector control). Efficient resuscitation can be

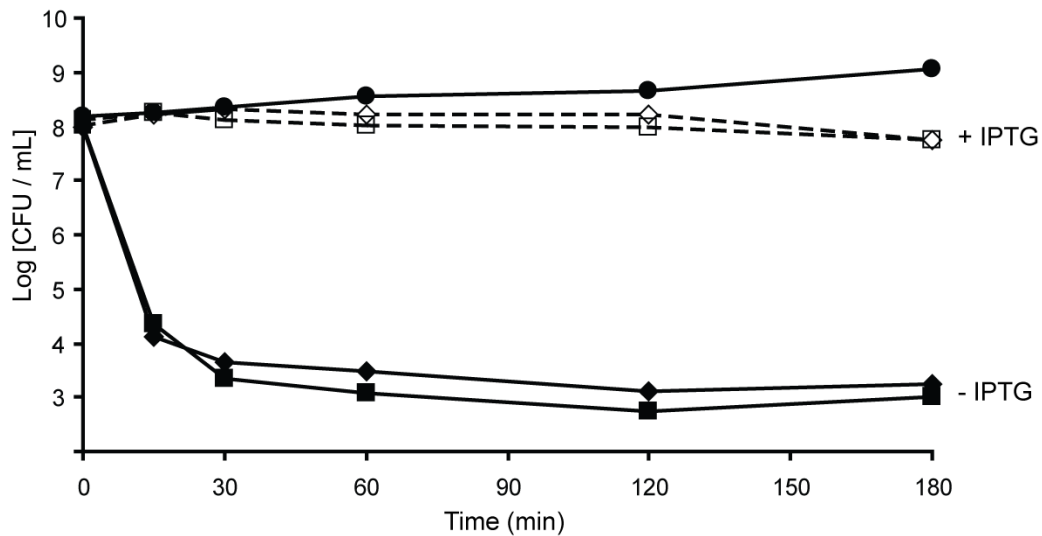


Figure 15 The *vapBC* locus from *S. typhimurium* LT2 and *vapBC* from *S. flexneri* pMYSH6000 are bona fide TA-loci. *E. coli* K-12 MG1655 carrying the following plasmids; pBAD33 and pNDM220 (vector) (●), pKW52 (pBAD::SD_{opt}::*vapC*_{LT2}) and pKW51 (pA1/04/03::SD_{opt}::*vapB*_{LT2}) (◆ -IPTG and ◊ +IPTG), pKW82 (pBAD::*vapC*) and pKW81 (pA1/04/03::*vapB*) (◼ -IPTG and ◻ +IPTG) were grown exponentially in LB medium containing Cm (25 µg/mL) and Amp (30 µg/mL). Transcription was induced at time zero by adding 0.2% arabinose. Samples were taken out at time points indicated, diluted and plated on plates containing Cm 25 µg/mL, Amp 30 µg/mL, 0,2% glucose and with or without 2 mM IPTG.

obtained even after extended periods of toxin expression (180 min), which clearly shows that the toxin is bacteriostatic rather than being bacteriocidal.

To identify the molecular target of VapC_{LT2} and VapC, rates of DNA, RNA and protein synthesis were measured after toxin induction. *E. coli* K-12 strains containing VapC_{LT2} and VapC were grown in AB minimal medium (antitoxins were included in these strains to decrease toxicity of toxin in uninduced cells) and samples collected before and after toxin induction were pulsed for 1 min with methyl-³H-thymidine (DNA synthesis), ³H-uridine (RNA synthesis) or ³⁵S-methionine (protein synthesis). From Figure 16 A and B it is observed that ectopic expression of VapC_{LT2} and VapC does not reduce the global level of replication and transcription after 60 min which is comparable to RelE induction. The rate of replication and transcription seems to slightly increase after toxin induction, however decreases to the pre-induction level after 30 min. The rates of transcription and replication seem to follow similar trends after toxin induction and do not indicate any decrease. The rate of translation on the other hand decreases rapidly upon *vapC*_{LT2} and *vapC* induction (Figure 16C) to <10% of pre-induction levels which is comparable to the levels generated by expression of mRNA interferase RelE. This indicates that VapC_{LT2} and VapC, similar to mRNA interferases (such as RelE), target the translation machinery.

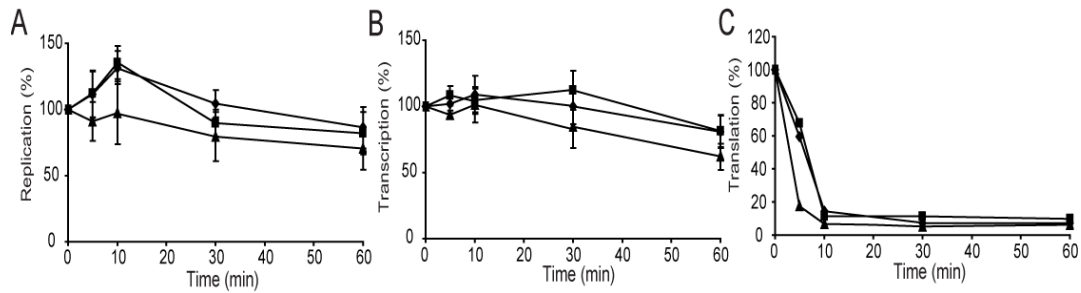


Figure 16 VapC toxins inhibit global translation. *E. coli* K-12 MG1655 carrying one of the following plasmids; pKP3035 (pBAD::*relE*) (▲), pKW52 (pBAD::*SD_{opt}::vapC_{LT2}*)/ pKW51 (pA1/03/04::*SD_{opt}::vapB_{LT2}*) (◆) or pKW82 (pBAD::*vapC*)/ pKW81 (pA1/03/04::*vapB*) (■) were grown exponentially in AB-minimal medium with 0.5% glycerol as carbon source and transcription of the toxins was induced by addition of arabinose (0.2%) at time zero. The rates of **A**) replication, **B**) transcription and **C**) translation were determined at time points indicated and the pre-induction rates were set to 100%. Results in A) and B) are shown as a mean \pm SE (n=4) and mean \pm SE (n=4), respectively.

VapC expression activates endogenous YoeB mRNA interferase to cleave mRNA at stop codons

VapC_{LT2} and VapC mediated inhibition of translation is consistent with the proposed nuclease activity of the PIN domain (see Introduction Chapter 2). In addition, the majority of the characterised mRNA interferases cleave mRNA and it is therefore plausible that VapC_{LT2} and VapC inhibit translation by mRNA cleavage. The tmRNA transcript was selected as a model RNA as it is translated, small, highly abundant and constitutively expressed during steady-state growth. The stability of the tmRNA transcript was monitored by Northern blot analysis before and after *vapC_{LT2}* and *vapC* induction. From Figure 17A (lanes 1-4 and 5-8) VapC_{LT2} and VapC expression slightly reduces the levels of matured full-length tmRNA indicating degradation. Interestingly, as the levels of tmRNA decrease (between 30 min and 60 min of induction) an RNA fragment of smaller size appears proportional to the decrease of full-length, which indicates specific cleavage. It is also observed that RelE expression decreases the level of full-length tmRNA (lanes 9-12), which is consistent with previous observations (Christensen and Gerdes, 2003). Furthermore, inhibition of translation by chloramphenicol does not affect the stability of tmRNA which suggests a specific effect of toxin induction (lanes 13-16).

To identify the location of the VapC_{LT2} dependent cleavage(s) observed in tmRNA, primer extension analysis was performed on RNA samples isolated in Figure 17A (Figure 17B). The specific cleavage is found to occur in the stop codon of the small reading frame inside tmRNA, which suggests that the cleavage is ribosome dependent

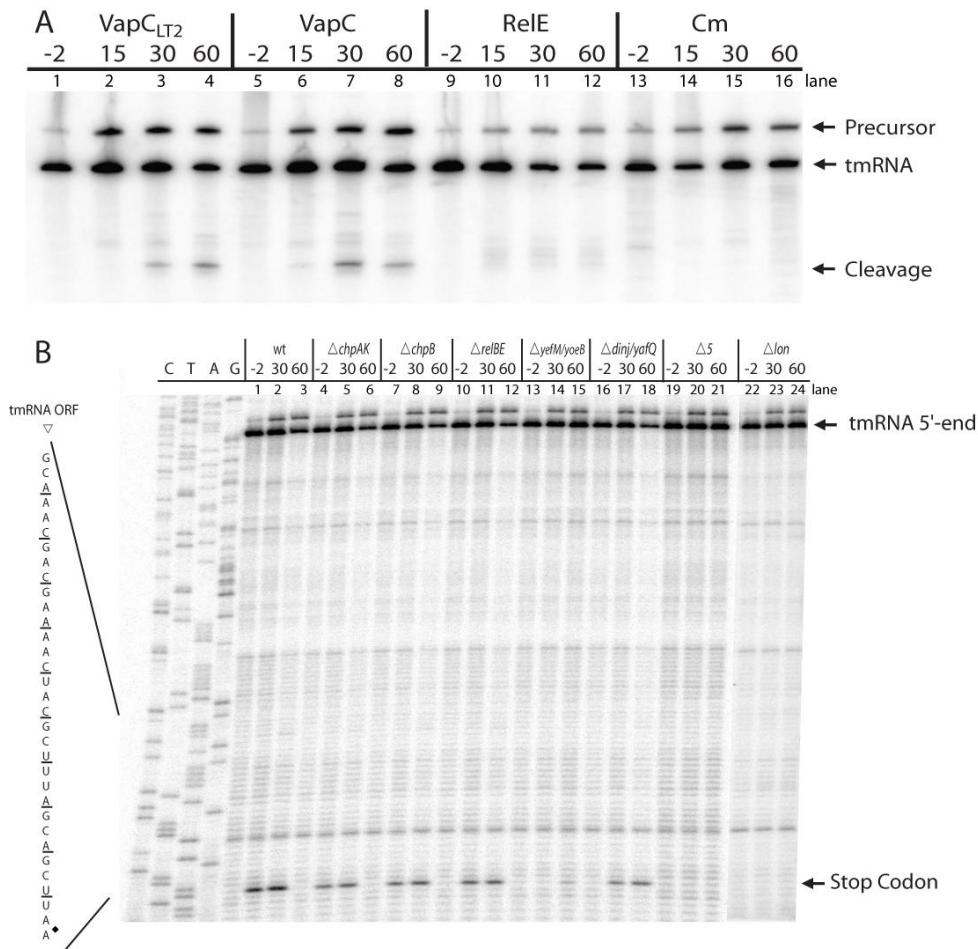


Figure 17 Expression of VapC toxins leads to activation of YoeB dependent cleavage in tmRNA. **A)** Northern blot analysis on tmRNA. *E. coli* K-12 MG1655 containing either; pKW52 (pBAD::SD_{opt}::vapCLT2), pKW82 (pBAD::vapC), pKP3035 (pBAD::relE) were grown exponentially in LB medium at 37°C. At time zero 0.2% arabinose was added to induce transcription. Cm (50 µg/mL) was added at time zero to MG1655 to inhibit translation and was used as a control. Total RNA was purified from the samples taken out at time points indicated (min) and fractionated by PAGE. **B)** Expression of VapC_{LT2} induces Lon-dependent YoeB cleavage in tmRNA. *E. coli* K-12 MG1655, MG1655 Δ chpAK (*mazF*), MG1655 Δ chpB, MG1655 Δ relBE, MG1655 Δ yefM/yoeB, MG1655 Δ dinJ/yafQ, MG1655 Δ 5 (lacks all five TA-loci) and MG1655 Δ lon carrying pKW52 (pBAD::SD_{opt}::vapC_{LT2}) were grown exponentially in LB medium at 37°C. At time zero 0.2% arabinose was added to induce expression of VapC_{LT2}. Bacterial samples were taken at time points indicated (min), RNA was isolated and primer extension analysis performed using primer 10SA-2.

(lanes 1-3). As VapC is found to inhibit global translation, it potentially also activates endogenous mRNA interferases present on the *E. coli* K-12 chromosome. This has previously been observed for Doc toxin expression (Garcia-Pino *et al.*, 2008). To confirm that this is not the case, primer extension was also performed on RNA purified from different mRNA interferase single deletion strains (Δ chpA, Δ chpB, Δ relBE, Δ yefM/yoeB and Δ dinJ/yafQ), as well as a strain deleted for the five mRNA interferases Figure 17B lanes 4-21). A Lon protease deficient strain is also investigated as Lon is the major protease responsible for antitoxin degradation (lanes

22-24). It is observed that cleavage occurs in all strains except strains lacking *yefM-yoeB* TA-locus and the Lon protease. YefM is a well known substrate for Lon protease (Christensen *et al.*, 2004). Surprisingly, this suggests that VapC_{LT2} and VapC mediated inhibition of global translation might *trans*-activate endogenous YoeB to cleave mRNA in the stop codon of RNA reading frames. Similar observation has been reported to occur as a result of global translation inhibition by Lon protease over-expression (Christensen *et al.*, 2004). Hence, ectopic expression of VapC_{LT2} and VapC does not directly affect the stability of tmRNA, but indirectly as inhibition of global translation activates YoeB mRNA interferase.

Ribosome dependent YoeB cleavage reveals possible ectopic initiation of translation at elongator codons, which depends on Shine & Dalgarno sequence

YoeB toxin is a ribosome dependent mRNA interferase *in vivo*, which cleaves between the 2nd and 3rd base in the A-site, but also degrades mRNA ribosome-independently *in vitro* (Christensen *et al.*, 2004; Kamada and Hanaoka, 2005; Christensen-Dalsgaard and Gerdes, 2008). To investigate whether VapC-induced YoeB activation leads to ribosome dependent cleavage as observed in the stop codon of tmRNA, primer extension analysis was performed on *dksA* mRNA after *vapC_{LT2}* induction. This was done by analysing different variants of *dksA* mRNA; one of which contains a premature termination codon and two which contains out of frame stop codons (Figure 18A). Using this setup it is predicted that if YoeB is ribosome dependent, YoeB will only cleave in genuine stop codons and will not recognise out of frame stop codons. As observed in Figure 18B after 30 min VapC_{LT2} triggered YoeB mRNA cleavage which only occurs in stop codons (lanes 1-3, 6-8, 11-13 and 16-18) and out of frame stop codons are not cleaved by YoeB (lanes 11-13 and 16-18). These observations suggest that cleavage is dependent on the translation machinery. Translation inhibition by chloramphenicol does not *trans*-activate YoeB cleavage hence the cleavage is induced specifically by VapC and not translation inhibition by chloramphenicol (lanes 4-5, 9-10, 14-15 and 19-20).

It is observed that YoeB is a ribosome dependent RNase and can therefore be used as a sensitive method to map position of ribosomes on mRNA during *vapC_{LT2}* and *vapC* expression. YoeB is a RelE homologue and RelE has previously successfully been used to map ribosome position with high resolution (Temperley *et al.*, 2010). To

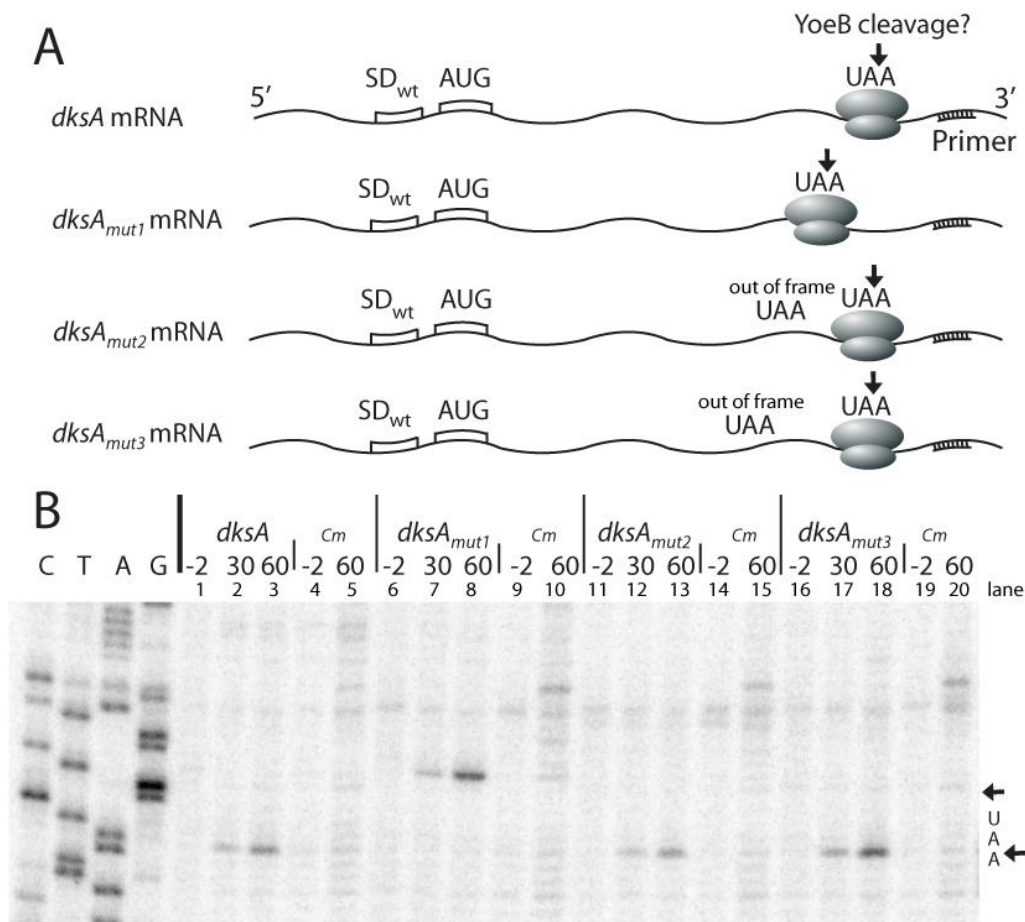


Figure 18 VapC_{LT2} activated YoeB stop codon cleavage is ribosome dependent. **A**) Presentation of wt and mutated version of *dksA* mRNA used to analyse the ribosome dependent cleavage in B). The *dksA* gene has been inserted in pKW254T creating pKW25420T (*dksA* mRNA). Plasmid pKW25423T (*dksA*_{mut1} mRNA) contains *dksA* were bases 448-450 GCT (codon 150) in the reading frame have been changed to TAA creating an in-frame premature stop codon. Plasmids pKW25424T (*dksA*_{mut2} mRNA) and pKW25425T (*dksA*_{mut3} mRNA) contains *dksA* were bases 447-449 GGC and 446-448 TGG have been changed to TAA, respectively. The TAA bases have been inserted out-of-frame and translation terminates at wild-type stop codon. YoeB cleavage is indicated by an arrow **B**) Primer extension analysis on VapC_{LT2} dependent stopcodon cleavage in *dksA* mutant. Strains MG1655Δ*dksA* /pKW25420T (wt *dksA*), MG1655Δ *dksA* /pKW25423T (*dksA*³, GCT448-450 changed to TAA), MG1655Δ *dksA* /pKW25424T (*dksA*⁴, GGC 447-449 changed to TAA) and MG1655Δ *dksA* /pKW25425T (*dksA*⁵, TGG446-448 changed to TAA) were co-transformed with pKW52 (pBAD::SD_{opt}::*vapC*_{LT2}) and grown exponentially in LB medium at 37°C. At time zero 0.2% arabinose was added to induce transcription. Cm 50μg/mL was added to strains without toxins and used as a control for translation inhibition. Total RNA was purified from samples taken out at time points indicated (min) and primer extension was performed using primer pKW71D-3#PE. Arrows indicate the position of YoeB cleavage.

investigate if VapC_{LT2} and VapC affect translation of *dksA*, three variants of *dksA* mRNA were constructed in which the Shine & Dalgarno (SD) sequence, the start codon or both were changed (Figure 19A). Primer extension analysis was then performed on RNA isolated before and 60 min after *vapC*_{LT2} and *vapC* induction. Consistent with previous results, *vapC*_{LT2} and *vapC* induction resulted in ribosome-dependent YoeB cleavage within the stop codon of wild-type *dksA* mRNA (denoted

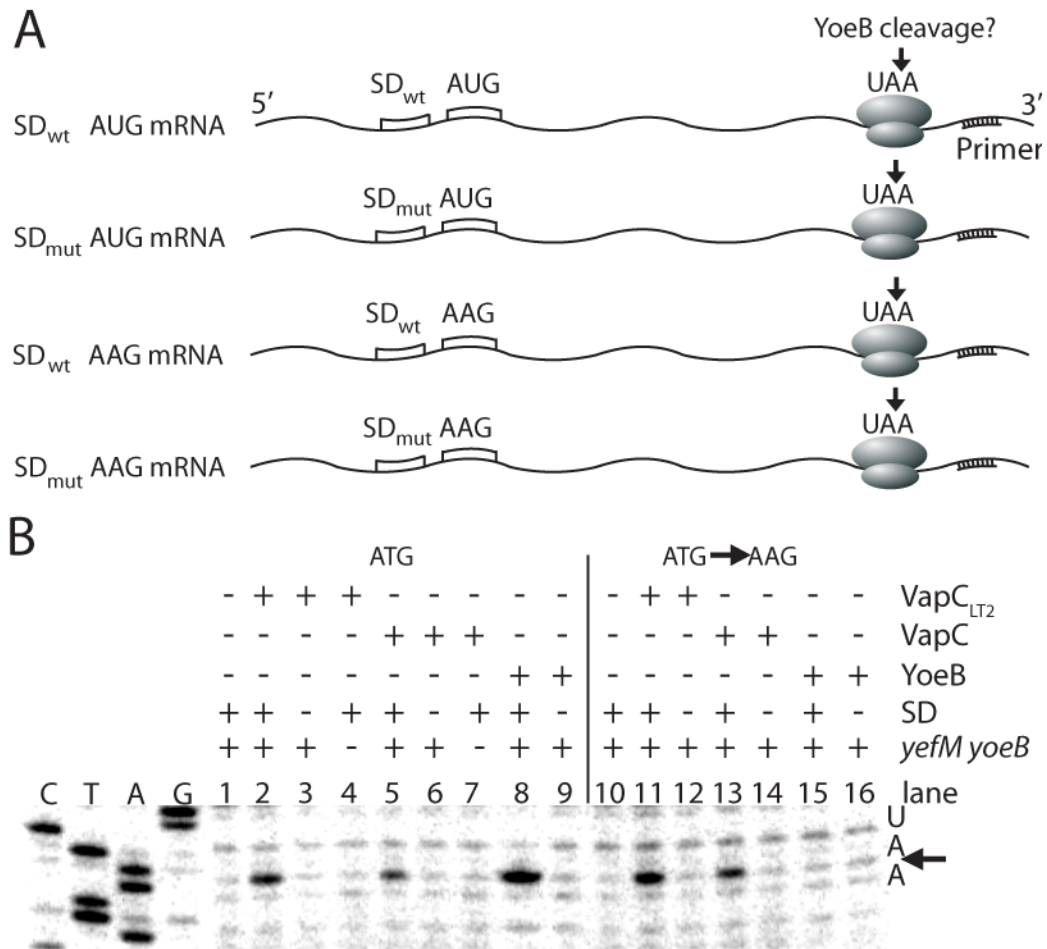


Figure 19 Ectopic production of VapC_{LT2} and VapC affects initiation of translation. (A) Drawing showing the four mRNAs analysed in (B). The top wavy lines symbolise wild type *dkSA* mRNA with SD, AUG start-codon and UAA stop codon. SD_{mut} indicates that the SD sequence of *dkSA* AGGAG, was changed to UCCUC. In the two bottom mRNAs, an AAG lysine codon replaces the AUG start codon. Arrows pointing at the UAA codons indicate possible YoeB cleavage in the stop codon of *dkSA*. (B) Primer extension analysis of VapC-mediated ribosome-dependent YoeB cleavage. MG1655 or MG1655Δ(*yefM-yoeB*) containing either pKW25420T (SD_{wt} AUG), pKW25421T (SD_{wt} AAG), pKW25427T (SD_{mut} AUG) or pKW25428T (SD_{mut} AAG) together with pKW3352HC (pBAD33::*vapC_{LT2}-H6*), pKW3382HC (pBAD33::*vapC-H6*) or pRB100 (pBAD33::*yoeB*) were grown exponentially in LB medium at 37°C. At time zero, 0.2% arabinose was added to induce transcription. Samples were taken before and 60 min after *vapC* induction. *yefM-yoeB* refers to experiments done in deletion strain, whereas SD indicates presence or absence of Shine&dalgarno sequence. VapC_{LT2}, VapC or YoeB refers to toxin induction.

SD_{wt} AUG mRNA in Figure 19A) (Figure 19B, left panel, lanes 1, 2 & 5). This cleavage disappeared if the *yefM yoeB* TA locus was deleted from the chromosome (lanes 4 & 7) showing that the cleavage depended on activation of YoeB. Consistently, induction of *yoeB* encoded by a plasmid led to efficient cleavage of the wild type *dkSA* mRNA (lane 8). Mutational change of the SD-sequence abolished stop codon cleavage in all three cases, showing that YoeB cleavage required that the mRNA was translated (lanes 3, 6 and 9). Next, a similar series of experiments was performed on mRNAs in which the AUG start-codon had been changed to an

elongator codon, AAG (Figure 19B, right panel). Induction of *yoeB* did not lead to cleavage of the SD_{wt} AAG mRNA, showing that the reading-frame starting with AAG was normally not translated (lanes 15, 16). In contrast, the SD_{wt} AAG mRNA was cleaved after *vapC* induction (lanes 11 and 13). VapC-induced cleavage of the SD_{wt} AAG mRNA was abolished by mutational change of the SD sequence (lanes 12 and 14). This observation is surprising and raises the possibility that VapC_{LT2} and VapC affect translation initiation as translation is initiated at the AAG codon of *dksA* mRNA if the codon is positioned correctly relative to an SD sequence leaving the reading frame intact.

VapC expression does not decrease stability of model mRNAs *in vivo* in the absence of YoeB activation but inhibits translation

In order to confirm that the observed decrease in mRNA stability is only due to the *trans*-activation of YoeB and not directly by the activity VapC_{LT2} and VapC mRNA interferase, northern blot analysis was performed on several model RNAs, *ompA*, *dksA* and *lpp* mRNA in the absence of *yefM-yoeB* TA-locus (Figure 20A). It is observed that neither *vapC*_{LT2} nor *vapC* induction significantly affect the stability of these mRNAs as full length mRNA is detected even 60 min after addition of arabinose. In all cases induction of mRNA interferase *relE* leads to efficient cleavage of model mRNAs. Translation inhibition by chloramphenicol also does not decrease the stability of these mRNA. This observation suggests that YoeB mRNA interferase is responsible for the majority of the observed mRNA cleavage. Weak degradation is observed in *dksA* mRNA in the absence of *yefM-yoeB*, but cannot account for the <10% inhibition of global translation (Figure 16C), which suggests that additional mRNA interferases might be active. To ensure that the observed activation of endogenous YoeB is not due to indirect effects such as VapC_{LT2} and VapC titrating YefM antitoxin and to confirm that VapC_{LT2} and VapC in fact inhibit translation, a second pulse-chase experiment was performed in a *lon* protease deficient strain (Figure 20B). It is observed that in the absence of YoeB activation (and the majority of mRNA interferases) both *vapC*_{LT2} and *vapC* induction leads to efficient inhibition of translation. This shows that both VapC_{LT2} and VapC are active and it is most likely the decrease in rates of translation by VapC_{LT2} and VapC which triggers the Lon-dependent activation of YoeB.

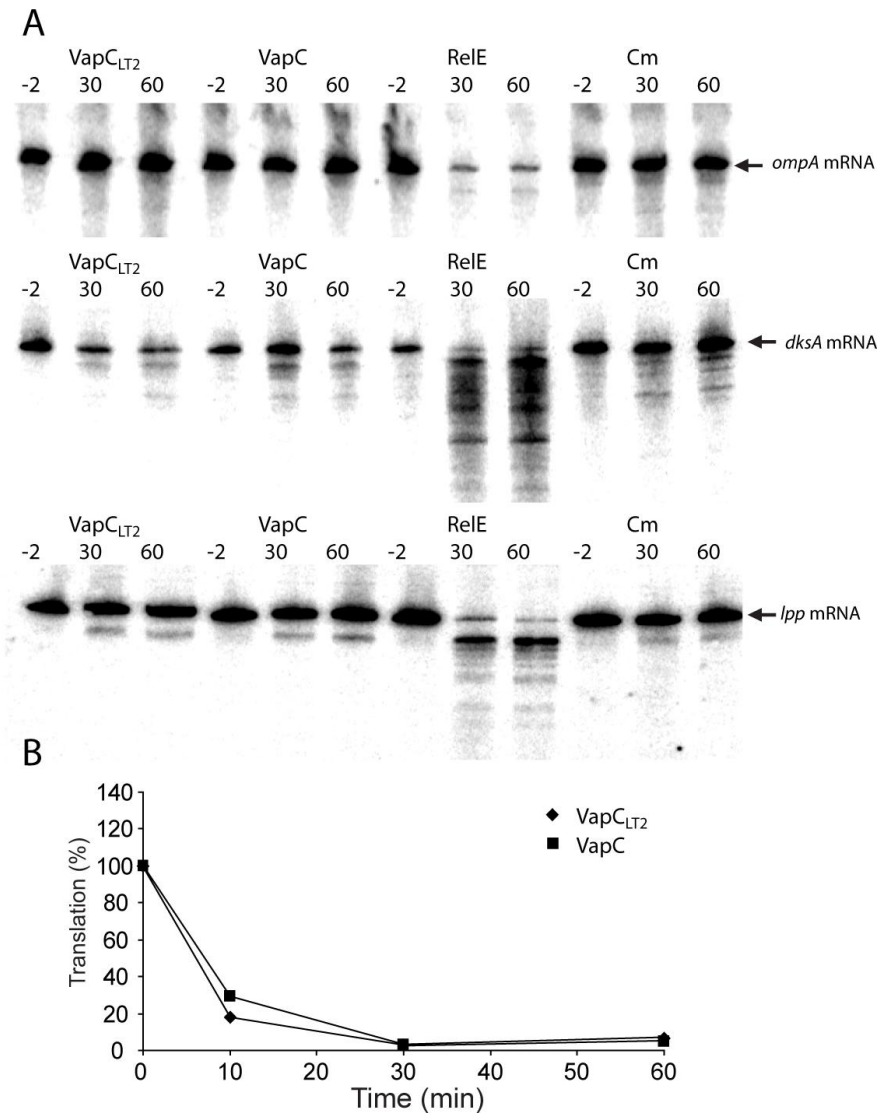


Figure 20 Vap_{CLT2} and VapC do not cleave mRNA in the absence of YoeB activation but inhibits translation. **A**) Northern blot analysis on *ompA*, *dksA* and *lpp* mRNA. *E. coli* K-12 MG1655 $\Delta 5$ ($\Delta chpAK$, $\Delta chpB$, $\Delta relBE$, $\Delta yefM/yoeB$ and $\Delta dinj/yafQ$) carrying pKW52 (pBAD::SD_{opt}::*vapCLT2*), pKW82 (pBAD::*vapC*) or pKP3035 (pBAD::*relE*) were grown exponentially in LB medium at 37°C. At time zero 0.2% arabinose was added to induce transcription. Cm (50µg/mL) was added at time zero to MG1655 $\Delta 5$ to inhibit translation and was used as a control. Total RNA was purified from the samples taken out at time points indicated (min). **B**) VapC toxins inhibit global translation in the absence of YoeB activation. *E. coli* K-12 MG1655 Δlon carrying pKW52 (pBAD::SD_{opt}::*vapCLT2*) /pKW51(pA1/03/04::SD_{opt}::*vapB*_{LT2}) (◆) or pKW82 (pBAD::*vapC*) / pKW81 (pA1/03/04::*vapB*) (■) were grown exponentially in AB-minimal medium with 0.5% glycerol as carbon source and transcription of the toxins was induced by addition of arabinose (0.2%) at time zero. The rate-of translation was measured by pulse-chase. Pre-induction levels were set to 100%.

VapC toxins decrease polysomes, but does not specifically associate with the ribosome or ribosomal subunits

Previous studies showed that mRNases, such as RelE, associate with the ribosome and cleave the mRNA at A-site codons (Pedersen et al., 2003; Neubauer et al., 2009).

Cleavage of mRNA by mRNA interferases leads to a decrease in the abundance of polysomes (e.g. chains of translating ribosomes on single mRNAs) as the mRNA is cleaved and ribosomes released by mechanisms such as *trans*-translation. Ribosome associating toxins such as Doc do not decrease polysomes, but rather stabilises polysomes (Liu et al., 2008). As VapC_{LT2} and VapC are observed to inhibit global translation without cleaving model mRNAs, it was interesting to see how these toxins affect polysomes. This was done by analysing fractions of an extract from cells expressing *vapC*_{LT2}, separated by sucrose gradient ultracentrifugation. As observed in Figure 21A ectopic expression VapC_{LT2} leads to a significant decrease in polysomes and corresponding increase in free 30S and 50S subunits. Co-expression of antitoxin VapB_{LT2} allows translation which is also observed as higher abundance of polysomes can be detected. The VapC_{LT2} induced decrease in polysome abundance is consistent with the observed inhibition of translation, however not with lack of degradation of mRNA. This indicates that VapC_{LT2} and VapC inhibit translation by a different mechanism compared to RelE and Doc.

Therefore it was investigated whether VapC_{LT2} and VapC would associate with ribosomes. Extracts of *E. coli* K-12 expressing VapC or VapC_{LT2} were separated on 5-40% sucrose gradients by ultracentrifugation and VapC detected by Western blot analysis. As seen, VapC and VapC_{LT2} were found in highest concentrations in the fractions that contained 5S ribosomal and tRNA (Figure 21B left and right). However, VapC_{LT2} was also detected in fractions containing ribosomal subunits and 70S. To investigate the specificity of the interaction observed with ribosomal subunit and 70S, total ribosomal RNA was separated into subunits under conditions of low concentration of magnesium ions. This condition also removes free 5S and tRNA (Figure 21C left and right). The Western blot revealed that VapC did not associate with ribosomal subunits. However, VapC_{LT2} was present in fractions containing ribosomal RNA but did not localise in a subunit-dependent manner as observed for other toxins. It is possible that this association is an artefact caused by VapC_{LT2} over expression as it might partly aggregate. It is also observed that gradients from VapC_{LT2} (Figure 21B) extracts appear to have less polysomes compared to extracts prepared from cells expressing VapC, which is most-likely caused by different contrast settings between the two experiments and the manual fractionation of the gradients. In all experiments performed, both VapC_{LT2} and VapC extracts contained less polysomes compared to non-induced extracts (data not shown).

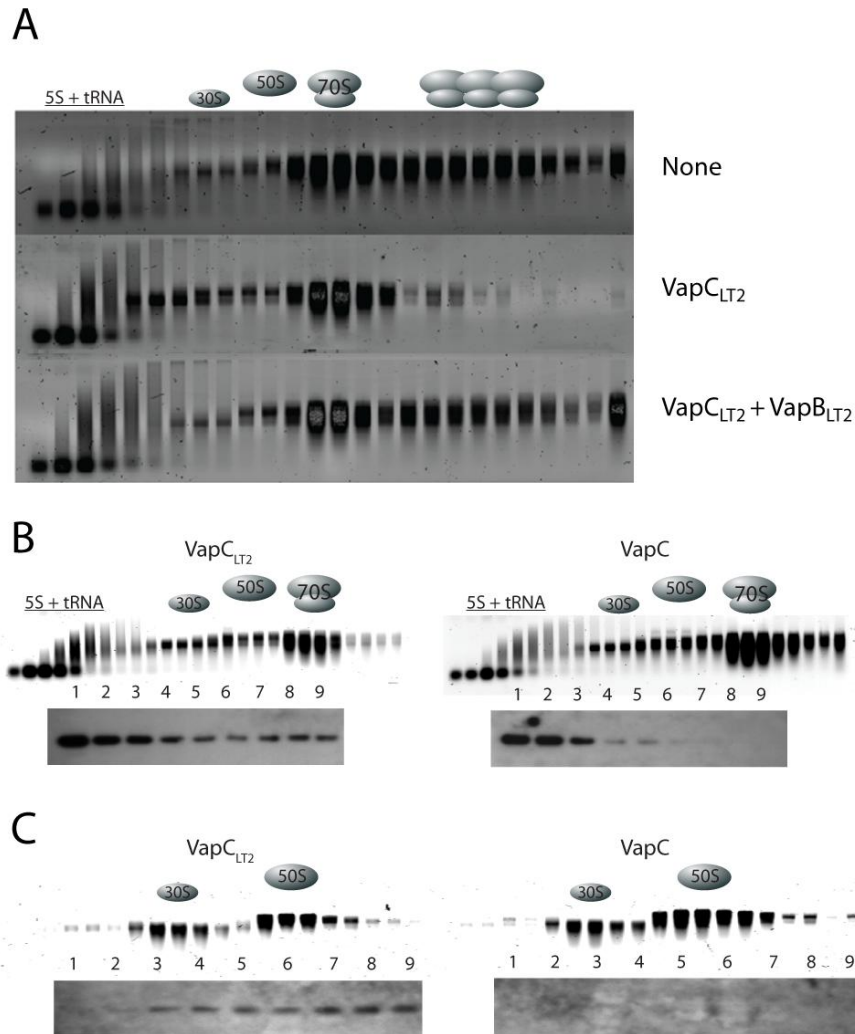


Figure 21 Ribosome profiles in response to VapC_{LT2} and VapC **A)** Ribosome profiles after vapC_{LT2} induction. *E. coli* K-12, MG1655 Δlon pKW3352HC (pBAD33::vapC_{LT2}-H₆)/pKW51 (pA1/03/04::SD_{opt}::vapB_{LT2}) were grown exponentially in LB medium and were collected after 20 min of vapC_{LT2} or vapC_{LT2} and vapB_{LT2} induction. Samples were separated in a 5-40% sucrose gradient at 35.000rpm at 4°C for 3h 30 min and fractions were visualised by agarose gel electrophoresis and EtBr staining. **B)** MG1655 Δlon carrying pKW3352HC (pBAD33::vapC_{LT2}-H₆) or pKW3382HC (pBAD33::vapC-H₆) were grown exponentially in LB medium and samples were collected after 15 min of toxin induction. The top panels show ribosome profiles of cells expressing VapC_{LT2}-H₆ (left) or VapC-H₆ (Right) while the lower panels shows His₆-tag detected by Western blotting using anti-his-tag antibodies. The numbers corresponds to fractions in the upper panels. In (B), 10 mM Mg²⁺ was present in the gradients to keep the ribosomal subunits assembled in 70S particles. **C)** Similar to B) but the ribosomal subunits disengaged due to conditions of low magnesium ions (1 mM Mg²⁺). Ribosomal RNA was visualized by agarose gel electrophoresis and EtBr staining.

In conclusion, the ribosome analysis showed that the majority of VapC_{LT2} and VapC was present in fractions containing tRNA and did not specifically associate with the ribosome or ribosomal subunits. This suggests that the target of VapC_{LT2} and VapC is not the ribosome directly. The toxins, nevertheless, somehow inhibit global translation as well as decrease polysome abundance without significantly affecting stability of mRNA.

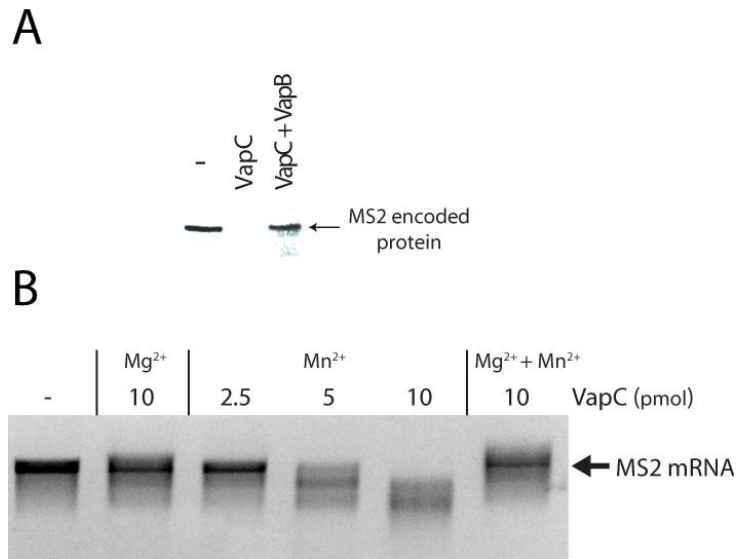


Figure 22 VapC inhibits translation *in vitro*. **A**) Native VapC inhibits translation *in vitro* and can be neutralized by VapB. Each reaction contained the following: 6 μ L Premix, 4.5 μ L S30 Extract, 1.5 μ L amino acid mix without methionine, 0.5 μ L ³⁵S-methionine and 4.5 pmol VapC with and without pre-incubation with 30 pmol VapB. The reaction was incubated for 5 min at 37°C before addition of 1 μ L MS2 RNA (~0.7 pmol) (Roche). The reactions were incubated for 1 h at 37°C before termination of the reaction by acetone precipitation. The protein products were visualized by SDS-PAGE and phosphorimaging. **B**) VapC degrades MS2 RNA in the presence of Mn²⁺, which can be reversed by Mg²⁺. 2.5, 5.0 or 10 pmol of VapC was incubated with 0.7 pmol of MS2 RNA in 10 mM HEPES pH 7.5 and 15 mM KCl in the presence of either 3 mM Mg²⁺ and/or 3 mM Mn²⁺ for 1 h at 37°C. RNA was visualized with EtBr staining. The right-most lane shows that addition of Mg²⁺ to the VapC reaction containing Mn²⁺ inhibited the non-specific activity of VapC. The stability of MS2 RNA did not change in the presence of only Mg²⁺ and Mn²⁺ during the course of the assay (Left-most lane). Neither Mg²⁺ nor Mn²⁺ activated VapC_{LT2} on any RNA substrate that we tested *in vitro*.

Purified VapC inhibits translation

To reduce the number of possible factors involved in the observed VapC activity in inhibiting translation, it was informative to reproduce the observed inhibition of translation *in vitro*. Translation was investigated using a cell free *in vitro* translation extract with purified VapC. Addition of purified, native VapC (4.5 pmol) to an *in vitro* translation reaction abolished translation even after 1 h of incubation with MS2 mRNA (~0.7 pmol) (Figure 22A, lanes 1 and 2). Pre-incubation with VapB antitoxin neutralized VapC activity, showing that VapCs inhibition of translation was specific (lane 3). Thus, the preparation of VapC was active *in vitro* and its activity could be counteracted by VapB. For reasons unknown, VapC_{LT2} was not active in *in vitro* assays and subsequent *in vitro* work was performed using VapC.

It is possible that VapC degrades the MS2 mRNA in the *in vitro* extract and causes inhibition of translation. To test this, MS2 mRNA (~0.7 pmol) was incubated with VapC (2.5 – 10 pmol) in the presence of divalent metal ions Mg²⁺ and/ or Mn²⁺

(Figure 22B). After 1 h of incubation, efficient degradation is only observed in the presence of Mn^{2+} . This shows that VapC is an RNase that can degrade MS2 RNA in the presence of Mn^{2+} . However, addition of equal amounts of Mg^{2+} and Mn^{2+} to the same reaction significantly decreases the degradation of MS2 RNA. The decreased RNase activity in the presence Mg^{2+} , could indicate that Mg^{2+} can displace Mn^{2+} from the PIN domain active site and might be the preferred metal ion..

As the cellular concentration of Mg^{2+} is significantly higher than Mn^{2+} might indicate that the observed Mn^{2+} dependent RNase activity is not physiological. In that case VapC could target something else than MS2 RNA in the extract. Incubation of MS2 RNA with Mg^{2+} and Mn^{2+} without VapC did not significantly change the RNA stability in the cleavage assay.

VapC specifically cleaves tRNA^{fMet} *in vitro* and *in vivo* without affecting stability of other tRNAs

Another possible target of VapC is tRNA, which would be consistent with all the previous observations. In addition, a plausible tRNA target would be tRNA^{fMet} considering the observed effects on translation initiation in response to VapC_{LT2} and VapC production. To test this idea purified VapC (5 pmol) was incubated with 2 pmol of tRNA^{fMet}, tRNA^{Val} and tRNA^{Phe} in the presence of Mg^{2+} (Figure 23A). VapC completely degraded purified *E. coli* tRNA^{fMet} in a 15 min reaction. In contrast, tRNA^{Val} and tRNA^{Phe} were not degraded, which shows specificity of VapC towards tRNA^{fMet}. Cleavage of tRNA^{fMet} was counteracted by the prior addition of VapB to VapC, which shows that it is the activity of VapC that is responsible for observed degradation. EDTA also inhibited the reaction, revealing that VapC activity required divalent cations or, more specifically, Mg^{2+} . The tRNA cleavage assay was not performed in the presence of Mn^{2+} .

To confirm this observation *in vivo*, *vapC*_{LT2} and *vapC* were induced in *E. coli* K-12 and stability of tRNA followed by northern blot analysis (Figure 23B). It is observed that both *vapC*_{LT2} and *vapC* induction leads to rapid decrease in the stability of full-length tRNA^{fMet} with the co-occurrence of a smaller cleavage product.

Consistent with this observation neither inhibition of translation by chloramphenicol nor expression of mRNA interferase RelE significantly affected the stability of this tRNA.

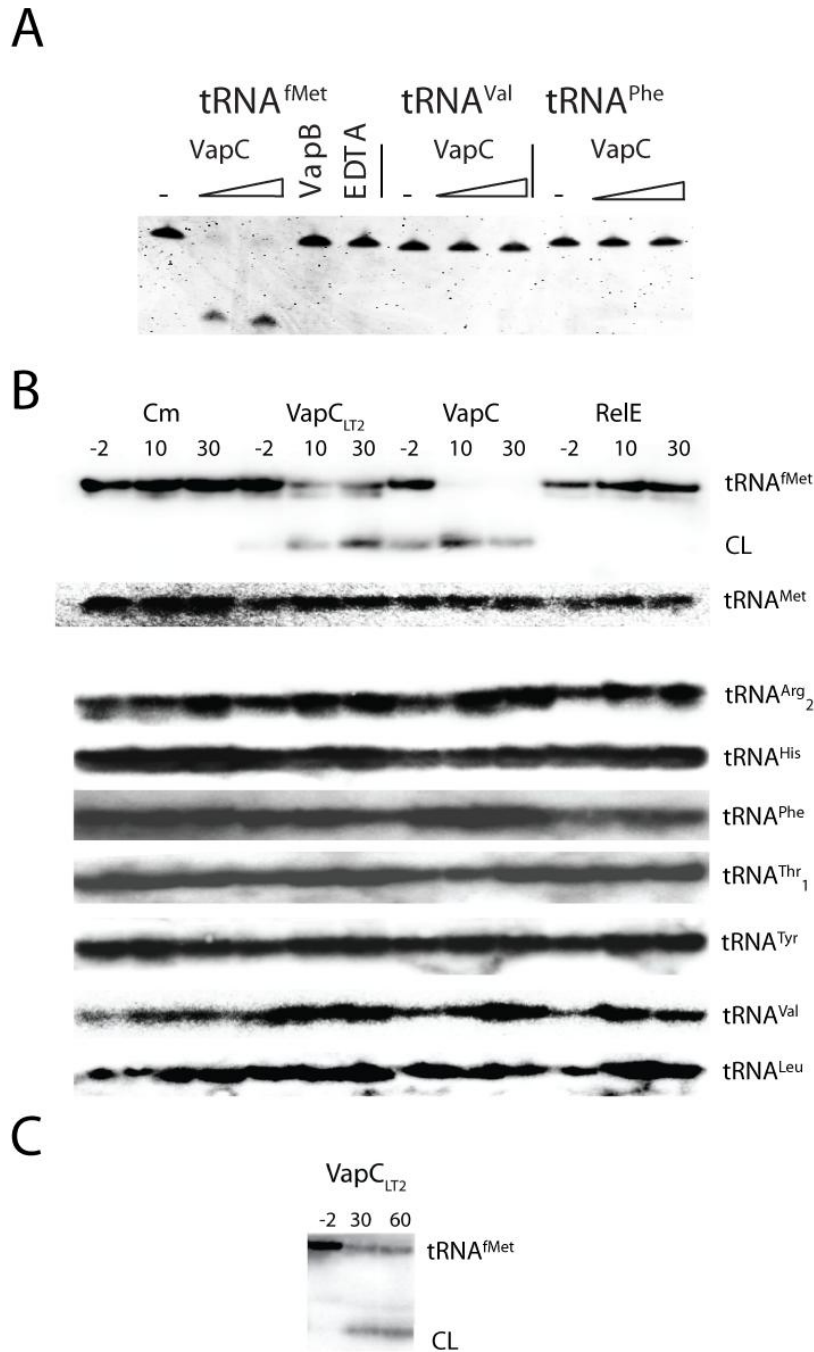


Figure 23 VapC cleaves tRNA^{fMet}. **A**) Cleavage of tRNA^{fMet} *in vitro*. VapC (2.5 pmol or 5 pmol) was incubated with 2 pmol tRNA^{fMet}, tRNA^{Val} or tRNA^{Phe} for 15 min. Controls: VapC (5 pmol) was pre-incubated with either VapB (30 pmol) or 12.5 mM EDTA before the addition of tRNA^{fMet}. tRNA was separated on an agarose gel and visualised by EtBr staining. **B**) Cleavage of tRNA^{fMet} *in vivo*. MG1655Δlon containing pKW3352HC (pBAD33::vapC_{LT2}-H₆), pKW3382HC (pBAD33::vapC-H₆) or pKP3035 (pBAD33::relE) were grown exponentially in LB medium at 37°C. At time zero, arabinose (0.2%) was added to induce transcription. Samples were taken at time points indicated (min). Chloramphenicol (50 μg/mL), Cm, was added to MG1655Δlon as a control. tRNAs (tRNA^{fMet}, tRNA^{Met}, tRNA^{Arg2}, tRNA^{His}, tRNA^{Phe}, tRNA^{Thr1}, tRNA^{Tyr}, tRNA^{Val} and tRNA^{Leu1}) were analysed by northern blot analysis. The use of a Δlon strain prevented fortuitous induction of mRNases by VapC over expression. **C**) Cleavage of tRNA^{fMet} in *S. enterica* LT2. KP1001 *S. enterica* LT2 containing pKW3352HC (pBAD33::vapC_{LT2}-H₆) were grown and induced as in B). Samples were taken at time points indicated (min). CL indicates cleavage fragments detected.

Interestingly, however, VapC seems to be more active than VapC_{LT2} as full-length tRNA^{fMet} cannot be detected after 10 min of *vapC* induction. In the case of *vapC*_{LT2} induction, full-length RNA can still be detected after 30 min. The stability of several elongator tRNAs including tRNA^{Met}, tRNA^{Arg2}, tRNA^{His}, tRNA^{Phe}, tRNA^{Thr1}, tRNA^{Tyr}, tRNA^{Val} and tRNA^{Leu1} was also not affected, which indicates the specificity of VapC_{LT2} and VapC towards tRNA^{fMet}. Weak tRNA^{fMet} cleavage is observed in the pre-induced samples (-2) which is most likely caused by low leakiness of the pBAD promoter.

It should be noted that tRNA^{fMet} are identical in both *E. coli* K-12, *S. enterica* LT2 and *S. flexneri* 2a and could therefore constitute a possible target,. Accordingly, *vapC*_{LT2} induction in *S. enterica* LT2 was also observed to induce tRNA^{fMet} cleavage (Figure 23C).

It was observed that VapC_{LT2} and VapC are bacteriostatic and inhibited cells can be resuscitated after 180 min of induction (Figure 15). As VapC_{LT2} and VapC most likely inhibit global translation by tRNA^{fMet} cleavage, the relation between growth rate and tRNA^{fMet} stability can be investigated by subsequent antitoxin induction in toxin inhibited cells. As observed in Figure 24A, both *vapC*_{LT2} and *vapC* induction efficiently inhibits growth which is resumed after a short delay upon *vapB*_{LT2} or *vapB* induction. Consistent with the growth inhibition, a decrease in full-length tRNA^{fMet} is observed (Figure 24B, left and middle panel). Furthermore, a transcriptional induction of *vapB*_{LT2} and *vapB* resulted in accumulation of full-length tRNA^{fMet} and resumption of growth is observed. Interestingly, the delay in resuming the growth is related to the accumulation of full-length tRNA^{fMet} and VapC, which produces a more efficient depletion, has a longer delay before growth resumption (~ 90 min for *vapB* induction compared to ~ 30 min for *vapB*_{LT2} induction).

As previously mentioned, the catalytic centers of PIN-domain proteins consist of quartets of conserved acidic residues (Figure 14). It is predicted that the aspartate in position +7 and +98 of VapC_{LT2} and VapC are required for the catalytic activity. To test this possibility, aspartates in these positions were changed to an alanine in VapC_{LT2} and tested for toxicity (Figure 24C). As observed, both VapC_{LT2}^{D7A} and VapC_{LT2}^{D98A} expression is less toxic compared to wild type VapC_{LT2}. It is observed that VapC_{LT2}^{D98A} expression decreases colony size, which suggests that this mutant still retains partial activity. To confirm the inactivity of VapC_{LT2}^{D7A} the activity was tested in a growth experiment.

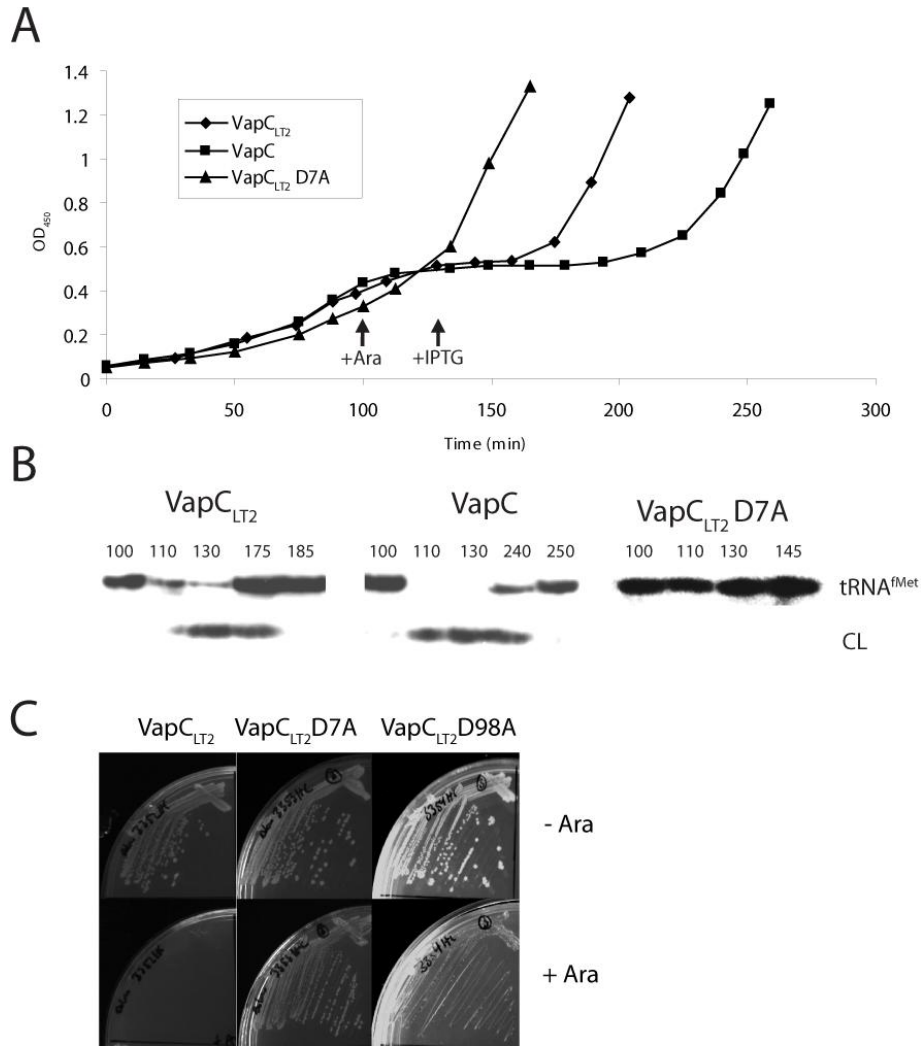


Figure 24 Regulation of the growth rate by tRNA^{fMet} cleavage. **(A)** Bacterial growth after VapC expression and subsequent VapB expression. Strains MG1655 Δ lon / pKW3352HC (pBAD33::vapC_{LT2}-H₆) / pKW51 (R1::pA1/O4/O3::vapB_{LT2}) (◆), MG1655 Δ lon / pKW3382HC (pBAD33::vapC-H₆) / pKW81 (pA1/O4/O3::vapB) (■) or MG1655 Δ lon / pKW3353 (pBAD33::vapC_{LT2}-H₆^{D7A}) (▲) were grown exponentially in LB medium at 37°C. At 100 min, vapC transcription was induced by the addition of 0.2% arabinose. In the case of strains carrying vapC and vapC_{LT2}, vapC expression was terminated at 130 min by the addition of 0.4% glucose and transcription of vapB and vapB_{LT2} was induced by addition of 2 mM IPTG. **(B)** Northern blotting analysis on tRNA^{fMet} of cell samples from (A) VapC_{LT2} (Left Panel), VapC (Middle Panel) and VapC_{LT2} D7A (Right Panel). **(C)** Toxicity of VapC_{LT2}D7A and VapC_{LT2}D98A. MG1655 Δ lon containing either pKW3352HC (pBAD33::vapC_{LT2}-H₆), pKW3353 (pBAD33::vapC_{LT2}-H₆^{D7A}) or pKW3354HC (pBAD33::vapC_{LT2}-H₆^{D98A}) were streaked onto NA plates with or without 0.2% arabinose.

As observed in Figure 24A vapC_{LT2}^{D7A} does not inhibit growth upon induction and is reflected in the levels of tRNA^{fMet}, which were not affected (Figure 24B right). This shows that D7A substitution renders VapC catalytically inactive and that the predicted active site is necessary for the observed RNase activity.

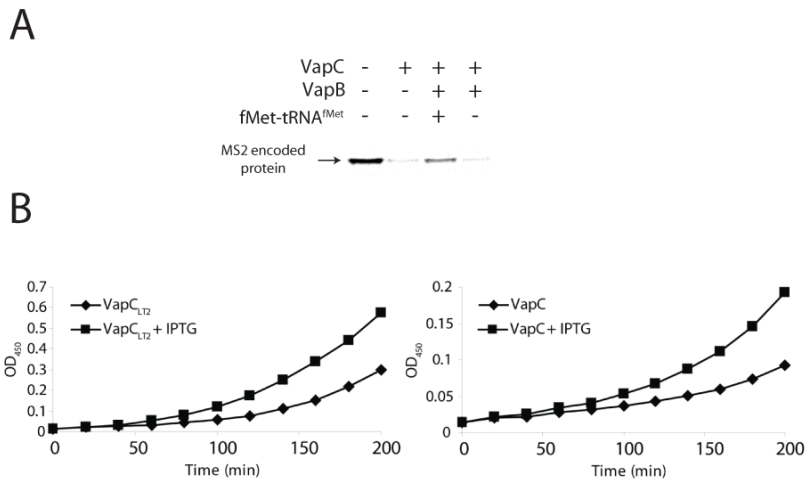


Figure 25 tRNA^{fMet} is the sole target of VapC and VapC_{LT2}. **A**) Inhibition of translation *in vitro* by VapC can be reversed by fMet-tRNA^{fMet}. VapC (9 pmol) (lanes 2, 3 and 4) or buffer (lane 1) were added to an *E. coli* S30 extract and incubated for 5 min before VapB (60 pmol) (lane 3 and 4) or buffer (lane 1 and 2) was added at +5 min and incubation was continued; at +10 min, fMet-tRNA^{fMet} (lane 3) or buffer (lane 1, 2 and 4) was added together with ³⁵S-met and MS2 RNA. The reaction was terminated after incubation for an additional 10 min. **B**) Ectopic overexpression of tRNA^{fMet} counteracts VapC-mediated growth inhibition. C41 (DE3)/pKW3221 (pT7::tRNA^{fMet}) / pKW3352HC (pBAD33::vapC_{LT2}-H₆) or C41 (DE3)/pKW3221 (pT7::tRNA^{fMet}) / pKW3382HC (pBAD33::vapC-H₆) were grown exponentially to OD₄₅₀ ≈ 0.5 in LB medium at 37°C. The cultures were diluted to OD₄₅₀ ≈ 0.05 in medium with or without 2 mM IPTG to induce production of T7 RNA polymerase and ultimately tRNA^{fMet}. The cells were grown exponentially to an OD₄₅₀ ≈ 0.4. A *vapC* transcription pulse was generated by the addition of arabinose (0.2%) for 2 min (*vapC*_{LT2}) or 1 min (*vapC*) which was terminated by the addition of 0.4% glucose. The cultures were diluted to OD₄₅₀ ≈ 0.01 in preheated medium with and without 2 mM IPTG and cell density was measured at the time points indicated. Right panel: *vapC*; left panel: *vapC*_{LT2}. Squares and diamonds indicate growth with and without IPTG, respectively.

tRNA^{fMet} is most-likely the sole target of VapC

VapC_{LT2} and VapC cleave tRNA^{fMet}, but it is not clear whether this tRNA is the sole target in the cell. Investigations to shed more light on this were done with an *in vitro* and *in vivo* approach. The *in vitro* approach was to reactivate a VapC-inhibited translation extract by addition of fresh charged fMet-tRNA^{fMet} (Figure 25A). Consistent with previous results, incubation of VapC with the extract inhibits translation (lane 1 and 2). Addition of VapB to the reaction does not affect the activity of the extract (lane 4); however subsequent addition of fresh fMet-tRNA^{fMet} to the extract reactivates translation (lane 3). This is a clear indication that tRNA^{fMet} is the only tRNA being targeted in the extract. To confirm this *in vivo*, *E. coli* cells are pulsed with VapC_{LT2} or VapC in the presence or absence of additional tRNA^{fMet} supplied from an inducible promoter on the chromosome (Figure 25B left and right). Due to the difference in toxicity, *vapC*_{LT2} is induced for 2 min and *vapC* for 1 min. As it can be observed for both toxins, cells which have excess of tRNA^{fMet} recover

growth more rapidly compared to cells with lower levels of tRNA^{fMet}. It is also observed that VapC_{LT2} is less toxic than VapC as growth resumes faster, which is consistent with previous results. It should be noted that expression of tRNA^{fMet} by itself does not affect the growth rate. This indicates that tRNA^{fMet} is probably the sole target of VapC_{LT2} or VapC *in vivo*, because if otherwise the toxins would have targeted additional tRNAs, tRNA^{fMet} production would not make a significant advantage for growth resumption. These observations also support that the observed Mn²⁺ dependent RNase activity on mRNA *in vitro* is unspecific.

VapC cleavage occurs at the anticodon stem-loop of tRNA^{fMet}

The tRNase activity observed by VapC_{LT2} and VapC produce tRNA^{fMet} fragments consistent with specific cleavage in the tRNA. To analyse this in detail, tRNA^{fMet} was radiolabelled in the 5'- and 3'-end and subsequently treated with increasing concentration of VapC (Figure 26 A), B) and C)). Incubation of tRNA^{fMet} with VapC produces one specific cleavage product, which is mapped to occur between position +38 and +39 in the anticodon loop, adjacent to the universally conserved GC stem (Figure 26D).

The cleavage site could also be mapped *in vivo* by analysing tRNA^{fMet} fragments isolated from *E. coli* K-12 cells expressing VapC_{LT2} and VapC. Cleavage fragments were isolated using a biotinylated primer specific for tRNA^{fMet} and subsequently radiolabelled. Using a tRNA^{fMet} specific probe, a cleavage fragment is isolated with the same size as 5'-labelled *in vitro* cleaved tRNA^{fMet} (Figure 27A). Interestingly, smaller fragments are also isolated which could be products of subsequent ribonuclease activity by other ribonucleases in the cell as the cleavage products might become unstable. Consistent with the Northern blots (Figure 23B) no cleavage products are isolated in cells expressing RelE or those treated with chloramphenicol, and only full-length tRNA^{fMet} can be recovered. As the VapC cleavage site is in the middle of tRNA^{fMet} sequence, the observed cleavage product could correspond to unspecific hybridisation to the 3'-end cleavage product as it would have similar size to the 5'-end cleavage product. In order to clarify this, two new biotinylated primers were designed, specific for either 5'-end or 3'-end cleavage fragment (Figure 27B and C). It can be observed that only weak cleavage fragment can be observed with the 5'-end specific primer, whereas the smaller ribonuclease degradation products are clearly visible. Conversely, with the 3'-end primer, only a specific cleavage fragment is

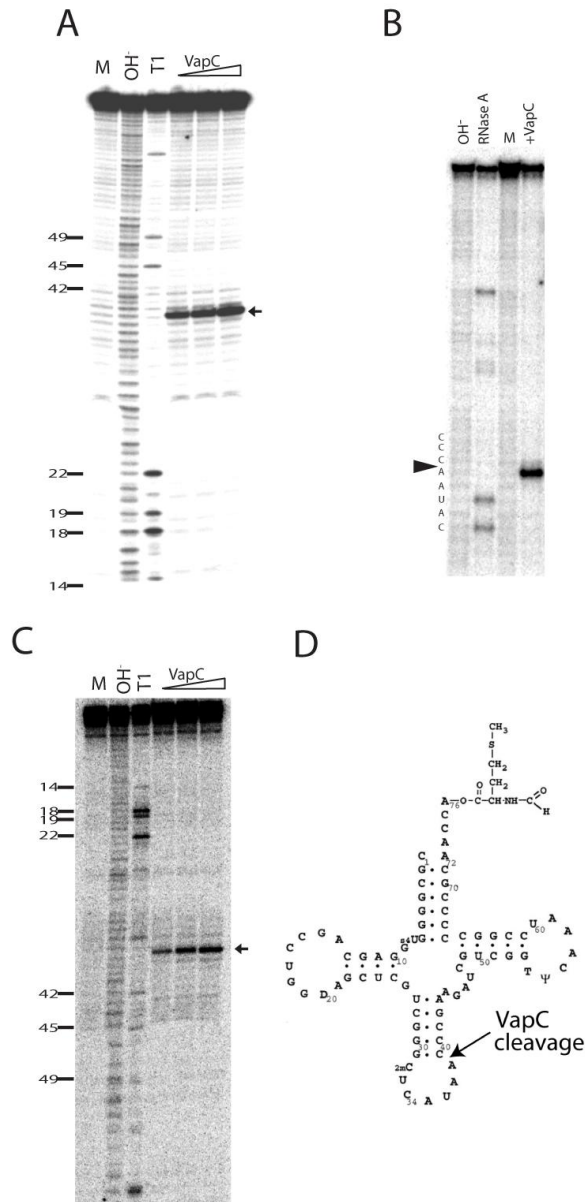


Figure 26 VapC cleaves tRNA^{fMet} in the anticodon stem-loop *in vitro*. **A)** and **B)** *In vitro* cleavage of 5'-labeled tRNA^{fMet}. **C)** *In vitro* cleavage of 3'-labeled tRNA^{fMet}. One pmol tRNA^{fMet} was treated with increasing concentrations (0.01, 0.025 and 0.05 pmol) or 0.05 pmol alone of VapC for 15 min. M: untreated tRNA^{fMet}; OH-: hydroxyl ladder of tRNA^{fMet}; T1: RNase T1 digestion of tRNA^{fMet} RNase A: RNase A digestion of tRNA^{fMet}. **D)** Primary and Secondary structures of *E. coli* fMet-tRNA^{fMet}. The arrow indicates the mapped cleavage site.

isolated. This could indicate that the GC stem prevents the 3'-end cleavage product from being degraded by other ribonucleases and 5'-end is more prone to degradation as it is unprotected (Figure 27D). A similar observation has been made for colicin D, which cleaves between position +38 and +39 of tRNA^{Arg}, which *in vivo* is subsequently degraded to +34 by other ribonucleases (Tomita *et al.*, 2000). This degradation can also be a result of the tRNA purification process as cellular ribonucleases are released upon lysis of the cells. In conclusion, VapC_{LT2} and VapC

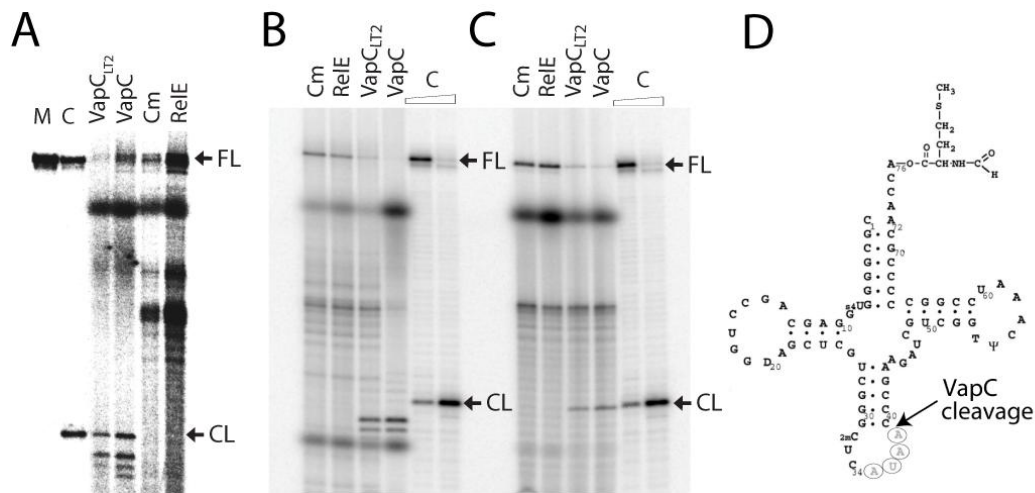


Figure 27 Analysis of the tRNA^{fMet} cleavage product *in vivo*. tRNA^{fMet} was isolated from total tRNA samples taken in Figure 23B) at 10 min by hybridization to a biotinylated probe complementary to the cleavage products of tRNA^{fMet} (Fmet-bio). The RNA/DNA hybrid was subsequently purified using Streptavidin sepharose and labelled with ³²P in its 5'-end. M is untreated tRNA^{fMet} and lane C is *in vitro* cleavage of tRNA^{fMet} by VapC (0.01 and/or 0.05 pmol of VapC). FL: Full-length tRNA^{fMet}; CL: Cleavage product of tRNA^{fMet}. **A**) tRNA^{fMet} specific probe (Fmet-bio) **B**) 5'-specific tRNA^{fMet} probe (FMET-BIO-N) **C**) 3'-specific tRNA^{fMet} probe (FMET-BIO-3). **D**) Primary and Secondary structures of *E. coli* fMet-tRNA^{fMet}. The arrow indicates the mapped cleavage site. Circled shaded bases in the anticodon loop are subsequently removed by cellular ribonucleases either in the cell or in the tRNA purification process.

act by endoribonucleolytic cleavage at a specific site in the anticodon stem-loop of tRNA^{fMet}. The anticodon stem is not conserved in the elongator tRNA^{Met}, which could explain why this tRNA is not cleaved (Figure 23B).

An abrupt decrease in the rate of translation induces VapC cleavage of tRNA^{fMet} from plasmid resident *vapBC* locus

Endoribonucleolytic cleavage of tRNA^{fMet} by VapC seems to be highly specific. Therefore Northern blot analysis of tRNA^{fMet} is a highly sensitive assay to analyse the activity of VapC. Previously it has been shown that when the *de novo* synthesis of antitoxin decreases, for example by treatment with chloramphenicol, transcription from the promoter increases (Described for *vapBC* in Results Part II) (Christensen *et al.*, 2001). It is therefore now possible to test the activity of VapC activated from the *vapBC* operon, when the synthesis of antitoxin and toxin is blocked. The *vapBC* or *vapBC*^{D7A} (Asp 7 to Ala substitution which is non-toxic) operon under the control of the native promoter were therefore cloned onto low-copy number plasmids and transformed into *E. coli* K-12. Translation was blocked by addition of chloramphenicol and the stability of tRNA^{fMet} followed by northern blot analysis. As

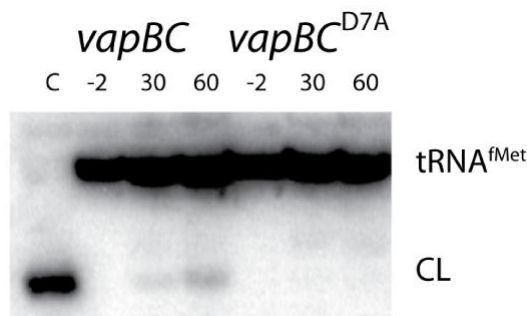


Figure 28 Cleavage of tRNA^{fMet} by VapC activated from *vapBC* operon during translation inhibition. *E. coli* K-12 MG1655/pKW254812 (*vapBC*) and MG1655/pKW254813 (*vapBC*^{D7A}) were grown exponentially in LB medium at 37 °C. At time zero, 50 µg/mL of chloramphenicol was added. Samples were taken at time points indicated (min). The lane marked C shows tRNA^{fMet} cleaved by VapC (10 min sample from Figure 23B). CL denotes the VapC cleavage product(s) of tRNA^{fMet}.

seen in Figure 28, blocking translation in cells carrying *vapBC* induces detectable cleavage. No such cleavage is detected in cells carrying non-toxic *vapBC*^{D7A}. This clearly shows that VapC can be activated by abrupt translation inhibition consistent with degradation of VapB during such conditions. Interestingly however, only weak cleavage is detected which can reflect either low intrinsic activity of VapC in this setup or that VapC is activated only in a sub population of cells.

Depletion of tRNA^{fMet} by VapC results in ectopic initiation of translation at elongator codons

As it is now clear that Vap_{CLT2} and VapC depletes the cells for tRNA^{fMet} this might explain the observed ectopic initiation on AAG lysine codons when they are positioned in optimal distance to the Shine & Dalgarno sequence (Figure 19B). Depletion of tRNA^{fMet} might promote the use of elongator tRNAs inserted in the ribosomal P-site during translation initiation. To investigate this conjecture in a simpler and more general context, a dual luciferase assay was performed to measure the fidelity of translation initiation (Kimura and Suzuki, 2010). Firefly luciferase gene (*lucF*) had its AUG start-codon changed to either AAA or AAG lysine codons; renilla luciferase (*lucR*) was included to normalize LucF activity (Figure 29). The LucF/LucR ratios were very low for the AAA and AAG constructs before induction of *vapCLT2*, consistent with the absence of initiation of translation from AAA and AAG elongator codons. Strikingly, induction of *vapCLT2* resulted in ≈20-fold (AAA) and ≈4-fold (AAG) increases in the LucF/LucR ratios. No increase was observed

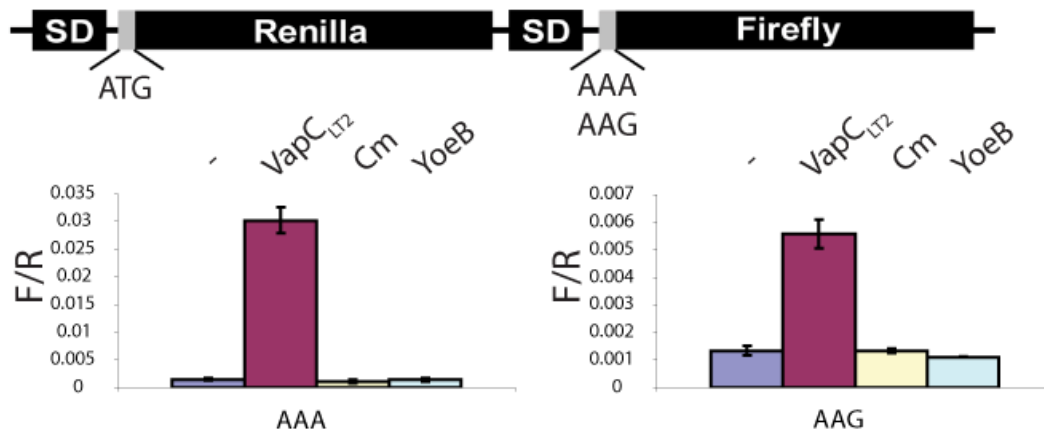


Figure 29 Measurement of relative translational initiation frequencies at elongator codons (AAA and AAG) by a dual luciferase assay. *E. coli* K-12 MG1655 Δlon containing plasmids pQE-AAA or pQE-AAG and pKW3352HC (pBAD33::*vapC_{LT2-H6}*) or pRB100 (pBAD33::*yoeB*) were grown exponentially in LB medium at 37°C. Samples were taken before and 30 min after induction of *vapC*. Cm, Cell samples treated with chloramphenicol (50 μ g/ml) were included as additional controls. F/R: Firefly/Renilla activity ratio.

when translation was inhibited with chloramphenicol or *yoeB* induction. These results confirm that *vapC* induction activated ectopic translation initiation at elongator codons positioned correctly in respect to a Shine & Dalgarno sequence. This observation also indirectly indicates that VapC_{LT2} and VapC only affect tRNA^{Met} as the rest of the translation machinery is left intact.

Discussion Section I

Extensive bioinformatic analysis of toxins, based on sequence similarity, led to the identification of at least ten different TA families (Anantharaman and Aravind, 2003; Pandey and Gerdes, 2005; Makarova *et al.*, 2009; Leplae *et al.*, 2011). Five of these toxin families have been shown to inhibit translation primarily by mRNA cleavage e.g. RelE, MazF, HigB, HicA, HipA. Two toxin families, CcdB and ParE, are known to inhibit replication by inhibiting DNA gyrase activity and one Zeta (ζ) has been identified to target cell wall synthesis. VapC is known to inhibit translation but the molecular target was so far unknown.

VapC is the largest family of toxins and in a recently published TA database with collected data from 964 prokaryotic genomes, 1316 loci were classified as *vapBC*, making this TA locus family the most abundant, representing approximately 43% of all identified TA loci (Shao *et al.*, 2011). In order to understand and elucidate the biological function of *vapBC* loci and TA loci in general, it is therefore of considerable interest to identify the cellular target of VapC.

It is shown here that expression of VapC homologue STM3033 (here referred to as VapC_{LT2}) from *S. enterica* LT2 and VapC homologue MvpT (here referred to as VapC) of *S. flexneri* 2a. YSH6000 virulence plasmid pMYSH6000 inhibits growth of *E. coli* K-12 cells and reduces viability (Figure 15). In addition, it has previously been shown that *mvpAT* locus efficiently stabilizes plasmids and that MvpA co-expression leads to loss of plasmid suggesting plasmid stabilization by the mechanism of PSK (Radnedge *et al.*, 1997; Sayeed *et al.*, 2000). This phenotype is a consequence of a difference in stability of the antitoxin (MvpA) compared to the toxin (MvpT) (Gerdes *et al.*, 2005). Daughter cells that lose the plasmid containing *mvpAT* experience rapid decay of the antitoxin by cellular proteases (Lon and/or Clp). Due to lack of continued antitoxin synthesis, the toxin is liberated from its inactive state in the complex and inhibits growth.

Here it was shown that VapC_{LT2} and VapC inhibited cells can be rescued to almost 100% viability after three hours by subsequent expression of antitoxins (Figure 15). This indicates that these toxins do not kill the cells, but rather are bacteriostatic and restrict cell growth when expressed. This is consistent with previous observations for other TA loci e.g. *relBE* and *mazEF* and suggests that the plasmid stabilization

observed by *mvpAT* is an indirect effect of toxin and antitoxin component properties (Pedersen *et al.*, 2002).

In this study evidence is also presented that VapC_{LT2} and VapC inhibit growth by reducing the rate of global translation (Figure 16 and 20B). Concomitantly, by Northern blotting and primer extension analysis it was observed that tmRNA and *dksA* mRNA is cleaved between the 2nd and 3rd base of the UAA stop codon (Figure 17A, 17B and 18B). Subsequent studies, however, carried out in strains lacking *yefM/yoeB* TA locus and the Lon protease, showed that the observed cleavage was mediated by endogenous YoeB and dependent on the activity of Lon protease and not directly by VapC (Figure 17B). Lon overproduction inhibits translation and has previously been shown to specifically activate YoeB mRNA interferase to cleave at mRNA stop codon, most-likely by Lon mediated degradation of YefM (Christensen *et al.*, 2004). Therefore, this observation suggests that VapC dependent inhibition of translation activates Lon protease, either directly or indirectly, to degrade YefM and in turn liberate endogenous YoeB to cleave mRNA. In addition to this, mutations in the *dksA* reading frame also revealed that the VapC_{LT2} and VapC activated YoeB cleavage was completely dependent on the ribosome which is consistent with previous observations (Christensen *et al.*, 2004; Christensen-Dalsgaard and Gerdes, 2008)

These results are interesting as there are other TA-systems present in *E. coli* K-12. The antitoxins of *relBE* and *mazEF* are also Lon protease substrates (e.g RelB and MazE) (Christensen *et al.*, 2001; Christensen and Gerdes, 2003). Accordingly, RelE- and MazF- mediated mRNA cleavage would also be expected to occur upon translation inhibition by VapC, however this is not observed.

The Doc toxin from *phd/doc* of phage P1 has been shown to inhibit translation elongation, which indirectly activates endogenous MazF and RelE to cleave mRNA (Hazan *et al.*, 2001; Garcia-Pino *et al.*, 2008). In addition, amino acid starvation (by addition of Serine hydroxymate which induces serine starvation) or by starving cells for specific amino acids leads to A-site cleavage in a amino acid codon specific manner, which could depend on mRNA Interferases (Li *et al.*, 2008b; Garza-Sanchez *et al.*, 2008). In this respect RelE and MazF toxin have also directly been linked to A-site cleavage during amino acid starvation (Christensen *et al.*, 2003). In conclusion, amino acid starvation and Lon overproduction both inhibit translation but activate different TA loci to cleave mRNA. This supports the idea that inhibition of

transcription and/or translation is the key activator of TA systems and can generate unbalanced amounts of toxin and antitoxin, as it has previously been shown for *relBE* and *mazEF* (Aizenman *et al.*, 1996; Christensen *et al.*, 2001). Thus, as shown here, the fact that VapC-induced inhibition of translation specifically activates YoeB, is consistent with the observation that the mechanism of translation inhibition might activate specific TA loci. In relation to this, it has previously been suggested that the mode of translation inhibition might leave the ribosomes in a state more or less accessible for specific toxins (Christensen *et al.*, 2004). This could also be the explanation why mRNA cleavage by other toxins is not observed after VapC induction and why cleavage is not observed in cells where translation is inhibited by chloramphenicol. Chloramphenicol inhibits peptidyl transfer activity and in such case, the ribosomal A-site may not be accessible for ribosome dependent mRNA interferases.

Nevertheless, in the absence of Lon protease, which is responsible for *trans*-activation of the majority of TAs, VapC_{LT2} and VapC still inhibit translation efficiently to a level similar to that caused by RelE expression (Figure 20C and 16C). Furthermore, in the absence of *yefM-yoeB* several mRNAs including *ompA*, *dksA* and *lpp* were found to be stable when *vapC_{LT2}* or *vapC* is induced (Figure 20A). This observation suggests that VapC_{LT2} and VapC inhibit translation by a mechanism different from RelE as RelE efficiently cleaved all the tested mRNAs.

Interestingly, VapC_{LT2} and VapC decreased polysomes, consistent with the inhibition of translation, but did not specifically associate to either the ribosome or ribosomal subunits (Figure 21A and 21B). This observation confirms that the activity is distinct from ribosome dependent mRNAses such as RelE or YoeB, as these toxins both associate with ribosomes and ribosomal subunits (Pedersen *et al.*, 2003; Zhang and Inouye, 2009). In addition, the mechanism of translation inhibition by VapC is most likely also distinct to the Doc toxin, which activity has been found to stabilise polysomes (Liu *et al.*, 2008).

However, the observation that the highest quantities of VapC_{LT2} and VapC are detected in sucrose gradient fractions containing 5S ribosomal subunits and tRNA, suggested that the target might be found there (Figure 21B). Previously performed primer extension analysis on 5S ribosomal RNA (*rrfD*) after VapC_{LT2} and VapC expression did not detect any difference in degradation compared with RelE expression or chloramphenicol treatment (data not shown here) (Winther and Gerdes,

2009). Furthermore, by analysing the quality of RNA extraction no significant difference in purified 5S was detected, suggesting that the target most-likely is not 5S and therefore could be a tRNA (data not shown). An interesting observation in relation to that was the observed VapC *trans*-activated YoeB dependent stop codon cleavage when the AUG start codon was changed to an AAG lysine codon which normally silences the reading frame (Figure 19B). Stop codon cleavage was dependent on a Shine & Dalgarno sequence positioned correctly in respect to the start codon, but occurred independently of a canonical initiation codon, which suggested that translation initiation was affected by VapC_{LT2} and VapC expression. As the observed YoeB cleavage occurred in the stop codon, the data suggested that translation elongation was not affected, as ribosomes reached the stop codon even in the absence of an AUG start codon (Figure 19B).

What could then be the target of VapC and the activity of its PIN domain? It has previously been proposed that PIN domains retain ribonuclease activity and share similarity with 5'-nuclease domain families (Clissold and Ponting, 2000). In addition, conserved acidic residues were identified and suggested to bind divalent cations similar to that observed by other metal-ion dependent nucleases. In a following study it was shown that the conserved putative active site residues from an Archeal PIN domain could be aligned with the active site residues of T4 RNase H facilitating Mg²⁺ binding. In addition, weak nuclease activity could be confirmed *in vitro* (Arcus *et al.*, 2004). In more recent studies using purified VapC from non-typable *Hemophilus influenzae*, *Mycobacterium tuberculosis*, *Sulfolobus solfataricus* and *Piscirickettsia salmonis*, it has been shown that VapC indeed possesses RNase activity *in vitro*, which in most cases can be inhibited by the presence of VapB antitoxin (Daines *et al.*, 2007; Ramage *et al.*, 2009; Maezato *et al.*, 2011; Gomez *et al.*, 2011) (see Table 2). These observations suggest that VapC is a ribonuclease..

In an attempt to simplify the system, native VapC was purified, and shown to inhibit translation in an *in vitro* translation extract. This inhibition could be counteracted by VapB (Figure 22A). VapC was observed to degrade MS2 RNA in the presence of Mn²⁺ (Figure 22B). However, Mn²⁺ dependent RNase activity could be counteracted by addition of Mg²⁺, which might suggest that in the presence of Mg²⁺ VapC does not degrade MS2 RNA and that Mg²⁺ could be the preferred ion of the active site.. Taking into account the higher cellular levels of Mg²⁺ the results possibly indicate that VapC does not specifically degrade mRNA and that the inhibition of translation does not

occur by mRNA cleavage. This idea is also consistent with the observation that *ompA*, *dksA* and *lpp* mRNAs and tmRNA are not cleaved by VapC *in vivo* (Figure 20A).

As it was observed that VapC_{LT2} and VapC expression might affect translation initiation a plausible target would be initiator tRNA. The presence of VapC in fractions containing 5S ribosomal RNA and tRNA also supported this idea.

In fact, it was observed that VapC_{LT2} and VapC are highly specific tRNA^{fMet} tRNases both *in vitro* in the presence of Mg²⁺ and *in vivo* (Figure 23A and 23B). Several tRNA species were investigated but only tRNA^{fMet} was cleaved under conditions tested. That tRNA^{fMet} most-likely is the sole target of VapC_{LT2} and VapC was further substantiated by the ability of additional tRNA^{fMet} to reactivate inhibited *in vitro* translation extract and counteract toxicity *in vivo* in growing cells (Figure 25A and 25B). The cleavage of tRNA^{fMet} could be correlated with the cellular growth and confirmed the results of the viable count assays, which showed that the tRNase activity was bacteriostatic (Figure 24A, Figure 24B left and middle and Figure 15). In addition, it was also observed that a conserved acidic residue predicted to be in the active site involved in configuring the metal ion is important for PIN domain activity as a mutation of Asp7 renders VapC_{LT2}^{D7A} inactive (Figure 24A and 24B Right).

Several other site-specific tRNases are known, which includes colicin D, colicin E and PrrC, but VapC is so far the only tRNase known that cleaves initiator tRNA. Colicin D cleaves four isoaccepting arginine tRNAs between positions +38 and +39 (Tomita *et al.*, 2000), while colicin E5 cleaves in the anticodon loop of 4 different elongator tRNAs, between +34 and +35 (Ogawa *et al.*, 1999). The tRNA cleaving colicins are considered to be bacteriocidal, and are in contrast to VapC, transported out of the producer cells to kill non-producing competitor cells. Colicin-producing cells produce immunity proteins that are analogous in function to antitoxins. PrrC, which cleaves lysine tRNA in the anticodon loop between +34 and +35, is activated by bacteriophage T₄ infection (Amitsur *et al.*, 1987).

The VapC_{LT2} and VapC dependent cleavage was mapped to occur between position +38 and +39 *in vivo* and *in vitro*, though *in vivo* cleaved fragments were subsequently degraded, most-likely by cellular ribonucleases (Figure 26 and 27). A similar observation has been reported for colicin D (Tomita *et al.*, 2000). Interestingly, the anticodon loop including position +38 and +39 is also conserved in elongator tRNA^{fMet} but is not cleaved (Figure 23B). A recent crystal structure of the tRNA^{fMet} anticodon stem-loop revealed unique conformational differences to elongator tRNA,

which in particular involves interaction between A38 and _{2m}C32 and C39 and A37 (Barraud *et al.*, 2008). This could indicate that either the GC stem, which is only present in tRNA^{fMet}, or these unique structural features of the anticodon loop might be the discriminator for VapC recognition. This however still remains to be tested.

Furthermore, in this study it was shown that VapC can be activated from the *vapBC* operon during abrupt translation inhibition (Figure 28). Surprisingly, only weak cleavage of tRNA^{fMet} was detected. This could either be caused by intrinsic low activity of VapC which might be due to the genetic context, as it is plasmid resident, which might affect the regulation. But it could also reflect activation of VapC in a subpopulation of cells. It has recently been shown that TAs might contribute to stochastic generation of a subpopulation of cells which are persistent to antibiotic treatment (Maisonneuve *et al.*, 2011). In relation to that the weak cleavage observed by VapC might reflect high cleavage in just a subpopulation of cells and indicating stochastic activation. This however remains to be tested.

However a very interesting occurrence was observed as depletion of tRNA^{fMet} by VapC cleavage activated initiation of translation at elongator codons positioned correctly relative to a ribosome binding site. This was observed indirectly by *trans*-activated ribosome YoeB cleavage and more directly in the dual luciferase system (Figure 19 and 29).

VapC was therefore found to inhibit global initiation of translation and simultaneously activating translation of reading frames that are normally silent. Whether this latter effect has physiological consequences (i.e. when endogenous VapC is activated in the wild type context) remains to be determined. However, Varshney and colleagues recently observed that a reduction of the cellular level of tRNA^{fMet} by mutations in the *metZ WV* promoter relaxed the stringency of initiator tRNA selection at the ribosomal P-site (Kapoor *et al.*, 2011). This result supports the idea that the reduced level of tRNA^{fMet} observed after *vapC*_{LT2} or *vapC* induction allows loading of elongator tRNAs in the P-site and thereby stimulates ectopic initiation of translation. The requirement for an SD sequence for ectopic initiation is in agreement with this interpretation. Another observation which favours this idea was the higher initiation of translation observed at AAA codons compared to AAG codons (Figure 29). There is a clear correlation between codon usage and cognate tRNA abundance (Dong *et al.*, 1996). In *E. coli* K-12, 73% of lysine codons are represented by AAA codons which suggest higher abundance of the cognate tRNA and could

explain the observed increased preference in initiation of translation from this codon compared to AAG lysine codon.

Like other components of the translational apparatus, production of tRNA^{fMet} is controlled by the stringent response (Nagase *et al.*, 1988). Moreover, the charging level of tRNA^{fMet} decreases in response to leucine starvation (Dittmar *et al.*, 2005). Thus, bacterial cells regulate the level of tRNA^{fMet} in response to environmental changes. This makes physiological sense, since a reduced rate of translation reduces both nutrient consumption and the translational error rate (Sorensen *et al.*, 1994) which, in turn, may increase cellular fitness. It is shown here that VapC can be activated by abrupt reduction of the growth rate (Figure 28). Thus *vapBC* may reduce the translational error rate during conditions of slow growth simply by reducing the drain on charged tRNA. In addition, it cannot be excluded that *vapBC* induces major changes in the proteome of slowly growing or starved cells. A possibility would be start codon selection shift from AUG and towards reading frames with alternative start codons (e. g. GUG and UUG) or maybe even to different reading frames, although this remains to be tested.

I propose that enteric VapCs represent a novel class of tRNases that could be beneficial during environmental stresses including virulence (Figure 30).

The Major human pathogen *Mycobacterium tuberculosis* has an expanded number of genes encoding VapC homologues on its chromosome, and 45 *vapBC* loci have been identified so far (Pandey and Gerdes, 2005; Ramage *et al.*, 2009). The majority of toxins induce a quasi-dormant growth state, which makes *M. tuberculosis* an interesting organism of study as it has the ability to arrest growth during intracellular phases of its lifecycle (Gerdes *et al.*, 2005). Interestingly, it has recently been shown that TAs, including loci of the *vapBC* family, are up-regulated during anoxic growth and during growth inside macrophages (Ramage *et al.*, 2009; Korch *et al.*, 2009). The *vapBC* locus has also previously been shown to affect the intracellular growth-rate of the human pathogen *Neisseria gonorrhoea*, which is consistent with a possible role in growth rate regulation during virulence (Hopper *et al.*, 2000).

Both *Shigella flexneri* 2a and *Salmonella enterica* serovar Typhimurium, which are the host organisms of the *vapBC* loci investigated in this study, show intracellular growth strategies during pathogenesis, which involve states of slow growth and *vapBC* might play a role (Tsolis *et al.*, 2008). It can not be excluded that *vapBC* loci

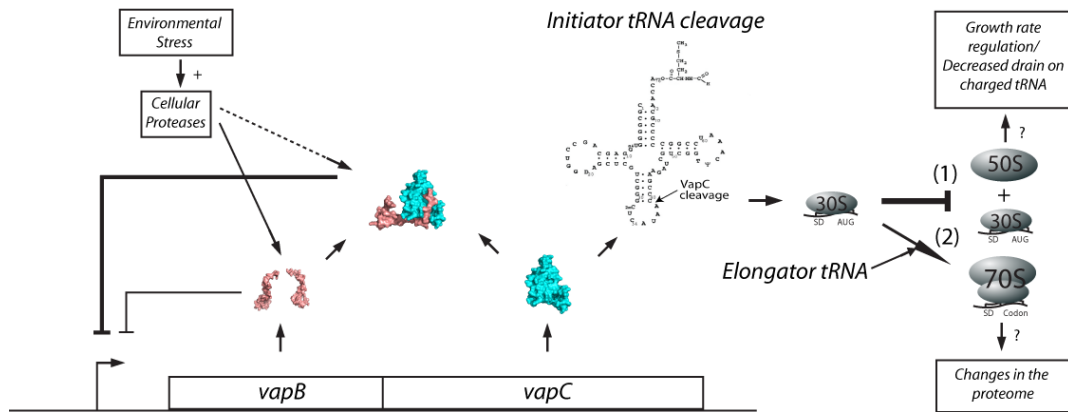


Figure 30 Model for VapC activation and activity. Environmental stress such as nutrient deprivation decrease *de novo* synthesis of antitoxin VapB (salmon) and increase protease activity which in turn liberates more stable VapC (cyan), either by degradation of antitoxin in free form or in complex. VapC is activated and cleaves initiator tRNA, which inhibits translation at the step of initiation. This may have several consequences; (1) VapC inhibits formation of 70S initiation complexes which decreases the growth rate and drain on charged pools of tRNA that in turn results in higher translational fidelity, (2) Removal of initiator tRNA allows alternative tRNA to compete for P-site occupation, which leads to translation initiation events and changes in the proteome.

also play other roles as they are present in non-pathogens and are highly abundant in Archaea (Olah *et al.*, 2001; Cooper *et al.*, 2009). In addition, a single *vapBC* locus has recently been linked to heat shock survival of *Sulfolobus solfataricus* (Maezato *et al.*, 2011).

These observations support that *vapBC* could contribute to growth rate regulation and benefit the cell during stress conditions. However, it does not exclude that *vapBC* TA loci may play additional roles in enterics or in other organisms.

The work presented here has opened the path to identify the cellular targets of VapC PIN-domain proteins from other organisms, including *M. tuberculosis*.

Future Perspectives for Results Section I

From the data presented Results Section I, it is clear the VapC_{LT2} and VapC are tRNases that specifically cleave tRNA^{fMet}. An obvious question that arises is how VapC_{LT2} and VapC distinguish this particular tRNA from 60 different species. It would be very interesting to investigate the substrate specificity VapC biochemically by introducing mutations in tRNA^{fMet} or the anticodon stem-loop which abolishes or enhances the activity of VapC. In general tRNAs are highly modified and it would also be interesting to investigate the importance of these modifications for tRNA cleavage. Alternatively, the unique structure of tRNA^{fMet} might also be important for substrate recognition and can be tested biochemically. In this case a crystal structure of VapC bound to its substrate would give crucial information about substrate recognition and the mechanism of cleavage.

Interestingly, it is observed that *vapB* induction in VapC inhibited cells, which are almost devoid of full-length tRNA^{fMet}, leads to relatively rapid accumulation of full length tRNA^{fMet} and resumption of growth. This suggests that additional mechanisms might be present which aids resuscitation. One possibility is that a small pool of tRNA^{fMet} is protected from VapC either by binding to aminoacyl tRNA synthetases or initiation factor 2. An alternative possibility is that some of the cleaved tRNA^{fMet} can be repaired by RNA ligases. Recently, a putative RNA repair operon has been identified in *E. coli* K-12 named *rtcBA* (Chakravarty and Shuman, 2011; Tanaka and Shuman, 2011). RtcB is an ATP-dependent 3'-5'-RNA ligase and RtcA is a 3'terminal RNA cyclase. RtcA has also been observed to have polynucleotide 5'-adenylation activity, which raises interesting questions for its biological activity. Interestingly Shuman and co-workers showed that tRNAses such as *Kleuveromyces lactis* γ -toxin produces substrates that can be ligated by RtcB, which suggests that RtcB has a function in tRNA repair (Tanaka and Shuman, 2011).

I have also obtained indirect evidence that VapC might produce substrates for RNA ligases such as RtcB, with a 3' terminus phosphate in the 5'-cleavage product and a 5'-OH in the 3' cleavage product. The 3'-terminus of the 5'-product of tRNA^{fMet} could not be ligated to pCp with T₄ RNA ligase, consistent with a 2',3'-cyclic phosphate. The 5'-terminus of the 3'-product could be phosphorylated without prior dephosphorylation, indicating a 5'-hydroxyl group. This is analogous to other known tRNases such as colicin D or colicin E5 (Ogawa *et al.*, 1999; Tomita *et al.*, 2000).

Furthermore, an *rtcB* deficient strain has been observed to show greater sensitivity to VapC than wild type as growth recovery in the mutant is delayed after a VapC pulse. This could indicate that RtcB alone or with RtcA could aid resuscitation. It would be very interesting to investigate this further to find out if this putative RNA repair operon is involved in tRNA^{fMet} repair.

A second interesting aspect would be the possible role in pathogenesis. In an early attempt, I created a *vapBC*_{LT2} deletion strain of pathogenic *S. enterica* SL1344, which is very similar to *S. enterica* LT2. Wild type and mutant were then tested in a virulence assay on mammalian epithelial cells (Collaboration with Paul Dean, Newcastle University). However, no significant differences were observed comparing wild type to *vapBC*_{LT2} deletion strain. This suggests that *vapBC*_{LT2} is not involved in invasion, but does not exclude that *vapBC*_{LT2} might be involved in regulating growth inside cells as has been observed for *fitAB* of *N. gonorrhoea* (Hopper *et al.*, 2000). An interesting experiment would be to measure the growth rate of *S. enterica* SL1344 Δ *vapBC*_{LT2} during vacuolar growth or growth inside macrophages. This can be performed using a gentamycin protection assay as bacterial cells are protected from gentamycin whilst inside a host cell (Elsinghorst, 1994). Recently it has been shown that TAs may contribute to increased frequencies of persisters, e.g. a sub population of cells which show high tolerance to antibiotic treatment (Maisonneuve *et al.*, 2011). It would be interesting to test whether a plasmid resident *vapBC* can complement or partially complement the decreased persister frequency phenotype of an *E. coli* K-12 strain lacking ten TAs.

Results Section II: Transcriptional regulation of *vapBC*_{LT2}

Introduction to experimental work

Type II Toxin-antitoxin (TA) loci are abundant on plasmids and chromosomes of free-living prokaryotes and generally make up a single transcriptional unit (Gerdes *et al.*, 2005). Transcription from the TA promoter is auto-regulated by the antitoxin, which contains an N-terminal DNA binding domain thus DNA-binding is enhanced by forming a stable, high affinity complex with the toxin via the antitoxin C-terminus. The antitoxin is unstable and is rapidly degraded by cellular proteases under conditions of stress or treatment with antibiotics, which in turn activates transcription from the TA promoter (Christensen *et al.*, 2001; Hazan *et al.*, 2004). Toxins of TAs have been divided into at least ten families of which *vapBC* is by far the most abundant in both bacteria and archaea (Pandey and Gerdes, 2005; Jorgensen *et al.*, 2009; Makarova *et al.*, 2009). In Results Section I, it was reported that VapC toxins from enterics are RNases that inhibit global translation by cleavage of tRNA^{fMet} in the anticodon stem-loop. The subject of Results Section II is the regulation of the *vapBC* operon.

It is now clear that VapBC, analogous to other toxin-antitoxin families, auto-regulates transcription by binding to inverted repeats in the promoter region (Wilbur *et al.*, 2005; Bodogai *et al.*, 2006; Robson *et al.*, 2009). The best studied example to date is FitAB (fast intracellular trafficking) from *Neisseria gonorrhoeae* which binds to a 36bp promoter DNA inverted repeat as (FitA₂-FitB₂)₂, an octamer of four FitA-FitB heterodimers, and illustrates how a FitB toxin dimer bridge enhance FitA antitoxin DNA-binding (Mattison *et al.*, 2006).

Several recent studies have shown that the toxin might not only enhance affinity of antitoxin for DNA binding, but also under certain conditions decrease affinity; this phenomenon has been observed for Kis-Kid, CcdAB, RelBE and Phd-Doc TA-systems (Monti *et al.*, 2007; Afif *et al.*, 2001; Overgaard *et al.*, 2008; Garcia-Pino *et al.*, 2010). This phenomenon is also referred to as conditional cooperativity.

In recent studies of RelBE and Phd-Doc it was observed that toxin in excess abolishes cooperativity in the DNA binding. In the reported examples conditional cooperativity is based on the presence of a high affinity and a low affinity binding site in the toxin. When the toxin and antitoxin levels are balanced both binding sites in the

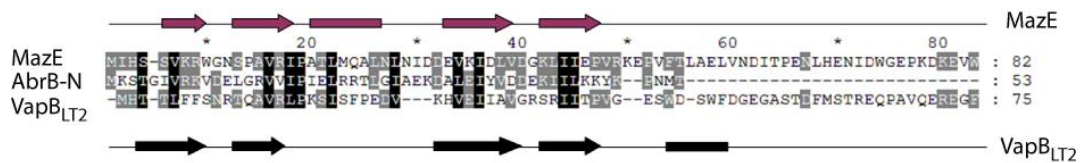


Figure 31 Sequence alignment of AbrB proteins. Alignment contains MazE, AbrB N-terminal domain and VapB_{LT2}. Secondary structure of MazE observed from crystal structure is shown in Magenta (Kamada *et al.*, 2003) and predicted secondary structure (<http://bioinf.cs.ucl.ac.uk/psipred/>) of VapB_{LT2} shown in black. (Arrows = β -sheets, Boxes = α -Helices).

toxin are occupied by antitoxin C-termini. When the toxin and antitoxin levels are unbalanced and the toxin is in excess of antitoxin, the high affinity binding sites on free toxins will compete for low affinity site bound antitoxin C-terminus, which will lead to decreased cooperativity and decreased affinity for DNA. This is by means an additional mechanism by which the TA locus can regulate and balance the expression of antitoxin and toxin in the cell. A dual role of the toxin in regulating DNA binding has not yet been reported for VapBC toxin antitoxin family.

VapB_{LT2} is the antitoxin and has been predicted to contain a N-terminal DNA binding domain belonging to the family of AbrB transcriptional repressors (predicted by Interpro, <http://www.ebi.ac.uk/interpro/>) (Figure 31). The MazE antitoxin of the *mazEF* TA-locus also belongs to this family (Kamada *et al.*, 2003). In this results section, Results Section II, the transcriptional regulation of *vapBC* from *Salmonella enterica* serovar Typhimurium LT2 is analysed (here referred to as VapBC_{LT2}).

Strict translational coupling between *vapB*_{LT2} and *vapC*_{LT2} ensures excess levels of VapB_{LT2} during steady state growth

Translation coupling has previously been described for *parD* (encoding *kis-kid* TA-locus) of plasmid R1, but has not been shown for *vapBC* TAs (Ruiz-Echevarria *et al.*, 1995).

The *vapB*_{LT2} and *vapC*_{LT2} reading frames overlap by one base such as the last A in *vapB*_{LT2} UGA stop codon is the first A in *vapC*_{LT2} AUG start codon, which indicates translational coupling. This possibility was analysed by making a series of mutations in the *vapB*_{LT2} gene of a translational *vapBC*_{LT2}^{D7A}-*lacZ* fusion under the control of a constitutive P_{tac} promoter. The ptac promoter here mimics a de-repressed *vapBC* promoter and the D7A substitution in *vapC*_{LT2} avoids potential toxicity (Figure 32A). It is observed that a start codon mutation in *vapB*_{LT2} abolishes all translation of *lacZ*, which indicates strict translational coupling (Figure 32B). It is also observed that a

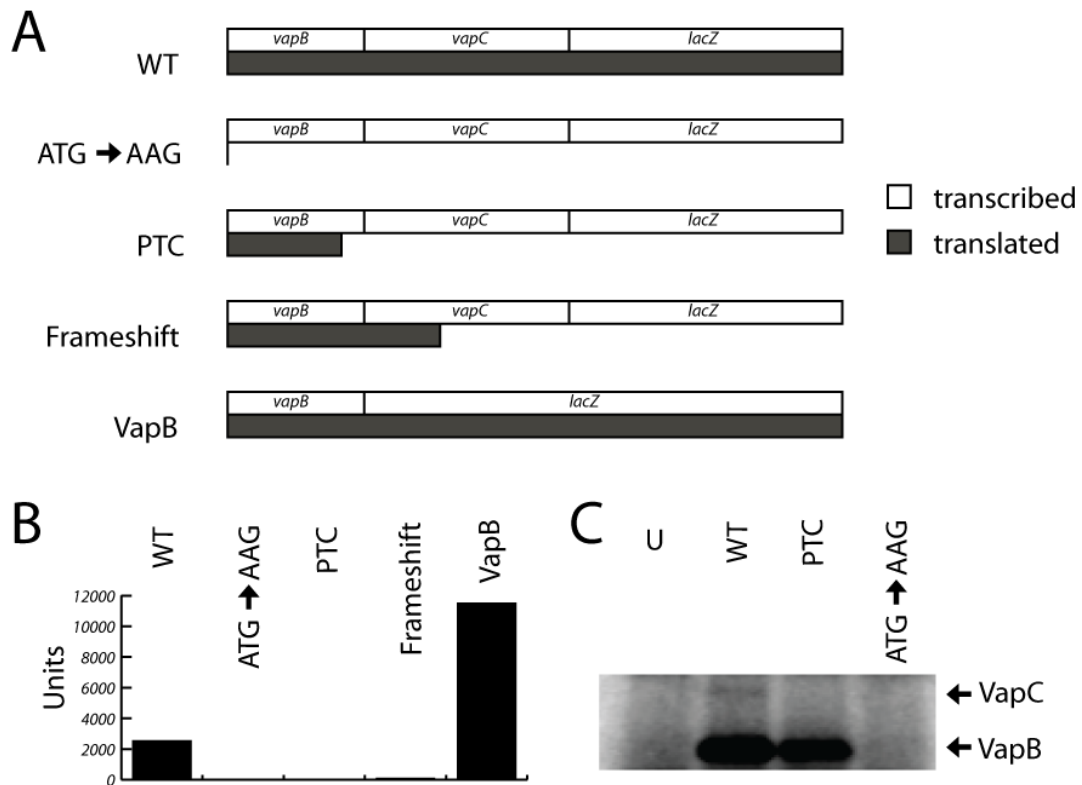


Figure 32 Translation of *vapBC*_{LT2} transcript from a constitutive promoter results in translation of VapB_{LT2} with strict translational coupling to VapC_{LT2}. **A**) Expected reading frames of different translational *lacZ* fusions; wildtype (WT), start codon substitution AUG → AAG in *vapB*, premature termination codon (PTC) in *vapB*_{LT2}, frameshift mutation in *vapB*_{LT2} and a direct fusion to *vapB*_{LT2}. Transcribed mRNA is shown in white and translated in grey. **B**) Analysis of translational coupling between *vapB*_{LT2} and *vapC*_{LT2} *in vivo*. TB28 (MG1655 Δ *lacZ*YIA) containing either pKW253-1 (p_{tac}::*vapBC*_{LT2}^{D7A}::*lacZ*YA), pKW253-2 (p_{tac}::*vapBC*_{LT2}^{D7A}::*lacZ*YA with *vapB*_{LT2} ATG→AAG), pKW253-3 (p_{tac}::*vapBC*_{LT2}^{D7A}::*lacZ*YA with PTC in *vapB*_{LT2}), pKW253-4 (p_{tac}::*vapBC*_{LT2}^{D7A}::*lacZ*YA with frameshift mutation in *vapB*_{LT2}) or pKW253-5 (p_{tac}::*vapB*_{LT2}::*lacZ*YA) were grown exponentially in LB medium at OD₆₀₀ = 0.5 samples were collected and the activity of β -galactosidase measured (Units). **C**) Analysis of translational coupling *in vitro*. Purified *vapBC*_{LT2} mRNA (1 pmol) without and with premature termination codon in *vapB*_{LT2} or *vapB*_{LT2} start codon mutation was added to a S30 *in vitro* translation extract containing ³⁵S-methionine and incubated at 37°C for 25 min. *In vitro* protein products resolved by SDS-PAGE and visualised by phosphor imaging.

premature stop codon in *vapB*_{LT2} (UAA stop codon at codon 61 instead of 77) and a frame-shift mutation which forces the ribosomes to terminate translation inside *vapC*_{LT2} (UGA stop codon at codon 82 instead of 77) also abolishes translation of *lacZ*. These observations confirm strict translational coupling between termination of translation in *vapB*_{LT2} to initiation of translation in *vapC*_{LT2}. A direct translational *vapB*_{LT2}-*lacZ* fusion results in an approximate ~4-fold higher β -galactosidase activity compared to a translational *vapBC*_{LT2}-*lacZ* fusion. This indicates a ~4-fold lower translation level of *vapC*_{LT2} compared to *vapB*_{LT2} resulting from the non-optimal coupling efficiency. This observation is confirmed *in vitro* using purified *vapBC*_{LT2}

mRNAs in a cell free *in vitro* translation system (Figure 32C). VapC_{LT2} is only produced with WT mRNA and not with mRNA containing either the premature termination codon or *vapB*_{LT2} start codon mutation. Only small amounts of VapC_{LT2} are detected, which might be caused by the uncoupling of transcription and translation in the *in vitro* assay. These *in vivo* and *in vitro* observations indicate that during steady state, VapB_{LT2} will always be produced in excess of VapC_{LT2}, thus is consistent with its role as an antitoxin.

Lon protease is responsible for VapB_{LT2} degradation which activates *vapBC*_{LT2} transcription during nutritional stress and by chloramphenicol

To locate the *vapBC*_{LT2} promoter, the transcriptional start site was identified by primer extension analysis. This was performed on RNA samples prepared from *S. enterica* LT2 and *E. coli* MG1655 containing pKW512 (pRBJ200::*vapBC*_{LT2}::*lacZ*). The primer used is complementary to a region inside *vapB*_{LT2} mRNA, making it possible to map the region upstream of *vapB*_{LT2} start codon and detect transcriptional start sites upstream of *vapB*_{LT2}. A specific band consistent with a transcriptional start site was detected upstream of *vapB*_{LT2}, which includes a short leader containing the Shine & Dalgarno sequence of *vapB*_{LT2} (Figure 33A). Inspection of the region upstream of the mapped transcriptional start site (+1) revealed putative -10 and -35 sequences (Figure 33D). Furthermore, two inverted repeats were observed in the promoter region, one perfect repeat overlapping with -10 sequences and another imperfect repeat overlapping the -35 sequence. These inverted repeats are likely to represent the binding sites of VapB_{LT2}.

Previously, it has been shown that transcription of *E. coli* toxin-antitoxin loci *relBE* and *mazEF* increases when cells are exposed to antibiotics and nutritional stress e.g. amino acid starvation (Aizenman *et al.*, 1996; Christensen *et al.*, 2001; Christensen *et al.*, 2003). To investigate whether *vapBC*_{LT2} responds in a similar manner, cells of *S. enterica* LT2 and *E. coli* MG1655 containing pKW512 (pRBJ200::*vapBC*_{LT2}::*lacZ*) were grown exponentially, and at time zero exposed to serine hydroxamate (SHT). SHT induces serine starvation by a competitive inhibition of seryl tRNA synthetase which prevents charging of serine tRNA (Tosa and Pizer, 1971). By semi-quantitative primer extension, promoter activity was analyzed (Figure 33A). It is observed that transcription of *vapBC*_{LT2} increases significantly upon SHT induced amino acid starvation. It is also observed that transcription increase by translational inhibition by

in protease deficient *E. coli* strains during translation inhibition. As observed in Figure 33B, *vapBC*_{LT2} transcription increases after 10 min both from chromosomal encoded *vapBC*_{LT2} of *S. enterica* LT2 and from plasmid resident *vapBC*_{LT2} in *E. coli* K-12 MG1655. Transcription also increased in MG1655 Δ *clpP* (lanes 10-12), but not in MG1655 Δ *lon* (lanes 7-9). This indicates that Lon protease is responsible for VapB_{LT2} degradation. This was also confirmed by Western blot analysis using VapB_{LT2} specific polyclonal antibodies in similar strains expressing VapB_{LT2} (Figure 33C). Consistent with the primer extension, it is observed, that after 10 min the stability of VapB rapidly decreases in MG1655 and MG1655 Δ *clp*, however not in the MG1655 Δ *lon* strain. This suggests that ATP-dependent Lon protease is responsible for VapB_{LT2} degradation and transcriptional activation during translation inhibition.

VapB_{LT2} specifically binds its own promoter DNA and VapC_{LT2} increase the affinity of VapB_{LT2} for DNA

Two inverted repeats which represent putative *vapB*_{LT2} binding sites were identified in the promoter region. To test this hypothesis, native VapB_{LT2} and VapC_{LT2} were purified, incubated with a DNA fragment containing promoter region, and analysed by electrophoretic mobility shift assays (EMSA) (Figure 34A). It is observed that VapB_{LT2}, which contains an AbrB-like DNA-binding domain, has affinity for DNA; however only at very high concentrations more significant DNA-VapB_{LT2} complexes are observed (lanes 3-7). This indicates that VapB_{LT2} by itself only has very low affinity for DNA. It is also observed that VapC_{LT2} toxin does not have affinity for DNA itself (lane 8). All EMSA reactions contain an excess of salmon sperm DNA to avoid unspecific DNA binding.

However, incubation of low concentrations of VapB_{LT2} with increasing concentrations of VapC_{LT2} gives a dramatic increase in affinity for DNA (lanes 9-13). This indicates that VapC_{LT2} greatly increases the affinity of VapB_{LT2} for DNA. It is also observed that the VapB_{LT2} DNA-binding is highly specific for promoter DNA as no binding to unspecific DNA (P) occurs. Formation of two DNA-protein complexes, C1 and C2, are observed, which could indicate binding to both inverted repeats in the promoter region (Figure 33C). To elucidate this in greater detail, a DNase I protection assay was performed on DNA bound complexes (Figure 34B). Promoter DNA was incubated with VapB_{LT2} and increasing concentrations of VapC_{LT2} (lanes 1-4) and analysed for DNase I protection. Two protected areas are observed, which overlap

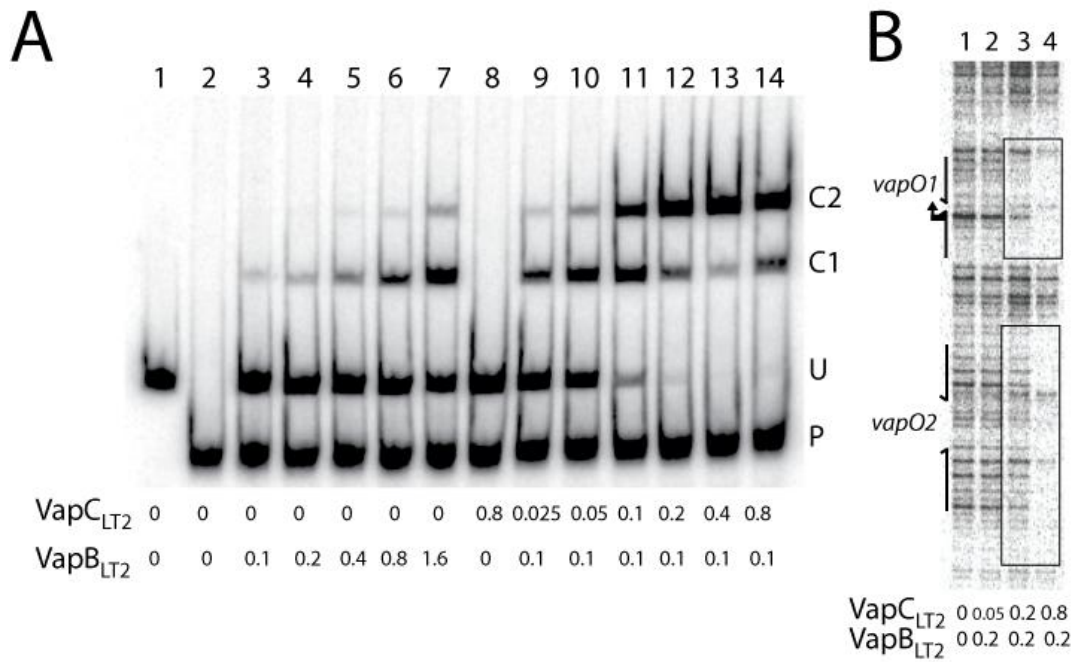


Figure 34 VapB_{LT2} binds to two inverted repeats in promoter region and VapC_{LT2} increases the affinity of VapB_{LT2} for DNA. **A)** Electrophoretic mobility shift assay on VapB_{LT2} binding to DNA. Purified VapB_{LT2} and VapC_{LT2} was added to a radio labelled DNA probe containing the *vapBC*_{LT2} promoter region (-179bp and +122bp of transcriptional start site) in concentrations shown (μ M) (lane 1-14). Bound complexes were separated on a 5% native PAGE gel and visualized by phosphor imaging. U is the unbound probe and C1 and C2 are the complexes formed when probe is bound. P is a ~200bp DNA fragment from pUC vector and used as control for unspecific binding. **B)** DNase I protection assay on *vapBC*_{LT2} promoter region. Purified VapB_{LT2} and VapC_{LT2} was added to a DNA probe as in A) and subsequently incubated with DNase I (lane 1-4). Digested DNA was then separated in an 8% Urea PAGE gel and analysed by phosphor imaging. The protected areas are enclosed by boxes and the position of the promoter and the two inverted repeats are marked with arrows.

with the two inverted repeats. This is consistent with VapB_{LT2} binding to and protecting both these sites, and could suggest that C1 and C2 complexes formed in Figure 34A correspond to one and two complexes of VapB_{LT2} and VapC_{LT2} bound to promoter DNA. On the basis of these data, I rename inverted repeat overlapping with -10 sequence to *vapO1* (*vap* Operator) and inverted repeat overlapping with -35 to *vapO2*.

Two inverted repeats represent four putative VapB_{LT2} dimer binding sites. However only two complexes are observed at high VapB_{LT2} concentrations, which could indicate low cooperative binding within each inverted repeat, similar to that shown by CcdA, Kis and RelB (Madl *et al.*, 2006;Monti *et al.*, 2007;Cherny *et al.*, 2007). However, the DNA-protein complexes (C1 and C2) observed in the absence of VapC_{LT2} (lanes 3-7) have similar sizes to those which occur in the presence of VapC_{LT2}, which could indicate that the VapB_{LT2} purification might be contaminated

by small amounts of VapC_{LT2}. VapB_{LT2} is purified from protein complex with VapC_{LT2}, which makes this explanation plausible.

Nevertheless, with increasing VapC_{LT2}/VapB_{LT2} ratio an increased affinity for DNA is observed. Interestingly, it can be observed from Figure 34A lane 14, that at a certain VapB_{LT2}/VapC_{LT2} ratio (~1:8), affinity for DNA is observed to decrease slightly as decreased amount of C2 complexes and increased amount of C1 are detected. This suggests that, at high concentrations, VapC_{LT2} might play an additional role in inhibiting DNA binding.

VapC_{LT2} in excess decreases the affinity of VapB_{LT2} for DNA which is reversible

To investigate this phenomenon in detail, additional EMSAs were performed with a greater excess of VapC_{LT2} compared to VapB_{LT2} (Figure 35A). It is observed that with increasing concentrations of VapC_{LT2}, VapC_{LT2} initially promotes binding of VapB_{LT2} to *vapBC*_{LT2} promoter DNA (lanes 2 and 3), but then drastically decreases the affinity of the complex for DNA (lanes 4-8). In lane 8 almost no C1 complex is observed. This suggests that at a certain VapB_{LT2}/VapC_{LT2} ratio of above ~1:8, VapC_{LT2} gradually decreases the affinity of VapB_{LT2} for *vapBC*_{LT2} promoter DNA.

To verify that this is in fact a direct effect of VapC_{LT2}, the VapB_{LT2}/VapC_{LT2} ratio was shifted by increasing the concentration of VapB_{LT2} (lanes 9-11). It is observed that addition of VapB_{LT2} to the reaction results in increased affinity for DNA, consistent with a direct reversible effect of VapC_{LT2}. This phenomenon is also confirmed by DNase I footprinting (Figure 35B). With increased concentrations of VapC_{LT2}, a decreased protection of both *vapO1* and *vapO2* is observed (lanes 1-7). Furthermore, it is observed that protection is decreased at lower VapC_{LT2} concentrations in *vapO2* that contains an imperfect inverted repeat (compare lane 2 and 3) than in *vapO1* (compare lanes 2-7), which suggests that the complex might have higher affinity for *vapO1*. As observed in the gel shift in figure 35A, when the VapB_{LT2}/VapC_{LT2} ratio is increased protection is regained (lanes 8 and 9). Again it is observed that *vapO1* is protected before *vapO2*, consistent with higher affinity of the complex for this site.

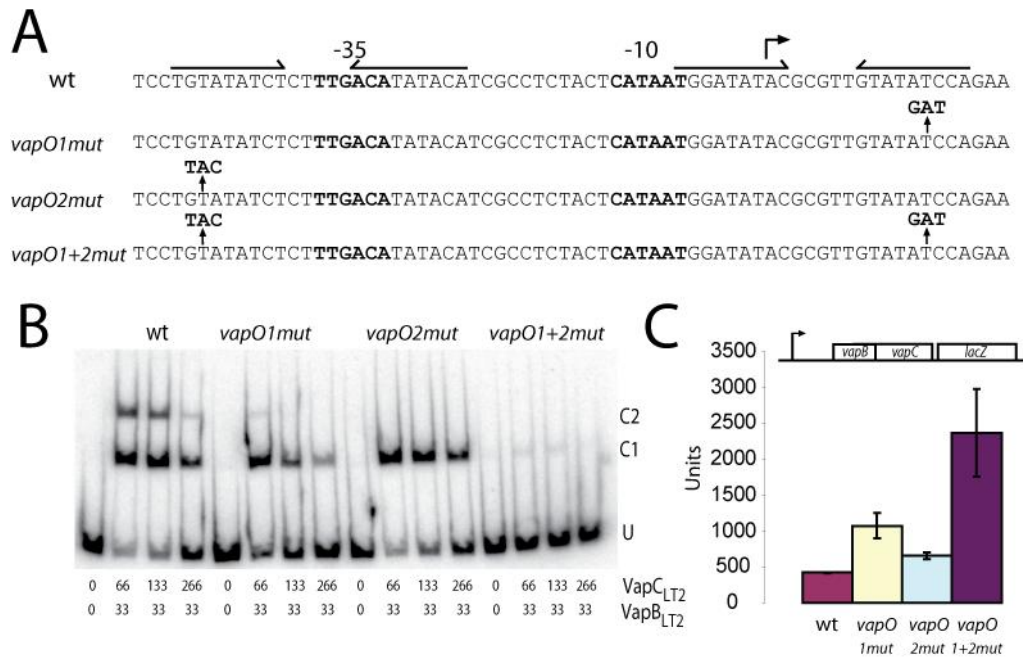


Figure 36 VapC_{LT2} mediated decrease in affinity of VapB_{LT2} for DNA acts on both inverted repeats independently. **A)** DNA sequences of *vapBC*_{LT2} promoter region showing positions of base substitutions in binding site (*vapO*) 1 and 2. The position of promoter and inverted repeats are indicated by arrows. **B)** Electrophoretic mobility shift assay of VapB_{LT2} binding to promoter DNA with binding site (*vapO*) mutations. VapB_{LT2} and VapC_{LT2} were incubated with promoter DNA containing base substitution mutations which scrambles binding site 1 and 2 in amounts shown (nM). Protein-DNA complexes were separated in a 5% native PAGE gel and analysed by phosphor imaging. U indicates unbound DNA probe C1 and C2 is promoter DNA bound by either one or two protein-DNA complexes, respectively. **C)** The *vapBC*_{LT2} promoter activity in binding site mutants. TB28 containing either pKW512TFZD7A (p_{wt}::*vapBC*_{LT2}^{D7A}::*lacZYA*), pKW512TFZD7A-1 (p_{VapOmut1}::*vapBC*_{LT2}^{D7A}::*lacZYA*), pKW512TFZD7A-2 (p_{VapOmut2}::*vapBC*_{LT2}^{D7A}::*lacZYA*) or pKW512TFZD7A-1-2 (p_{VapOmut1+2}::*vapBC*_{LT2}^{D7A}::*lacZYA*) were grown exponentially in LB medium at 37°C. At OD₆₀₀ ~ 0.5 samples were collected out and the activity of β-galactosidase measured (Units).

were selected from the DNA sequence not to affect the binding of RNA polymerase (Figure 36A). Subsequently, EMSAs were performed using DNA probes containing mutations from Figure 36A. As observed previously, when a DNA probe containing wild type promoter is incubated with VapC_{LT2} and VapB_{LT2}, two complexes are observed (C1 and C2). The complexes decrease in intensity with increased concentration of VapC_{LT2}, consistent with a decrease of VapB_{LT2} in affinity for DNA (Figure 36B). However, this is also the case when using *vapO1mut* and *vapO2mut* scrambled probes, which shows that both operator sites are not needed to decrease the affinity of VapB_{LT2} for DNA. Primarily complex C1 is observed in both mutants, consistent with only one operator site being occupied and that C1 formed in both cases is of similar size..

Interestingly, it is observed that *vapO1mut* decreases the amount of protein bound to DNA more significantly than *vapO2mut*, as C1 complex is less intense for the *vapO1mut* than *vapO2mut*. This is consistent with the observation that the protein complex has higher affinity for *vapO1*. It is also observed that when both sites are simultaneously mutated only a very weak C1 complex is detected, which is consistent with the weak C2 complex in the *vapO1mut* probe. This is most likely due to a incomplete disruption of the DNA binding in the *vapO1mut* mutation. To confirm these observations the effect of the binding site mutations on transcriptional repression with transcriptional *vapBC_{LT2}^{D7A}-lacZ* fusions, was tested (Figure 36C). As can be observed, both *vapO1mut* and *vapO2mut* independently allow repression to some degree compared to wt promoter. With a functional *vapO1* (*vapO2mut*), ~ 0.5-fold up regulation is observed compared to wild type. This is more efficient than a functional *vapO2* (*vapO1mut*) as ~ 1.5-fold up regulation is observed compared to wild type. When both operator sites are mutated (*vapO12mut*), ~4.6-fold up regulation is observed compared to wild type. This observation not only suggests that both operator sites contribute to transcriptional repression, but also that the sites independently can repress transcription. It is observed that *vapO1* contributes more efficient to transcriptional repression than *vapO2*, which is consistent with the higher affinity of VapB_{LT2} observed for this operator site. From the data presented it can not be excluded that an increase in transcription is caused by change in affinity of RNA polymerase for DNA in *vapO* mutants. However, the observed increase in transcription is consistent with the observed decrease in affinity of VapB_{LT2} for *vapO* mutants. In summary these observations indicate that the two inverted repeats may act as repressor sites independently and can be used isolated to investigate the DNA binding of VapB_{LT2}.

VapC_{LT2} toxin in excess disrupts DNA-binding of VapB_{LT2} to *vapO1* and shows conditional repression *in vitro* and *in vivo*

To test the repressor sites independently, EMSAs were performed using a DNA fragment containing only *vapO1* (Figure 37A). Consistent with previous experiments, increasing the concentration of VapC_{LT2} in respect to VapB_{LT2}, results in increased affinity of VapB_{LT2} for DNA (lanes 2-5). At a certain VapB_{LT2}/VapC_{LT2} ratio however (1:8, lane 6), affinity for DNA gradually decreases with increased VapC_{LT2} concentration. This can be reverted by changing the VapB_{LT2}/VapC_{LT2} ratio by

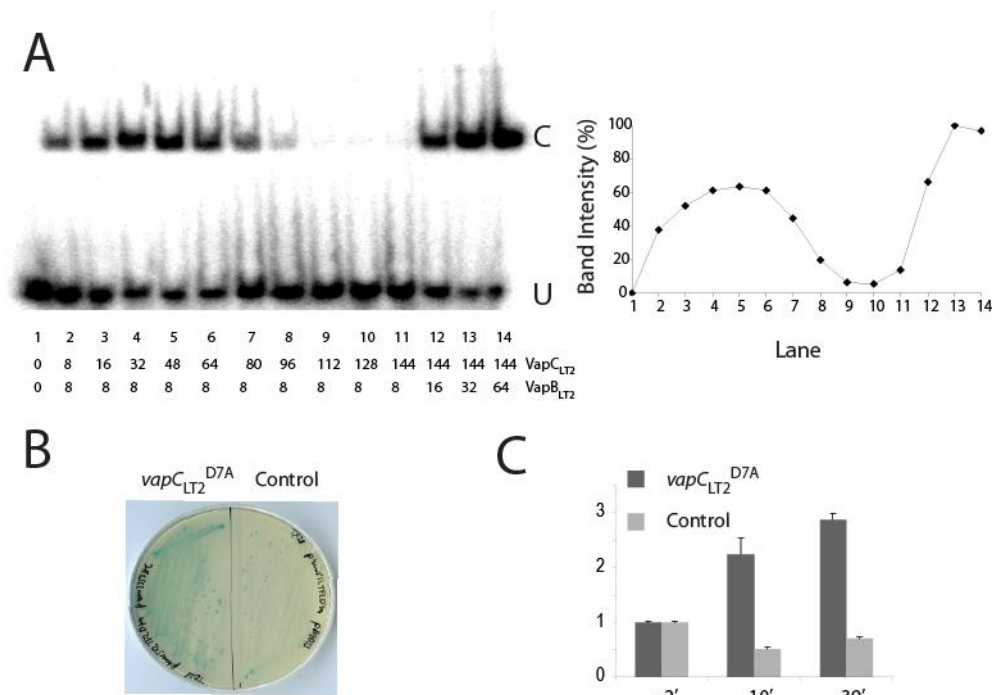


Figure 37 The *vapBC*_{LT2} locus shows conditional DNA binding. **A**) Electrophoretic mobility shift assay with purified VapC_{LT2} and VapB_{LT2} with promoter DNA containing *vapO1*. (Left panel) VapB_{LT2} and VapC_{LT2} were mixed with radio labelled promoter DNA containing *vapO1* binding site (36bp fragment, -14bp and +21bp of +1) in amount shown (nM) (lane 1-14). Protein-DNA complexes were separated by 6% native PAGE and analysed by phosphor imaging. U and C indicate position of unbound and bound DNA, respectively. (Right panel) Image J quantitated Band intensities plotted in a graph with C band intensity (%) as a function of the lane number. **B**) Ectopic induction of *vapC*_{LT2}^{D7A} *In vivo* increases *vapBC*_{LT2} transcription. TB28 (MG1655 Δ *lacIZYA*) pKW512TFZD7A (*vapBC*_{LT2}^{D7A}::*lacZYA*) containing either pKW3353HC (pBAD::SD_{opt}::*vapC*_{LT2}^{D7A}-H6) or pBAD33 were streaked to single colonies on LB plates containing X-gal and 0.2% arabinose. **C**) *vapC*_{LT2}^{D7A} induced transcription as quantified by qPCR. TB28 (MG1655 Δ *lacIZYA*) pKW512TFZD7A (*vapBC*_{LT2}^{D7A}::*lacZYA*) with pKW3353HC (pBAD::SD_{opt}::*vapC*_{LT2}^{D7A}-H6) or pBAD33 empty vector were grown exponential in LB medium at time zero 0.2% arabinose was added to induce transcription from pBAD promoter. Samples were taken at times indicated (min) and total RNA extracted. Quantitative PCR was performed and fold-change in respect to house keeping gene *rpsA* was calculated by $\Delta\Delta C_t$ relative quantification method.

addition of VapB_{LT2} to the reaction through which the affinity is regained (lanes 12-14). This suggests that protein complex bound to single operator site can be liberated when VapC_{LT2} is in excess.

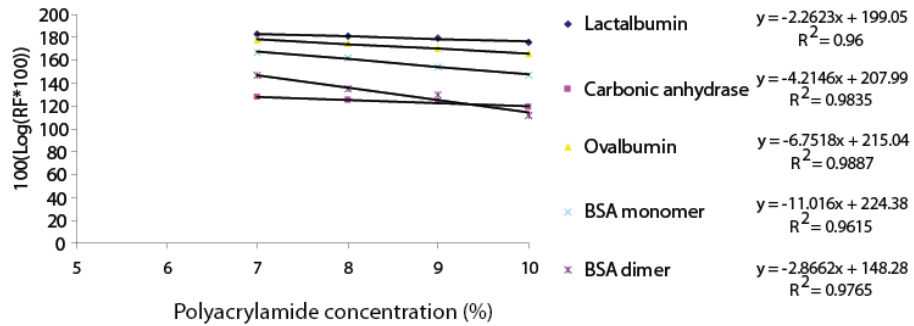
To investigate the biological significance of the conditional repression *in vivo*, *vapBC*_{LT2} was transcriptionally fused to the *lacZ* gene encoding β -galactosidase and analysed in the presence of a plasmid expressing VapC_{LT2} in *trans* (Figure 37B). When inducing a non-toxic *vapC*_{LT2}^{D7A} in *trans* on plates containing X-gal, the colonies are observed to be significantly more blue compared to an empty vector control, consistent with higher *vapBC*_{LT2} promoter activity. Up-regulation of *vapBC*_{LT2} was confirmed by quantitative PCR (Figure 37C). It is observed that after induction of *vapC*_{LT2}^{D7A} the transcription of *vapBC*_{LT2} reaches a ~3-fold increase after

30 min of expression. Furthermore, no increase is observed when inducing empty vector which is consistent with Figure 37B. Summarising these observations, VapC_{LT2} clearly seems to play an additional role by decreasing repression of transcription..

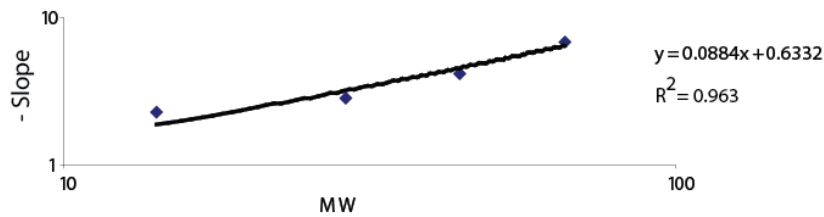
To investigate the protein complex formed on *vapO1* into more detail, the molecular weight (MW) of DNA-protein complex was estimated. The MW was determined by an EMSA based method in which the relative mobility (R_f) in different percentages of polyacrylamide (7-10%) is used to calculate the MW (Figure 38A-D). The relative mobility of MW marker proteins and protein complex with DNA are plotted against the polyacrylamide concentration (Figure 38A and 38C). Slopes of the MW marker proteins were then plotted against their MW and the regression equation was used to calculate the MW of protein complex bound to DNA (Figure 38B and 38D).

The MW of protein complex without DNA was calculated to be 91.74 kD. In a recent study on a VapC homologue, FitB from *N. gonorrhoea*, the crystal structure revealed a FitAB complex binding to DNA as an octamer of four FitAB heterodimers [FitA₂-FitB₂]₂ where FitB dimerisation mediates strong cooperative binding (Mattison *et al.*, 2006). The calculated MW of a [VapB₂-VapC₂]₂ octamer is 93.2 kD, in accordance with the EMSA estimate for protein complex. In the EMSAs presented here (containing *vapO1*) no intermediate complex was observed even at low VapBC_{LT2} concentrations, which if the proteins bind DNA as an [VapB₂-VapC₂]₂ octamer are indicative of very strong cooperative binding. VapC_{LT2} may contribute to cooperativity by forming a bridge between VapB_{LT2} dimers bound to each half-site of *vapO*. However as observed VapC_{LT2} can also destroy DNA binding when in excess of VapB_{LT2}. This suggests that VapC_{LT2} might regulate DNA binding by conditional cooperativity. In the FitAB crystal structure, FitA-FitB heterodimers are very similar and FitB does not contain any obvious low affinity binding sites for FitA as observed for CcdAB, RelBE and Phd-Doc TA complexes (De *et al.*, 2009;Overgaard *et al.*, 2009;Garcia-Pino *et al.*, 2010). This observation opens the possibility that VapB_{LT2} and VapC_{LT2} forms an octameric complex and the mechanism of conditional cooperativity might lie in the dimerisation of VapC_{LT2}.

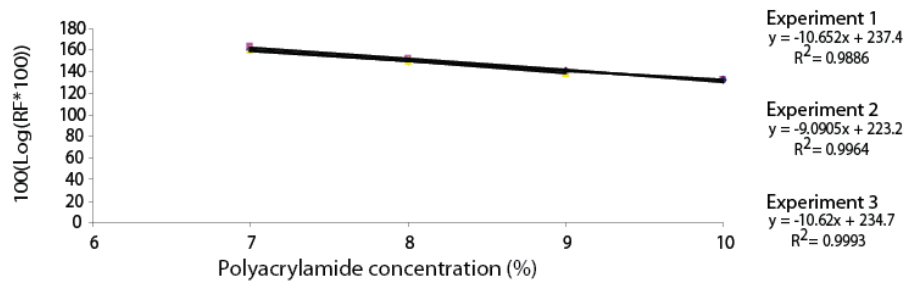
A



B



C



D

	-slope	MW (kD)	MW - DNA (kD)
Exp 1	10.652	119.8645	97.74854
Exp 2	9.0905	102.2005	80.08451
Exp 3	10.62	119.5025	97.38655

Mean 91.74 kD

Figure 38 Estimation of the Molecular weight (MW) of protein complex bound to *vapO1* DNA. **A)** A graph showing the logarithm of the relative mobility (RF) of marker proteins; Lactalbumin (blue), Carbonic anhydrase (magenta), Ovalbumin (Yellow), BSA monomer (teal) and BSA dimer (purple) plotted as a function of polyacrylamide concentration (%). The calculated slopes of regression equations are shown on the right. **B)** The slopes of the marker protein regressions are plotted as a function of the molecular weight. The value of the regression equation of the plot is shown on the right. **C)** A graph showing the logarithm of the relative mobility of protein-DNA complex of three independent experiments. The calculated slopes of regression equations of the three experiments are shown on the right. **D)** Table with the molecular weight of protein-DNA complexes and protein complex (subtracted with mass of promoter DNA fragment 22.106 kD) extrapolated according to the equation $y = 0.0884x + 0.6332$. The average mass of three experiments is 91.74 ± 10.09 kD.

VapC_{LT2} dimerisation is important for transcriptional repression and conditional cooperativity

To investigate the possible role of VapC_{LT2} dimerisation in conditional cooperativity, a mutational analysis was performed on residues that could be important for dimerisation (Figure 40A). To select residues involved in dimerisation, the tertiary structure of VapC_{LT2} was predicted using PHYRE (Kelley and Sternberg, 2009) and the predicted structure superimposed onto FitB (Figure 39A). It can be observed that although VapC_{LT2} and FitB show limited similarity on the level of primary sequence (Figure 14) a high scoring model (FitB was used as a model by PHYRE) can be build which aligns with FitB (Figure 39A). From the possible VapC_{LT2} dimer structure residues can be predicted which might be important for dimerisation (Figure 39B and Figure 40A). Putative residues involved in dimerisation were initially tested by substitution mutations in *vapC_{LT2}* in a transcriptional *vapBC_{LT2}-lacZ* fusion by changing residues in VapC_{LT2} to either alanine or serine (Figure 40A and 40B). As dimerisation is crucial for cooperativity of FitAB DNA-binding, mutations that interfere with dimerisation of VapC_{LT2} should decrease the ability of the complex to repress transcription. It is observed that four residues are of particular interest; leucine 43 to alanine (~ 5.2-fold up-regulation), isoleucine 44 to alanine (~ 1.4-fold up-regulation), tyrosine 72 to alanine (~ 7-fold up-regulation) and alanine 76 to serine (~ 1.9-fold up-regulation).

Tyrosine 72 aligns perfectly with phenylalanine 78 in FitB, which has been shown to be a key residue for FitB dimerisation (Mattison *et al.*, 2006) (Figure 39A). The transcriptional up-regulation observed when residues are mutated suggests that these residues might be important for VapC_{LT2} dimerisation as well.. Interestingly, mutations in the dimerisation interface that affect transcriptional repression also affect toxicity of VapC_{LT2} (Figure 42B). Particularly, L43A and Y72A decrease toxicity, however A76S also seem less toxic as small colonies are observed. This indicates that VapC_{LT2} dimerisation could also be important for toxicity, possibly by affecting the configuration of the acidic catalytic residues in the active site. The decrease in toxicity might also be caused by tertiary structure changes resulting from introducing mutations into VapC_{LT2}.

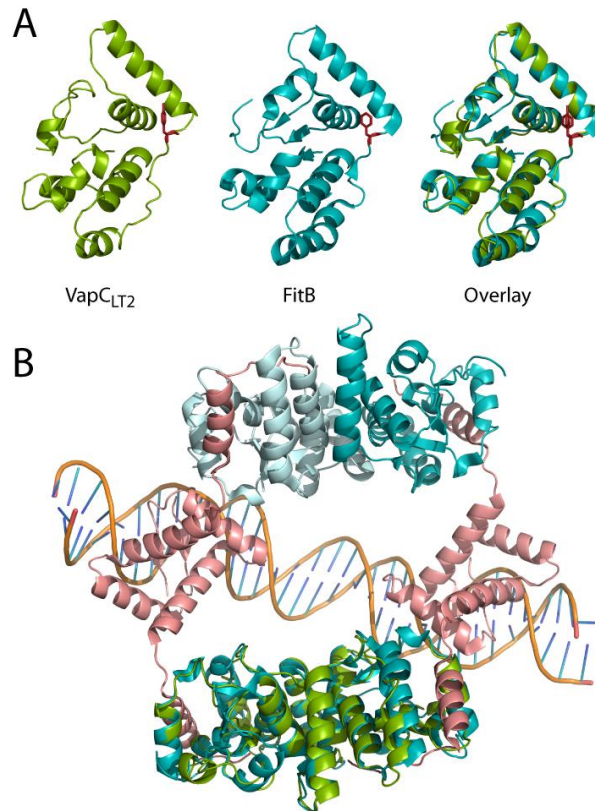


Figure 39 Structural alignment of VapC_{LT2} with FitAB. **A)** The tertiary structure of VapC_{LT2} (STM3033) from *S. enterica* LT2 was predicted using Protein Homology/analogY Recognition Engine (PHYRE (Kelley and Sternberg, 2009), <http://www.sbg.bio.ic.ac.uk/~phyre/index.cgi>) the top scoring prediction had an E-value of $3.850249e^{-15}$ and was build on a model of FitB . The predicted VapC structure was aligned with the structure of *N. gonorrhoea* VapC homologue, FitB (2BSQ chain A) (Mattison et al., 2006) using PYMOL v1.3. Tyr72 of VapC_{LT2} and Phe78 of FitB is highlighted in red **B)** Proposed VapC dimer (Teal blue) aligned with FitB dimer (Violet) in FitAB complex bound to DNA inverted repeat. FitA dimers binding to DNA repeats are shown in green. The FitAB protein structure was obtained from the protein data bank PDB ID; 2BSQ.

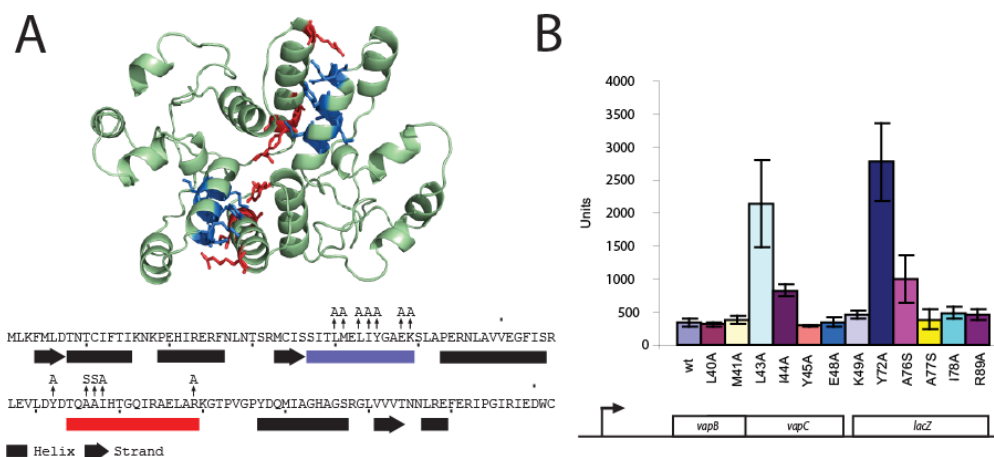


Figure 40 Isolation of mutants in the dimerisation interface that affect repression. **A)** Predicted tertiary and secondary structure of VapC_{LT2} dimer including positions of substitution mutations in predicted dimer interface. Helix 3 and 5 is marked in blue and red, respectively. **B)** Transcriptional activity of vopBC_{LT2} transcriptional fusion to lacZ with mutations in VapC_{LT2} dimer interface. TB28 (MG1655 $\Delta lacZ$ IYA) containing pKW254BC (vopBC_{LT2}::lacZYA) and substitution mutant derivatives were grown exponentially in LB medium at 37°C. At OD₆₀₀ of 0.5 samples were collected and the activity of β -galactosidase (Units) measured.

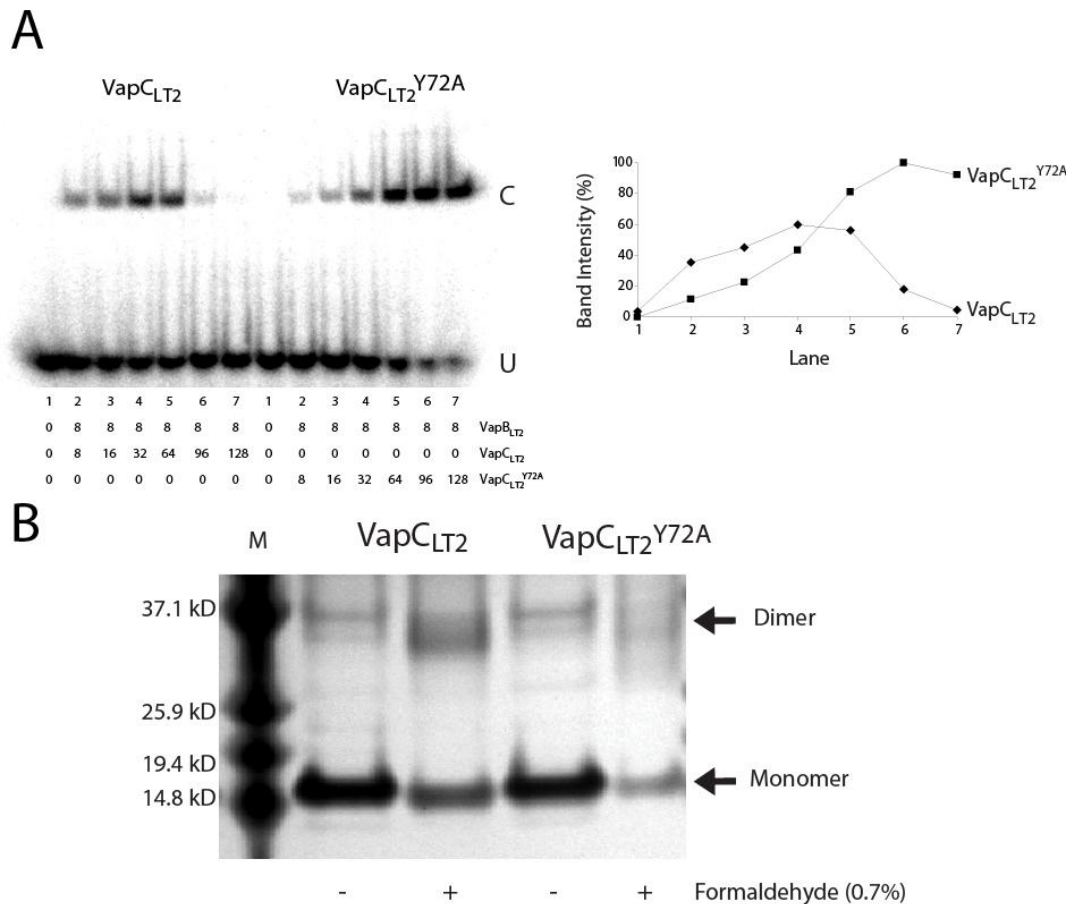


Figure 41 VapC_{LT2}^{Y72A} affects dimerisation and abolishes conditional cooperativity **A**) Electrophoretic mobility shift assay with purified VapC_{LT2}, VapC_{LT2}^{Y72A} and VapB_{LT2} with promoter DNA. (Left panel) VapB_{LT2}, VapC_{LT2} or VapC_{LT2}^{Y72A} were mixed with radio labelled promoter DNA containing *vapO1* in amounts shown (nM) (lanes 1-7). Protein-DNA complexes were separated by 6% native PAGE and analysed by phosphor imaging. U and C indicate position of unbound and complex bound DNA, respectively. (Right panel). Image J quantitated Band intensities plotted in a graph with C band intensity (%) as a function of the lane number. **B**) *In vitro* crosslinking of VapC_{LT2} reveals Y72A mutant as being deficient in dimerisation. 5 pmol Purified VapC_{LT2} or VapC_{LT2}^{Y72A} was *in vitro* cross linked by incubation with 0.7% formaldehyde or storage buffer for 15 min at 37°C. Cross linked complexes were resolved by SDS-PAGE and subsequent silver staining. M is a molecular weight marker and position of monomer and dimer complexes are indicated with arrows.

However, mutants VapC_{LT2}^{L34A}, VapC_{LT2}^{Y72A}, VapC_{LT2}^{A76S} and VapC_{LT2}^{I44A} were initially purified from complex with His-tagged VapB_{LT2} which suggest that the mutations do not interfere with antitoxin binding and that the mutants, in that respect, are correctly folded.

To investigate the importance of substitution Y72A in dimerisation and subsequent DNA-binding, EMSAs were performed using purified VapB_{LT2}, VapC_{LT2} and VapC_{LT2}^{Y72A} together with *vapO1* DNA (Figure 41A). VapC_{LT2} increases the affinity of VapB_{LT2} for DNA (lane 2-4) and at a certain VapB_{LT2}/VapC_{LT2} ratio of ~1:8 (lane 5) the affinity decreases with increasing VapC_{LT2} concentration. Interestingly, when

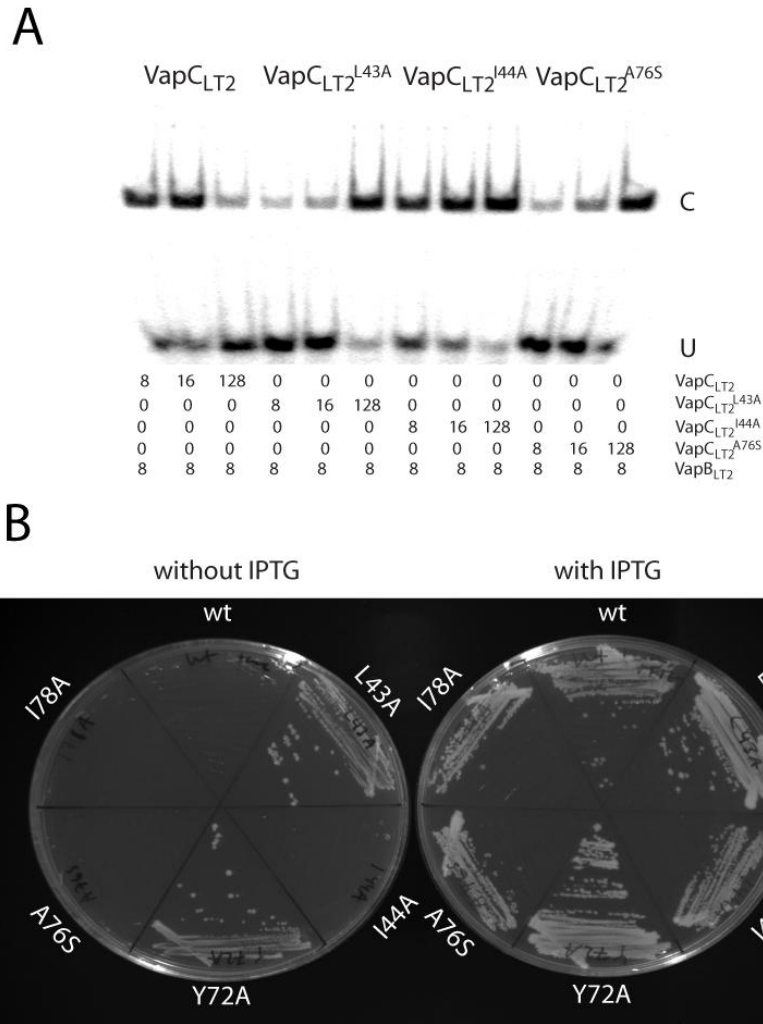


Figure 42 Effect of substitution mutations in VapC_{LT2} dimerisation interface on conditional cooperativity. **A)** Electrophoretic mobility shift assay with purified VapC_{LT2}, VapC_{LT2}^{L43A}, VapC_{LT2}^{I44A}, VapC_{LT2}^{A76S} and VapB_{LT2} with *vapO1* DNA in amounts shown (nM). The proteins were mixed with radio labelled promoter DNA containing VapO1. Protein-DNA complexes were separated by 6% native PAGE and analysed by phosphor imaging. U and C indicate position of unbound and bound DNA, respectively. **B)** Toxicity of dimerisation mutants on plates. MG1655 (*E. coli* K-12) containing pKW51(pA1/03/04:: SD_{opt}::*vapB*_{LT2}) and either pKW52 (PBAD::SD_{opt}::*vapC*_{LT2}), pKW3352L43A (PBAD::SD_{opt}::*vapC*_{LT2}^{L43A}), pKW3352I44A (PBAD::SD_{opt}::*vapC*_{LT2}^{I44A}), pKW3352Y72A (PBAD::SD_{opt}::*vapC*_{LT2}^{Y72A}), pKW3352A76S (PBAD::SD_{opt}::*vapC*_{LT2}^{A76S}), pKW3352I78A (PBAD::SD_{opt}::*vapC*_{LT2}^{I78A}) were single colony streaked on NA plates containing 0.2% arabinose with or without 2 mM IPTG.

VapC_{LT2}^{Y72A} is incubated with VapB_{LT2}, VapC_{LT2}^{Y72A} increases the affinity of VapB_{LT2} for DNA (lanes 1-7). However, as it can be observed from the band intensity profiles (right panel), VapC_{LT2}^{Y72A} only poorly contributes to DNA-binding compared to VapC_{LT2} at low concentrations.

Furthermore, it can also be observed that VapC_{LT2}^{Y72A} does not exhibit conditional cooperativity as it continues to increase the affinity of VapB_{LT2} for promoter DNA even at a VapB_{LT2}/ VapC_{LT2}^{Y72A} ratio of ~1:16 (lane 7). A possible explanation is that

VapC_{LT2}^{Y72A} has decreased affinity for VapB_{LT2}. This however does not explain the lack of conditional cooperativity at high concentrations and that VapC_{LT2}^{Y72A} can promote binding of more VapB_{LT2} to DNA. Consistent with weaker dimerisation, *in vitro* cross linking with formaldehyde, showed that VapC_{LT2}^{Y72A} only weakly crosslinked, whereas VapC_{LT2} made stronger dimer sized crosslinks (Figure 41B). Similar to VapC_{LT2}^{Y72A}, dimerisation mutants of VapC_{LT2}^{L43A}, VapC_{LT2}^{I44A} and VapC_{LT2}^{A76S} were also analysed by EMSA and were also observed to lose the ability to exert conditional cooperativity at VapB_{LT2}/VapC_{LT2} ratio of ~1:16 (Figure 42A). Consistent with the observed increase in *vapBC*_{LT2} transcription, mutants VapC_{LT2}^{L43A} and VapC_{LT2}^{A76S} also significantly affected binding of VapB_{LT2} to DNA. The VapC_{LT2}^{I44A} mutant did so to a lesser extent, which is also consistent with the subtle effect on transcription repression (Figure 40B). These observations support that dimerisation of VapC_{LT2} toxin is important for conditional cooperativity.

Discussion for Results Section II

Previous studies on Toxin-Antitoxin systems such as *Escherichia coli* K-12 *relBE* locus have shown that, under steady-state growth, the *relBE* promoter is transcriptionally repressed (Christensen *et al.*, 2001). Under conditions with decreased rate of translation, by treatment with chloramphenicol or amino acid starvation, transcription from *relBE* promoter is induced, which is dependent on Lon protease. This is due to a decrease in the RelB/RelE ratio as RelB levels are decreased under such conditions (Christensen *et al.*, 2001; Overgaard *et al.*, 2008).

As demonstrated above amino acid starvation or treatment with chloramphenicol also increases transcription from the *vapBC_{LT2}* promoter and is also dependent on Lon protease (Figure 33A and 33B). Furthermore, it was observed that the increase in transcription could be linked to Lon-dependent decrease in the stability of antitoxin VapB_{LT2} (Figure 33C). Interestingly, *vapBC_{LT2}* transcript was also detected before addition of chloramphenicol, indicative of constitutive low level of transcription during steady state growth. A consequence of low basal transcription could suggest rapid turnover of VapB_{LT2} or the presence of a cellular pool of VapBC_{LT2} complex that does not repress transcription. Several studies have reported differential TA transcription within the same organism during steady state growth, whereas some TAs are repressed and others induced (Cooper *et al.*, 2009; Ramage *et al.*, 2009).

S. enterica LT2 VapB_{LT2} contains a predicted N-terminal AbrB DNA-binding domain, similar to MazE antitoxin of *E. coli* K-12 MazEF toxin-antitoxin system. Transcription of *mazEF* was shown to occur primarily from a promoter (P₂), which is located within an unusual inverted repeat which is DNase I protected by MazEF cell extracts (Marianovsky *et al.*, 2001). The crystal structure of MazEF complex revealed a MazF₂-MazE₂-MazF₂ hexamer of two heterotrimers in which both toxin MazF and antitoxin MazE dimerise and is proposed to bind DNA in a MazE:MazF ratio of 1:2 (Zhang *et al.*, 2003a; Kamada *et al.*, 2003). Analysing the region flanking the identified *vapBC_{LT2}* promoter revealed two inverted repeats as potential VapB_{LT2} binding sites (Figure 33D). When native purified VapB_{LT2} was incubated with promoter DNA, binding was only observed at high concentrations, indicating low affinity for DNA; however when VapB_{LT2} was added together with VapC_{LT2}, the binding of VapB_{LT2} to DNA was observed at much lower concentrations (Figure 34A). This indicates that VapC_{LT2} greatly increases the affinity of VapB_{LT2} for DNA.

DNase I protection by VapB_{LT2} bound at the inverted repeats 1 and 2 in the promoter region is also observed. This is consistent with protein complex binding to these sites (Figure 34B). For simplicity I rename the two inverted repeats, *vapO1* and *vapO2*.

Other homologues of VapBC_{LT2} have been characterised for their ability to bind promoter DNA. These include; FitAB from *N. gonorrhoea*, NtrPR from *S. meliltoi*, and more recently VapBC from *M. smegmatis* (Wilbur *et al.*, 2005; Bodogai *et al.*, 2006; Robson *et al.*, 2009). In the case of FitAB, it was shown that FitA antitoxin, which contains a Ribbon-helix-helix (RHH) DNA-binding domain, forms a homodimer which binds promoter DNA with low affinity and with high affinity when in complex with toxin FitB. This is in good accordance with the observations in this work. Interestingly, it was observed that NtrPR containing cell extracts, in which NtrP antitoxin contains an AbrB DNA-binding domain, seems to bind a direct repeat rather than an inverted repeat in the promoter region and therefore this complex might be different.

It has recently been shown that toxins RelE and Doc can either positively or negatively regulate repression of transcription by a mechanism known as conditional cooperativity (Overgaard *et al.*, 2008; Garcia-Pino *et al.*, 2010). When VapC_{LT2} was in excess of VapB_{LT2}, VapC_{LT2} decreased the affinity of VapB_{LT2} for DNA (Figure 35A). The affinity of the VapB_{LT2} for DNA could be recovered by increasing the VapB_{LT2}/VapC_{LT2} ratio, which confirmed that it likely is an active mechanism. Consistently it was observed that VapC_{LT2} in excess results in decreased DNase I protection by VapB_{LT2}; first in *vapO2* and then in *vapO1* indicating higher affinity of the protein complex for *vapO1* (Figure 35B). The observed decrease in affinity of VapB_{LT2} for DNA when VapC_{LT2} is in excess is similar to the effect observed by RelE and Doc.

To address the importance of the two operator sites for the conditional repression mechanism, EMSAs with VapB_{LT2}, VapC_{LT2} and promoter fragments containing scrambled *vapO1* and *vapO2* were performed (Figure 36B). It was observed that mutations in these operator sites do indeed affect binding of VapB_{LT2}, confirming the DNase I protection by protein at these sites. This was also confirmed by transcriptional *lacZ* fusions *in vivo* as each site can contribute to repression of transcription, with *vapO1* being more important than *vapO2*, which can be explained by higher affinity of VapB_{LT2} for the *vapO1* site (Figure 36C). It can however not be

excluded that the transcriptional increase is caused by increased promoter activity in these mutants but is consistent with the *in vitro* observations.

Nevertheless, it was observed that the conditional repression mechanism acts on both operator sites independently as protein complexes bound to either of the operator sites seem to decrease with increasing VapC_{LT2} concentration, suggesting that each inverted repeat is an independent functional repressor site. This was also confirmed by EMSAs of VapB_{LT2} and VapC_{LT2} with isolated *vapOI* which also showed the conditional repression mechanism in excess of VapC_{LT2} and could be reverted by increasing the VapB_{LT2}/VapC_{LT2} ratio (Figure 37A). In addition, VapC_{LT2} mediated increase transcription could also be observed *in vivo* as ectopic overexpression of non-toxic VapC_{LT2}^{D7A} increases transcription of *vapBC*_{LT2} (Figure 37B and 37C).

The crystal structure of FitAB bound to DNA revealed an octamer of four heterodimers binding promoter DNA inverted repeat in a [FitA₂-FitB₂]₂ complex (Mattison *et al.*, 2006). In this complex FitB was found to dimerise forming a bridge between FitA bound to two different half sites of the inverted repeat. It would be expected that such bridging would result in strong cooperativity in DNA binding of FitA. The molecular weight of the protein complex bound to one operator site was estimated to be ~91.74kD which is in good accordance with DNA bound to a [VapB₂-VapC₂]₂-complex (Calculated MW 93.8kD, 4 VapB_{LT2} of 8.514 kD and 4 VapC of 14.938 kD) (Figure 38A,B,C and D). It is observed that DNA binding of VapB to DNA with increasing VapC_{LT2} gives a cooperative saturation profile without binding intermediates (Figure 37A). Another observation which favours a strong cooperative binding of a [VapB₂-VapC₂]₂-complex to DNA is observed when one half-site is scrambled in each of the inverted repeats which results in a complete loss of DNA-binding (Figure 36B).

The explanation for the observed conditional repression mechanism or conditional cooperativity could lie in the dimerisation bridge formed by VapC_{LT2} dimers, which would be crucial for this type of complex. Superimposing the predicted tertiary structure of VapC_{LT2} onto FitB dimer structure made it possible to predict residues involved in VapC_{LT2} dimerisation (Figure 39 and 40A). Mutations which interfere with VapC_{LT2} dimerisation are predicted to result in less stable [VapB₂-VapC₂]₂-complexes and will affect the ability of the complex to repress transcription. A mutational analysis of selected residues in VapC_{LT2} dimer interface was performed, which revealed residues L43A, I44A, Y72A and A76S to affect transcriptional

repression (Figure 40B). Especially, residues L43A and Y72A appeared to be important, as the mutations lead to strong decrease in transcriptional repression. Interestingly, it was also observed that these mutations seem to affect VapC_{LT2} toxicity, which could be linked to the importance of dimerisation in configuring the active site of VapC (Figure 42B). This possibility has readily been discussed for crystal structures of VapCs from *P. aerophilum*; PAE2754, PAE0151 and FitAB of *N. gonorrhoea* (Arcus *et al.*, 2004;Bunker *et al.*, 2008;Mattison *et al.*, 2006). However, this effect might also be caused by significant structural changes as a consequence of the substitution mutations.

It has been shown that FitB has a dimer interface with extensive interactions between α -helix 3 in one dimer with α -helix 5 in the other dimer, which involves several hydrophobic residues. However, especially F78 seem to be the key residue forming several important hydrophobic interactions (Mattison *et al.*, 2006). In the predicted VapC_{LT2} structure, Y72A aligns perfectly with F78 in FitB, which is interesting in respect to the observed effect on *vapBC*_{LT2} transcriptional repression (Figure 39A). To assess this, EMSAs with VapB_{LT2} and promoter DNA with increasing concentrations of VapC_{LT2} or VapC_{LT2}^{Y72A} were performed (Figure 41A). Surprisingly, not only did VapC_{LT2}^{Y72A} decrease the binding of complex to promoter DNA compared to VapC_{LT2} but also abolished the anti-repression mechanism, which is observed by VapC_{LT2} at VapB_{LT2}/VapC_{LT2} ratio of ~1:16. This in turn resulted in even more VapB_{LT2} being bound to DNA at very high VapC_{LT2}^{Y72A} amounts. Taking into consideration that the Y72A mutation does not significantly decrease the affinity of VapC_{LT2}^{Y72A} for VapB_{LT2} it could indicate that a dimer/monomer equilibrium exists in solution in which the dimer favors DNA binding of the complex. The observed stimulation of VapB_{LT2} binding in the presence of high VapC_{LT2}^{Y72A} concentrations is most likely due the fact that the interaction between toxin and antitoxin promotes the folding of the otherwise unstructured antitoxin. This in turn stimulates non-cooperative DNA binding of the antitoxin to the operator sites. Binding is however only observed at very high VapC_{LT2}^{Y72A} concentrations, which is in agreement with its poor ability to stimulate repression of transcription (Figure 40B). Interaction induced folding of the antitoxin has also previously been described for CcdA and Phd antitoxins (De *et al.*, 2009;Garcia-Pino *et al.*, 2010).

That VapC_{LT2}^{Y72A} might produce weaker dimers was also observed by *in vitro* cross linking whereas VapC_{LT2}^{Y72A} showed no or low amounts of dimer (Figure 41B) This

observation could also be confirmed for other purified mutants of VapC_{LT2}; VapC_{LT2}^{L43A}, VapC_{LT2}^{I44A}, and VapC_{LT2}^{A76S}, which had a similar effect on DNA binding of VapB_{LT2} (Figure 42A). These observations all suggest that VapC_{LT2} dimerisation might be important for conditional cooperativity.

It has been shown for CcdB, RelE and Doc that small changes in the antitoxin/toxin ratio results in rapid decrease in affinity of toxin-antitoxin complex for DNA (Afif *et al.*, 2001; Overgaard *et al.*, 2008; Garcia-Pino *et al.*, 2010). For RelE and Doc this has been explained by the presence of a low and a high affinity antitoxin binding site in the toxin. Analysing the crystal structure of DNA bound FitAB reveals a complete symmetry in the FitB dimer interface which means that FitA most likely is bound to the same site in all FitB heterodimers (Figure 39B) (In FitA monomers 9-13 Amino acid C-termini are not visible in the structure) (Mattison *et al.*, 2006). This suggests two mechanisms by which excess VapC_{LT2} can break cooperative complex bound to DNA: (1) VapC_{LT2} in excess directly competes for antitoxin VapB_{LT2} in the DNA bound VapBC_{LT2} complex which could also result in loss cooperativity in the complex. This is highly unlikely since as the VapB_{LT2}-VapC_{LT2} interaction is very strong and can only be broken using high amounts of urea during the purification process and is also the case for VapC_{LT2}^{Y72A} which does not mediate conditional cooperativity. (2) A more likely mechanism is that VapC_{LT2} directly interferes with cooperativity by competing for dimerisation with VapC_{LT2} in the DNA bound VapBC_{LT2} complex, which would eventually lead to decreased DNA affinity by disruption of cooperativity (Figure 43). This mechanism would also predict that a higher concentration of VapC_{LT2} is needed to compete as a dimer equilibrium would not only exist in VapBC_{LT2} complex but also between free VapC_{LT2}. This model is also consistent with the presence of a pool of VapBC_{LT2} complex in the cell during steady-state growth which does not inhibit transcription.

The mechanism of conditional cooperativity allows cells which are inhibited by toxin to return from a dormant state to a state that permits growth. The outcome of a de-repressed promoter on VapB_{LT2} and VapC_{LT2} production was investigated using a constitutive promoter which could mimic a de-repressed *vapBC*_{LT2} promoter (Figure 32B and C). It is observed that VapC_{LT2} synthesis is limited by strict translational coupling from VapB_{LT2} both *in vivo* and *in vitro*, which indicates that if translation resumes by change in conditions, VapB_{LT2} will be synthesized in excess of VapC_{LT2} and favour VapBC_{LT2} DNA-binding. Conditional cooperativity has previously been

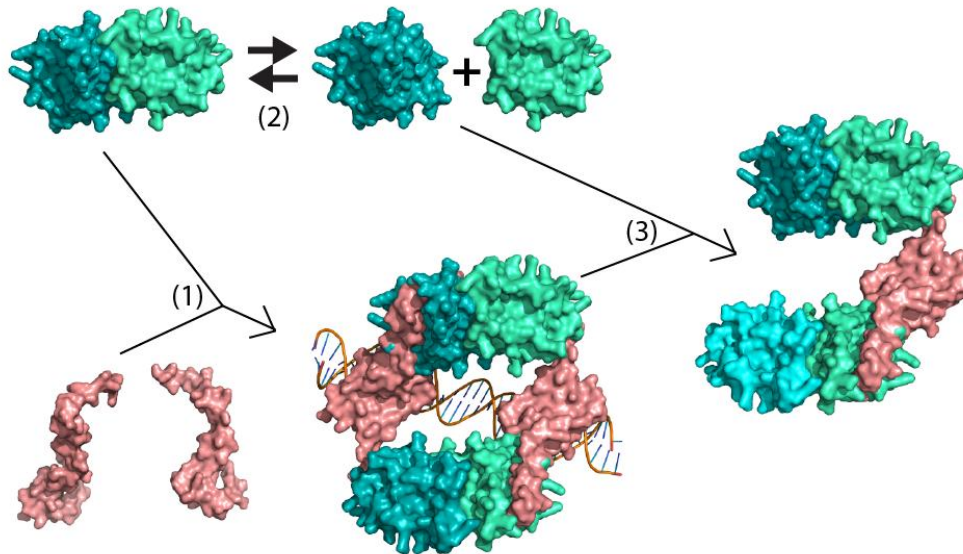


Figure 43 Model for how VapC_{LT2} in Excess can exert conditional cooperativity. (1) VapB_{LT2} (salmon) and VapC_{LT2} dimer (teal and cyan) forms an octameric (VapB₂-VapC₂)₂-complex which binds cooperatively to *vapO1* and *vapO2* operator sites and represses transcription. When the translation rate is decreased or protease activity is increased as a result of nutritional stress or treatment with antibiotics, VapB_{LT2} levels decrease and more stable VapC_{LT2} becomes in excess. (2) VapC_{LT2} forms a dimer in solution which exists in monomer/dimer equilibrium. (3) Free VapC_{LT2} monomer can interfere with the VapC_{LT2} dimer bound in complex, which abolishes cooperative binding to DNA. This in turn activates transcription, which will facilitate VapB_{LT2} production, as VapB_{LT2} is produced in excess of VapC_{LT2}.

reported for *ccdAB*, *relBE* and *phd-doc* (De *et al.*, 2009; Overgaard *et al.*, 2008; Garcia-Pino *et al.*, 2010). In these systems, conditional cooperativity is mediated by the presence of two distinct antitoxin binding sites in the toxin. The antitoxin binds to these sites with different affinity which makes the complexes very sensitive to very small changes in the antitoxin/toxin ratio. The mechanism of conditional cooperativity presented here for *vapBC*_{LT2}, depends on breaking of the dimerisation of VapC_{LT2} in the DNA bound [VapB₂-VapC₂]₂-complex. Consistent with this interpretation the VapBC_{LT2} complex is less sensitive to changes in the VapB_{LT2}/VapC_{LT2} ratio and complex breakage occurs gradually with increased VapC_{LT2}, when VapC_{LT2} is in excess. Nevertheless, this study could represent an exciting new mechanism by which toxins can exert conditional cooperativity to regulate transcription.

Future Perspectives for Results Section II

It is clear from the data presented in Results Section II that dimerisation of VapC_{LT2} is important not only for the cooperative binding of VapB_{LT2} to *vapO* but also for the mechanism of conditional cooperativity. To investigate this possibility further, a crystal structure of VapBC_{LT2} complex bound to DNA would give fundamental insights to the mechanism of regulation. Alternatively, a crystal structure of the complex formed when VapC_{LT2} is in excess would also give interesting clues to the mechanism of conditional cooperativity. Some of these questions might also be answered by analytical ultracentrifugation of the VapBC_{LT2} complex as well as information about the affinities between the antitoxin and the toxin. This could be done in parallel with mutant VapBC_{LT2}^{Y72A} complex which would give interesting clues to the difference between wt and mutant.

Alternatively, the affinities between antitoxin and toxin could be analysed by Surface Plasmon Resonance (SPR) with immobilised VapB_{LT2}, VapC_{LT2} or VapC_{LT2}^{Y72A}. This experiment is however limited by the low solubility of the toxin proteins. However, the affinities of VapBC_{LT2} and VapBC_{LT2}^{Y72A} for DNA could also be analysed by immobilising promoter DNA with a biotin tag as the complexes are more soluble.

Finally, an interesting experiment would be to analyse the observed increase in affinity of VapB_{LT2} for DNA in the presence of high concentrations of VapC_{LT2}^{Y72A} mutants. This could be done by analysing the binding of VapB_{LT2} to a half operator site in the presence of VapC_{LT2} and VapC_{LT2}^{Y72A}. A half operator site would not allow cooperative binding to occur and if the toxin induces folding of the antitoxin upon interaction, VapC_{LT2} and VapC_{LT2}^{Y72A} would do so to a similar extent.

Conclusion

I demonstrate here that *vapBC* from *Shigella flexneri* 2a YSH6000 virulence plasmid pMYSH6000 and *Salmonella enterica* serovar Typhimurium LT2 is bona fide TA loci, which, like other Type II TAs, encodes an antitoxin *vapB* and toxin *vapC*. Furthermore, I show that *vapB* and *vapC* are translationally coupled which ensures that VapB is produced in excess of VapC. The *vapBC* locus is transcribed from a single promoter, which is repressed and transcribed only at low level during steady-state growth.

VapB contains an N-terminal DNA binding domain and forms a dimer which represses transcription by binding to two inverted repeats (*vapO*, operator sites) in the promoter region. The affinity of VapB for *vapOs* is greatly increased in the presence of VapC, which act as a co-repressor. The VapC toxin does so possibly by forming a complex with VapB by direct protein-protein interaction, which might not only neutralise the activity of VapC but also cooperatively enhance the binding of VapB to *vapOs* by forming VapC dimer bridge between two VapB dimers.

Consistent with other Type II TAs, transcription of *vapBC* is increased during nutritional stress and treatment with antibiotics that is caused by decreased cellular levels of VapB, which is degraded by ATP-dependent Lon protease. The decrease in cellular levels of VapB leads to free VapC, which is activated to act on its cellular target. Apart from activation it also directly stimulates *vapBC* transcription as the cooperative binding of [VapB₂-VapC₂]₂ complex to DNA is conditional and VapC in excess of VapB might interfere with VapC dimerisation in the DNA bound complex, which leads to de-repression of the promoter. Transcriptional induction ensures efficient VapB production when translation resumes by a change in the environment. The VapC toxin contains a PIN domain, which specifically cleaves tRNA^{fMet} between position +38 and +39 dependent on Mg²⁺. Hereby, VapC inhibits global translation at the step of translation initiation. This inhibition is bacteriostatic as cells rapidly recover by subsequent induction of VapB. The cleavage of tRNA^{fMet} results in a reduced growth rate and may be beneficial to translation fidelity during slow growth as the drain on charged pools of charged tRNA is adjusted to a slower growth rate, which results in increased translation fidelity. VapC activation might also play another role by altering the proteome as decreased levels of tRNA^{fMet} result in increased competition by elongator tRNAs for P-site occupation which could lead to

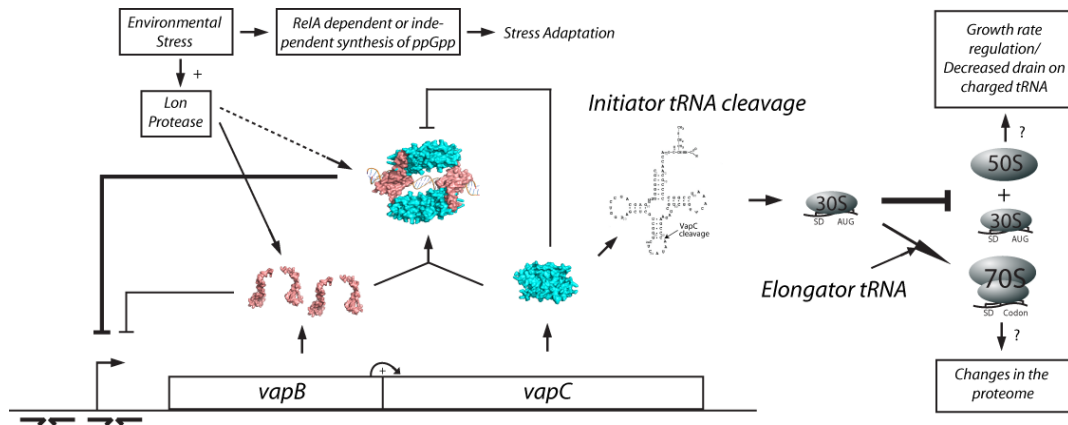


Figure 44 The complete model for *vapBC* regulation and activity. Two dimers of VapC (cyan) forms a complex with two dimers of VapB (salmon), which promotes cooperative binding to two operator sites (*vapO*) in the promoter region. This in turn represses transcription of the *vapBC* operon. VapB is an efficient Lon protease substrate. During environmental stress e.g. amino acid starvation, protease activity of Lon is increased, which leads to decreased cellular levels of VapB. This results in increased transcription as VapB_{LT2} is degraded and Free VapC interferes with the cooperative binding of the complex to DNA. Free VapC is also activated to act on its cellular target tRNA^{fMet}, which leads to inhibition of global translation and results in decreased growth rate and drain on charged tRNA species with a consequent increase in fidelity of the translation machinery on mRNA which are translated. A possibility is also that VapC might regulate the proteome as it might affect translation initiation, which could be beneficial to the cell under certain conditions. Environmental stress also induces ppGpp production (See Introduction Chapter 4), which helps the cell to adapt to the environment with a slower growth rate. Changes in the environment to more favourable conditions results in immediate toxin neutralisation as the synthesis of toxin is strictly coupled to the antitoxin.

translation initiation events to occur on elongator codons positioned in optimal distance to a Shine & Dalgarno sequence. The complete model for *vapBC* regulation and activity is shown in Figure 44.

Materials and Methods

Bacterial Strains, Plasmids and Growth Conditions

Bacterial cultures were grown in either Luria-Bertani medium (For 1L LB medium, 10g Bacto-Tryptone, 5g Yeast Extract, 10g NaCl, PH 7.5) or AB minimal medium (For 1L AB medium, 0.4g (NH₄)₂SO₄, 1.2g Na₂HPO₄, 0.6g KH₂PO₄, 0.6g NaCl, 0.08mM CaCl₂, 0.8mM MgCl₂ and 2.4μM FeCl₃) supplemented with 0.5% glycerol, 1μg/μL thiamine and defined concentrations of amino acids. When appropriate, the medium was supplemented with 30 μg/mL (low-copy) or 100μg/mL (high-copy) ampicillin, 50 μg/mL chloramphenicol, 25 μg/mL kanamycin and 10 μg/mL tetracycline. Amino acid starvation is induced by adding serine hydroxymate (SHT, purchased from Sigma Aldrich) to a final concentration 1 mg/mL. Transcription from LacI-regulated promoters was induced by the addition of 2 mM Isopropyl-β-D-1-thiogalactopyranoside (IPTG). Transcription from AraC-regulated promoters was induced by the addition of 0.2% arabinose.

Indicator plates were supplemented with X-gal (5-bromo-4-chloro-3-indoyl-b-D-galactoside) to a final concentration of 40 μg/ml. Strains and plasmids constructed are listed in table 3 and 4, respectively. Oligonucleotides used in this study are listed in table 5.

Standard procedures

The molecular cloning work in this study was done according to (Sambrook *et al.*, 1989). Amplification of DNA fragments was performed using Phusion™ High-Fidelity DNA polymerase (Finnzymes) and DNA purifications performed using illustra GFX PCR & gel band purification kit™ (GE healthcare). All other amplification was carried out using Gotaq® Flexi DNA polymerase (Promega). Correct recombinant clones were confirmed by sequence obtained from DNA Sequencing & Services™, Dundee, Scotland. Plasmid preparations were carried out using QIAprep spin MiniPrep kit (Qiagen) and Nucleobond® AX-100 (ClonTech). DNA restriction digestions and ligations were performed using enzymes purchased from Roche or Promega.

Table 3. Strains constructed and used in this study

Strains	Genotype	Reference
MG1655	Wild-type <i>E. coli</i> K-12	Laboratory Collection
KP1001	Wild-type <i>S. enterica</i> LT2	Laboratory Collection
TB28	MG1655 $\Delta lacIZYA$	Laboratory Collection
C41	BL21 derivative (DE3)	Laboratory Collection
SC301467	MG1655 $\Delta mazF \Delta chpB \Delta relBE \Delta dinJ-yafQ \Delta yefM-yoeB$	(Christensen <i>et al.</i> , 2004)
SC30	MG1655 $\Delta mazF$	(Christensen <i>et al.</i> , 2003)
SC31	MG1655 $\Delta chpB$	(Christensen <i>et al.</i> , 2003)
SC34	MG1655 $\Delta relBE$	(Christensen <i>et al.</i> , 2003)
SC36	MG1655 $\Delta dinJ-yafQ$	(Christensen <i>et al.</i> , 2004)
SC37	MG1655 $\Delta yefM-yoeB$	(Christensen <i>et al.</i> , 2004)
MG1655 Δlon	MO11, MG1655 $\Delta lon146::tet$	(Overgaard <i>et al.</i> , 2008)
KW10	$\Delta lon::kan$	This study
KW11	$\Delta clp::kan$	This study

Table 4 Plasmids constructed and used in this study

Plasmid	Plasmid properties	Reference
pNDM71	Plasmid R1 derivative, <i>bla</i>	Laboratory Collection
pKW71512	pNDM71:: <i>vapBC</i> _{LT2}	This study
pNDM220	R1 <i>bla lacI^f pA1/O4/O3</i>	(Gottfredsen and Gerdes, 1998)
pRBJ200	R1 <i>bla mcs-lacZYA</i>	(Jensen <i>et al.</i> , 1995)
pKW512	pRBJ200 <i>vapBC</i> _{LT2} :: <i>lacZYA</i>	This work
pMG25	<i>pA1/O3/O4</i>	Laboratory collection
pKW512HB	<i>pA1/O3/O4::H6-vapB</i> _{LT2} - <i>vapC</i> _{LT2}	This study
pKW512HC	<i>pA1/O3/O4::vapB</i> _{LT2} -H6- <i>vapC</i> _{LT2}	This study
pBAD33	<i>pBAD</i>	(Guzman <i>et al.</i> , 1995)
pKW3352HC	<i>pBAD::SD</i> _{opt} :: <i>vapC</i> _{LT2} -H6	This study
pKW3353HC	<i>pBAD::SD</i> _{opt} :: <i>vapC</i> _{LT2} ^{D7A} -H6	This study
pKW3354HC	<i>pBAD::SD</i> _{opt} :: <i>vapC</i> _{LT2} ^{D98A} -H6	This Study
pKW3382HC	<i>pBAD::SD</i> _{opt} :: <i>vapC</i> -H6	This study
pKW52	<i>pBAD::SD</i> _{opt} :: <i>vapC</i>	This study
pKW51	<i>pA1/O3/O4::SD</i> _{opt} :: <i>vapB</i> _{LT2}	This study
pKW82	<i>pBAD33 pBAD::vapC (mvpT)</i>	This study
pKW81	pNDM220 <i>pA1/O4/O3::vapB (mvpA)</i>	This study
pKW3221	<i>T7::tRNA^{Met}</i>	This study
pKW812HB	<i>pA1/O4/O3:H6-vapB-vapC</i>	This study
pKW812HC	<i>pA1/O4/O3:vapB-H6-vapC</i>	This study
pKW254812	<i>pOU254::vapBC</i>	This study
pKW254813	<i>pOU254::vapBC</i> ^{D7A}	This study
pKP3035	<i>pBAD::relE</i>	(Pedersen <i>et al.</i> , 2002)
pRB100	<i>pBAD::yoeB</i>	(Christensen-Dalsgaard and Gerdes, 2008)
pOU254	<i>lacZYA</i> transcriponal fusion vector	Laboratory collection
pKW512TFZD7A	<i>pOU254, vapBC</i> _{LT2} ^{D7A} :: <i>lacZYA</i>	This study
pKW512TFZD7A-1	pKW512TFZD7A, mutation in <i>vapO1</i>	This study
pKW512TFZD7A-2	pKW512TFZD7A, mutation in <i>vapO2</i>	This study
pKW512TFZD7A-1-2	pKW512TFZD7A, mutation in <i>vapO1</i> and <i>vapO2</i>	This study
pKW254BC	<i>pOU254, vapBC</i> _{LT2} :: <i>lacZYA</i>	This study
pKW254BCL40A	pKW254BC, L40A substitution	This study

pKW254BCM41A	pKW254BC, M41A substitution	This study
pKW254BCL43A	pKW254BC, L43A substitution	This study
pKW254BCI44A	pKW254BC, I44A substitution	This study
pKW254BCY45A	pKW254BC, Y45A substitution	This study
pKW254BCE48A	pKW254BC, E48A substitution	This study
pKW254BCK49A	pKW254BC, K49A substitution	This study
pKW254BCY72A	pKW254BC, Y72A substitution	This study
pKW254BCA76S	pKW254BC, A76S substitution	This study
pKW254BCA77S	pKW254BC, A77S substitution	This study
pKW254BCI78A	pKW254BC, I78A substitution	This study
pKW254BCR89A	pKW254BC, R89A substitution	This study
pOU253	<i>lacZYA</i> translational fusion vector	Laboratory collection
pKW253-1	pOU253, p _{lac} :: <i>vapB</i> _{LT2} ^{D7A} :: <i>lacZYA</i>	This study
pKW253-2	pKW253-1, Start codon mutation	This study
pKW253-3	pKW253-1, Premature termination codon (PTC)	This study
pKW253-4	pKW253-1, Frameshift mutation	This study
pKW253-5	pOU253, p _{lac} :: <i>vapB</i> _{LT2} :: <i>lacZYA</i>	This study
pKW512HBL43A	pKW512HB, with <i>vapC</i> _{LT2} ^{L43A}	This study
pKW512HBI44A	pKW512HB, with <i>vapC</i> _{LT2} ^{I44A}	This study
pKW512HBY72A	pKW512HB, with <i>vapC</i> _{LT2} ^{Y72A}	This study
pKW512HBA76S	pKW512HB, with <i>vapC</i> _{LT2} ^{A76S}	This study
pKW3352L43A	p _{BAD} ::SD _{opt} :: <i>vapC</i> _{LT2} ^{L43A}	This study
pKW3352I44A	p _{BAD} ::SD _{opt} :: <i>vapC</i> _{LT2} ^{I44A}	This study
pKW3352Y72A	p _{BAD} ::SD _{opt} :: <i>vapC</i> _{LT2} ^{Y72A}	This study
pKW3352A76S	p _{BAD} ::SD _{opt} :: <i>vapC</i> _{LT2} ^{A76S}	This study
pKW3352I78A	p _{BAD} ::SD _{opt} :: <i>vapC</i> _{LT2} ^{I78A}	This study
pKW254T	pOU254 contains terminator from pMG25	(Christensen-Dalsgaard <i>et al.</i> , 2008)
pKW25420T	pKW254T <i>dksA</i>	This work
pKW25421T	pKW254T <i>dksA</i> ATG→AAG	This work
pKW25423T	pKW254T <i>dksA</i> in frame TAA 2nd codon before stop codon	This work
pKW25424T	pKW254T <i>dksA</i> out of frame TAA before stop codon	This work
pKW25425T	pKW254T <i>dksA</i> out of frame TAA before stop codon	This work
pKW25427T	pKW254T <i>dksA</i> –SD	This work
pKW25428T	pKW254T <i>dksA</i> –SD ATG→AAG	This work
pEQ AAA	<i>lucR lucF</i> ATG→AAA	(Kimura and Suzuki, 2010)
pEQ AAG	<i>lucR lucF</i> ATG→AAG	This study
pSC333	pGEM3, <i>bla</i> , T _γ :: <i>lpp</i>	(Christensen and Gerdes, 2003)
pSC334	pGEM3, <i>bla</i> , T _γ :: <i>ssrA</i>	(Christensen and Gerdes, 2003)

Table 5 Oligonucleotides used in this study

Oligo name	Sequence
VAPC-1_LT2#1	CCCCCGCATGCGAATTCATGCAGAAATTAGCACCAGTCTTC
VAPC-1_LT2#12	CCCCCGGTACCGGATCCAAAATAAGGAGGAAAAAAAATGCTGAAATTCATGCTTGATAC
VAPC-1_SF_#1	CCCCAAGCTTGAATTCGATTTCTGATGAACAGGTCAGC
VAPC-1_SF_#2	CCCCCGGTACCGGATCCGAAAGAAAGGGAGTCATTCTGA
VAPB-1_LT2#1	CCCCCGCATGCGAATTCGCATCAAAATCCTTCCCGTTCC
VAPB-1_LT2#12	CCCCCGGTACCGGATCCAAAATAAGGAGGAAAAAAAATGCACACAACACTTTTTTTTAG
VAPB-1_SF_#1	CCCCAAGCTTGAATTCCTTCAGCATCAGAATGACTCCC
VAPB-1_SF_#2	CCCCCGGTACCGGATCCCACATAAGGAGGCAATAATG
VAPBC_LT2#2	CCCCGAATTCGAATCCGGGGATAACATCTGA

VAPBC_LT2#1	CCCCCGGATCCGACAAGGATGCCTGCGGAG
VAPB_LT2#HIS61	CCCCCGAATTCAAAATAAGGAGGAAAAAAAAATGCACACAACACTTTTTTTTAG
VAPB_LT1#HIS62	CCCCCGGATCCAGCATCAAAATCCTTCCCG
VAPC_LT2#HIS61	CCCCCGGATCCAAAATAAGGAGGAAAAAAAAATGCATCACCATCACCATCACCTG AAATTCATGCTTGATACCAA
VAPC_LT2#HIS62	CCCCAAGCTTGAGAAATTAGCACCAGTCTTC
TRANSTERM#CCW	CCCCGAATTCGATTCAACCCCTTCTTCGATC
DKSA_UAA1#UP	CGAAAAACAGATGTAAGGCTAATTACAGC
DKSA_UAA1#DOWN	GCTGTAATTAGCCTTACATCTGTTTTTCG
DKSA_UAA2#UP	GCGAAAAACAGATTAATGGCTAATTACAG
DKSA_UAA2#DOWN	CTGTAATTAGCCATTAATCTGTTTTTCGC
DKSA_UAA3#UP	CGCGAAAAACAGATAACTGGCTAATTACAG
DKSA_UAA3#DOWN	CTGTAATTAGCCAGTTATCTGTTTTTCGC
rp1N-3#CCW	CGATAACTTCGTCATCACGACGG
rpsJ-3#CCW2	CCAATCATTGTTTCAACCTCTC
rrsA-1#up	GGTGATCCAACCGCAGGTTCCCTAC
rnpB#up	AGGTGAAACTGACCGATAAGCCGG
pKW71D-3#PE	GAGGTCATTACTGGATCTATCAAC
T7/pmoA	GGGCCTAATACGACTCACTATAGGGACCAGGTGTATCTTTTCGGAGCGCCTGCCG
pmoA-forw	CGGCATAAGCCGAAGATATCGG
dksA probe- f	CAACTTCCCGGACCCGGTAG
dksA T7 probe- r	GGGCCTAATACGACTCACTATAGGGGATGCACAGATCGGCTGTCC
10SA-2	GCCCCTCGGCATGCATGCACC
vapB-5#PE	GGCAATCTGACTGCCGTTGGTCC
H6-VAPB#SF-DOWN	CCCCCGAATTCAAAATAAGGAGGAAAAAAAAATGCATCACCATCACCATCACGAAACCACCGT ATTTCTCAGCAAC
H6-VAPB#SF-UP	CCCCCGGATCCCTTCAGCATCAGAATGACTCCC
VAPB#SF-ECORI-DOWN	CCCCCGAATTCAAAATAAGGAGGAAAAAAAAATGGAAACCACCGTATTTCTCAGCAAC
VAPC#SF-UP	CCCCCAAGCTTGAATTCGATTTCTGATGAACAGGTCAGC
H6C-down-BamHI-KpnI	CCCCCGGATCCGGTACCAAAAATAAGGAGGAAAAAAAAATGCTGAAATTCATGCTTGATACCAA TAC
H6C-up-HindIII	CCCCCAAGCTTCAGAAATTAGTGATGGTGATGGTGATGGCACCAGTCTTCGATTCGGATAC
VAPC#SF-DOWN	CCCCCGGATCCGGTACCAAAAATAAGGAGGAAAAAAAAATGCTGAAGTTTATGCTCGATACC
VAPC-H6#SF-ECORI-HINDIII-UP	CCCCCGAATTCAGCTTGTCAGTGATGGTGATGGTGATGGTCCAGTCTTCAGTTCTCAG
H6-VapC_SF_Down_N	CCCCCGGTACCGGATCCAAAATAAGGAGGAAAAAAAAATGCATCACCATCACCATCAC CTGAAGTTTATGCTCGATAC
H6C-down-D7A	CATGCTGCGACCAATACCTGTATTTTC
D7A-up-N	GTATTGGTCGCAAGCATGAATTTACG
H6C-down-D98A	GCCTTATGCGCAGATGATTGCTGGC
H6C-up-D98A	CATCTGCGCATAAGGCCCGACAGG
VapBC_SF_BamHI_Down	CCCCCGGATCCGCACATAGTAATTATCCTTGTGCG
VapCpMYSHD7A-up	CAGATGTGGTTCGCGAGCATAAACTTCAGCAT
VapCpMYSHD7A-down	GTTTATGCTCGCGACCAACATCTGCATTTTTTAC
T7-fMet-tRNA-f	CCCCCGGTACCGAATTCGGGCTAATACGACTCACTATAGACGGGGTGGAGCAGCCTG
T7-fMet-tRNA-rv	CCCCCGGATCCAGCTTAGAAACAAAAAACACCCGTTAGGGTG
tRNAVal	CCCTCCTTGTAAGGGAGG
tRNAphe	GACACGGGGATTTTCAATC
tRNAMet	CCATCATTATGAGTGATGTG
tRNA2Arg	TCCGACCGCTCGGTTCTGTAGC
tRNAHis	CACGACAACCTGGAATCAATCC
tRNA1Leu	GTAAGGACACTAACACCTGAAGC
tRNA1Thr	TGGGGACCTCACCCTTACCAA
tRNAFmet	CTTCGGGTTATGAGCCGACGAGCTA
tRNATyr	CAGATTACAGTCTGCTCCCTTTGGCCGCTCGGGAACCCAC
Fmet-bio	ATGAGTGATGTGCTCTAACCAACTGAG
FMET-BIO-N	CCCGACGAGCTACCAGGCTGTCCAC
FMET-BIO-3	GCCGGATTTGAACCGACGACCTTCGG
dksA-bamHI-sacI#CW	CCCCCGGATCCGAGCTCGTCGCTGCGCAAATACGC
TRANSTERM#CCW	CCCCGAATTCGATTCAACCCCTTCTTCGATC
dksA 1AAG-cw	GTTAAGGAGAAGCAACAAGCAAGAAGGGCAAAC
dksA 1AAG-ccw	GTTTTGCCCTTCTTGCTTGTTGCTTCTCCTTAAAC
dksA-antiSD-cw	CGATAGTGCGTGTATCTCTCAAGCAACATGCAAGAAG
dksA-antiSD-ccw	CTTCTTGATGTGCTTGAGGATAACACGCATATCG
dksA-antiSD-1AAG-cw	CGATAGTGCGTGTATCTCTCAAGCAACAAGCAAGAAG
dksA-antiSD-1AAG-ccw	CTTCTTGCTTGTTGCTTGAGGATAACACGCATATCG

CCW	
pKW71D-3#PE	GAGGTCATTACTGGATCTATCAAC
Fluc_AAG-AfeI-f	CCCCCAGCGTGTAAAGAGGAGAAATTAACCAAGGAAGACGCCAAAAACATAAAG
Fluc_SphI-r	CCCCCGCATGCGAGAATCTGACGCAGGCAG
Fmet-bio	ATGAGTGTGTGCTCTAACCAACTGAG- TEG biotin
VAPBC LT2#1	CCCCCGGATCCGACAAGGATGCCTGCGGAG
VAPBC LT2#2	CCCCCGAATTCGAATCCGGGGATAACATCTGA
H6B-down-EcoRI	CCCCCGAATTCAAAATAAGGAGGAAAAAAAATGCATCACCATCACCATCACCACACAACACT TTTTTTTAG
VAPB LT1#HIS62	CCCCCGGATCCCAGCATCAAAATCCTTCCC
VAPC-1 LT2#12	CCCCCGGTACCGGATCCAAAATAAGGAGGAAAAAAAATGCTGAAATTCATGCTTGATAC
VAPC LT2#HIS62	CCCCCAAGCTTGCAGAAATTAGCACCAGTCTTC
VAPB LT2#HIS61	CCCCCGAATTCAAAATAAGGAGGAAAAAAAATGCACACAACACTTTTTTTTTTAG
VAPC_LT2#HIS61	CCCCCGGATCCAAAATAAGGAGGAAAAAAAATGCATCACCATCACCATCACCTGAAATTCAT GCTTGATACCAA
vapBC down#EcoRI	CCCCGAATTCGACAAGGATGCCTGCGGAG
vapC-1 LT2up#BamHI	CCCCGGATCCATGCAGAAATTAGCACCAGTCTTC
H6C- down-D7A	CATGCTT CGC ACCAATACCTGTATTTTC
D7A-up-N	GTATTGGT CGC AAGCATGAATTTTCAG
pOU254 CW	TAGGGGTCCGCGCA
pOU254 CCW	TGTGGGATTAAGTGC
PBC-10 MUT DOWN	ATATACGCGTTGTATGATCAGAAAGGAGGCAGTTATGCAC
PBC-10 MUT UP	CTGCCTCCTTTCTGATCATAACCGGTATATCCATTATGAG
PBC-35 MUT DOWN	GGATTATTTTTCTCTACTATCTCTTTGACATATACATCGCCTC
PBC-35 MUT UP	ATATGTCAAAAGAGATAGTAAGGAAAAAATAATCCAGTCACATGACG
VAPC-L40A-f	CAGCTCCATCACCGCGATGGAGCTGATTTACGGTGC
VAPC-L40A-rv	GTAAATCAGCTCCATCGCGGTGATGGAGCTGATACAC
VapC-M41A-f	CAGCTCCATCACCTTAGCGGAGCTGATTTACGGTGCCTG
VapC-M41A-rv	CACCGTAAATCAGCTCCGCTAAGGTGATGGAGCTGATAC
VapC-L43A-f	CATCACCTTAATGGAGGCGATTACGGTGCAGAAAAAG
VapC-L43A-rv	TTTCAGCACCGTAAATCGCCTCCATTAAGGTGATGGAGC
VAPC-I44A-f	CCTTAATGGAGCTGGCGTACGGTGCTGAAAAAGCCTG
VAPC-I44A-rv	CTTTTTTCAGCACCGTACGCCAGCTCCATTAAGGTGATGG
VAPC-Y45A-f	CTTAATGGAGCTGATTTGCGGGTGCTGAAAAAGCCTGGC
VAPC-Y45A-rv	GCTTTTTTCAGCACCGCAATCAGCTCCATTAAGGTGATG
VapC-E48A-f	CTGATTTACGGTGCCTGCGAAAAGCCTGGCGCCGGAGCG
VapC-E48A-rv	CGGCGCCAGGCTTTTCGCGACCGTAAATCAGCTCC
VapC-K49A-f	GATTTACGGTGCCTGAAGCGAGCCTGGCGCCGGAGCGTAATC
VapC-K49A-rv	CTCCGGCGCCAGGCTCGCTTACGACCGTAAATCAGCTC
VapC-F72A-f	GCCTTGAGGTTTGGATGCGGATACACAGGCAGCGATAC
VapC-F72A-rv	TCGCTGCCTGTGTATCCGCATCCAAAACCTCAAGGCGG
VAPC-A76S-f	GGATTACGATACACAGTCGGCGATACATACCGGTCAAATC
VAPC-A76S-rv	GACCGGTATGTATCGCCGACTGTGTATCGTAATCCAAAAAC
VAPC-A77S-f	TTACGATACACAGGCATCGATACATCCGGTCAAATCCG
VAPC-A77S-rv	TTTGACCGGTATGTATCGATGCCTGTGTATCGTAATCC
VAPC-I78A-f	GATACACAGGCAGCGGCATACCGGTCAAATCCGTGC
VAPC-I78A-rv	GATTTGACCGGTATGCGCCGCTGCCTGTGTATCGTAATC
VapC-R89A-f	CCGTGCCAAGTGGCCGGAAGGGAACACCTGTCCGGCC
VapC-R89A-rv	GACAGGTGTTCCCTTCGCGGCCAGTTCCGACAGGATTTG
BC_253-ECORI_DOWN	CCCCCGAATTCGAGCTGTGACAATTAATCATCGGCTCGTATAATGTGTGGACGCGTTGTATA TCCAGAAAGGAGG
BC_253-BAMHI-UP	CCCCCGGATCCGCACCAGTCTTCGATTCGGATAC
BC_253_PRESTOPB_DOWN	GCCAGTACTGATTTTTAAAGTACCAGAGAACAACCCGCAG
BC_253_PRESTOPB_UP	GTTGTTCTCTGGTACTTTAAAAATCAGTACTGGCGCCTTCGC
BC_253_STARTB_DOWN	CAGAAAGGAGGAGTAAAGCACACAACACTTTTTTTTAGTAACCG
BC_253_STARTB_UP	CTAAAAAAAAGTGTGTGTGCTTAACCTGCCTCCTTTCTGGATATAC
BC_253_STOPFB_DOWN	ACGGGAAGGATTTTATGCTGAAATTCATGCTTGATACC
BC_253_STOPFB_UP	CATGAATTTTCAGCATAAAAATCCTTCCCGTTCCCTGTAC
BC_253_FUSB_UP	CCCCCGGATCCCGTTCCTGTACTGCGGGTTG
H6C-down-BamHI-KpnI	CCCCCGGATCCGGTACCAAAAATAAGGAGGAAAAAAAATGCTGAAATTCATGCTTGATACCAA TAC
VAPBC T7 DOWN	CGGGATCCTGTAATACGACTACTATAGACGGTGTATATCCAGAAAGGAG
VAPBC_T7_RRNBT1_UP	CAAAAAACCCCTCAAGACCCGTTTAGAGGCCCAAGGGTTGATAACATCTGATGCAGAAATT AGCAC
vapBC EMSA down	CAGAAGCCATGGGCACATATG
vapBC EMSA up	GATTTTCGACATGTTTCACATCC
VapBCbinding#small-down	CTCATAATGGATATACGCGTTGTATATCCAGAAAGG
VapBCbinding#small-up	CCTTTCTGGATATACAACGCGTATATCCATTATGAG
q-vapB-f	GCAGTCAGATTGCCTAAATCG

q-vapB-rv	AAATCAGTACTGGCGCCTTC
rpsA qPCR-f	CTGGGTCTGAAACAGTGCAA
rpsA qPCR-r	TCCAAGCCGATGAAGATACC
171SR14	GGGGCAGCTGGCGAAAGGGGGATGTGCTGC
171SR16	GGGGCAGCTGAATTTCACACAGGAAACAGCTA

Strains Constructed

KW10. The *lon* gene was deleted from the chromosome of MG1655 by P1 transduction as described in (Sambrook *et al.*, 1989). Insertion of kanamycin resistance cassette (Acquired from KEIO collection strain JW0429) into the correct location on the chromosome was confirmed by colony PCR using primers flanking the *lon* gene.

KW11. the *clpP* gene was deleted from the chromosome of MG1655 by P1 transduction as described in (Sambrook *et al.*, 1989). Insertion of kanamycin resistance cassette (Acquired from KEIO collection strain JW0427) into the correct location on the chromosome was confirmed by colony PCR using primers flanking the *clpP* gene.

Plasmids Constructed

pKW52. *vapC*_{LT2} (STM3033) of *S. enterica* LT2 amplified by colony PCR with primers VAPC-1_LT2#1 and VAPC-1_LT2#12. The PCR product was digested with *KpnI* and *SphI* and inserted into pBAD33. Cells carrying pKW52 express VapC_{LT2} upon addition of arabinose.

pKW82. *vapC* (*mvpT*) of *S. flexneri* 2a strain YSH6000 virulence plasmid pMYSH6000 was amplified from purified total DNA of strain YSH6000 with primers VAPC-1_SF_#1 and VAPC-1_SF_#2. The PCR product was digested with *KpnI* and *HindIII* and inserted into pBAD33. Cells carrying pKW82 express VapC upon addition of arabinose.

pKW51. *vapB*_{LT2} (STM3034) of *S. enterica* LT2 was amplified by colony PCR with primers VAPB-1_LT2#1 and VAPB-1_LT2#12. The PCR product was digested with *BamHI* and *EcoRI* and inserted into pNDM220. Cells carrying pKW51 express VapB_{LT2} upon addition of IPTG.

pKW81. *vapB* (*mvpA*) of *S. flexneri* 2a YSH6000 virulence plasmid pMYSH6000 was amplified from purified total DNA of strain YSH6000 with primers VAPB-1_SF_#1 and VAPB-1_SF_#2. The PCR product was digested with *Bam*HI and *Eco*RI and inserted into pNDM220. Cells carrying pKW81 express VapB upon addition of IPTG.

pKW512. *vapBC* of *S. enterica* LT2 was amplified by colony PCR was amplified by colony PCR with primers VAPBC_LT2#1 and VAPBC_LT2#2. The PCR product was digested with *Bam*HI and *Eco*RI and inserted into pRBJ200. Cells carrying pKW512 contains *vapBC*_{LT2} transcriptional fused to *lacZYA*.

pKW3352HC. *vapC*_{LT2} (STM3033)-encoding DNA was synthesized by PCR using *S. enterica* LT2 template DNA and primers H6C-down-BamHI-KpnI and H6C-up-HindIII. The resulting PCR product was digested with *Kpn*I and *Hind*III and ligated into pBAD33. The resulting plasmid expresses C-terminal His-tagged (Six histidine residues) VapC_{LT2} upon addition of arabinose

pKW3353HC. Two parts of *vapC*_{LT2} was PCR amplified from a pKW3352HC template using primers H6C-down-BamHI-KpnI and D7A-up-N, and primers H6C-up-HindIII and H6C- down-D7A. The resulting two overlapping PCR products were used as templates in an additional amplification using primers primers H6C-down-BamHI-KpnI and primers H6C-up-HindIII. The resulting PCR product was digested with *Kpn*I and *Hind*III and ligated into pBAD33. The resulting plasmid expresses C-terminal His-tagged VapC_{LT2} with Aspartate at +7 changed to Alanine upon addition of arabinose.

pKW3354HC. Two parts of *vapC*_{LT2} was PCR amplified from a pKW3352HC template using primers H6C-down-BamHI-KpnI and H6C-up-D98A, and primers H6C-up-HindIII and H6C-down-D98A. The resulting two overlapping PCR products were used as templates in an additional amplification using primers primers H6C-down-BamHI-KpnI and primers H6C-up-HindIII. The resulting PCR product was digested with *Kpn*I and *Hind*III and ligated into pBAD33. The resulting plasmid expresses C-terminal His-tagged VapC_{LT2} with Aspartate at +98 changed to Alanine upon addition of arabinose.

pKW3382HC. *vapC* (*mvpT*) of *S. flexneri* 2a strain YSH6000 virulence plasmid pMYSH6000 was amplified using strain YSH6000 DNA as a template with primers VAPC#SF-DOWN and VAPC-H6#SF-ECORI-HINDIII-UP. The PCR product was digested with *KpnI* and *HindIII* and inserted into pBAD33. Cells carrying pKW3382HC express C-terminal His-tagged (six histidine residues) VapC upon addition of arabinose.

pKW3221. *metV* of *E. coli* K-12 was amplified from chromosomal DNA using primers T7-fMet-tRNA-f and T7-fMet-tRNA-rv. The resulting PCR product was digested with *EcoRI* and *BamHI* and ligated into pBR322. C41 (DE3) carries the T₇ RNA polymerase gene under *p_{lac}* control and C41 cells containing pKW3221 therefore express tRNA^{fMet} upon addition of IPTG.

pKW254812. *vapBC* (*mvpT*) of *S. flexneri* 2a strain YSH6000 virulence plasmid pMYSH6000 was amplified using strain YSH6000 DNA as a template with primers VAPC#SF-UP and VapBC_SF_BamHI_Down. The PCR product was digested with *BamHI* and *EcoRI* and inserted into pOU254. Cells carrying pKW254812 express *vapBC* from its native promoter.

pKW254813. Two parts of *vapBC* were PCR amplified from a pKW254812 template using primers VapBC_SF_BamHI_Down and VapCpMYSHD7A-up, and VAPC#SF-UP and VapCpMYSHD7A-down. The resulting two overlapping PCR products were used as templates in an additional amplification reaction using primers VapBC_SF_BamHI_Down and primer VAPC#SF-UP. The resulting PCR product was digested with *BamHI* and *EcoRI* and ligated into pOU254. Cells carrying pKW254813 express *vapBC* from its native promoter with VapC having an Aspartate at +7 changed to Alanine.

pQE AAG. The Firefly luciferase gene (*lucF*) was amplified from purified plasmid pQE ATG with primers Fluc_AAG-AfeI-f and Fluc_SphI-r. The PCR product was then digested with *AfeI* and *SphI* and inserted into similarly digested pQE ATG. Cells carrying pQE AAG contains the dual luciferase plasmid with a start-codon substitution in *lucF*.

pKW25420T. The *dksA* gene of *E. coli* K-12 was amplified from chromosomal DNA with primers *dksA*-*bam*H1-*sac*I#CW and *dksA*-*pml*I-*xho*I#CCW. The PCR product was digested with *Bam*H1 and *Xho*I and inserted into pKW254T. Cells carrying pKW25420T express *dksA*.

pKW25421T. Two parts of the *dksA* gene of *E. coli* K-12 were amplified from purified pKW25420T with primers *dksA*-*bam*H1-*sac*I#CW and *dksA* 1AAG-*ccw* in addition to *dksA* 1AAG-*cw* and TRANSTERM#CCW. The two overlapping PCR products were used as a template in a second amplification with primers *dksA*-*bam*HI-*sac*I#CW and TRANSTERM#CCW. The product was digested with *Bam*HI and *Eco*RI and inserted into pOU254. Cells carrying pKW25421T express *dksA* mRNA with the start codon changed to AAG.

pKW25423T. Two parts of the *dksA* gene of *E. coli* K-12 was amplified from purified pKW25420T with primers *dksA*-*bam*H1-*sac*I#CW and DKSA_UAA1#DOWN in addition to DKSA_UAA1#UP and TRANSTERM#CCW. These two overlapping PCR products were used as template in a second amplification with primers *dksA*-*bam*H1-*sac*I#CW and TRANSTERM#CCW. The product was digested with *Bam*HI and *Eco*RI and inserted into pOU254. Cells carrying pKW25423T express *dksA* with an in-frame UAA substitution and translation will terminate incorrectly.

pKW25424T. Two parts of the *dksA* gene of *E. coli* K-12 was amplified from purified pKW25420T with primers *dksA*-*bam*H1-*sac*I#CW and DKSA_UAA2#DOWN in addition to DKSA_UAA2#UP and TRANSTERM#CCW. These two overlapping PCR products were used as template in a second amplification with primers *dksA*-*bam*H1-*sac*I#CW and TRANSTERM#CCW. The product was digested with *Bam*HI and *Eco*RI and inserted into pOU254. Cells carrying pKW25424T express *dksA* with an out-of frame UAA substitution and translation will terminate correctly.

pKW25425T. Two parts of the *dksA* gene of *E. coli* K-12 was amplified from purified pKW25420T with primers *dksA*-*bam*H1-*sac*I#CW and DKSA_UAA3#DOWN in addition to DKSA_UAA3#UP and TRANSTERM#CCW. These two overlapping PCR products were used as template in a second amplification with primers *dksA*-*bam*H1-*sac*I#CW and TRANSTERM#CCW. The product was digested with *Bam*HI

and *EcoRI* and inserted into pOU254. Cells carrying pKW25425T express *dksA* with an out-of frame UAA substitution and translation will terminate correctly.

pKW25427T. Two parts of the *dksA* gene of *E. coli* K-12 was amplified from purified pKW25420T with primers *dksA*-*bamHI*-*sacI*#CW and *dksA*-antiSD-ccw in addition to *dksA*-antiSD-cw and TRANSTERM#CCW. The two overlapping PCR products were used as a template in a second amplification with primers *dksA*-*bamHI*-*sacI*#CW and TRANSTERM#CCW. The product was digested with *BamHI* and *EcoRI* and inserted into pOU254. Cells carrying pKW25427T express *dksA* mRNA with an inverted SD sequence.

pKW25428T. Two parts of the *dksA* gene of *E. coli* K-12 was amplified from purified pKW25420T with primers *dksA*-*bamHI*-*sacI*#CW and *dksA*-antiSD-1AAG-ccw in addition to *dksA*-antiSD-1AAG-cw and TRANSTERM#CCW. The two overlapping PCR products were used as a template in a second amplification with primers *dksA*-*bamHI*-*sacI*#CW and TRANSTERM#CCW. The product was digested with *BamHI* and *EcoRI* and inserted into pOU254. Cells carrying pKW25428T express *dksA* mRNA with an inverted SD sequence and the AUG start-codon changed to AAG.

pKW71512. A DNA fragment containing *vapBC* from *S. enterica* LT2 was generated using primers VAPBC_LT2#1 and VAPBC_LT2#2. The PCR product was digested with *BamHI* and *EcoRI* and inserted in pNDM71, a mini R1cloning vector. pKW71512 contain *vapBC*_{LT2} under transcriptional control of its native promoter.

pKW512HB. Two PCR products containing either *vapB* or *vapC* from *S. enterica* LT2 was generated using primers H6B-down-*EcoRI* and VAPB_LT1#HIS62 or VAPC-1_LT2#12 and VAPC_LT2#HIS62, respectively. PCR product containing *vapB*_{LT2} was digested with *EcoRI* and *BamHI* and PCR product containing *vapC*_{LT2} was digested with *BamHI* and *HindIII*. The digests were then inserted into pMG25. pKW512HB produces *VapB*_{LT2} with a N-terminal tag of six histidines and *VapC*_{LT2} upon addition of IPTG.

pKW512HC. Two PCR products containing either *vapB* or *vapC* from *S. enterica* LT2 was generated using primers VAPB_LT2#HIS61 and VAPB_LT1#HIS62 or

VAPC_LT2#HIS61 and VAPC_LT2#HIS62, respectively. PCR product containing *vapB*_{LT2} was digested with *EcoRI* and *BamHI* and PCR product containing *vapC*_{LT2} was digested with *BamHI* and *HindIII*. The digests were then inserted into pMG25. pKW512HC produces VapC_{LT2} with an N-terminal tag of six histidines and VapB_{LT2} upon addition of IPTG.

pKW812HB. Two PCR products, one encoding *vapB* and one encoding *vapC* were amplified from *S. flexneri* strain YSH6000 DNA as template and primers H6-VAPB#SF-DOWN and H6-VAPB#SF-UP, and VAPC#SF-UP and VAPC#SF-DOWN. The resulting PCR product containing *vapB* was digested with *EcoRI* and *BamHI*, whereas the PCR product containing *vapC* was digested with *BamHI* and *HindIII*. The products were ligated into pMG25, a pUC-derived vector that carries *lacI^q* and the synthetic LacI-regulated pA1/O3/O4 promoter. Cells containing pKW812HB express N-terminal His-tagged VapB and native VapC upon addition of IPTG.

pKW812HC. Two PCR products, one containing *vapB* and one containing *vapC* were amplified from *S. flexneri* strain YSH6000 DNA as template and primers VAPB#SF-ECORI-DOWN and H6-VAPB#SF-UP, and VAPC#SF-UP and H6-VapC_SF_Down_N. The resulting PCR product encoding *vapB* was digested with *EcoRI* and *BamHI*, whereas the PCR product encoding *vapC* was digested with *BamHI* and *HindIII*. Digested products were ligated into pMG25. Cells containing pKW812HC express VapB and N-terminal His-tagged VapC upon addition of IPTG.

pKW512TFZD7A. Two PCR products were generated using primers *vapBC*_down#*EcoRI* and D7A-up-N or *vapBC*-1LT2up#*BamHI* and H6C-down-D7A using *S. enterica* LT2 as DNA template. The resulting products were then used as templates in a second round of PCR using primers *vapBC*_down#*EcoRI* and *vapBC*-1LT2up#*BamHI*. The PCR product was then digested with *EcoRI* and *BamHI* and inserted into pOU254. pKW512TFZD7A contains non-toxic *vapBC*^{D7A} in a transcriptional fusion to *lacZYA*.

pKW512TFZD7A-1. Two PCR products were generated using primers pOU254_CW and PBC-10_MUT_UP, or PBC-10_MUT_DOWN and pOU254_CCW using

pKW512TFZD7A as template. Overlapping PCR products were then used as templates in a second round of PCR with primers pOU254_CW and pOU254_CCW. The PCR product was digested with *Bam*HI and *Eco*RI and inserted in pOU254. pKW512TFZD7A-1 contains non-toxic vapBC_{LT2}^{D7A} in a transcriptional fusion with *lacZYA* with ATC for GAT substitution mutation in promoter

pKW512TFZD7A-2. Two PCR products were generated using primers pOU254_CW and PBC-35_MUT_UP, or PBC-35_MUT_DOWN and pOU254_CCW using pKW512TFZD7A as template. Overlapping PCR products were then used as templates in a second round of PCR with primers pOU254_CW and pOU254_CCW. The PCR product was digested with *Bam*HI and *Eco*RI and inserted in pOU254. pKW512TFZD7A-2 contains non-toxic vapBC_{LT2}^{D7A} in a transcriptional fusion with *lacZYA* with GTA for TAC substitution mutation in promoter

pKW512TFZD7A-1-2. Two PCR products were generated using primers pOU254_CW and PBC-10_MUT_UP, or PBC-10_MUT_DOWN and pOU254_CCW using pKW512TFZD7A-2 as template. Overlapping PCR products were then used as templates in a second round of PCR with primers pOU254_CW and pOU254_CCW. The PCR product was digested with *Bam*HI and *Eco*RI and inserted in pOU254. pKW512TFZD7A-1-2 contains non-toxic vapBC_{LT2}^{D7A} in a transcriptional fusion with *lacZYA* with GTA for TAC and ATC for GAT substitution mutation in promoter

pKW254BC. A DNA fragment containing *vapBC* from *S. enterica* LT2 was generated using primers vapBC_down#EcoRI and vapC-1_LT2up#BamHI. The PCR product was digested with *Bam*HI and *Eco*RI and inserted in pOU254. pKW254BC contains *vapBC*_{LT2} in a transcriptional fusion with *lacZYA*.

pKW254BCL40A. Two PCR products were generated using primers vapBC_down#EcoRI and VAPC-L40A-rv or vapC-1_LT2up#BamHI and VAPC-L40A-f using *S. enterica* LT2 as DNA template. The resulting products were then used as templates in a second round of PCR using primers vapBC_down#EcoRI and vapC-1_LT2up#BamHI. The PCR product was then digested with *Eco*RI and *Bam*HI and inserted into pOU254. pKW254BCL40A contains *vapBC*_{LT2}^{L40A} in a transcriptional fusion to *lacZYA*.

pKW254BCM41A. Two PCR products were generated using primers vapBC_down#EcoRI and VAPC-M41A-rv or vapC-1_LT2up#BamHI and VAPC-M41A-f using *S. enterica* LT2 as DNA template. The resulting products were then used as templates in a second round of PCR using primers vapBC_down#EcoRI and vapC-1_LT2up#BamHI. The PCR product was then digested with *EcoRI* and *BamHI* and inserted into pOU254. pKW254BCM41A contains $vapBC_{LT2}^{M41A}$ in a transcriptional fusion to *lacZYA*.

pKW254BCL43A. Two PCR products were generated using primers vapBC_down#EcoRI and VAPC-L43A-rv or vapC-1_LT2up#BamHI and VAPC-L43A-f using *S. enterica* LT2 as DNA template. The resulting products were then used as templates in a second round of PCR using primers vapBC_down#EcoRI and vapC-1_LT2up#BamHI. The PCR product was then digested with *EcoRI* and *BamHI* and inserted into pOU254. pKW254BCL43A contains $vapBC_{LT2}^{L43A}$ in a transcriptional fusion to *lacZYA*.

pKW254BCI44A. Two PCR products were generated using primers vapBC_down#EcoRI and VAPC-I44A-rv or vapC-1_LT2up#BamHI and VAPC-I44A-f using *S. enterica* LT2 as DNA template. The resulting products were then used as templates in a second round of PCR using primers vapBC_down#EcoRI and vapC-1_LT2up#BamHI. The PCR product was then digested with *EcoRI* and *BamHI* and inserted into pOU254. pKW254BCI44A contains $vapBC_{LT2}^{I44A}$ in a transcriptional fusion to *lacZYA*.

pKW254BCY45A. Two PCR products were generated using primers vapBC_down#EcoRI and VAPC-Y45A-rv or vapC-1_LT2up#BamHI and VAPC-Y45A-f using *S. enterica* LT2 as DNA template. The resulting products were then used as templates in a second round of PCR using primers vapBC_down#EcoRI and vapC-1_LT2up#BamHI. The PCR product was then digested with *EcoRI* and *BamHI* and inserted into pOU254. pKW254BCY45A contains $vapBC_{LT2}^{Y45A}$ in a transcriptional fusion to *lacZYA*.

pKW254BCE48A. Two PCR products were generated using primers vapBC_down#EcoRI and VAPC-E48A-rv or vapC-1_LT2up#BamHI and VAPC-E48A-f using *S. enterica* LT2 as DNA template. The resulting products were then used as templates in a second round of PCR using primers vapBC_down#EcoRI and vapC-1_LT2up#BamHI. The PCR product was then digested with *EcoRI* and *BamHI* and inserted into pOU254. pKW254BCE48A contains *vapBC*^{E48A} in a transcriptional fusion to *lacZYA*.

pKW254BCK49A. Two PCR products were generated using primers vapBC_down#EcoRI and VAPC-K49A-rv or vapC-1_LT2up#BamHI and VAPC-K49A-f using *S. enterica* LT2 as DNA template. The resulting products were then used as templates in a second round of PCR using primers vapBC_down#EcoRI and vapC-1_LT2up#BamHI. The PCR product was then digested with *EcoRI* and *BamHI* and inserted into pOU254. pKW254BCK49A contains *vapBC*^{K49A} in a transcriptional fusion to *lacZYA*.

pKW254BCY72A. Two PCR products were generated using primers vapBC_down#EcoRI and VAPC-Y72A-rv or vapC-1_LT2up#BamHI and VAPC-Y72A-f using *S. enterica* LT2 as DNA template. The resulting products were then used as templates in a second round of PCR using primers vapBC_down#EcoRI and vapC-1_LT2up#BamHI. The PCR product was then digested with *EcoRI* and *BamHI* and inserted into pOU254. pKW254BCY72A contains *vapBC*^{Y72A} in a transcriptional fusion to *lacZYA*.

pKW254BCA76S. Two PCR products were generated using primers vapBC_down#EcoRI and VAPC-A76S-rv or vapC-1_LT2up#BamHI and VAPC-A76S-f using *S. enterica* LT2 as DNA template. The resulting products were then used as templates in a second round of PCR using primers vapBC_down#EcoRI and vapC-1_LT2up#BamHI. The PCR product was then digested with *EcoRI* and *BamHI* and inserted into pOU254. pKW254BCA76S contains *vapBC*^{A76S} in a transcriptional fusion to *lacZYA*.

pKW254BCA77S. Two PCR products were generated using primers vapBC_down#EcoRI and VAPC-A77S-rv or vapC-1_LT2up#BamHI and VAPC-

A77S-f using *S. enterica* LT2 as DNA template. The resulting products were then used as templates in a second round of PCR using primers vapBC_down#EcoRI and vapC-1_LT2up#BamHI. The PCR product was then digested with *EcoRI* and *BamHI* and inserted into pOU254. pKW254BCA77S contains $vapBC_{LT2}^{A77S}$ in a transcriptional fusion to *lacZYA*.

pKW254BCI78A. Two PCR products were generated using primers vapBC_down#EcoRI and VAPC-I78A-rv or vapC-1_LT2up#BamHI and VAPC-I78A-f using *S. enterica* LT2 as DNA template. The resulting products were then used as templates in a second round of PCR using primers vapBC_down#EcoRI and vapC-1_LT2up#BamHI. The PCR product was then digested with *EcoRI* and *BamHI* and inserted into pOU254. pKW254BCI78A contains $vapBC_{LT2}^{I78A}$ in a transcriptional fusion to *lacZYA*.

pKW254BCR89A. Two PCR products were generated using primers vapBC_down#EcoRI and VAPC-R89A-rv or vapC-1_LT2up#BamHI and VAPC-R89A-f using *S. enterica* LT2 as DNA template. The resulting products were then used as templates in a second round of PCR using primers vapBC_down#EcoRI and vapC-1_LT2up#BamHI. The PCR product was then digested with *EcoRI* and *BamHI* and inserted into pOU254. pKW254BCR89A contains $vapBC_{LT2}^{R89A}$ in a transcriptional fusion to *lacZYA*.

pKW253-1. A DNA fragment containing *vapBC* from *S. enterica* LT2 was generated using primers BC_253-ECORI_DOWN and BC_253-BAMHI-UP using pKW512TFZD7A as template. The PCR product was digested with *BamHI* and *EcoRI* and inserted in pOU253. pKW253-1 contains $vapBC_{LT2}^{D7A}$ with a p_{tac} promoter in a translational fusion with *lacZYA*.

pKW253-2. Two PCR products were generated using primers BC_253-ECORI_DOWN and BC_253_PRESTOPB_UP or BC_253-BAMHI-UP and BC_253_PRESTOPB_DOWN using pKW512TFZD7A as template. The resulting products were then used as templates in a second round of PCR using primers BC_253-ECORI_DOWN and BC_253-BAMHI-UP. The PCR product was then digested with *EcoRI* and *BamHI* and inserted into pOU253. pKW253-2 contains

*vapBC*_{LT2}^{D7A} with a premature termination codon in *vapB*_{LT2} in a translational fusion with *lacZYA* under the control of a constitutive p_{tac} promoter.

pKW253-3. Two PCR products were generated using primers BC_253-ECORI_DOWN and BC_253_STARTB_UP or BC_253-BAMHI-UP and BC_253_STARTB_DOWN using pKW512TFZD7A as template. The resulting products were then used as templates in a second round of PCR using primers BC_253-ECORI_DOWN and BC_253-BAMHI-UP. The PCR product was then digested with *EcoRI* and *BamHI* and inserted into pOU253. pKW253-3 contains *vapBC*_{LT2}^{D7A} with a start codon mutation in *vapB*_{LT2} in a translational fusion with *lacZYA* under the control of a constitutive p_{tac} promoter.

pKW253-4. Two PCR products were generated using primers BC_253-ECORI_DOWN and BC_253_STOPFB_UP or BC_253-BAMHI-UP and BC_253_STOPFB_DOWN using pKW512TFZD7A as template. The resulting products were then used as templates in a second round of PCR using primers BC_253-ECORI_DOWN and BC_253-BAMHI-UP. The PCR product was then digested with *EcoRI* and *BamHI* and inserted into pOU253. pKW253-4 contains *vapBC*_{LT2}^{D7A} with a frameshift mutation in *vapB*_{LT2} in a translational fusion with *lacZYA* under the control of a constitutive p_{tac} promoter.

pKW253-5. A DNA fragment containing *vapB* from *S. enterica* LT2 was generated using primers BC_253-ECORI_DOWN and BC_253_FUSB_UP using pKW512TFZD7A as template. The PCR product was digested with *BamHI* and *EcoRI* and inserted in pOU253. pKW253-5 contains *vapB*_{LT2} with a p_{tac} promoter in a translational fusion with *lacZYA*.

pKW512HBL43A. A PCR product containing *vapC* from *S. enterica* LT2 was generated using primers H6C-down-BamHI-KpnI and VAPC_LT2#HIS62 using pKW254BCL43A as template. PCR product containing *vapC*^{L43A} was digested with *BamHI* and *HindIII* and inserted into *BamHI* and *HindIII* digested pKE512HB. pKW512HBL43A produces VapB_{LT2} with a N-terminal tag of six histidines and VapC_{LT2}^{L43A} upon addition of IPTG.

pKW512HBI44A. A PCR product containing *vapC* from *S. enterica* LT2 was generated using primers H6C-down-BamHI-KpnI and VAPC_LT2#HIS62 using pKW254BCI44A as template. PCR product containing *vapC*^{I44A} was digested with *Bam*HI and *Hind*III and inserted into *Bam*HI and *Hind*III digested pKE512HB. pKW512HBI44A produces VapB_{LT2} with a N-terminal tag of six histidines and VapC_{LT2}^{I44A} upon addition of IPTG.

pKW512HBY72A. A PCR product containing *vapC* from *S. enterica* LT2 was generated using primers H6C-down-BamHI-KpnI and VAPC_LT2#HIS62 using pKW254BCY72A as template. PCR product containing *vapC*^{Y72A} was digested with *Bam*HI and *Hind*III and inserted into *Bam*HI and *Hind*III digested pKE512HB. pKW512HBY72A produces VapB_{LT2} with a N-terminal tag of six histidines and VapC_{LT2}^{Y72A} upon addition of IPTG.

pKW512HBA76S. A PCR product containing *vapC* from *S. enterica* LT2 was generated using primers H6C-down-BamHI-KpnI and VAPC_LT2#HIS62 using pKW254BCA76S as template. PCR product containing *vapC*^{A76S} was digested with *Bam*HI and *Hind*III and inserted into *Bam*HI and *Hind*III digested pKE512HB. pKW512HBA76S produces VapB_{LT2} with a N-terminal tag of six histidines and VapC_{LT2}^{A76S} upon addition of IPTG.

pKW3352L43A. A PCR product containing *vapC* from *S. enterica* LT2 was generated using primers VAPC-1_LT2#12 and VAPC_LT2#HIS62 using pKW254BCL43A as template. PCR product containing *vapC*_{LT2}^{L43A} was digested with *kpn*I and *Hind*III and inserted into pBAD33 pKW3352L43A produces VapC_{LT2}^{L43A} upon addition of arabinose.

pKW3352I44A. A PCR product containing *vapC* from *S. enterica* LT2 was generated using primers VAPC-1_LT2#12 and VAPC_LT2#HIS62 using pKW254BCI44A as template. PCR product containing *vapC*_{LT2}^{I44A} was digested with *kpn*I and *Hind*III and inserted into pBAD33. pKW3352I44A produces VapC_{LT2}^{I44A} upon addition of arabinose.

pKW3352Y72A. A PCR product containing *vapC* from *S. enterica* LT2 was generated using primers VAPC-1_LT2#12 and VAPC_LT2#HIS62 using pKW254BCY72A as template. PCR product containing *vapC*_{LT2}^{Y72A} was digested with *kpnI* and *HindIII* and inserted into pBAD33. pKW3352Y72A produces VapC_{LT2}^{Y72A} upon addition of arabinose.

pKW3352A76S. A PCR product containing *vapC* from *S. enterica* LT2 was generated using primers VAPC-1_LT2#12 and VAPC_LT2#HIS62 using pKW254BCA76S as template. PCR product containing *vapC*_{LT2}^{A76S} was digested with *kpnI* and *HindIII* and inserted into pBAD33. pKW3352A76S produces VapC_{LT2}^{A76S} upon addition of arabinose.

pKW3352I78A. A PCR product containing *vapC* from *S. enterica* LT2 was generated using primers VAPC-1_LT2#12 and VAPC_LT2#HIS62 using pKW254BCI78A as template. PCR product containing *vapC*_{LT2}^{I78A} was digested with *kpnI* and *HindIII* and inserted into pBAD33. pKW3352I78A produces VapC_{LT2}^{I78A} upon addition of arabinose.

Rates-of protein, RNA and DNA synthesis

Cells were grown in AB minimal at 37°C supplemented with 0.5% glycerol and 1X FN18 amino acid mix (For 200mL 20x FN18 mix, 0.710g Ala, 0.700g Arg, 0.310g His, 0.580g His, 0.580g His, 0.580g Lys, 0.460g Pro, 0.480g Thr, 0.600g Gly, 0.530g Asn, 0.870 Gln, 0.520g Iso, 0.240g Phe, 0.360g Tyr, 0.700g Val, 0.530g Asp, 0.880 Glu, 0.120 Cys, 10g Ser, 0.200 Trp) to an optical density OD₄₅₀= 0.5. Cultures were diluted to OD₄₅₀ of 0.05 and at an OD₄₅₀ of 0.3 cultures were induced by adding 0.2% arabinose. Samples of 0.5 mL were taken out at time points 0, 5, 10, 30, 60 min and added to preheated 5 µCi of [³⁵S]methionine (protein synthesis), 2 µCi [³H]uridine (RNA synthesis) or 2 µCi [methyl-³H]thymidine (DNA synthesis). After 1 min of pulse incorporation, samples were chased for 10 min with 0.5 mg cold methionine, 0.5 mg uridine or 0.5 mg thymidine, respectively. Protein, RNA and DNA was precipitated by addition of 100 µL ice-cold 40% trichloroacetic acid (TCA) and centrifuged at 14,300 rpm for 30 min at 4°C. Samples were then washed twice in cold 96% ethanol. Precipitates were transferred to scintillation vials and the amount of radioactivity incorporated counted in a liquid scintillation counter.

RNA purification

Cells were grown in LB at 37°C. At an OD₄₅₀ of 0.5 the cultures were diluted an OD of 0.05 and grown to an OD of 0.5 and transcription of the toxin was induced by appropriate inducer. Translation was inhibited by adding 50µg/mL chloramphenicol. 15 mL samples were taken at appropriate time points (see text) and immediately cooled, harvested and stored at -80°C.

Total RNA purification

Sample cell pellets were resuspended in 200 µL ice cold solution 1 [0.3 M sucrose, 0.01 M Na-Ac (pH 4.5)] and transferred to 1.5 mL microfuge tubes containing 200 µL solution 2 [2% SDS, 0.01 M Na-Ac (pH 4.5)]. 400µL of RNA phenol [saturated with 0.03M Na-Ac (pH 4.5), 0.1% 8-hydroxyquinoline] is then added to the cell suspension and it is heated at 65°C for 3 min. The solution was then frozen in liquid nitrogen for 15 s and spun at max-speed for 5 min. at room temperature. The aqueous phase is transferred into a new microfuge tube and extraction is repeated. The extraction is completed by addition of 200 µL phenol and 200 µL chloroform. The RNA was then precipitated ON in 900 µL 96% ethanol and 80 µL 1.5 M K-Ac (pH 4.8). In the final step the precipitated RNA was pelleted by centrifugation at 20.000 g for 20 min at 4 °C and washed with 70% ethanol. The RNA was then dried in a speed-vac for 5 min and resuspended in appropriate amounts of TE-buffer (10 mM Tris-HCl and 1 mM EDTA, pH 8) or nuclease free dH₂O. Alternatively, total RNA was purified using the RNeasy[®] minprep kit (Qiagen) according to manufactures instructions. The RNA was then quantified at OD₂₆₀ and the quality checked by agarose gel electrophoresis and ethidium bromide (EtBr) staining

tRNA purification

Total tRNA was purified according to (Varshney *et al.*, 1991). Cell pellets of 10 mL samples were resuspend 0.3 ml of 0.3 M Na-Ac (pH 4.5) and 10 mM Na₂EDTA, transferred to 1.5-ml Eppendorf tubes, and subjected to two extractions with equal volumes of phenol. The aqueous layer was transferred to new tubes, mixed with 2.5 volumes of ethanol, and left on ice for 1-2 h. Total nucleic acids were recovered by centrifugation for 15 min. The pellet was dissolved in 60 µL of 0.3 M Na-Ac (pH 4.5). Nucleic acids were re-precipitated with 2.5 volumes of ethanol,

left on ice for 2-3 h, and recovered by centrifugation for 15 min. The pellet was dissolved in 20 μ l of 10 mM Na-Ac (pH 4.5) and 1 mM Na₂EDTA. The RNA was then quantified at OD₂₆₀ and the quality checked by agarose gel electrophoresis and EtBr staining.

Preparation of VapC and VapB

VapC and VapC_{LT2} was purified from complex with N-terminal His-tagged VapB essentially as described for ReIE (Pedersen *et al.*, 2002) with some modifications. Strain C41 containing either pKW512HB (h6-*vapB*_{LT2}-*vapC*_{LT2}) or pKW812HB (h6-*vapB*-*vapC*) were grown under aeration in LB at 37°C. At OD₄₅₀ = 0.5 expression was induced by addition of 2 mM IPTG. After 3 h of growth, the cultures were harvested and resuspended in ice-cold lysis buffer (50mM NaH₂PO₄, 0.3M NaCl, 10mM imidazole, 5mM β -mercaptoethanol pH8 supplemented with EDTA-free protease inhibitor, Roche). Cells were disrupted using a Constant Cell disruption system and lysate cleared by centrifugation at 15,000 rpm for 30 min at 4°C. The cleared lysates were then incubated with Ni-NTA agarose (Qiagen) for at least 2 h at 4°C and subsequently loaded onto a gravity column. The columns were then washed extensively in wash buffer (50mM NaH₂PO₄, 0.3M NaCl, 35mM imidazole, 5mM β -mercaptoethanol pH8). VapC_{LT2} or VapC could then be separated and isolated from VapBC complex under denaturing conditions by incubating the column overnight (ON) at room-temperature in 10 column volumes of denaturing buffer (100mM NaH₂PO₄, 10mM Tris-HCl, 9.8M Urea, pH8). Denatured protein was collected refolded by four step dialysis; (1) 1 x PBS 0.1% Triton X-100 5mM DTT, (2) 1 x PBS 5mM DTT, (3) 1 x PBS 5mM DTT, and (4) 1 X PBS 20% glycerol 5 mM DTT. The authenticity and purity analysed by SDS-PAGE. VapB_{LT2}, VapB or VapC_{LT2} mutants were purified in a similar way using strain C41 carrying pKW512HC (*vapB*_{LT2}-h6-*vapC*_{LT2}), pKW812HC (*vapB*-h6-*vapC*), pKW512HBL43A (h6-*vapB*_{LT2}-*vapC*_{LT2}^{L43A}), pKW512HBI44A (h6-*vapB*_{LT2}-*vapC*_{LT2}^{I44A}), pKW512HBA76S (h6-*vapB*_{LT2}-*vapC*_{LT2}^{A76S}) and pKW512HBY72A (h6-*vapB*_{LT2}-*vapC*_{LT2}^{Y72A}).

Inhibition of *in vitro* translation extract

Purified VapC was tested for inhibition of MS2 RNA translation in a cell-free *E. coli* S30 *in vitro* translation Extract (Promega).

VapC activity assay

Each reaction contained the following: 6 μL Premix, 4.5 μL S30 Extract, 1.5 μL amino acid mix without methionine, 0.5 μL ^{35}S -methionine and 4.5 pmol VapC with and without pre-incubation with 30 pmol VapB. The reaction was incubated for 5 min at 37°C before addition of 1 μL MS2 RNA (~0.7 pmol) (Roche). The reactions were incubated for 1 h at 37°C before termination of the reaction by acetone precipitation. The protein products were separated on a 12% SDS-PAGE and visualised by phosphor imaging.

Resuming translation in a VapC inhibited extract

Each reaction contained the following: 20 μL Premix, 15 μL S30 Extract, 5 μL amino acid mix without methionine, and with 9 pmol VapC or storage buffer. The reaction was incubated for 5 min at 37°C before addition of either VapB (~60 pmol) or storage buffer. The incubation was continued for 5 min at 37°C. Finally, 2 μL MS2 RNA (~1.4 pmol, Roche) template was added together with 1 μL ^{35}S -methionine with or without 8 pmol of fMet-tRNA^{fMet} (A generous gift from Daniel Castro-Roa, Nikolay Zenkin' lab, Newcastle University) and incubation was continued for 10 min at 37°C. A 20 μL sample was taken and reaction terminated by acetone precipitation. The proteins synthesized by the *in vitro* translation reactions were separated on a 12% SDS-PAGE gel and visualised by phosphor imaging.

***In vitro* RNA cleavage analysis**

VapC tRNase activity was tested *in vitro* by incubating 2.5 pmol or 5 pmol of purified VapC with 2 pmol of purified tRNA^{fMet}, tRNA^{Val} or tRNA^{Phe} (Sigma-Aldrich) in cleavage buffer (10 mM HEPES pH7.5, 15 mM KCl, 3 mM MgCl₂ and a final glycerol concentration of 10%.) for 15 min at 37°C. VapC activity was counteracted by either pre-incubation with 30 pmol of VapB or by addition of 12.5mM of EDTA. Reactions were stopped by the addition of formamide buffer (FD, 10mL Formamide, 0.1 mM EDTA, 0.1% xylene cyanol, 0.1% bromphenol blue) and tRNAs could be separated by 8% PAGE (1:37.5) containing 8M Urea in 1 x TBE (for 1L 5 x TBE stock; 54g Tris, 27.5g boric acid and 20 mL 0.5M EDTA pH 8) and subsequent Ethidium bromide (EtBr) staining.

***In vitro* cleavage site mapping**

The cleavage site of VapC was identified by incubation with either 5'-end or 3'-end radio-labelled tRNA^{fMet}. 5'-end labelling was achieved by phosphorylating dephosphorylated tRNA^{fMet} using T₄ polynucleotide kinase (NEB) and [γ -³²P]-ATP, whereas 3'-end labelling of tRNA^{fMet} was achieved by ligation of radiolabelled pCp using T₄ RNA ligase (NEB). A hydroxyl ladder was created by incubating 1 pmol of tRNA^{fMet} in ladder buffer (50 mM NaCO₃ pH9.2, 1mM EDTA) for 5 min at 95°C. An RNase T1 ladder was created by incubating 1 pmol tRNA^{fMet} with 4U of RNase T1 (Fermentas) for 3 min at 37°C in RNase T1 buffer (50 mM Tris-HCl pH7.5, 2 mM EDTA). VapC cleavage was performed in cleavage buffer containing 1 pmol tRNA^{fMet} and 0.01 pmol, 0.025 pmol and 0.05 pmol of VapC for 15 min at 37°C. In the cleavage control, VapC was omitted. The reactions were stopped by addition of FD buffer and the tRNA separated on a 10% PAGE (1:37.5) gel containing 8M Urea in 1 x TBE and visualised by subsequent phosphor imaging.

Analysis of the *in vivo* cleavage site in tRNA^{fMet}

To determine the cleavage site *in vivo*, tRNA^{fMet} was isolated from total tRNA by hybridization to tRNA^{fMet} specific biotinylated DNA probes Fmet-bio, FMET-BIO-N or FMET-BIO-3 (see Table 5). Five micrograms of dephosphorylated total tRNA was mixed with 5 pmol of Fmet-bio oligo in 10 μ L RNA buffer (10 mM HEPES pH 7.5, 15 mM KCl). The mixture was denatured at 80 °C for 10 min and incubated on ice for 5 min. The hybrid was added to 20 μ L of Streptavidin Sepharose HP (GE Healthcare) and incubated for 5 min at room temperature during gentle mixing. The sepharose was then washed three times in RNA buffer to remove non-specific hybridization. The sepharose beads were resuspended in 15 μ L RNA buffer with 2 μ L polynucleotide kinase buffer, 1 μ L kinase was added together with 2 μ L [γ -³²P]-ATP. The solution was incubated for 30 min at 37 °C. Finally, the sepharose was washed three times in RNA buffer to remove excess un-incorporated [³²P]-ATP and the reaction stopped by addition of FD buffer. The fragments could be resolved by 10% Urea PAGE (1:37.5) in 1 x TBE and visualized by phosphor imaging.

Ribosome Profiles generated by ultracentrifugation

Ribosome profiles and subsequent Western analysis was done according to (Liu *et al.*, 2008), however with modifications. MG1655 Δ lon containing either pKW3352HC

(pBAD33::*vapC_{LT2}*-H6) or pKW3382HC (pBAD33::*vapC*-H6) were grown exponentially in 400mL of LB. At $OD_{450} = 0.4$, transcription was induced by the addition of 0.2% arabinose and expression was allowed to continue for 20' before the cultures were harvested. Pellets were washed in Ribosome buffer (10 mM $MgCl_2$ 50 mM NH_4Cl 10 mM Tris, pH 7.4 and 5 mM DTT) and stored at $-80^\circ C$. Pellet was then resuspended in 5 mL ice-cold Ribosome buffer with EDTA-free protease inhibitor and 5U of RNase-free DNase (Roche). The Cells were lysed by passing through Cell Disrupter at 16,000 bar once and the lysate cleared by centrifugation at 15,000 rpm for 20 min. 500 μ L of cleared lysate was loaded onto a 5-40% continuous sucrose gradient in Ribosome buffer and centrifuged either at 35,000 rpm for 3.5 h or at 28,000 rpm for 12 hr at $4^\circ C$ in a Beckman SW40Ti rotor. Gradients were fractionated in 500 μ L fractions and visualized in a 1% agarose gel stained with EtBr. In an attempt to separate ribosomal subunits, 1 mL of lysate was initially centrifuged through a 1.1 M sucrose cushion in ribosome buffer at 35,000 rpm for 14hr at $4^\circ C$. The clear ribosome pellet, which appeared was then washed gently with low magnesium ribosome buffer (1 mM $MgCl_2$ 50 mM NH_4Cl 10 mM Tris, pH 7.4 and 5 mM DTT) and resuspended in 1 mL low magnesium ribosome buffer by gentle agitation on ice. 500 μ L of the resuspend ribosome solution was then loaded onto a 5-40% continuous sucrose gradient in low magnesium ribosome buffer and centrifuged at 28,000 rpm for 12hr at $4^\circ C$. Gradients were then fractionated in 500 μ L fraction and visualized in a 1% agarose gel stained with EtBr.

Luciferase activity assays

The assay was carried out in accordance with (Kimura and Suzuki, 2010), however with modifications. *E. coli* K-12 MG1655 Δlon containing pKW3352HC (BAD::*vapC_{LT2}*) with pQE AAA or pQE AAG were grown exponentially in LB medium at $37^\circ C$. At $OD_{450} = 0.4$, 0.2% arabinose was added and after 30 min of expression, 0.5 mL samples were harvested by centrifugation. The cell pellet was then resuspended in 100 μ L of luciferase lysis buffer (50 mM HEPES pH 7.5, 100 mM KCl, 10 mM $MgCl_2$, 7 mM β -Mercaptoethanol and 400 μ M lysozyme). The suspension was then shock-frozen in liquid nitrogen and thawed on ice. The lysate was cleared by centrifugation and 10 μ L of lysate was used in the Dual-Luciferase® Reporter Assay System (Promega) in accordance with manufactures protocol. The

translation efficiency on the start codon of *lucF* was determined as the LucF/LucR ratio.

Northern blot analysis

Northern analysis was used for detection and quantification of mRNA and tRNA levels.

mRNA Northern blot analysis

For mRNA quantification 10 µg of total RNA was fractionated in a 5% PAGE (1:37.5) gel containing 1x TBE and 8M Urea and electroblotted to a Zeta-probe nylon membrane (Bio Rad) and hybridized with a single-stranded ³²P-labelled riboprobe, complementary to the RNA in PerfectHyb™ Plus hybridization buffer (Sigma) ON at 65 °C. The riboprobes for *lpp* and tmRNA were generated using *pstI* linerized pSC333 and pSC334 as template. The *dksA* and *ompA* specific riboprobes were generated with a PCR product template including a T7 promoter made with primers *dksA* probe-f and *dksA* T7 probe-r and T7/*pmoA* and *pmoA*-forw, respectively. Templates were *in vitro* transcribed for 2 h at 37°C [T7 RNA polymerase (Promega); 0.1 µM DTT; 1x transc. buffer; 2.5 mM of ATP, GTP and UTP; 0.2µg template; [³²Pα]-CTP (50 mCi); 100µM CTP; RNase inhibitor]. DNA template was removed by adding DNase. The membranes were washed in 2 x SSC (0.3M NaCl, 0.03M Na-citrate, pH 7) with 0.1 % SDS twice at room temperature, to wash increase stringency, membrane were additionally washed one – two times for 30 min in 0.5 x SSC with 0.1% SDS at hybridisation temperature. Finally the blot was detected by phosphor imaging

tRNA Northern blot analysis

Northern blot analysis was also applied to determine the stability of different tRNA species after VapC or VapC_{LT2} expression. Five micrograms of purified tRNA was mixed with loading buffer (0.1 M Na-Acetate pH 5, 8 M Urea, 0.05% bromphenol blue and 0.05% xylene cyanol) and separated in an 8% PAGE (1:37.5) gel containing 8 M urea and 0.1 M Na-acetate pH 5. The part of the gel containing tRNA of interest was then electroblotted onto a Hybond-N membrane (GE Healthcare) in transfer buffer (40 mM Tris-Acetate, 2 mM EDTA pH 8.1). The separated tRNA was UV-crosslinked. The membrane was pre-hybridized in PerfectHyb™ Plus hybridization buffer (Sigma) for 5 min at 42 °C following addition of an appropriate ³²P-labelled

DNA oligo probe; tRNA^{Val}, tRNA^{Phe}, tRNA^{Met}, tRNA^{Arg2}, tRNA^{His}, tRNA^{Leu1}, tRNA^{Thr1}, tRNA^{fMet} or tRNA^{Tyr} (see the oligonucleotide list) and subsequent hybridization for at least 4 h at 42 °C. After hybridization, the membrane was washed two - three times 5 min in 2 x SSC with 0.1% SDS at room temperature and the blot was analysed by phosphor imaging.

Primer extension analysis

Primer extension analysis was used semi-quantitatively, and to identify mRNA 5'-ends generated either as transcript 5'-ends or by mRNA interferase cleavage.

Identification of the transcriptional start site of the vapBC_{LT2} promoter

To map the promoter *vapBC_{LT2}* from *S. enterica* LT2, primer extension analysis was performed on total RNA from KP1001 *S. typhimurium* LT2 or *E. coli* K-12 variants containing a plasmid with *vapBC* operon. The *vapB*-5#PE primer (4 pmol) which is specific to *vapB* in *vapBC* mRNA was labelled in a reaction with 4µL [γ -³²P]-ATP and T₄ polynucleotide kinase (NEB) for 30 min at 37°C. Labelled primer (0.2 pmol) was hybridized with 10 µg of total RNA. Hybridization with primer was followed by reverse transcription using 0.1 U of SuperScript II Reverse transcriptase (Invitrogen) in 1 x FirstStrand buffer, 10 mM DTT and 1 mM dNTP for 1 h at 42°C. Radiolabelled cDNA was separated in a 6% PAGE (1:37.5) gel containing 8 M Urea with 1 x TBE and visualized by phosphor imaging.

Identification of cleavage sites generated by YoeB mRNA interferase

To identify the cleavage sites of ribosome dependent YoeB mRNAse, primer extension analysis was performed on genetically modified versions of the *dksA* mRNA. The pKW71D-3#PE primer (4 pmol) which is specific to the 3'-end of *dksA* mRNA deriving from pKW25420T (*dksA* with native promoter), pKW25421T (*dksA*, ATG→AAG), pKW25423T (*dksA*, in frame premature termination codon), pKW25424T (*dksA*, out of frame TAA), pKW25425T (*dksA*, out of frame TAA), pKW25427T (*dksA* without SD sequence) and pKW25428T (*dksA*, ATG→AAG, without SD sequence) was labelled in a reaction with 4µL [γ -³²P]-ATP and T₄ polynucleotide kinase (NEB) for 30 min at 37°C. Labelled primer (0.2 pmol) was hybridized with 20 µg of total RNA isolated from *E. coli* K-12 expressing *dksA* derivatives together with *vapC*, *vapC_{LT2}* or YoeB. The hybridization was followed by

reverse transcription using 0.1 U of SuperScript II Reverse transcriptase (Invitrogen) in 1 x FirstStrand buffer, 10 mM DTT and 1 mM dNTP. The tmRNA 5'-end and the small reading frame was mapped using primer 10SA-2. Radiolabelled cDNA was fractionated in a 6% PAGE (1:37.5) gel containing 8 M Urea with 1 x TBE and visualized by phosphor imaging.

Western blot analysis

Western blot analysis was used to detect specific proteins in protein samples either using protein specific or tag specific antibodies

Degradation of VapB_{LT2} in the cell

The stability of VapB_{LT2} after addition of chloramphenicol was determined by Western Blot Analysis. The *vapB_{LT2}* transcription was induced from pKW51, a low copy plasmid, by addition of 1 mM IPTG for 10min to exponentially growing MG1655, KW10 (MG1655 Δlon) and KW11 (MG1655 Δclp). Translation was inhibited by addition of 50 μ g/mL chloramphenicol and 1 mL samples were taken at time points indicated. Samples were rapidly harvested at 4°C and cell pellet resuspend in 50 μ L leammli buffer (Buffer stock, 4mL 50% glycerol, 1mL Mercaptoethanol, 5.75mL 10% SDS, 2.5mL 0.5M Tri-HCl pH 6.8 and 1mL 0.1% Bromophenol blue) and boiled for 2 min. Proteins from 10 μ L samples were separated by SDS-PAGE and electroblotted onto a PVDF transfer membrane (GE healthcare) and membrane blocked 1hr at ambient temperature in PBS-T (Phosphate Buffered Saline (Oxoid) with 0.1% Tween) with 5% milk powder. The membrane was briefly washed in PBS-T and then incubated for at least 1 h at room temperature with VapB_{LT2} polyclonal antibodies (Eurogentec) in PBS-T and 2% milk powder. After 2 x 5 min washing steps in PBS-T was followed by incubation with HRP (Horseradish Peroxidase) conjugated anti-rabbit IgG antibodies (Sigma) in PBS-T with 2% milk powder for 1 h at room temperature. The membrane was then washed 2 x 5 min and 15 min in PBS-T and the blot detected by chemiluminescence using ECL plus western blotting detection system (GE Healthcare).

Western blot analysis on ribosome fractions

VapC-H₆ and VapC_{LT2}-H₆ were detected in sucrose gradient fractions by western blot analysis. 10 μ L relevant ribosome gradient fractions were mixed with 10 μ L of

laemmli buffer and proteins separated in a 4-12% SDS-PAGE gel (Invitrogen). Proteins were then electro blotted onto a PVDF transfer membrane (GE healthcare) at 115mA for 60 min and membrane blocked ON at 4°C in PBS-T (PBS with 0.1% Tween) and 5% milk powder. The membrane was then incubated for at least 3 h at 4°C with Penta-His monoclonal antibodies (Qiagen) in PBS-T and 2% milk powder. The membrane was then briefly washed in PBS-T followed by incubation with HRP conjugated mouse IgG antibodies (Sigma) for 2 h at 4°C. The membrane was finally washed in PBS-T and the blot detected using ECL plus western blotting detection system (GE Healthcare).

Electrophoretic mobility shift assays and DNase I footprinting

DNA fragments containing either one binding site, *vapO1* (using hybridised oligos VapBCbinding#small-down and VapBCbinding#small-up), or two binding sites, *vapO1* and *vapO2* (PCR product with oligos vapBC_EMSA_down and vapBC_EMSA_up), were 5'-end-labelled with [γ -³²P]ATP using T4 polynucleotide Kinase (NEB). Binding site mutations in *vapO1* or *vapO2* were introduced by PCR using primers PBC-10_MUT_DOWN and PBC-10_MUT_UP for *vapO1mut* and PBC-35_MUT_DOWN and PBC-35_MUT_UP for *vapO2mut*. Binding Control DNA (199bp) was amplified from pUC plasmid DNA using primer 171SR14 and 171SR16 and was 5'-labelled as described above.

Labelled probes (0.5-2nM) were incubated with purified proteins in binding buffer (20 mM Tris-HCl pH 7.5, 100 mM KCl, 2 mM MgCl₂, 1 mM DTT, 50 µg/mL BSA and 10% glycerol) in a volume of 20uL or 30uL. To avoid unspecific DNA binding sonicated salmon sperm DNA (ssDNA) was added to a final concentration 0.1 mg/ml. Reactions were incubated for 20 min at 37°C before DNA bound complexes were separated by native PAGE in 5% or 6% acrylamide gels (1:37.5) with 0.5x TBE for two and one binding site probes, respectively. The separation was followed by phosphor imaging.

DNase I footprinting

For DNase I footprinting, binding reactions prepared as described above, were incubated with 0.01 U/µl DNase I and 1 x DNase I buffer (Roche) at 37°C for 2 min, followed by addition of 100 µl of Stop buffer (2 M ammonium acetate, 20 mM EDTA, 10 mg/ml ssDNA). The resulting DNA fragments were extracted once in

phenol, once in chloroform, precipitated in ethanol equalized for total radioactivity and separated on an 8% PAGE gel (1:37.5) containing 8M Urea in 1 x TBE along with a dideoxyNTP sequencing ladder. The digestion pattern was detected by phosphor imaging.

MW estimation of VapBC_{LT2} complex bound to DNA

The molecular weight (MW) of VapBC_{LT2} bound to DNA was estimated according to an EMSA-based method (Orchard and May, 1993). 50 pmol of VapC_{LT2} was incubated with 50 pmol of VapB_{LT2} and 5 pmol DNA probe (containing *vapO1*) in binding buffer as described above. The binding reactions were analyzed on a series of polyacrylamide gels (7%-10%) including four molecular weight markers (Lactal Albumin, 14.2kD, Carbonic Anhydrase, 29kD, Ovoalbumin, 44kD, Bovine Serum Albumin, 66kD). The gels were silver stained and the distance from the well to stained protein band was measured and divided by the bromophenol blue migration distance to give the relative mobility (R_f). The logarithm of the R_f values for protein complex and molecular weight marker was plotted against the gel acrylamide concentration and a best-line fit was obtained. The negative slopes of these fits were plotted against the molecular weights of the protein standards on a double-logarithmic scale and a best-line fit was obtained. The slope of VapBC_{LT2} bound to DNA could then extrapolated according to the equation ($y = 0.0884x + 0.6332$) and the MW of the DNA (22.116 kD) was subtracted to give MW of VapBC_{LT2}.

β -galactosidase assays

Overnight cultures were diluted to an $OD_{600} \sim 0.05$ in LB supplemented with appropriate antibiotics and grown at 37°C to an OD_{600} of 0.5 and diluted to OD_{600} of 0.05. At OD_{600} of 0.4-0.5 samples of 500 μ L were taken. Activity of the fusion was measured by monitoring β -galactosidase activity (Units) in samples from cells carrying pOU254 and pOU253 derivatives using the chloroform protocol variant as described (Miller, 1972). Experiments were carried out in triplicates.

Quantitative PCR

Total RNA was extracted from cell samples using RNeasy mini kit (Qiagen). After elution, RNA was treated with DNase in an additional step to ensure that RNA was completely DNA free. Total RNA was converted to cDNA in 20 μ L standard

reactions with 0.32 μg of RNA and random primers using MultiScribe™ reverse transcriptase (Applied Biosystems) according to manufacturer's instructions. The cDNA was diluted 100-fold and 6 μL used in 20 μL standard reactions containing 2 μL of each primer and 10 μL 2x Sybr Green PCR mastermix (Qiagen). Primers used were q-vapB-f and q-vapB-rv for *vapB* mRNA and rpsA qPCR-f and rpsA qPCR-rv for internal reference gene (*rpsA*). The cDNA was amplified in a Rotor-Gene Q real-time PCR cycler (Qiagen) and the quantification performed using Rotor-Gene Q software by the $\Delta\Delta C_t$ relative quantification method (Livak and Schmittgen, 2001). Standard curves for primer efficiencies were performed using 10, 100, 10^3 and 10^4 dilutions of cDNA and was taken into consideration in the C_t values obtained.

***In vitro* translation of *vapBC*_{LT2} mRNA**

The *vapBC*_{LT2} mRNA variants were purified as T7 transcripts from DNA templates. For wild type *vapBC* mRNA primers VAPBC_T7_DOWN and VAPBC_T7_RRNBT1_UP were used. PCR products using BC_253_PRESTOPB_DOWN and BC_253_PRESTOPB_UP or BC_253_STARTB_DOWN and BC_253_STARTB_UP were used as templates in a PCR with VAPBC_T7_DOWN and VAPBC_T7_RRNBT1_UP to create T7 templates for *vapBC*_{LT2} mRNA containing premature stop codon in *vapB*_{LT2} and *vapB*_{LT2} start codon mutation, respectively. The DNA templates were transcribed using T7 RNA polymerase (Promega) in accordance with manufacturer's instructions. T7 transcripts were purified by extraction from denaturing PAGE gel. Transcripts were then *in vitro* translated using a cell free *in vitro* translation S30 extract (Promega). Each reaction contained 8 μL S30 premix, 2 μL amino acid mix, 5 μL S30 extract, 1 μL ³⁵S-methionine which was preincubated for 5 min at 37°C before addition of 1 pmol of mRNA. Incubation was continued for 25 min before reaction was terminated by acetone precipitation. Protein product was visualized by SDS-PAGE and phosphor imaging.

***In vitro* cross-linking of purified VapC_{LT2}**

The presence of VapC_{LT2} dimer in solution was verified by *in vitro* cross linking with formaldehyde. 5 pmol Purified VapC_{LT2} or VapC_{LT2}^{Y72A} mutant was incubated with 0.7% formaldehyde in storage buffer (PBS + 20% glycerol) for 15 min at 37°C. The cross linking reaction was terminated by addition of glycine to final concentration of

0.25M and leammli buffer. The cross linked complexes were separated by 4-12% SDS-PAGE and visualised by silver staining.

References

- Afif,H., Allali,N., Couturier,M., and Van,M.L. (2001) The ratio between CcdA and CcdB modulates the transcriptional repression of the ccd poison-antidote system. *Mol Microbiol* **41**: 73-82.
- Ahidjo,B.A., Kuhnert,D., McKenzie,J.L., Machowski,E.E., Gordhan,B.G., Arcus,V. *et al.* (2011) VapC Toxins from Mycobacterium tuberculosis Are Ribonucleases that Differentially Inhibit Growth and Are Neutralized by Cognate VapB Antitoxins. *PLoS One* **6**: e21738.
- Aizenman,E., Engelberg-Kulka,H., and Glaser,G. (1996) An Escherichia coli chromosomal "addiction module" regulated by guanosine [corrected] 3',5'-bispyrophosphate: a model for programmed bacterial cell death. *Proc Natl Acad Sci U S A* **93**: 6059-6063.
- Amitsur,M., Levitz,R., and Kaufmann,G. (1987) Bacteriophage T4 anticodon nuclease, polynucleotide kinase and RNA ligase reprocess the host lysine tRNA. *EMBO J* **6**: 2499-2503.
- Amitsur,M., Morad,I., Chapman-Shimshoni,D., and Kaufmann,G. (1992) HSD restriction-modification proteins partake in latent anticodon nuclease. *EMBO J* **11**: 3129-3134.
- Anantharaman,V., and Aravind,L. (2003) New connections in the prokaryotic toxin-antitoxin network: relationship with the eukaryotic nonsense-mediated RNA decay system. *Genome Biol* **4**: R81.
- Antoun,A., Pavlov,M.Y., Lovmar,M., and Ehrenberg,M. (2006) How initiation factors maximize the accuracy of tRNA selection in initiation of bacterial protein synthesis. *Mol Cell* **23**: 183-193.
- Aoki,S.K., Diner,E.J., de Roodenbeke,C.T., Burgess,B.R., Poole,S.J., Braaten,B.A. *et al.* (2010) A widespread family of polymorphic contact-dependent toxin delivery systems in bacteria. *Nature* **468**: 439-442.
- Aoki,S.K., Pamma,R., Hernday,A.D., Bickham,J.E., Braaten,B.A., and Low,D.A. (2005) Contact-dependent inhibition of growth in Escherichia coli. *Science* **309**: 1245-1248.
- Aoki,S.K., Webb,J.S., Braaten,B.A., and Low,D.A. (2009) Contact-dependent growth inhibition causes reversible metabolic downregulation in Escherichia coli. *J Bacteriol* **191**: 1777-1786.
- Arbing,M.A., Handelman,S.K., Kuzin,A.P., Verdon,G., Wang,C., Su,M. *et al.* (2010) Crystal structures of Phd-Doc, HigA, and YeeU establish multiple evolutionary links between microbial growth-regulating toxin-antitoxin systems. *Structure* **18**: 996-1010.
- Arcus,V.L., Backbro,K., Roos,A., Daniel,E.L., and Baker,E.N. (2004) Distant structural homology leads to the functional characterization of an archaeal PIN domain as an exonuclease. *J Biol Chem* **279**: 16471-16478.

- Arcus, V.L., McKenzie, J.L., Robson, J., and Cook, G.M. (2011) The PIN-domain ribonucleases and the prokaryotic VapBC toxin-antitoxin array. *Protein Eng Des Sel* **24**: 33-40.
- Barends, S., Karzai, A.W., Sauer, R.T., Wower, J., and Kraal, B. (2001) Simultaneous and functional binding of SmpB and EF-Tu-TP to the alanyl acceptor arm of tmRNA. *J Mol Biol* **314**: 9-21.
- Barrangou, R., Fremaux, C., Deveau, H., Richards, M., Boyaval, P., Moineau, S. *et al.* (2007) CRISPR provides acquired resistance against viruses in prokaryotes. *Science* **315**: 1709-1712.
- Barraud, P., Schmitt, E., Mechulam, Y., Dardel, F., and Tisne, C. (2008) A unique conformation of the anticodon stem-loop is associated with the capacity of tRNA^{fMet} to initiate protein synthesis. *Nucleic Acids Res* **36**: 4894-4901.
- Bech, F.W., Jorgensen, S.T., Diderichsen, B., and Karlstrom, O.H. (1985) Sequence of the relB transcription unit from Escherichia coli and identification of the relB gene. *EMBO J* **4**: 1059-1066.
- Belitsky, M., Avshalom, H., Erental, A., Yelin, I., Kumar, S., London, N. *et al.* (2011) The Escherichia coli extracellular death factor EDF induces the endoribonucleolytic activities of the toxins MazF and ChpBK. *Mol Cell* **41**: 625-635.
- Bernard, P., and Couturier, M. (1992) Cell killing by the F plasmid CcdB protein involves poisoning of DNA-topoisomerase II complexes. *J Mol Biol* **226**: 735-745.
- Bernard, P., Kezdy, K.E., Van, M.L., Steyaert, J., Wyns, L., Pato, M.L. *et al.* (1993) The F plasmid CcdB protein induces efficient ATP-dependent DNA cleavage by gyrase. *J Mol Biol* **234**: 534-541.
- Bernardo, L.M., Johansson, L.U., Solera, D., Skarfstad, E., and Shingler, V. (2006) The guanosine tetraphosphate (ppGpp) alarmone, DksA and promoter affinity for RNA polymerase in regulation of sigma-dependent transcription. *Mol Microbiol* **60**: 749-764.
- Black, D.S., Irwin, B., and Moyed, H.S. (1994) Autoregulation of hip, an operon that affects lethality due to inhibition of peptidoglycan or DNA synthesis. *J Bacteriol* **176**: 4081-4091.
- Black, D.S., Kelly, A.J., Mardis, M.J., and Moyed, H.S. (1991) Structure and organization of hip, an operon that affects lethality due to inhibition of peptidoglycan or DNA synthesis. *J Bacteriol* **173**: 5732-5739.
- Bleichert, F., Granneman, S., Osheim, Y.N., Beyer, A.L., and Baserga, S.J. (2006) The PINc domain protein Utp24, a putative nuclease, is required for the early cleavage steps in 18S rRNA maturation. *Proc Natl Acad Sci U S A* **103**: 9464-9469.
- Bloomfield, G.A., Whittle, G., McDonagh, M.B., Katz, M.E., and Cheetham, B.F. (1997) Analysis of sequences flanking the vap regions of Dichelobacter nodosus: evidence for multiple integration events, a killer system, and a new genetic element. *Microbiology* **143 (Pt 2)**: 553-562.

- Blower, T.R., Salmond, G.P., and Luisi, B.F. (2011a) Balancing at survival's edge: the structure and adaptive benefits of prokaryotic toxin-antitoxin partners. *Curr Opin Struct Biol* **21**: 109-118.
- Blower, T.R., Pei, X.Y., Short, F.L., Fineran, P.C., Humphreys, D.P., Luisi, B.F., and Salmond, G.P. (2011b) A processed noncoding RNA regulates an altruistic bacterial antiviral system. *Nat Struct Mol Biol* **18**: 185-190.
- Bobay, B.G., Andreeva, A., Mueller, G.A., Cavanagh, J., and Murzin, A.G. (2005) Revised structure of the AbrB N-terminal domain unifies a diverse superfamily of putative DNA-binding proteins. *FEBS Lett* **579**: 5669-5674.
- Bodogai, M., Ferenczi, S., Bashtovyy, D., Miclea, P., Papp, P., and Dusha, I. (2006) The ntrPR operon of *Sinorhizobium meliloti* is organized and functions as a toxin-antitoxin module. *Mol Plant Microbe Interact* **19**: 811-822.
- Bordes, P., Cirinesi, A.M., Ummels, R., Sala, A., Sakr, S., Bitter, W., and Genevoux, P. (2011) SecB-like chaperone controls a toxin-antitoxin stress-responsive system in *Mycobacterium tuberculosis*. *Proc Natl Acad Sci U S A* **108**: 8438-8443.
- Bowman, C.M., Dahlberg, J.E., Ikemura, T., Konisky, J., and Nomura, M. (1971) Specific inactivation of 16S ribosomal RNA induced by colicin E3 in vivo. *Proc Natl Acad Sci U S A* **68**: 964-968.
- Bravo, A., de, T.G., and Diaz, R. (1987) Identification of components of a new stability system of plasmid R1, ParD, that is close to the origin of replication of this plasmid. *Mol Gen Genet* **210**: 101-110.
- Brown, B.L., Grigoriu, S., Kim, Y., Arruda, J.M., Davenport, A., Wood, T.K. *et al.* (2009) Three dimensional structure of the MqsR:MqsA complex: a novel TA pair comprised of a toxin homologous to RelE and an antitoxin with unique properties. *PLoS Pathog* **5**: e1000706.
- Brown, J.M., and Shaw, K.J. (2003) A novel family of *Escherichia coli* toxin-antitoxin gene pairs. *J Bacteriol* **185**: 6600-6608.
- Browning, D.F., Grainger, D.C., and Busby, S.J. (2010) Effects of nucleoid-associated proteins on bacterial chromosome structure and gene expression. *Curr Opin Microbiol* **13**: 773-780.
- Budde, P.P., Davis, B.M., Yuan, J., and Waldor, M.K. (2007) Characterization of a higBA toxin-antitoxin locus in *Vibrio cholerae*. *J Bacteriol* **189**: 491-500.
- Bunker, R.D., McKenzie, J.L., Baker, E.N., and Arcus, V.L. (2008) Crystal structure of PAE0151 from *Pyrobaculum aerophilum*, a PIN-domain (VapC) protein from a toxin-antitoxin operon. *Proteins* **72**: 510-518.
- Butala, M., Zgur-Bertok, D., and Busby, S.J. (2009) The bacterial LexA transcriptional repressor. *Cell Mol Life Sci* **66**: 82-93.
- Buts, L., Lah, J., Dao-Thi, M.H., Wyns, L., and Loris, R. (2005) Toxin-antitoxin modules as bacterial metabolic stress managers. *Trends Biochem Sci* **30**: 672-679.

Button,J.E., Silhavy,T.J., and Ruiz,N. (2007) A suppressor of cell death caused by the loss of sigmaE downregulates extracytoplasmic stress responses and outer membrane vesicle production in Escherichia coli. *J Bacteriol* **189**: 1523-1530.

Cascales,E., Buchanan,S.K., Duche,D., Kleanthous,C., Lloubes,R., Postle,K. *et al.* (2007) Colicin biology. *Microbiol Mol Biol Rev* **71**: 158-229.

Chadani,Y., Ono,K., Kutsukake,K., and Abo,T. (2011) Escherichia coli YaeJ protein mediates a novel ribosome-rescue pathway distinct from SsrA- and ArfA-mediated pathways. *Mol Microbiol* **80**: 772-785.

Chadani,Y., Ono,K., Ozawa,S., Takahashi,Y., Takai,K., Nanamiya,H. *et al.* (2010) Ribosome rescue by Escherichia coli ArfA (YhdL) in the absence of trans-translation system. *Mol Microbiol* **78**: 796-808.

Chakravarty,A.K., and Shuman,S. (2011) RNA 3'-phosphate cyclase (RtcA) catalyzes ligase-like adenylation of DNA and RNA 5'-monophosphate ends. *J Biol Chem* **286**: 4117-4122.

Chang,D.E., Smalley,D.J., and Conway,T. (2002) Gene expression profiling of Escherichia coli growth transitions: an expanded stringent response model. *Mol Microbiol* **45**: 289-306.

Cherny,I., Overgaard,M., Borch,J., Bram,Y., Gerdes,K., and Gazit,E. (2007) Structural and thermodynamic characterization of the Escherichia coli RelBE toxin-antitoxin system: indication for a functional role of differential stability. *Biochemistry* **46**: 12152-12163.

Christensen,S.K., and Gerdes,K. (2003) RelE toxins from bacteria and Archaea cleave mRNAs on translating ribosomes, which are rescued by tmRNA. *Mol Microbiol* **48**: 1389-1400.

Christensen,S.K., and Gerdes,K. (2004) Delayed-relaxed response explained by hyperactivation of RelE. *Mol Microbiol* **53**: 587-597.

Christensen,S.K., Maenhaut-Michel,G., Mine,N., Gottesman,S., Gerdes,K., and Van,M.L. (2004) Overproduction of the Lon protease triggers inhibition of translation in Escherichia coli: involvement of the yefM-yoeB toxin-antitoxin system. *Mol Microbiol* **51**: 1705-1717.

Christensen,S.K., Mikkelsen,M., Pedersen,K., and Gerdes,K. (2001) RelE, a global inhibitor of translation, is activated during nutritional stress. *Proc Natl Acad Sci U S A* **98**: 14328-14333.

Christensen,S.K., Pedersen,K., Hansen,F.G., and Gerdes,K. (2003) Toxin-antitoxin loci as stress-response-elements: ChpAK/MazF and ChpBK cleave translated RNAs and are counteracted by tmRNA. *J Mol Biol* **332**: 809-819.

Christensen-Dalsgaard,M., and Gerdes,K. (2006) Two higBA loci in the Vibrio cholerae superintegron encode mRNA cleaving enzymes and can stabilize plasmids. *Mol Microbiol* **62**: 397-411.

- Christensen-Dalsgaard,M., and Gerdes,K. (2008) Translation affects YoeB and MazF messenger RNA interferase activities by different mechanisms. *Nucleic Acids Res* **36**: 6472-6481.
- Christensen-Dalsgaard,M., Jorgensen,M.G., and Gerdes,K. (2010) Three new RelE-homologous mRNA interferases of Escherichia coli differentially induced by environmental stresses. *Mol Microbiol* **75**: 333-348.
- Christensen-Dalsgaard,M., Overgaard,M., Winther,K.S., and Gerdes,K. (2008) RNA decay by messenger RNA interferases. *Methods Enzymol* **447**: 521-535.
- Clissold,P.M., and Ponting,C.P. (2000) PIN domains in nonsense-mediated mRNA decay and RNAi. *Curr Biol* **10**: R888-R890.
- Cole,S.T., Eiglmeier,K., Parkhill,J., James,K.D., Thomson,N.R., Wheeler,P.R. *et al.* (2001) Massive gene decay in the leprosy bacillus. *Nature* **409**: 1007-1011.
- Cooper,C.R., Daugherty,A.J., Tachdjian,S., Blum,P.H., and Kelly,R.M. (2009) Role of vapBC toxin-antitoxin loci in the thermal stress response of Sulfolobus solfataricus. *Biochem Soc Trans* **37**: 123-126.
- Couturier,M., Bahassi,e., and Van,M.L. (1998) Bacterial death by DNA gyrase poisoning. *Trends Microbiol* **6**: 269-275.
- Daines,D.A., Wu,M.H., and Yuan,S.Y. (2007) VapC-1 of nontypeable Haemophilus influenzae is a ribonuclease. *J Bacteriol* **189**: 5041-5048.
- Dalebroux,Z.D., Svensson,S.L., Gaynor,E.C., and Swanson,M.S. (2010) ppGpp conjures bacterial virulence. *Microbiol Mol Biol Rev* **74**: 171-199.
- Dalton,K.M., and Crosson,S. (2010) A conserved mode of protein recognition and binding in a ParD-ParE toxin-antitoxin complex. *Biochemistry* **49**: 2205-2215.
- Dao-Thi,M.H., Charlier,D., Loris,R., Maes,D., Messens,J., Wyns,L., and Backmann,J. (2002) Intricate interactions within the ccd plasmid addiction system. *J Biol Chem* **277**: 3733-3742.
- Dao-Thi,M.H., Van,M.L., De,G.E., Afif,H., Buts,L., Wyns,L., and Loris,R. (2005) Molecular basis of gyrase poisoning by the addiction toxin CcdB. *J Mol Biol* **348**: 1091-1102.
- Dao-Thi,M.H., Van,M.L., De,G.E., Buts,L., Ranquin,A., Wyns,L., and Loris,R. (2004) Crystallization of CcdB in complex with a GyrA fragment. *Acta Crystallogr D Biol Crystallogr* **60**: 1132-1134.
- David,M., Borasio,G.D., and Kaufmann,G. (1982) Bacteriophage T4-induced anticodon-loop nuclease detected in a host strain restrictive to RNA ligase mutants. *Proc Natl Acad Sci U S A* **79**: 7097-7101.
- Davies,D.G., Parsek,M.R., Pearson,J.P., Iglewski,B.H., Costerton,J.W., and Greenberg,E.P. (1998) The involvement of cell-to-cell signals in the development of a bacterial biofilm. *Science* **280**: 295-298.

- de la Hoz,A.B., Ayora,S., Sitkiewicz,I., Fernandez,S., Pankiewicz,R., Alonso,J.C., and Ceglowski,P. (2000) Plasmid copy-number control and better-than-random segregation genes of pSM19035 share a common regulator. *Proc Natl Acad Sci U S A* **97**: 728-733.
- De,J.N., Garcia-Pino,A., Buts,L., Haesaerts,S., Charlier,D., Zangger,K. *et al.* (2009) Rejuvenation of CcdB-poisoned gyrase by an intrinsically disordered protein domain. *Mol Cell* **35**: 154-163.
- Dennis,P.P., and Bremer,H. (1974) Differential rate of ribosomal protein synthesis in *Escherichia coli* B/r. *J Mol Biol* **84**: 407-422.
- Depew,R.E., and Cozzarelli,N.R. (1974) Genetics and physiology of bacteriophage T4 3'-phosphatase: evidence for involvement of the enzyme in T4 DNA metabolism. *J Virol* **13**: 888-897.
- Diderichsen,B., Fiil,N.P., and Lavallo,R. (1977) Genetics of the *relB* locus in *Escherichia coli*. *J Bacteriol* **131**: 30-33.
- Dittmar,K.A., Sorensen,M.A., Elf,J., Ehrenberg,M., and Pan,T. (2005) Selective charging of tRNA isoacceptors induced by amino-acid starvation. *EMBO Rep* **6**: 151-157.
- Dong,H., Nilsson,L., and Kurland,C.G. (1996) Co-variation of tRNA abundance and codon usage in *Escherichia coli* at different growth rates. *J Mol Biol* **260**: 649-663.
- Dong,T., and Schellhorn,H.E. (2010) Role of RpoS in virulence of pathogens. *Infect Immun* **78**: 887-897.
- Dorr,T., Vulic,M., and Lewis,K. (2010) Ciprofloxacin causes persister formation by inducing the TisB toxin in *Escherichia coli*. *PLoS Biol* **8**: e1000317.
- Driessen,A.J., and Nouwen,N. (2008) Protein translocation across the bacterial cytoplasmic membrane. *Annu Rev Biochem* **77**: 643-667.
- Elsinghorst,E.A. (1994) Measurement of invasion by gentamicin resistance. *Methods Enzymol* **236**: 405-420.
- Englert,M., Sheppard,K., Aslanian,A., Yates,J.R., III, and Soll,D. (2011) Archaeal 3'-phosphate RNA splicing ligase characterization identifies the missing component in tRNA maturation. *Proc Natl Acad Sci U S A* **108**: 1290-1295.
- Fineran,P.C., Blower,T.R., Foulds,I.J., Humphreys,D.P., Lilley,K.S., and Salmond,G.P. (2009) The phage abortive infection system, ToxIN, functions as a protein-RNA toxin-antitoxin pair. *Proc Natl Acad Sci U S A* **106**: 894-899.
- Fleischmann,R.D., Adams,M.D., White,O., Clayton,R.A., Kirkness,E.F., Kerlavage,A.R. *et al.* (1995) Whole-genome random sequencing and assembly of *Haemophilus influenzae* Rd. *Science* **269**: 496-512.

- Fozo,E.M., Makarova,K.S., Shabalina,S.A., Yutin,N., Koonin,E.V., and Storz,G. (2010) Abundance of type I toxin-antitoxin systems in bacteria: searches for new candidates and discovery of novel families. *Nucleic Acids Res* **38**: 3743-3759.
- Francuski,D., and Saenger,W. (2009) Crystal structure of the antitoxin-toxin protein complex RelB-RelE from *Methanococcus jannaschii*. *J Mol Biol* **393**: 898-908.
- Garcia-Pino,A., Balasubramanian,S., Wyns,L., Gazit,E., De,G.H., Magnuson,R.D. *et al.* (2010) Allosteric and intrinsic disorder mediate transcription regulation by conditional cooperativity. *Cell* **142**: 101-111.
- Garcia-Pino,A., Christensen-Dalsgaard,M., Wyns,L., Yarmolinsky,M., Magnuson,R.D., Gerdes,K., and Loris,R. (2008) Doc of Prophage P1 Is Inhibited by Its Antitoxin Partner Phd through Fold Complementation. *J Biol Chem* **283**: 30821-30827.
- Garza-Sanchez,F., Gin,J.G., and Hayes,C.S. (2008) Amino acid starvation and colicin D treatment induce A-site mRNA cleavage in *Escherichia coli*. *J Mol Biol* **378**: 505-519.
- Garza-Sanchez,F., Shoji,S., Fredrick,K., and Hayes,C.S. (2009) RNase II is important for A-site mRNA cleavage during ribosome pausing. *Mol Microbiol* **73**: 882-897.
- Ge,Z., Mehta,P., Richards,J., and Karzai,A.W. (2010) Non-stop mRNA decay initiates at the ribosome. *Mol Microbiol* **78**: 1159-1170.
- Gentry,D.R., and Cashel,M. (1996) Mutational analysis of the *Escherichia coli* *spoT* gene identifies distinct but overlapping regions involved in ppGpp synthesis and degradation. *Mol Microbiol* **19**: 1373-1384.
- Gerdes,K. (2000) Toxin-antitoxin modules may regulate synthesis of macromolecules during nutritional stress. *J Bacteriol* **182**: 561-572.
- Gerdes,K., Christensen,S.K., and Lobner-Olesen,A. (2005) Prokaryotic toxin-antitoxin stress response loci. *Nat Rev Microbiol* **3**: 371-382.
- Gerdes,K., Moller-Jensen,J., Ebersbach,G., Kruse,T., and Nordstrom,K. (2004) Bacterial mitotic machineries. *Cell* **116**: 359-366.
- Gerdes,K., Nielsen,A., Thorsted,P., and Wagner,E.G. (1992) Mechanism of killer gene activation. Antisense RNA-dependent RNase III cleavage ensures rapid turnover of the stable *hok*, *srnB* and *pndA* effector messenger RNAs. *J Mol Biol* **226**: 637-649.
- Gerdes,K., Rasmussen,P.B., and Molin,S. (1986) Unique type of plasmid maintenance function: postsegregational killing of plasmid-free cells. *Proc Natl Acad Sci U S A* **83**: 3116-3120.
- Gerdes,K., and Wagner,E.G. (2007) RNA antitoxins. *Curr Opin Microbiol* **10**: 117-124.

- Glavan,F., Behm-Ansmant,I., Izaurralde,E., and Conti,E. (2006) Structures of the PIN domains of SMG6 and SMG5 reveal a nuclease within the mRNA surveillance complex. *EMBO J* **25**: 5117-5125.
- Gomez,F.A., Cardenas,C., Henriquez,V., and Marshall,S.H. (2011) Characterization of a functional toxin-antitoxin module in the genome of the fish pathogen *Piscirickettsia salmonis*. *FEMS Microbiol Lett* **317**: 83-92.
- Gonzalez Barrios,A.F., Zuo,R., Hashimoto,Y., Yang,L., Bentley,W.E., and Wood,T.K. (2006) Autoinducer 2 controls biofilm formation in *Escherichia coli* through a novel motility quorum-sensing regulator (MqsR, B3022). *J Bacteriol* **188**: 305-316.
- Gotfredsen,M., and Gerdes,K. (1998) The *Escherichia coli* relBE genes belong to a new toxin-antitoxin gene family. *Mol Microbiol* **29**: 1065-1076.
- Gronlund,H., and Gerdes,K. (1999) Toxin-antitoxin systems homologous with relBE of *Escherichia coli* plasmid P307 are ubiquitous in prokaryotes. *J Mol Biol* **285**: 1401-1415.
- Guzman,L.M., Belin,D., Carson,M.J., and Beckwith,J. (1995) Tight regulation, modulation, and high-level expression by vectors containing the arabinose PBAD promoter. *J Bacteriol* **177**: 4121-4130.
- Hallez,R., Geeraerts,D., Sterckx,Y., Mine,N., Loris,R., and Van,M.L. (2010) New toxins homologous to ParE belonging to three-component toxin-antitoxin systems in *Escherichia coli* O157:H7. *Mol Microbiol* **76**: 719-732.
- Hanawa-Suetsugu,K., Takagi,M., Inokuchi,H., Himeno,H., and Muto,A. (2002) SmpB functions in various steps of trans-translation. *Nucleic Acids Res* **30**: 1620-1629.
- Hartz,D., McPheeters,D.S., and Gold,L. (1989) Selection of the initiator tRNA by *Escherichia coli* initiation factors. *Genes Dev* **3**: 1899-1912.
- Hayes,C.S., Aoki,S.K., and Low,D.A. (2010) Bacterial contact-dependent delivery systems. *Annu Rev Genet* **44**: 71-90.
- Hayes,C.S., and Low,D.A. (2009) Signals of growth regulation in bacteria. *Curr Opin Microbiol* **12**: 667-673.
- Hayes,C.S., and Sauer,R.T. (2003) Cleavage of the A site mRNA codon during ribosome pausing provides a mechanism for translational quality control. *Mol Cell* **12**: 903-911.
- Hazan,R., and Engelberg-Kulka,H. (2004) *Escherichia coli* mazEF-mediated cell death as a defense mechanism that inhibits the spread of phage P1. *Mol Genet Genomics*.
- Hazan,R., Sat,B., and Engelberg-Kulka,H. (2004) *Escherichia coli* mazEF-mediated cell death is triggered by various stressful conditions. *J Bacteriol* **186**: 3663-3669.

- Hazan,R., Sat,B., Reches,M., and Engelberg-Kulka,H. (2001) Postsegregational killing mediated by the P1 phage "addiction module" phd-doc requires the Escherichia coli programmed cell death system mazEF. *J Bacteriol* **183**: 2046-2050.
- Hopper,S., Wilbur,J.S., Vasquez,B.L., Larson,J., Clary,S., Mehr,I.J. *et al.* (2000) Isolation of Neisseria gonorrhoeae mutants that show enhanced trafficking across polarized T84 epithelial monolayers. *Infect Immun* **68**: 896-905.
- Huntzinger,E., Kashima,I., Fauser,M., Sauliere,J., and Izaurralde,E. (2008) SMG6 is the catalytic endonuclease that cleaves mRNAs containing nonsense codons in metazoan. *RNA*.
- Jensen,R.B., and Gerdes,K. (1995) Programmed cell death in bacteria: proteic plasmid stabilization systems. *Mol Microbiol* **17**: 205-210.
- Jensen,R.B., Grohmann,E., Schwab,H., az-Orejas,R., and Gerdes,K. (1995) Comparison of ccd of F, parDE of RP4, and parD of R1 using a novel conditional replication control system of plasmid R1. *Mol Microbiol* **17**: 211-220.
- Jiang,Y., Meidler,R., Amitsur,M., and Kaufmann,G. (2001) Specific interaction between anticodon nuclease and the tRNA(Lys) wobble base. *J Mol Biol* **305**: 377-388.
- Jiang,Y., Pogliano,J., Helinski,D.R., and Konieczny,I. (2002) ParE toxin encoded by the broad-host-range plasmid RK2 is an inhibitor of Escherichia coli gyrase. *Mol Microbiol* **44**: 971-979.
- Jishage,M., and Ishihama,A. (1998) A stationary phase protein in Escherichia coli with binding activity to the major sigma subunit of RNA polymerase. *Proc Natl Acad Sci U S A* **95**: 4953-4958.
- Jishage,M., Kvint,K., Shingler,V., and Nystrom,T. (2002) Regulation of sigma factor competition by the alarmone ppGpp. *Genes Dev* **16**: 1260-1270.
- Jorgensen,M.G., Pandey,D.P., Jaskolska,M., and Gerdes,K. (2009) HicA of Escherichia coli defines a novel family of translation-independent mRNA interferases in bacteria and archaea. *J Bacteriol* **191**: 1191-1199.
- Julio,S.M., Heithoff,D.M., and Mahan,M.J. (2000) ssrA (tmRNA) plays a role in Salmonella enterica serovar Typhimurium pathogenesis. *J Bacteriol* **182**: 1558-1563.
- Kamada,K., and Hanaoka,F. (2005) Conformational change in the catalytic site of the ribonuclease YoeB toxin by YefM antitoxin. *Mol Cell* **19**: 497-509.
- Kamada,K., Hanaoka,F., and Burley,S.K. (2003) Crystal structure of the MazE/MazF complex: molecular bases of antidote-toxin recognition. *Mol Cell* **11**: 875-884.
- Kamphuis,M.B., Monti,M.C., van den Heuvel,R.H., Santos-Sierra,S., Folkers,G.E., Lemonnier,M. *et al.* (2007) Interactions between the toxin Kid of the bacterial parD system and the antitoxins Kis and MazE. *Proteins* **67**: 219-231.

- Kapoor,S., Das,G., and Varshney,U. (2011) Crucial contribution of the multiple copies of the initiator tRNA genes in the fidelity of tRNA(fMet) selection on the ribosomal P-site in Escherichia coli. *Nucleic Acids Res* **39**: 202-212.
- Karzai,A.W., Susskind,M.M., and Sauer,R.T. (1999) SmpB, a unique RNA-binding protein essential for the peptide-tagging activity of SsrA (tmRNA). *EMBO J* **18**: 3793-3799.
- Kasari,V., Kurg,K., Margus,T., Tenson,T., and Kaldalu,N. (2010) The Escherichia coli mqsR and ygiT genes encode a new toxin-antitoxin pair. *J Bacteriol* **192**: 2908-2919.
- Keiler,K.C., and Ramadoss,N.S. (2011) Bifunctional transfer-messenger RNA. *Biochimie* **93** (11): 1993-1997
- Keiler,K.C., and Shapiro,L. (2003) tmRNA in Caulobacter crescentus is cell cycle regulated by temporally controlled transcription and RNA degradation. *J Bacteriol* **185**: 1825-1830.
- Kelley,L.A., and Sternberg,M.J. (2009) Protein structure prediction on the Web: a case study using the Phyre server. *Nat Protoc* **4**: 363-371.
- Keren,I., Shah,D., Spoering,A., Kaldalu,N., and Lewis,K. (2004) Specialized persister cells and the mechanism of multidrug tolerance in Escherichia coli. *J Bacteriol* **186**: 8172-8180.
- Khoo,S.K., Loll,B., Chan,W.T., Shoeman,R.L., Ngoo,L., Yeo,C.C., and Meinhart,A. (2007) Molecular and structural characterization of the PezAT chromosomal toxin-antitoxin system of the human pathogen Streptococcus pneumoniae. *J Biol Chem* **282**: 19606-19618.
- Kim,Y., Wang,X., Ma,Q., Zhang,X.S., and Wood,T.K. (2009) Toxin-antitoxin systems in Escherichia coli influence biofilm formation through YjgK (TabA) and fimbriae. *J Bacteriol* **191**: 1258-1267.
- Kim,Y., Wang,X., Zhang,X.S., Grigoriu,S., Page,R., Peti,W., and Wood,T.K. (2010) Escherichia coli toxin/antitoxin pair MqsR/MqsA regulate toxin CspD. *Environ Microbiol* **12**: 1105-1121.
- Kim,Y., and Wood,T.K. (2010) Toxins Hha and CspD and small RNA regulator Hfq are involved in persister cell formation through MqsR in Escherichia coli. *Biochem Biophys Res Commun* **391**: 209-213.
- Kimura,S., and Suzuki,T. (2010) Fine-tuning of the ribosomal decoding center by conserved methyl-modifications in the Escherichia coli 16S rRNA. *Nucleic Acids Res* **38**: 1341-1352.
- Kleanthous,C. (2010) Swimming against the tide: progress and challenges in our understanding of colicin translocation. *Nat Rev Microbiol* **8**: 843-848.
- Koga,M., Otsuka,Y., Lemire,S., and Yonesaki,T. (2011) Escherichia coli rnlA and rnlB compose a novel toxin-antitoxin system. *Genetics* **187**: 123-130.

- Kolodkin-Gal,I., and Engelberg-Kulka,H. (2006) Induction of Escherichia coli chromosomal mazEF by stressful conditions causes an irreversible loss of viability. *J Bacteriol* **188**: 3420-3423.
- Kolodkin-Gal,I., Hazan,R., Gaathon,A., Carmeli,S., and Engelberg-Kulka,H. (2007) A linear pentapeptide is a quorum-sensing factor required for mazEF-mediated cell death in Escherichia coli. *Science* **318**: 652-655.
- Kolodkin-Gal,I., Verdiger,R., Shlosberg-Fedida,A., and Engelberg-Kulka,H. (2009) A differential effect of E. coli toxin-antitoxin systems on cell death in liquid media and biofilm formation. *PLoS One* **4**: e6785.
- Komine,Y., Kitabatake,M., Yokogawa,T., Nishikawa,K., and Inokuchi,H. (1994) A tRNA-like structure is present in 10Sa RNA, a small stable RNA from Escherichia coli. *Proc Natl Acad Sci U S A* **91**: 9223-9227.
- Koonin,E.V., and Wolf,Y.I. (2008) Genomics of bacteria and archaea: the emerging dynamic view of the prokaryotic world. *Nucleic Acids Res* **36**: 6688-6719.
- Korch,S.B., Contreras,H., and Clark-Curtiss,J.E. (2009) Three Mycobacterium tuberculosis Rel toxin-antitoxin modules inhibit mycobacterial growth and are expressed in infected human macrophages. *J Bacteriol* **191**: 1618-1630.
- Korch,S.B., Henderson,T.A., and Hill,T.M. (2003) Characterization of the hipA7 allele of Escherichia coli and evidence that high persistence is governed by (p)ppGpp synthesis. *Mol Microbiol* **50**: 1199-1213.
- Korch,S.B., and Hill,T.M. (2006) Ectopic overexpression of wild-type and mutant hipA genes in Escherichia coli: effects on macromolecular synthesis and persister formation. *J Bacteriol* **188**: 3826-3836.
- Kramer,E.B., and Farabaugh,P.J. (2007) The frequency of translational misreading errors in E. coli is largely determined by tRNA competition. *RNA* **13**: 87-96.
- Krell,T., Lacal,J., Busch,A., Silva-Jimenez,H., Guazzaroni,M.E., and Ramos,J.L. (2010) Bacterial sensor kinases: diversity in the recognition of environmental signals. *Annu Rev Microbiol* **64**: 539-559.
- Kuroda,A. (2006) A polyphosphate-lon protease complex in the adaptation of Escherichia coli to amino acid starvation. *Biosci Biotechnol Biochem* **70**: 325-331.
- Kuroda,A., Murphy,H., Cashel,M., and Kornberg,A. (1997) Guanosine tetra- and pentaphosphate promote accumulation of inorganic polyphosphate in Escherichia coli. *J Biol Chem* **272**: 21240-21243.
- Kuroda,A., Nomura,K., Ohtomo,R., Kato,J., Ikeda,T., Takiguchi,N. et al. (2001) Role of inorganic polyphosphate in promoting ribosomal protein degradation by the Lon protease in E. coli. *Science* **293**: 705-708.
- Kvint,K., Hosbond,C., Farewell,A., Nybroe,O., and Nystrom,T. (2000) Emergency derepression: stringency allows RNA polymerase to override negative control by an active repressor. *Mol Microbiol* **35**: 435-443.

- Lamanna,A.C., and Karbstein,K. (2009) Nob1 binds the single-stranded cleavage site D at the 3'-end of 18S rRNA with its PIN domain. *Proc Natl Acad Sci U S A* **106**: 14259-14264.
- Laursen,B.S., Sorensen,H.P., Mortensen,K.K., and Sperling-Petersen,H.U. (2005) Initiation of protein synthesis in bacteria. *Microbiol Mol Biol Rev* **69**: 101-123.
- Lehnherr,H., Maguin,E., Jafri,S., and Yarmolinsky,M.B. (1993) Plasmid addiction genes of bacteriophage P1: doc, which causes cell death on curing of prophage, and phd, which prevents host death when prophage is retained. *J Mol Biol* **233**: 414-428.
- Lehnherr,H., and Yarmolinsky,M.B. (1995) Addiction protein Phd of plasmid prophage P1 is a substrate of the ClpXP serine protease of Escherichia coli. *Proc Natl Acad Sci U S A* **92**: 3274-3277.
- Leplae,R., Geeraerts,D., Hallez,R., Guglielmini,J., Dreze,P., and Van,M.L. (2011) Diversity of bacterial type II toxin-antitoxin systems: a comprehensive search and functional analysis of novel families. *Nucleic Acids Res.*
- Lewis,K. (2010) Persister cells. *Annu Rev Microbiol* **64**: 357-372.
- Li,G.Y., Zhang,Y., Chan,M.C., Mal,T.K., Hoeflich,K.P., Inouye,M., and Ikura,M. (2006) Characterization of dual substrate binding sites in the homodimeric structure of Escherichia coli mRNA interferase MazF. *J Mol Biol* **357**: 139-150.
- Li,G.Y., Zhang,Y., Inouye,M., and Ikura,M. (2008a) Structural mechanism of transcriptional autorepression of the Escherichia coli RelB/RelE antitoxin/toxin module. *J Mol Biol* **380**: 107-119.
- Li,G.Y., Zhang,Y., Inouye,M., and Ikura,M. (2009) Inhibitory mechanism of Escherichia coli RelE-RelB toxin-antitoxin module involves a helix displacement near an mRNA interferase active site. *J Biol Chem* **284**: 14628-14636.
- Li,X., Yagi,M., Morita,T., and Aiba,H. (2008b) Cleavage of mRNAs and role of tmRNA system under amino acid starvation in Escherichia coli. *Mol Microbiol* **68**: 462-473.
- Li,X., Yokota,T., Ito,K., Nakamura,Y., and Aiba,H. (2007) Reduced action of polypeptide release factors induces mRNA cleavage and tmRNA tagging at stop codons in Escherichia coli. *Mol Microbiol* **63**: 116-126.
- Lies,M., and Maurizi,M.R. (2008) Turnover of endogenous SsrA-tagged proteins mediated by ATP-dependent proteases in Escherichia coli. *J Biol Chem* **283**: 22918-22929.
- Liu,M., Zhang,Y., Inouye,M., and Woychik,N.A. (2008) Bacterial addiction module toxin Doc inhibits translation elongation through its association with the 30S ribosomal subunit. *Proc Natl Acad Sci U S A* **105**: 5885-5890.
- Livak,K.J., and Schmittgen,T.D. (2001) Analysis of relative gene expression data using real-time quantitative PCR and the 2(-Delta Delta C(T)) Method. *Methods* **25**: 402-408.

- Loh,P.G., and Song,H. (2010) Structural and mechanistic insights into translation termination. *Curr Opin Struct Biol* **20**: 98-103.
- Loris,R., Dao-Thi,M.H., Bahassi,E.M., Van,M.L., Poortmans,F., Liddington,R. *et al.* (1999) Crystal structure of CcdB, a topoisomerase poison from *E. coli*. *J Mol Biol* **285**: 1667-1677.
- Loris,R., Marianovsky,I., Lah,J., Laeremans,T., Engelberg-Kulka,H., Glaser,G. *et al.* (2003) Crystal structure of the intrinsically flexible addiction antidote MazE. *J Biol Chem* **278**: 28252-28257.
- Madl,T., Van,M.L., Mine,N., Respondek,M., Oberer,M., Keller,W. *et al.* (2006) Structural basis for nucleic acid and toxin recognition of the bacterial antitoxin CcdA. *J Mol Biol* **364**: 170-185.
- Maezato,Y., Daugherty,A., Dana,K., Soo,E., Cooper,C., Tachdjian,S. *et al.* (2011) VapC6, a ribonucleolytic toxin regulates thermophilicity in the crenarchaeote *Sulfolobus solfataricus*. *RNA* **17**: 1381-1392.
- Magnuson,R., Lehnerr,H., Mukhopadhyay,G., and Yarmolinsky,M.B. (1996) Autoregulation of the plasmid addiction operon of bacteriophage P1. *J Biol Chem* **271**: 18705-18710.
- Magnuson,R., and Yarmolinsky,M.B. (1998) Corepression of the P1 addiction operon by Phd and Doc. *J Bacteriol* **180**: 6342-6351.
- Magnusson,L.U., Farewell,A., and Nystrom,T. (2005) ppGpp: a global regulator in *Escherichia coli*. *Trends Microbiol* **13**: 236-242.
- Maisonneuve,E., Shakespeare,L.J., Jorgensen,M.G., and Gerdes,K. (2011) Bacterial persistence by RNA endonucleases. *Proc Natl Acad Sci U S A* **108**: 13206-13211.
- Makarova,K.S., Grishin,N.V., and Koonin,E.V. (2006) The HicAB cassette, a putative novel, RNA-targeting toxin-antitoxin system in archaea and bacteria. *Bioinformatics* **22**: 2581-2584.
- Makarova,K.S., Wolf,Y.I., and Koonin,E.V. (2009) Comprehensive comparative-genomic analysis of type 2 toxin-antitoxin systems and related mobile stress response systems in prokaryotes. *Biol Direct* **4**: 19.
- Marianovsky,I., Aizenman,E., Engelberg-Kulka,H., and Glaser,G. (2001) The regulation of the *Escherichia coli* mazEF promoter involves an unusual alternating palindrome. *J Biol Chem* **276**: 5975-5984.
- Masuda,Y., Miyakawa,K., Nishimura,Y., and Ohtsubo,E. (1993) chpA and chpB, *Escherichia coli* chromosomal homologs of the pem locus responsible for stable maintenance of plasmid R100. *J Bacteriol* **175**: 6850-6856.
- Mattison,K., Wilbur,J.S., So,M., and Brennan,R.G. (2006) Structure of FitAB from *Neisseria gonorrhoeae* bound to DNA reveals a tetramer of toxin-antitoxin heterodimers containing pin domains and ribbon-helix-helix motifs. *J Biol Chem* **281**: 37942-37951.

- Maurizi, M.R. (1992) Proteases and protein degradation in *Escherichia coli*. *Experientia* **48**: 178-201.
- Meinhart, A., Alonso, J.C., Strater, N., and Saenger, W. (2003) Crystal structure of the plasmid maintenance system epsilon/zeta: functional mechanism of toxin zeta and inactivation by epsilon 2 zeta 2 complex formation. *Proc Natl Acad Sci U S A* **100**: 1661-1666.
- Meyer, A.S., and Baker, T.A. (2011) Proteolysis in the *Escherichia coli* heat shock response: a player at many levels. *Curr Opin Microbiol* **14**: 194-199.
- Miallau, L., Faller, M., Chiang, J., Arbing, M., Guo, F., Cascio, D., and Eisenberg, D. (2009) Structure and proposed activity of a member of the VapBC family of toxin-antitoxin systems. VapBC-5 from *Mycobacterium tuberculosis*. *J Biol Chem* **284**: 276-283.
- Miller, J.H. (1972) Experiments in Molecular Genetics. *Cold Spring Harbor Laboratory Press*.
- Monti, M.C., Hernandez-Arriaga, A.M., Kamphuis, M.B., Lopez-Villarejo, J., Heck, A.J., Boelens, R. *et al.* (2007) Interactions of Kid-Kis toxin-antitoxin complexes with the parD operator-promoter region of plasmid R1 are piloted by the Kis antitoxin and tuned by the stoichiometry of Kid-Kis oligomers. *Nucleic Acids Res* **35**: 1737-1749.
- Moyed, H.S., and Bertrand, K.P. (1983) hipA, a newly recognized gene of *Escherichia coli* K-12 that affects frequency of persistence after inhibition of murein synthesis. *J Bacteriol* **155**: 768-775.
- Mutschler, H., Gebhardt, M., Shoeman, R.L., and Meinhart, A. (2011) A novel mechanism of programmed cell death in bacteria by toxin-antitoxin systems corrupts peptidoglycan synthesis. *PLoS Biol* **9**: e1001033.
- Nagase, T., Ishii, S., and Imamoto, F. (1988) Differential transcriptional control of the two tRNA(fMet) genes of *Escherichia coli* K-12. *Gene* **67**: 49-57.
- Nakamoto, T. (2009) Evolution and the universality of the mechanism of initiation of protein synthesis. *Gene* **432**: 1-6.
- Nariya, H., and Inouye, M. (2008) MazF, an mRNA interferase, mediates programmed cell death during multicellular *Myxococcus* development. *Cell* **132**: 55-66.
- Neubauer, C., Gao, Y.G., Andersen, K.R., Dunham, C.M., Kelley, A.C., Hentschel, J. *et al.* (2009) The structural basis for mRNA recognition and cleavage by the ribosome-dependent endonuclease RelE. *Cell* **139**: 1084-1095.
- Nieto, C., Pellicer, T., Balsa, D., Christensen, S.K., Gerdes, K., and Espinosa, M. (2006) The chromosomal relBE2 toxin-antitoxin locus of *Streptococcus pneumoniae*: characterization and use of a bioluminescence resonance energy transfer assay to detect toxin-antitoxin interaction. *Mol Microbiol* **59**: 1280-1296.

Nieto,C., Sadowy,E., de la Campa,A.G., Hryniewicz,W., and Espinosa,M. (2010) The relBE2Spn toxin-antitoxin system of *Streptococcus pneumoniae*: role in antibiotic tolerance and functional conservation in clinical isolates. *PLoS One* **5**: e11289.

Nollmann,M., Crisona,N.J., and Arimondo,P.B. (2007) Thirty years of *Escherichia coli* DNA gyrase: from in vivo function to single-molecule mechanism. *Biochimie* **89**: 490-499.

Ogata,H., Audic,S., Renesto-Audiffren,P., Fournier,P.E., Barbe,V., Samson,D. *et al.* (2001) Mechanisms of evolution in *Rickettsia conorii* and *R. prowazekii*. *Science* **293**: 2093-2098.

Ogawa,T., Tomita,K., Ueda,T., Watanabe,K., Uozumi,T., and Masaki,H. (1999) A cytotoxic ribonuclease targeting specific transfer RNA anticodons. *Science* **283**: 2097-2100.

Ogura,T., and Hiraga,S. (1983) Mini-F plasmid genes that couple host cell division to plasmid proliferation. *Proc Natl Acad Sci U S A* **80**: 4784-4788.

Okan,N.A., Mena,P., Benach,J.L., Bliska,J.B., and Karzai,A.W. (2010) The smpB-ssrA mutant of *Yersinia pestis* functions as a live attenuated vaccine to protect mice against pulmonary plague infection. *Infect Immun* **78**: 1284-1293.

Olah,B., Kiss,E., Gyorgypal,Z., Borzi,J., Cinege,G., Csanadi,G. *et al.* (2001) Mutation in the ntrR gene, a member of the vap gene family, increases the symbiotic efficiency of *Sinorhizobium meliloti*. *Mol Plant Microbe Interact* **14**: 887-894.

Orchard,K., and May,G.E. (1993) An EMSA-based method for determining the molecular weight of a protein-DNA complex. *Nucleic Acids Res* **21**: 3335-3336.

Osterberg,S., Del Peso-Santos,T., and Shingler,V. (2011) Regulation of Alternative Sigma Factor Use. *Annu Rev Microbiol*.

Overgaard,M., Borch,J., and Gerdes,K. (2009) RelB and RelE of *Escherichia coli* form a tight complex that represses transcription via the ribbon-helix-helix motif in RelB. *J Mol Biol* **394**: 183-196.

Overgaard,M., Borch,J., Jorgensen,M.G., and Gerdes,K. (2008) Messenger RNA interferase RelE controls relBE transcription by conditional cooperativity. *Mol Microbiol* **69**: 841-857.

Pandey,D.P., and Gerdes,K. (2005) Toxin - antitoxin loci are highly abundant in free-living but lost from host-associated prokaryotes. *Nucleic Acids Res* **33**: 966-976.

Paul,B.J., Berkmen,M.B., and Gourse,R.L. (2005) DksA potentiates direct activation of amino acid promoters by ppGpp. *Proc Natl Acad Sci U S A* **102**: 7823-7828.

Pedersen,K., Christensen,S.K., and Gerdes,K. (2002) Rapid induction and reversal of a bacteriostatic condition by controlled expression of toxins and antitoxins. *Mol Microbiol* **45**: 501-510.

- Pedersen,K., and Gerdes,K. (1999) Multiple hok genes on the chromosome of *Escherichia coli*. *Mol Microbiol* **32**: 1090-1102.
- Pedersen,K., Zavialov,A.V., Pavlov,M.Y., Elf,J., Gerdes,K., and Ehrenberg,M. (2003) The bacterial toxin RelE displays codon-specific cleavage of mRNAs in the ribosomal A site. *Cell* **112**: 131-140.
- Peebles,C.L., Gegenheimer,P., and Abelson,J. (1983) Precise excision of intervening sequences from precursor tRNAs by a membrane-associated yeast endonuclease. *Cell* **32**: 525-536.
- Perederina,A., Svetlov,V., Vassylyeva,M.N., Tahirov,T.H., Yokoyama,S., Artsimovitch,I., and Vassylyev,D.G. (2004) Regulation through the secondary channel--structural framework for ppGpp-DksA synergism during transcription. *Cell* **118**: 297-309.
- Pertschy,B., Schneider,C., Gnadig,M., Schafer,T., Tollervey,D., and Hurt,E. (2009) RNA helicase Prp43 and its co-factor Pfa1 promote 20 to 18 S rRNA processing catalyzed by the endonuclease Nob1. *J Biol Chem* **284**: 35079-35091.
- Petry,S., Weixlbaumer,A., and Ramakrishnan,V. (2008) The termination of translation. *Curr Opin Struct Biol* **18**: 70-77.
- Picard,F., Dressaire,C., Girbal,L., and Coccagn-Bousquet,M. (2009) Examination of post-transcriptional regulations in prokaryotes by integrative biology. *C R Biol* **332**: 958-973.
- Pimentel,B., Madine,M.A., and de,l.C.-M. (2005) Kid cleaves specific mRNAs at UUACU sites to rescue the copy number of plasmid R1. *EMBO J* **24**: 3459-3469.
- Potrykus,K., and Cashel,M. (2008) (p)ppGpp: still magical? *Annu Rev Microbiol* **62**: 35-51.
- Prysak,M.H., Mozdierz,C.J., Cook,A.M., Zhu,L., Zhang,Y., Inouye,M., and Woychik,N.A. (2009) Bacterial toxin YafQ is an endoribonuclease that associates with the ribosome and blocks translation elongation through sequence-specific and frame-dependent mRNA cleavage. *Mol Microbiol* **71**: 1071-1087.
- Pullinger,G.D., and Lax,A.J. (1992) A *Salmonella dublin* virulence plasmid locus that affects bacterial growth under nutrient-limited conditions. *Mol Microbiol* **6**: 1631-1643.
- Puskas,L.G., Nagy,Z.B., Kelemen,J.Z., Ruberg,S., Bodogai,M., Becker,A., and Dusha,I. (2004) Wide-range transcriptional modulating effect of ntrR under microaerobiosis in *Sinorhizobium meliloti*. *Mol Genet Genomics* **272**: 275-289.
- Radnedge,L., Davis,M.A., Youngren,B., and Austin,S.J. (1997) Plasmid maintenance functions of the large virulence plasmid of *Shigella flexneri*. *J Bacteriol* **179**: 3670-3675.

- Raffaello, M., Kanin, E.I., Vogt, J., Burgess, R.R., and Ansari, A.Z. (2005) Holoenzyme switching and stochastic release of sigma factors from RNA polymerase in vivo. *Mol Cell* **20**: 357-366.
- Ramage, H.R., Connolly, L.E., and Cox, J.S. (2009) Comprehensive functional analysis of Mycobacterium tuberculosis toxin-antitoxin systems: implications for pathogenesis, stress responses, and evolution. *PLoS Genet* **5**: e1000767.
- Redfield, R.J., Cameron, A.D., Qian, Q., Hinds, J., Ali, T.R., Kroll, J.S., and Langford, P.R. (2005) A novel CRP-dependent regulon controls expression of competence genes in Haemophilus influenzae. *J Mol Biol* **347**: 735-747.
- Ren, D., Bedzyk, L.A., Thomas, S.M., Ye, R.W., and Wood, T.K. (2004) Gene expression in Escherichia coli biofilms. *Appl Microbiol Biotechnol* **64**: 515-524.
- Reynolds, N.M., Lazazzera, B.A., and Ibb, M. (2010) Cellular mechanisms that control mistranslation. *Nat Rev Microbiol* **8**: 849-856.
- Roberts, R.C., and Helinski, D.R. (1992) Definition of a minimal plasmid stabilization system from the broad-host-range plasmid RK2. *J Bacteriol* **174**: 8119-8132.
- Robson, J., McKenzie, J.L., Cursons, R., Cook, G.M., and Arcus, V.L. (2009) The vapBC operon from Mycobacterium smegmatis is an autoregulated toxin-antitoxin module that controls growth via inhibition of translation. *J Mol Biol* **390**: 353-367.
- Rotem, E., Loinger, A., Ronin, I., Levin-Reisman, I., Gabay, C., Shoshitaishvili, N. *et al.* (2010) Regulation of phenotypic variability by a threshold-based mechanism underlies bacterial persistence. *Proc Natl Acad Sci U S A* **107**: 12541-12546.
- Ruiz-Echevarria, M.J., Berzal-Herranz, A., Gerdes, K., and az-Orejas, R. (1991) The kis and kid genes of the parD maintenance system of plasmid R1 form an operon that is autoregulated at the level of transcription by the co-ordinated action of the Kis and Kid proteins. *Mol Microbiol* **5**: 2685-2693.
- Ruiz-Echevarria, M.J., de la, C.G., and az-Orejas, R. (1995) Translational coupling and limited degradation of a polycistronic messenger modulate differential gene expression in the parD stability system of plasmid R1. *Mol Gen Genet* **248**: 599-609.
- Saavedra De, B.M., Mine, N., and Van, M.L. (2008) Chromosomal toxin-antitoxin systems may act as antiaddiction modules. *J Bacteriol* **190**: 4603-4609.
- Sambrook, J., Fritsch, E.F., and Maniatis, T. (1989) *Molecular cloning: a laboratory manual*. Cold Spring Harbor Laboratory Press **2nd Edition**.
- Sat, B., Hazan, R., Fisher, T., Khaner, H., Glaser, G., and Engelberg-Kulka, H. (2001) Programmed cell death in Escherichia coli: some antibiotics can trigger mazEF lethality. *J Bacteriol* **183**: 2041-2045.
- Sat, B., Reches, M., and Engelberg-Kulka, H. (2003) The Escherichia coli mazEF suicide module mediates thymineless death. *J Bacteriol* **185**: 1803-1807.

- Sayeed,S., Brendler,T., Davis,M., Reaves,L., and Austin,S. (2005) Surprising dependence on postsegregational killing of host cells for maintenance of the large virulence plasmid of *Shigella flexneri*. *J Bacteriol* **187**: 2768-2773.
- Sayeed,S., Reaves,L., Radnedge,L., and Austin,S. (2000) The stability region of the large virulence plasmid of *Shigella flexneri* encodes an efficient postsegregational killing system. *J Bacteriol* **182**: 2416-2421.
- Schaeffer,D., Tsanova,B., Barbas,A., Reis,F.P., Dastidar,E.G., Sanchez-Rotunno,M. *et al.* (2009) The exosome contains domains with specific endoribonuclease, exoribonuclease and cytoplasmic mRNA decay activities. *Nat Struct Mol Biol* **16**: 56-62.
- Schmidt,O., Schuenemann,V.J., Hand,N.J., Silhavy,T.J., Martin,J., Lupas,A.N., and Djuranovic,S. (2007) prfF and yhaV encode a new toxin-antitoxin system in *Escherichia coli*. *J Mol Biol* **372**: 894-905.
- Schneider,C., Anderson,J.T., and Tollervey,D. (2007) The exosome subunit Rrp44 plays a direct role in RNA substrate recognition. *Mol Cell* **27**: 324-331.
- Schneider,C., Leung,E., Brown,J., and Tollervey,D. (2009) The N-terminal PIN domain of the exosome subunit Rrp44 harbors endonuclease activity and tethers Rrp44 to the yeast core exosome. *Nucleic Acids Res* **37**: 1127-1140.
- Schumacher,M.A., Piro,K.M., Xu,W., Hansen,S., Lewis,K., and Brennan,R.G. (2009) Molecular mechanisms of HipA-mediated multidrug tolerance and its neutralization by HipB. *Science* **323**: 396-401.
- Seshadri,A., and Varshney,U. (2006) Mechanism of recycling of post-termination ribosomal complexes in eubacteria: a new role of initiation factor 3. *J Biosci* **31**: 281-289.
- Sevin,E.W., and Barloy-Hubler,F. (2007) RASTA-Bacteria: a web-based tool for identifying toxin-antitoxin loci in prokaryotes. *Genome Biol* **8**: R155.
- Shah,D., Zhang,Z., Khodursky,A., Kaldalu,N., Kurg,K., and Lewis,K. (2006) Persisters: a distinct physiological state of *E. coli*. *BMC Microbiol* **6**: 53.
- Shao,Y., Harrison,E.M., Bi,D., Tai,C., He,X., Ou,H.Y. *et al.* (2011) TADB: a web-based resource for Type 2 toxin-antitoxin loci in bacteria and archaea. *Nucleic Acids Res* **39**: D606-D611.
- Shinohara,M., Guo,J.X., Mori,M., Nakashima,T., Takagi,H., Nishimoto,E. *et al.* (2010) The structural mechanism of the inhibition of archaeal RelE toxin by its cognate RelB antitoxin. *Biochem Biophys Res Commun* **400**: 346-351.
- Shoji,S., Walker,S.E., and Fredrick,K. (2009) Ribosomal translocation: one step closer to the molecular mechanism. *ACS Chem Biol* **4**: 93-107.
- Singh,R., Barry,C.E., III, and Boshoff,H.I. (2010) The three RelE homologs of *Mycobacterium tuberculosis* have individual, drug-specific effects on bacterial antibiotic tolerance. *J Bacteriol* **192**: 1279-1291.

- Singletary,L.A., Gibson,J.L., Tanner,E.J., McKenzie,G.J., Lee,P.L., Gonzalez,C., and Rosenberg,S.M. (2009) An SOS-regulated type 2 toxin-antitoxin system. *J Bacteriol* **191**: 7456-7465.
- Sinha,S., Cameron,A.D., and Redfield,R.J. (2009) Sxy induces a CRP-S regulon in Escherichia coli. *J Bacteriol* **191**: 5180-5195.
- Skruzny,M., Schneider,C., Racz,A., Weng,J., Tollervey,D., and Hurt,E. (2009) An endoribonuclease functionally linked to perinuclear mRNP quality control associates with the nuclear pore complexes. *PLoS Biol* **7**: e8.
- Smith,A.S., and Rawlings,D.E. (1997) The poison-antidote stability system of the broad-host-range Thiobacillus ferrooxidans plasmid pTF-FC2. *Mol Microbiol* **26**: 961-970.
- Sorensen,M.A. (2001) Charging levels of four tRNA species in Escherichia coli Rel(+) and Rel(-) strains during amino acid starvation: a simple model for the effect of ppGpp on translational accuracy. *J Mol Biol* **307**: 785-798.
- Sorensen,M.A., Jensen,K.F., and Pedersen,S. (1994) High concentrations of ppGpp decrease the RNA chain growth rate. Implications for protein synthesis and translational fidelity during amino acid starvation in Escherichia coli. *J Mol Biol* **236**: 441-454.
- Stewart,G.R., Robertson,B.D., and Young,D.B. (2003) Tuberculosis: a problem with persistence. *Nat Rev Microbiol* **1**: 97-105.
- Sunohara,T., Jojima,K., Yamamoto,Y., Inada,T., and Aiba,H. (2004) Nascent-peptide-mediated ribosome stalling at a stop codon induces mRNA cleavage resulting in nonstop mRNA that is recognized by tmRNA. *RNA* **10**: 378-386.
- Sussman,A.J., and Gilvarg,C. (1969) Protein turnover in amino acid-starved strains of Escherichia coli K-12 differing in their ribonucleic acid control. *J Biol Chem* **244**: 6304-6306.
- Suzuki,M., Zhang,J., Liu,M., Woychik,N.A., and Inouye,M. (2005) Single protein production in living cells facilitated by an mRNA interferase. *Mol Cell* **18**: 253-261.
- Szekeres,S., Dauti,M., Wilde,C., Mazel,D., and Rowe-Magnus,D.A. (2007) Chromosomal toxin-antitoxin loci can diminish large-scale genome reductions in the absence of selection. *Mol Microbiol* **63**: 1588-1605.
- Tachdjian,S., and Kelly,R.M. (2006) Dynamic metabolic adjustments and genome plasticity are implicated in the heat shock response of the extremely thermoacidophilic archaeon Sulfolobus solfataricus. *J Bacteriol* **188**: 4553-4559.
- Takagi,H., Kakuta,Y., Okada,T., Yao,M., Tanaka,I., and Kimura,M. (2005) Crystal structure of archaeal toxin-antitoxin RelE-RelB complex with implications for toxin activity and antitoxin effects. *Nat Struct Mol Biol* **12**: 327-331.
- Tam,J.E., and Kline,B.C. (1989) Control of the ccd operon in plasmid F. *J Bacteriol* **171**: 2353-2360.

- Tan, Q., Awano, N., and Inouye, M. (2011) YeeV is an Escherichia coli toxin that inhibits cell division by targeting the cytoskeleton proteins, FtsZ and MreB. *Mol Microbiol* **79**: 109-118.
- Tanaka, N., and Shuman, S. (2011) RtcB is the RNA ligase component of an Escherichia coli RNA repair operon. *J Biol Chem* **286**: 7727-7731.
- Temperley, R., Richter, R., Dennerlein, S., Lightowlers, R.N., and Chrzanowska-Lightowlers, Z.M. (2010) Hungry codons promote frameshifting in human mitochondrial ribosomes. *Science* **327**: 301.
- Thisted, T., and Gerdes, K. (1992) Mechanism of post-segregational killing by the hok/sok system of plasmid R1. Sok antisense RNA regulates hok gene expression indirectly through the overlapping mok gene. *J Mol Biol* **223**: 41-54.
- Tian, Q.B., Ohnishi, M., Tabuchi, A., and Terawaki, Y. (1996) A new plasmid-encoded proteic killer gene system: cloning, sequencing, and analyzing hig locus of plasmid Rts1. *Biochem Biophys Res Commun* **220**: 280-284.
- Tomecki, R., and Dziembowski, A. (2010) Novel endoribonucleases as central players in various pathways of eukaryotic RNA metabolism. *RNA* **16**: 1692-1724.
- Tomita, K., Ogawa, T., Uozumi, T., Watanabe, K., and Masaki, H. (2000) A cytotoxic ribonuclease which specifically cleaves four isoaccepting arginine tRNAs at their anticodon loops. *Proc Natl Acad Sci U S A* **97**: 8278-8283.
- Tosa, T., and Pizer, L.I. (1971) Effect of serine hydroxamate on the growth of Escherichia coli. *J Bacteriol* **106**: 966-971.
- Tsolis, R.M., Young, G.M., Solnick, J.V., and Baumler, A.J. (2008) From bench to bedside: stealth of enteroinvasive pathogens. *Nat Rev Microbiol* **6**: 883-892.
- Tu, G.F., Reid, G.E., Zhang, J.G., Moritz, R.L., and Simpson, R.J. (1995) C-terminal extension of truncated recombinant proteins in Escherichia coli with a 10Sa RNA decapetide. *J Biol Chem* **270**: 9322-9326.
- Ullers, R.S., Luirink, J., Harms, N., Schwager, F., Georgopoulos, C., and Genevoux, P. (2004) SecB is a bona fide generalized chaperone in Escherichia coli. *Proc Natl Acad Sci U S A* **101**: 7583-7588.
- van Melderen, L. (2010) Toxin-antitoxin systems: why so many, what for? *Curr Opin Microbiol* **13**: 781-785.
- van Melderen, L., Thi, M.H., Lecchi, P., Gottesman, S., Couturier, M., and Maurizi, M.R. (1996) ATP-dependent degradation of CcdA by Lon protease. Effects of secondary structure and heterologous subunit interactions. *J Biol Chem* **271**: 27730-27738.
- Varshney, U., Lee, C.P., and RajBhandary, U.L. (1991) Direct analysis of aminoacylation levels of tRNAs in vivo. Application to studying recognition of Escherichia coli initiator tRNA mutants by glutamyl-tRNA synthetase. *J Biol Chem* **266**: 24712-24718.

- Vazquez-Laslop,N., Lee,H., and Neyfakh,A.A. (2006) Increased persistence in Escherichia coli caused by controlled expression of toxins or other unrelated proteins. *J Bacteriol* **188**: 3494-3497.
- Wall,D., and Kaiser,D. (1999) Type IV pili and cell motility. *Mol Microbiol* **32**: 1-10.
- Wang,X., Kim,Y., Hong,S.H., Ma,Q., Brown,B.L., Pu,M. *et al.* (2011) Antitoxin MqsA helps mediate the bacterial general stress response. *Nat Chem Biol* **7**: 359-366.
- Wang,X., and Wood,T.K. (2011) Toxin/Antitoxin Systems Influence Biofilm and Persist Cell Formation and the General Stress Response. *Appl Environ Microbiol*.
- Wendrich,T.M., Blaha,G., Wilson,D.N., Marahiel,M.A., and Nierhaus,K.H. (2002) Dissection of the mechanism for the stringent factor RelA. *Mol Cell* **10**: 779-788.
- Wilbur,J.S., Chivers,P.T., Mattison,K., Potter,L., Brennan,R.G., and So,M. (2005) Neisseria gonorrhoeae FitA interacts with FitB to bind DNA through its ribbon-helix-helix motif. *Biochemistry* **44**: 12515-12524.
- Williams,K.P., Martindale,K.A., and Bartel,D.P. (1999) Resuming translation on tmRNA: a unique mode of determining a reading frame. *EMBO J* **18**: 5423-5433.
- Winther,K.S., and Gerdes,K. (2009) Ectopic production of VapCs from Enterobacteria inhibits translation and trans-activates YoeB mRNA interferase. *Mol Microbiol* **72**: 918-930.
- Wozniak,R.A., and Waldor,M.K. (2009) A toxin-antitoxin system promotes the maintenance of an integrative conjugative element. *PLoS Genet* **5**: e1000439.
- Yamaguchi,Y., Park,J.H., and Inouye,M. (2009) MqsR, a crucial regulator for quorum sensing and biofilm formation, is a GCU-specific mRNA interferase in Escherichia coli. *J Biol Chem* **284**: 28746-28753.
- Yang,M., Gao,C., Wang,Y., Zhang,H., and He,Z.G. (2010) Characterization of the interaction and cross-regulation of three Mycobacterium tuberculosis RelBE modules. *PLoS One* **5**: e10672.
- Yuan,J., Sterckx,Y., Mitchenall,L.A., Maxwell,A., Loris,R., and Waldor,M.K. (2010) Vibrio cholerae ParE2 poisons DNA gyrase via a mechanism distinct from other gyrase inhibitors. *J Biol Chem* **285**: 40397-40408.
- Zaher,H.S., and Green,R. (2009) Fidelity at the molecular level: lessons from protein synthesis. *Cell* **136**: 746-762
- Zhang,J., Zhang,Y., and Inouye,M. (2003a) Characterization of the interactions within the mazEF addiction module of Escherichia coli. *J Biol Chem* **278**: 32300-32306.
- Zhang,Y., and Inouye,M. (2009) The inhibitory mechanism of protein synthesis by YoeB, an Escherichia coli toxin. *J Biol Chem* **284**: 6627-6638.
- Zhang,Y., Yamaguchi,Y., and Inouye,M. (2009) Characterization of YafO, an Escherichia coli toxin. *J Biol Chem* **284**: 25522-25531.

Zhang, Y., Zhang, J., Hoeflich, K.P., Ikura, M., Qing, G., and Inouye, M. (2003b) MazF cleaves cellular mRNAs specifically at ACA to block protein synthesis in *Escherichia coli*. *Mol Cell* **12**: 913-923.

Zhang, Y., Zhu, L., Zhang, J., and Inouye, M. (2005) Characterization of ChpBK, an mRNA interferase from *Escherichia coli*. *J Biol Chem* **280**: 26080-26088.

Zhang, Y.X., Li, J., Guo, X.K., Wu, C., Bi, B., Ren, S.X. *et al.* (2004) Characterization of a novel toxin-antitoxin module, VapBC, encoded by *Leptospira interrogans* chromosome. *Cell Res* **14**: 208-216.

Zhu, L., Inoue, K., Yoshizumi, S., Kobayashi, H., Zhang, Y., Ouyang, M. *et al.* (2009) *Staphylococcus aureus* MazF specifically cleaves a pentad sequence, UACAU, which is unusually abundant in the mRNA for pathogenic adhesive factor SraP. *J Bacteriol* **191**: 3248-3255.

Zhu, L., Phadtare, S., Nariya, H., Ouyang, M., Husson, R.N., and Inouye, M. (2008) The mRNA interferases, MazF-mt3 and MazF-mt7 from *Mycobacterium tuberculosis* target unique pentad sequences in single-stranded RNA. *Mol Microbiol*.

Zhu, L., Zhang, Y., Teh, J.S., Zhang, J., Connell, N., Rubin, H., and Inouye, M. (2006) Characterization of mRNA interferases from *Mycobacterium tuberculosis*. *J Biol Chem* **281**: 18638-18643.

Zielenkiewicz, U., and Ceglowski, P. (2005) The toxin-antitoxin system of the streptococcal plasmid pSM19035. *J Bacteriol* **187**: 6094-6105.

Publications

Some of the work presented in this thesis has resulted in publications. These are listed chronologically below.

Christensen-Dalsgaard, M., Overgaard, M., **Winther, K.S.**, and Gerdes, K. (2008) RNA decay by messenger RNA interferases. *Methods Enzymol* 447: 521-535.

Winther, K.S., and Gerdes, K. (2009) Ectopic production of VapCs from Enterobacteria inhibits translation and trans-activates YoeB mRNA interferase. *Mol Microbiol* 72: 918-930.

Winther, K.S., and Gerdes, K. (2011) Enteric virulence associated protein VapC inhibits translation by cleavage of initiator tRNA. *Proc Natl Acad Sci U S A* 108: 7403-7407.

Winther, K.S., and Gerdes K. (2011) Regulation of enteric *vapBC* transcription: induction by toxin dimer breaking. (*In prep*)